Investigating non-canonical, 5’ UTR-dependent translation of MYC and its impact on colorectal cancer development

Untersuchung der nicht-kanonischen, 5' UTR-abhängigen Translation von MYC und ihres Einflusses auf die Entwicklung von Darmkrebs

Doctoral thesis

for a doctoral degree
at the Graduate School of Life Sciences,
Julius-Maximilians-Universität Würzburg,
Section Biomedicine

submitted by

Sarah Hahn

from Aschaffenburg

Würzburg 2023

Submitted on:

Office stamp

Members of the Thesis Committee

Chairperson:	Prof. Dr. Alexander Buchberger
Primary Supervisor:	Prof. Dr. Armin Wiegering
Supervisor (Second):	Prof. Dr. Martin Eilers
Supervisor (Third):	Prof. Dr. Utz Fischer
Supervisor (Fourth):	Prof. Dr. Anne Willis

Table of content

Zusammenfassung

Das kolorektale Karzinom (KRK) ist die zweithäufigste Tumorerkrankung in Deutschland, wobei die sequenzielle Akkumulation bestimmter Mutationen eine entscheidende Rolle beim Übergang vom Adenom zum Karzinom spielt. Insbesondere die Deregulation des Wnt-Signalweges und die damit verbundene deregulierte Expression des MYC-Onkoproteins spielen eine entscheidende Rolle. MYC ist ein zentraler Vermittler von Zellfunktionen und reguliert als Transkriptionsfaktor die Expression fast aller Gene sowie verschiedener RNA-Spezies. Selbst kleine Veränderungen der zellulären MYC-Konzentration können das Proliferationsverhalten beeinflussen und die Entstehung und das Fortschreiten von Tumoren fördern. Die gezielte Beeinflussung von *MYC* stellt daher einen wichtigen therapeutischen Ansatz für die Behandlung von Tumoren dar. Da eine direkte Hemmung von MYC aufgrund seiner Struktur herausfordernd ist, wurden bisher verschiedene Ansätze verfolgt, um MYC indirekt zu beeinflussen, etwa über seinen Interaktionspartner MAX oder auf Ebene der Stabilität, Transkription oder Translation. In unserer eigenen Forschungsgruppe lag der Schwerpunkt in den letzten Jahren speziell auf der Translation von *MYC* im KRK. Es konnte gezeigt werden, dass die Hemmung der kanonischen cap-abhängigen Translation nicht wie erwartet zu einer Verringerung der zellulären MYC-Level führt, was auf einen alternativen Mechanismus der *MYC*-Translation hindeutet, der unabhängig vom eIF4F-Komplex abläuft. Die 5'-UTR von *MYC* enthält eine interne ribosomale Eintrittsstelle (IRES), die eine besondere Rolle bei der Initiierung der *MYC*-Translation spielt, insbesondere im Multiplen Myelom. Als Grundlage für diese Arbeit wurde daher die Hypothese aufgestellt, dass die Translation von *MYC* im KRK möglicherweise ebenfalls über die IRES erfolgt. Auf dieser Grundlage wurden zunächst zwei publizierte IRES-Inhibitoren auf ihr Potenzial zur Regulierung der MYC-Expression in KRK-Zellen getestet. J007-IRES hatte keine Auswirkungen auf die MYC-Proteinmenge, und Cymarin scheint weitaus globalere Auswirkungen zu haben, die nicht ausschließlich auf die Verringerung der MYC-Proteinmenge zurückzuführen sind. Daher wurde weiter untersucht, inwieweit die alternative Translation von *MYC* generell von der 5'-UTR und damit interagierenden Faktoren abhängig ist. EIF3D wurde als MYC-5'-UTR-Bindungsprotein identifiziert, dessen Knockdown zu reduzierten MYC-Leveln, einem Proliferationsdefizit sowie einer Verringerung der globalen Proteinsynthese in KRK-Zellen führte. Darüber hinaus führte die Depletion von *EIF3D* zu ähnlichen Veränderungen im zellulären Genexpressionsmuster wie die Depletion von *MYC*, wobei viele tumorassoziierte Signalwege betroffen waren. Mittels eCLIP-seq wurde die Bindung von eIF3D an die *MYC* mRNA nachgewiesen, der genaue Mechanismus einer

möglicherweise durch eIF3D vermittelten Translation von *MYC* muss jedoch weiter untersucht werden. Die Ergebnisse dieser Arbeit deuten darauf hin, dass eine Verbindung zwischen eIF3D und der *MYC*-Expression/Translation besteht, wodurch eIF3D zu einem potenziellen therapeutischen Ziel für MYC-getriebene KRKs wird.

Summary

Colorectal cancer (CRC) is the second most common tumour disease in Germany, with the sequential accumulation of certain mutations playing a decisive role in the transition from adenoma to carcinoma. In particular, deregulation of the Wnt signalling pathway and the associated deregulated expression of the MYC oncoprotein play a crucial role. MYC is a central mediator of cellular functions and, as a transcription factor, regulates the expression of almost all genes as well as various RNA species. Even small changes in cellular MYC levels can influence proliferation behaviour and promote tumour initiation and progression. Targeting *MYC* thus represents an important therapeutic approach in the treatment of tumours. Since direct inhibition of MYC is challenging, various approaches have been pursued to date to target MYC indirectly, such as via its interaction partner MAX or at the level of stability, transcription, or translation. In our own research group, the focus in recent years has been specifically on the translation of *MYC* in CRC. It was shown that inhibition of canonical cap-dependent translation does not lead to a reduction in cellular MYC levels as expected, suggesting an alternative mechanism of *MYC* translation that occurs independently of the eIF4F complex. The *MYC* 5' UTR contains an internal ribosomal entry site (IRES), which has a particular role in the initiation of *MYC* translation, especially in multiple myeloma. As basis for this work, it was therefore hypothesised that translation of *MYC* potentially occurs via its IRES in CRC as well. Based on this, two IRES inhibitors were first tested for their potential to regulate MYC expression in CRC cells. J007-IRES had no effect on MYC levels and cymarin appears to produce much more global effects that are not exclusively due to reduced MYC levels. The extent to which alternative translation of *MYC* is generally dependent on its 5' UTR and interacting factors was therefore further investigated. EIF3D was identified as a *MYC* 5' UTR binding protein, whereby knockdown resulted in reduced MYC levels, a proliferation deficit as well as a reduction in global protein synthesis in CRC cells. Furthermore, depletion of *EIF3D* led to similar changes in cellular gene expression patterns as depletion of *MYC*, with many tumour-related pathways being affected. Using eCLIP-seq, the binding of eIF3D to the *MYC* mRNA was verified, but the exact mechanism of a potentially eIF3D-mediated translation of *MYC* requires further investigation. The results of this work suggest that there is a link between eIF3D and *MYC* expression/translation, rendering eIF3D a potential therapeutic target for MYC-driven CRCs.

1 Introduction

1.1 Mechanisms of eukaryotic translation

mRNA translation represents one of the most important and fundamental cellular processes and consumes much of the cellular energy (Buttgereit & Brand, 1995). Errors in the production of new proteins can lead to serious cellular defects and abnormalities, so this process is tightly controlled by several factors. By regulating protein synthesis, cells can respond in a matter of minutes to a wide range of environmental conditions, e.g. to ensure cell maintenance or to initiate programmed cell death (Sonenberg & Hinnebusch, 2009). For example, canonical cap-dependent translation is shut down under certain stress conditions and alternative pathways are utilised (see section 1.1.3), e.g. to translate stress-responsive genes that are 'switched off' under normal conditions (Harvey & Willis, 2018). The deregulated expression of essential translation factors can lead to a change in the translation spectrum and to uncontrolled growth of a cell, which illustrates the importance of translation control (Chu, Cargnello, Topisirovic, & Pelletier, 2016). Translation can be divided into four main steps, namely initiation, elongation, termination, and recycling of ribosomes (Dever & Green, 2012; Hinnebusch, 2014). In this work the focus is on the initiation process.

1.1.1 Canonical cap-dependent translation initiation

Almost all mRNAs possess a 5' terminal 7-methylguanosine (m7G) cap as well as a 50 - 300 nucleotide long 3' poly-adenine (A) tail. Both structures are of great importance for canonical translation initiation, with the m7G cap in particular - as the name suggests - and interacting factors playing a major role for cap-dependent translation (Hashem & Frank, 2018; Safaee et al., 2012).

1.1.1.1 Ternary complex formation and mRNA activation

Translation initiation begins with the formation of a ternary complex (TC) consisting of the methionine initiator transfer (t) RNA (Met-tRNA$_i$) and guanosine-triphosphate (GTP)-bound eukaryotic translation initiation factor (eIF) 2 (**Figure 1,** step 1). This complex associates with the 40S ribosomal subunit, promoted by eIFs 1, 1A, 3 and 5, to form the

so-called pre-initiation complex (PIC) (**Figure 1,** step 2) (Hashem & Frank, 2018). At the same time, mRNA is prepared for its recruitment to the PIC by interacting with eIF4 factors and the poly(A)-binding protein (PABP) (**Figure 1,** step 3a) (Jackson, Hellen, & Pestova, 2010; Sonenberg & Hinnebusch, 2009). In detail, eIF4E recognizes and binds the m7G cap, thereby anchoring the RNA helicase eIF4A to the 5' untranslated region (UTR) of the mRNA which is promoted by the scaffolding protein eIF4G. Subsequently, eIF4A, in conjunction with eIF4B, unwinds structures in the 5' UTR to clear a path for the associating PIC. The poly(A) tail is bound by PABP and interactions with eIF4G and E can bring the mRNA's 5' and 3' ends together (Aitken & Lorsch, 2012). It is assumed that this 'closed-loop mRNP' on the one hand ensures that only intact mRNAs are translated. On the other hand, it enables coupling of termination or recycling events to a new round of translation of the same mRNA. In general, the involvement of PABP does not appear to be essential for translation initiation, but it plays a role under competitive conditions and tends to enhance the translation rate (Aitken & Lorsch, 2012). After activation of the mRNA, it is recruited to the PIC most likely by interaction of eIF4G and eIF3, which is bound to the 40S ribosomal subunit (**Figure 1,** step 3b) (LeFebvre et al., 2006). EIF3 is a multi-subunit complex (eIF3A-M) with a molecular mass of 800 kDa and thus the largest of all translation factors, to which a wide variety of functions in translation are ascribed (Cate, 2017).

1.1.1.2 Scanning and start codon recognition

Once at the 5' end of the mRNA, it is thought that the PIC makes its way to the start codon via a linear, base-by-base scanning process (**Figure 1,** step 4) (Aitken & Lorsch, 2012). The process of start codon recognition and the factors involved have been characterised in detail over the past decades. mRNA translation in eukaryotes is typically initiated at an AUG start codon which is located within variants of the consensus Kozak sequence (GCCACCAUGG) to ensure translation begins in the proper reading frame (Kozak, 1986). Upon start codon recognition, eIF1 is released from the PIC and eIF2-bound GTP is converted to GDP, leading to arrest of the scanning process (**Figure 1,** step 5). Subsequently, eIF2-GDP and eIF5 dissociate from the complex, thereby enabling eIF5B to join and mediate 60S subunit association (**Figure 1,** step 6). This is followed by GTP hydrolysis by eIF5B and translation factor release to form the 80S initiation complex (IC) (**Figure 1,** step 7) (Aitken & Lorsch, 2012).

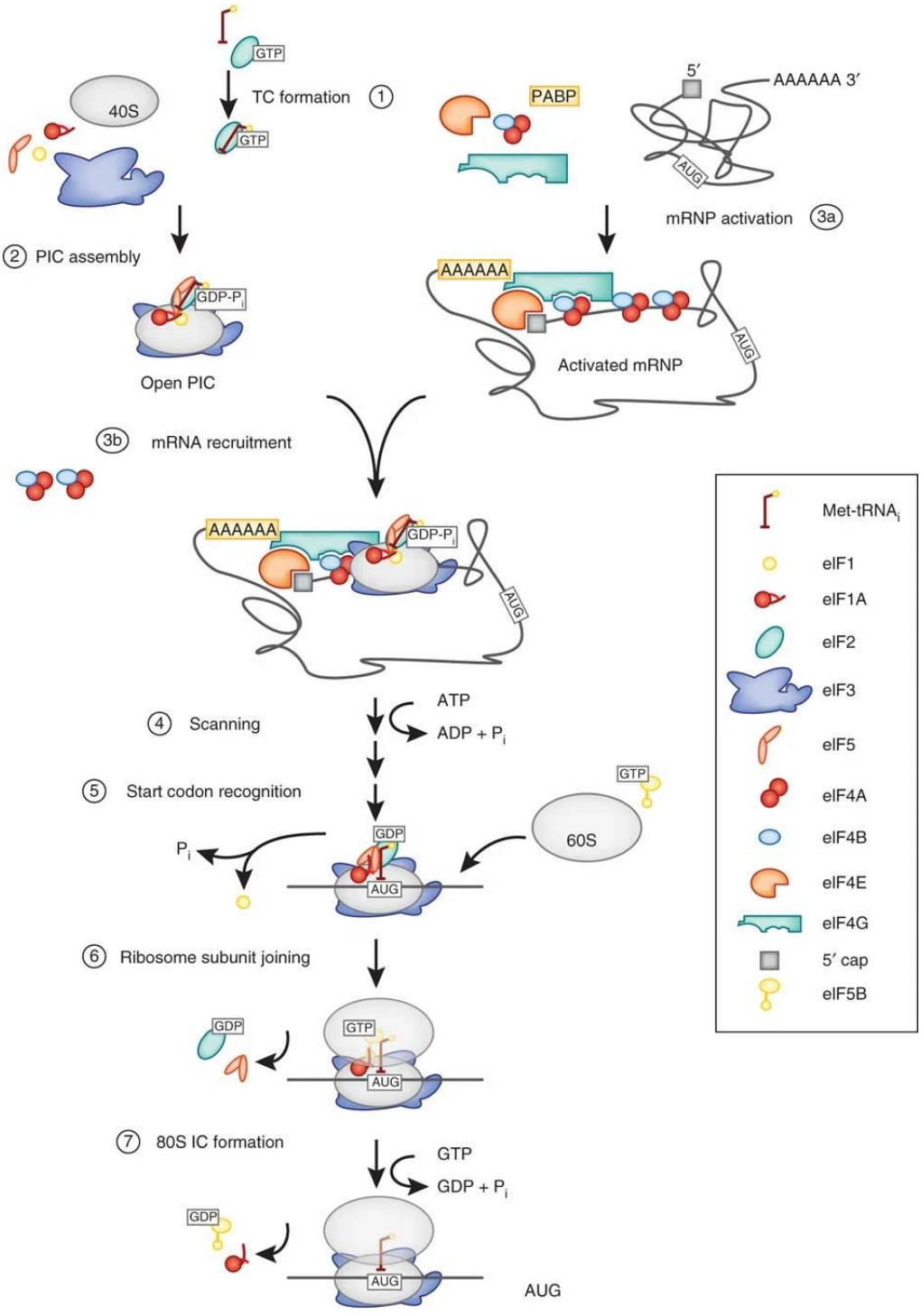

Figure 1: Mechanism of canonical cap-dependent translation initiation. *Ternary complex (TC) formation (1) is followed by pre-initiation complex (PIC) assembly (2). Activated mRNP (3a) is recruited to the PIC (3b) and the scanning process of the 5' UTR is initiated (4). Upon start codon recognition (5), the 60S ribosomal subunit joins the initiation complex (6) to form the elongation-competent 80S initiation complex (IC) (7). While most of the initiation factors (IF) dissociate upon 80S IC formation, eIF3 remains bound to the complex during elongation. Adapted from (Aitken & Lorsch, 2012) and reprinted with permission.*

The only factor remaining bound to the 40S ribosomal subunit during elongation is eIF3, thereby participating in downstream reinitiation events (Szamecz et al., 2008). The IC is then ready to accept the appropriate aminoacyl-tRNA within the aminoacyl (A) site of the ribosome and to synthesize the first peptide bond upon entering the elongation step (Sonenberg & Hinnebusch, 2009).

1.1.2 Regulation of cap-dependent translation initiation

In general, overall translation rates can be regulated by the activity and availability of the components of the eIF4F complex and the TC, which is of special importance under non-physiological conditions. When cells are faced with external or physiological stress, they can induce the so-called Integrated Stress Response (ISR), a complex cell response in which mRNA translation can be modulated via various signalling pathways and regulators (Dever, 2002; Ryoo & Vasudevan, 2017). In principle, during translation initiation, the eIF2-bound GTP is hydrolysed to GDP and must be replaced by GTP for the next round of translation which is performed by the guanine exchange factor eIF2B. Stressful conditions lead to phosphorylation of eIF2α (P-eIF2α) by stress-related kinases and increased binding to eIF2B, thereby inhibiting translation of most transcripts (Dever, 2002; Jennings, Zhou, Mohammad-Qureshi, Bennett, & Pavitt, 2013; Ryoo & Vasudevan, 2017). However, conditions of increased P-eIF2α promote alternative ways of mRNA translation such as internal ribosome entry site (IRES)- or upstream open reading frame (uORF)-mediated initiation (Godet et al., 2019; Ryoo & Vasudevan, 2017). Another node of translational inhibition in the ISR is mediated by the activity of the so-called 4E-binding proteins (4EBP). 4EBP is a transcriptional target of ATF4, which is activated upon eIF2α phosphorylation (Yamaguchi et al., 2008). However, activity of 4EBPs and interaction with their target eIF4E is dependent on their phosphorylation status (Somers et al., 2013). Under physiological conditions, various stimuli such as growth factors or hormones lead to phosphorylation of Akt, followed by mammalian target of rapamycin (mTOR) and finally 4EBPs are phosphorylated via the phosphoinositide 3-kinase (PI3K) pathway (Somers et al., 2013). In the hyperphosphorylated state, 4EBPs are unable to bind to eIF4E, making it available for the formation of the eIF4F complex and cap-dependent translation can be initiated (**Figure 2**). In contrast, it is assumed, that endoplasmic reticulum (ER) stress inactivates mTOR, which in turn is not able to phosphorylate 4EBP anymore (Preston & Hendershot, 2013). 4EBPs in the

hypophosphorylated state bind more strongly to eIF4E and sequester it leading to inhibition of canonical translation initiation (Gingras, Gygi, et al., 1999).

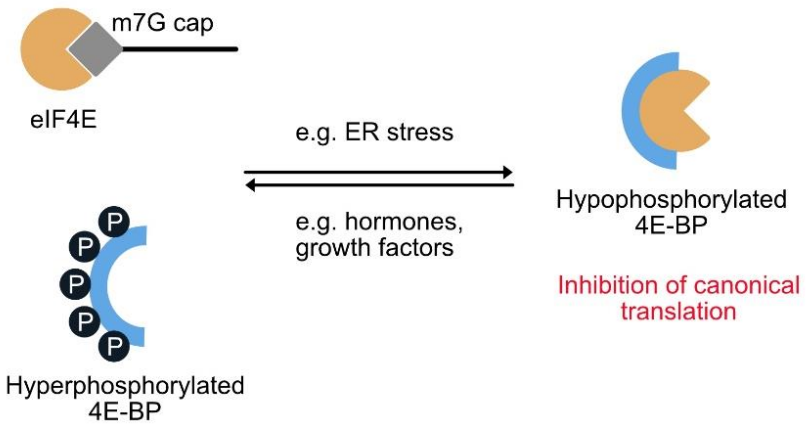

Figure 2: Canonical, cap-dependent translation initiation is dependent on the phosphorylation status of 4EBPs. *Under physiological conditions upon respective stimuli, 4EBPs are phosphorylated and thus not able to bind eIF4E, making it available for assembling the eIF4F complex. However, stressful conditions induce dephosphorylation of 4EBPs and their enhanced binding to eIF4E. eIF4E is thus no longer available for eIF4F complex assembly and canonical translation is inhibited. Adapted and modified from (Somers, Poyry, & Willis, 2013).*

1.1.3 Alternative ways of translation initiation

Although canonical cap-dependent initiation is the most studied mode of mRNA translation, alternative mechanisms also exist, such as ribosome shunting, leaky scanning, re-initiation-dependent, internal ribosome entry site (IRES)-dependent, m^6A-dependent or cap-independent translation enhancers (CITE) translation (Martinez-Salas, Pineiro, & Fernandez, 2012). Under particular circumstances, these modes of translation initiation can become even more important than cap-dependent translation, which is inhibited by stresses such as hypoxia, nutrient deprivation, oxidative stress or genotoxic stress (Sriram et al., 2018).

1.1.3.1 Alternative start codon usage

It is possible that several AUG start codons are present in different strength contexts on a transcript. For example, if the first AUG is in a sequence context of medium strength, the ribosome may sometimes initiate at this site or scan past it and start translation at a downstream AUG. This process is also known as leaky scanning (Kozak, 2002; X. Q. Wang & Rothnagel, 2004). If the two AUG codons are in frame with each other, two isoforms of the same protein are synthesised, one with an N-terminal extension. If there are two overlapping ORFs with different reading frames, two different proteins are expressed from the same mRNA. Both mechanisms thus play an important physiological role in mRNA translation (Sriram et al., 2018). Although AUG start codons are the most commonly used codons for translation initiation, it has been known since the 1980s that non-AUG start codons can also be used for translation initiation, albeit with lower efficiency. These usually differ from the AUG by only one nucleotide, e.g. CUG, GUG or UUG, and are referred to as near-cognate start codons (Peabody, 1989; Zitomer, Walthall, Rymond, & Hollenberg, 1984). Many endogenous and viral mRNAs are translated exclusively via non-AUG codons, such as the alternative translation initiation factor *EIF4G2* (also called *DAP5*), which plays an important role in IRES-mediated initiation (see also chapter 1.1.3.2.2) (Kearse & Wilusz, 2017; Takahashi et al., 2005). Thousands of other non-AUG initiation events have been discovered by ribosome profiling, with CUG, GUG, ACG and AUU being used with decreasing efficiency (Ingolia, Ghaemmaghami, Newman, & Weissman, 2009; Ingolia, Lareau, & Weissman, 2011).

1.1.3.2 IRES-dependent translation initiation

First being discovered in picornaviruses, IRESs were identified as *cis*-acting translation regulatory elements able to recruit ribosomes cap-independently via RNA structural domains. Viral IRESs are divided into four classes that differ in the way they recruit ribosomes and in their secondary/tertiary structure (Godet et al., 2019). Type I and II IRESs, which occur predominantly in picornaviruses, are 400 - 500 nucleotide long sequences with a highly conserved primary and secondary structure (K. M. Lee, Chen, & Shih, 2017; S. R. Thompson, 2012). In contrast, the shorter type III IRESs are characterised by the presence of a pseudoknot and the requirement of part of the coding sequence and are found, for example, in hepatitis C virus (HCV) (Tsukiyama-Kohara, Iizuka, Kohara, & Nomoto, 1992; C. Wang, Sarnow, & Siddiqui, 1994). Type IV IRESs

can initiate translation without an AUG start codon and are particularly represented in viruses with bicistronic mRNA, e.g. cricket paralysis virus (CrPV) (K. M. Lee et al., 2017; Wilson, Pestova, Hellen, & Sarnow, 2000). An exception to the four classes is the retroviridae family, whose mRNA is capped and thus resembles cellular IRESs (see below) (Godet et al., 2019). The example of picornaviruses illustrates the probability of an alternative translation initiation mechanism. Generally, picornavirus mRNAs are uncapped and start codons are located several hundred nucleotides downstream of the mRNA 5' end, rendering initiation of translation via the canonical, 5' end-dependent scanning mechanism unlikely. Furthermore, these viruses express an eIF4G-cleaving protease, which generally leads to a shutdown of cap-dependent translation in infected animal cells (Godet et al., 2019). Although it was initially assumed that only viral mRNAs had such structures, short time later an IRES-like sequence was identified in the cellular immunoglobulin heavy-chain binding protein (BiP) mRNA (Macejak & Sarnow, 1991).

1.1.3.2.1 Physiological role of IRES translation

Cellular IRES-mediated translation is thought to play a role especially under stress conditions where cap-dependent initiation is blocked, e.g. during the G2-M phase of the cell cycle, heat shock or - as already mentioned - by viral infections (Godet et al., 2019). Searching for the physiological role of IRES translation, such more or less complex secondary structures were identified in many other mRNAs, e.g. *MYC*, *fibroblast growth factors* (FGFs), *vascular endothelial growth factors* (VEGFs), as well as other master regulators of cell responses (Godet et al., 2019; Huez et al., 1998; A. C. Prats & Prats, 2002; Stoneley, Paulin, Le Quesne, Chappell, & Willis, 1998). It has been shown that these capped IRES-containing mRNAs can be translated both cap-dependently and IRES-mediated, depending on the condition. For example, a switch from cap- to IRES-dependent translation has been demonstrated for *VEGF* and *HIF1α* in breast cancer cells, resulting from the overexpression of eIF4G and 4EBP (Braunstein et al., 2007). The function of cellular IRES elements is clearly demonstrated by bi- or multicistronic mRNAs expressing two or more proteins, in most cases via IRES structures (Karginov, Pastor, Semler, & Gomez, 2017). For example, *FGF2* mRNA contains four CUGs and one AUG start codon, thereby expressing five FGF2 isoforms, which have different localisations and functions (Arnaud et al., 1999; H. Prats et al., 1989). Interestingly, translation of the upstream CUG is cap-dependent, whereas all other start codons are initiated in an IRES-mediated way.

1.1.3.2.2 Mechanism of IRES-mediated translation

IRES-mediated translation usually requires an alternative spectrum of canonical translation factors, with the so-called IRES trans-acting factors (ITAFs) playing an important additional role. Numerous ITAFs have been identified for a wide variety of IRES-containing mRNAs, which can act as activators or repressors and often have other functions in the cell. Most of them play a role in alternative splicing (e.g. hnRNPs), ribosome biogenesis (e.g. nucleolin), stabilisation of mRNAs (e.g. HuR), or transcription (e.g. p54nrb, hnRNPK and -M) (Godet et al., 2019). In relation to IRES-mediated translation, several ITAF mechanisms have been documented. On the one hand, they act as chaperones to induce conformational changes in the IRES's secondary structure or compete with other ITAFs to regulate the translation of IRESs (Ji et al., 2017; S. A. Mitchell, Spriggs, Coldwell, Jackson, & Willis, 2003). Furthermore, they may contribute to the nucleocytoplasmic translocation of IRES-containing mRNAs or interact with other translation initiation factors or 4EBPs to regulate translation (Braunstein et al., 2007; Liberman, Marash, & Kimchi, 2009; J. C. Lin, Hsu, & Tarn, 2007; W. Lin et al., 2014). The coupling of transcription and translation and concomitant promoter-dependent recruitment of ITAFs has also been documented (Conte et al., 2009). In addition, canonical eIFs (e.g. eIF4GI, DAP5, eIF4A, eIF5B and eIF3) as well as eukaryotic elongation factors (eEFs) also play a role in IRES activity (Braunstein et al., 2007; Miura et al., 2010; T. A. Nevins, Harder, Korneluk, & Holcik, 2003; Spriggs et al., 2009; Thakor & Holcik, 2012). Finally, some ITAFs are associated with the ribosome or are even ribosomal proteins (RPs), thereby promoting IRES-mediated translation initiation (Colon-Ramos et al., 2006; Landry, Hertz, & Thompson, 2009; Majzoub et al., 2014; Y. Yu, Ji, Doudna, & Leary, 2005) (**Figure 3**). If eIF2α is present in the phosphorylated form upon cell stress, this affects the availability of the TC (see 1.1.2). This in turn leads to the inhibition of cap-dependent translation initiation and instead to a preference for uORF- or IRES-mediated initiation (M. J. Kang et al., 2017; Ryoo & Vasudevan, 2017). Although eIF2α is generally required for both cap-dependent and -independent translation, IRES-mediated initiation increases selectively under P-eIF2α (Fernandez et al., 2002; M. J. Kang et al., 2017; Thakor & Holcik, 2012). Two models exist that could explain this observation. First, it is hypothesised that eIF5B may support ribosome recruitment and IC formation by delivering initiator tRNA directly to the P site of the ribosome, thereby contributing to the formation of a translation-competent IC (Holcik, 2015; Thakor & Holcik, 2012) (**Figure 3**). Second, GCN2 (in addition to phosphorylating eIF2α) has been shown to activate the stress response gene and transcription factor ATF4, which in turn

induces 4EBP (M. J. Kang et al., 2017). Thus, when the availability of the TC is limited, the blockade of cap-dependent translation by 4EBP can lead to enhanced IRES-mediated translation.

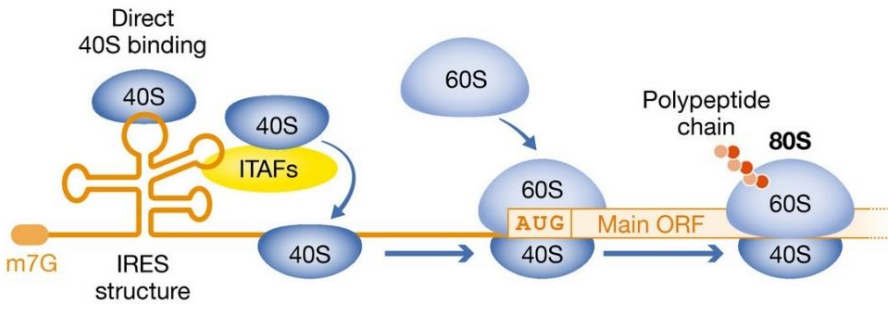

Figure 3: Schematics of IRES-mediated translation initiation. *It is hypothesised that the 40S ribosome with help of eIF5B may directly bind to the IRES or transcript-specific ITAFs could promote its binding and translocation to the vicinity of a suitable start codon. Adapted from (Sriram, Bohlen, & Teleman, 2018) and reprinted with permission.*

1.1.3.3 m^{6}A-dependent translation initiation

RNAs are generally subject to many modifications, with the N_6-methyladenosine (m^{6}A) modification being the most common. Originally, this type of modification was predominantly assigned to 3' UTRs of mRNAs, where it is thought to contribute to RNA binding protein recruitment and mRNA stability (Meyer et al., 2012). However, it is now known that m^{6}A modifications are also found in 5' UTRs of many mRNAs and thereby mediate translation initiation of uncapped mRNAs, independent of the eIF4F complex (Meyer et al., 2015; S. F. Mitchell & Parker, 2015; Niu et al., 2013). In addition, it has been shown that eIF3 can bind directly to m^{6}A modifications in the 5' UTR, thereby recruiting the 43S complex for translation initiation (Meyer et al., 2015).

1.1.3.4 eIF4E-independent cap-recognition

It was shown that under cellular stress conditions, in the early developmental phase and during cell cycle progression, translation of certain mRNAs required for these processes is ensured despite eIF4E inactivation (Gingras, Raught, & Sonenberg, 1999). A possible underlying mechanism was later described for the mRNA of the cell cycle regulator *JUN*,

whose 5' UTR harbours an inhibitory RNA element that blocks eIF4E recruitment (A. S. Lee, Kranzusch, Doudna, & Cate, 2016). The eIF3 complex is thought to make specific contacts to the cap via its cap-binding subunit eIF3D and these interactions are essential for the assembly of initiation complexes on eIF3-specialised mRNAs (A. S. Lee, Kranzusch, & Cate, 2015). As in the case of m^6A-dependent translation, the eIF3 complex plays a crucial role in this alternative mechanism.

1.2 Colorectal cancer and underlying mechanisms of development

Colorectal cancer (CRC) is the second most common tumour disease in Germany, with about 80,000 new cases per year (Siegel, Desantis, & Jemal, 2014). The majority of CRCs develop from adenomas that arise from normal mucosa through monoclonal expansion, a process that takes years to decades. It is characterised by continuous growth, dedifferentiation of cell populations and increasing independence from external factors. In particular, a sequential accumulation of mutations is responsible for tumour development, which are assigned to different time points of tumour initiation and progression (**Figure 4**) (Vogelstein et al., 1988; Walther et al., 2009).

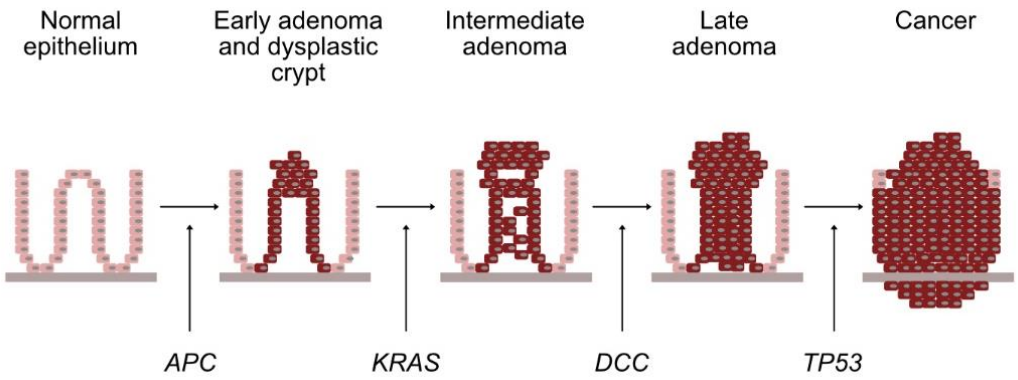

***Figure 4: Simplified adenoma–carcinoma sequence model in colorectal cancer**. Inactivation of APC initially leads to early adenoma and dysplastic crypt formation. KRAS mutations induce development of intermediate adenomas, which can develop into late adenomas upon, for example, DCC mutations. Loss of the tumour suppressor TP53 eventually results in formation of colorectal carcinomas that also invade underlying tissues and form metastases. Adapted and modified from (Walther et al., 2009).*

Inactivation of the *adenomatous polyposis coli* (*APC*) tumour suppressor gene usually comes first, followed by mutation of the protooncogene *KRAS*. This is often followed by

mutations in the *deleted in colorectal cancer* (DCC) tumour suppressor gene, and eventually the loss of the tumour suppressor *TP53*. More than 95 % of all CRCs harbour a mutation in the Wnt signaling pathway and in 80 % of cases these are located in the *APC* gene (Cancer Genome Atlas, 2012). The Wnt signalling pathway is a complex network of interacting proteins and plays a central role in embryonic development, cell cycle regulation, inflammation and tumourigenesis (Tai et al., 2015). The canonical Wnt/β-catenin pathway is characterised by the binding of Wnt to the LRP5/6 receptor complex (**Figure 5**). In the absence of the Wnt ligand, cytoplasmic β-catenin is phosphorylated by a complex of glycogen synthase kinase 3β (GSK-3β), casein kinase Iα (CKIα), Axin and APC. Subsequently, APC mediates the ubiquitin-mediated proteasomal degradation of phosphorylated β-catenin, keeping cytoplasmic β-catenin levels low and defining APC's role as a tumour suppressor. The presence of Wnt and its binding to the LRP5/6 receptor complex leads to activation of the pathway and recruitment of the cytosolic *Dishevelled* protein, which forms a complex with GSK-3β. This leads to disruption of the Axin/GSK-3β/APC complex, inhibition of β-catenin degradation and its accumulation in the cytoplasm. β-catenin translocates to the nucleus and, together with the transcription factor complex T cell factor/lymph enhancer factor 1 (TCF/LEF1), induces activation of Wnt target genes (H. Zhao et al., 2022). Loss of *APC* during colorectal tumourigenesis leads to deregulated β-catenin activity and overexpression of Wnt target genes, including *MYC* (He et al., 1998), *CCND1* (Shtutman et al., 1999), *JUN* (Mann et al., 1999), *Tcf-1* (Roose et al., 1999), *LEF1* (Hovanes et al., 2001), *VEGF* (X. Zhang, Gaspard, & Chung, 2001) and *AXIN2* (Jho et al., 2002), resulting in stimulation of cell proliferation and inhibition of differentiation. Interestingly, in a CRC model, the loss of *MYC* counteracted *APC* deficiency and highlights the tumourigenic role of *MYC* in the context of *APC* loss (Sansom et al., 2007). In addition, 5 – 10 % of all CRCs exhibit high-copy amplification of the *MYC* gene and moderate increases in copy number and *MYC* mRNA expression are present in more than 30 % (Camps et al., 2009; Leary et al., 2008). Overall, MYC is one of the essential factors in CRC development and its physiological role is described in more detail in the following sections.

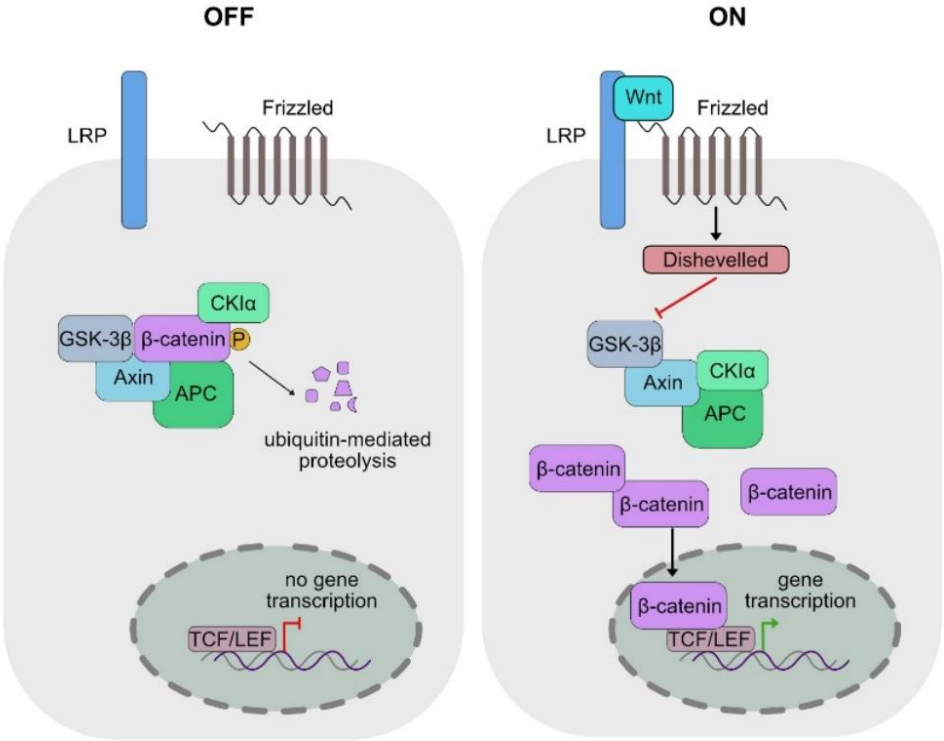

***Figure 5: Canonical Wnt signalling pathway**. In the absence of Wnt ligand ('OFF'), cytoplasmic β-catenin is phosphorylated by a complex of GSK-3β, CKIα, Axin and APC. Subsequently, APC mediates the ubiquitin-mediated proteasomal degradation of phosphorylated β-catenin. The presence of Wnt and its binding to the LRP5/6 receptor complex leads to activation of the pathway and recruitment of the cytosolic Dishevelled protein, which forms a complex with GSK-3β. This leads to disruption of the Axin/GSK 3β/APC complex, inhibition of β-catenin degradation and its accumulation in the cytoplasm. β-catenin translocates to the nucleus and, together with TCF/LEF1, induces transcription of Wnt target genes. Adapted from (H. Zhao et al., 2022).*

1.3 The oncoprotein MYC

The proto-oncogene *MYC* belongs to the MYC family of transcription factors which also includes *MYCN* and *MYCL*. All three genes of the *MYC* family encode nuclear phosphoproteins that share similar biological functions and affect various cellular functions including cell cycle progression, signal transduction, mRNA translation, metabolism, transcription and DNA repair (H. Chen, Liu, & Qing, 2018). Furthermore, deregulated expression of all *MYC* genes has been implicated in the development of a wide range of cancers, highlighting the need of understanding how these proteins are regulated (Dhanasekaran et al., 2022). In this work, MYC will be the primary focus as it appears to play the largest role in the development of cancer.

1.3.1 Models of MYC function

In general, MYC is considered a basic-region/helix–loop–helix/leucine-zipper (BR/HLH/LZ) domain transcription factor that interacts with its partner protein MAX to bind E-box sequences in promoter regions thereby regulating expression of virtually all active promoters (Adhikary & Eilers, 2005). When bound to DNA, the MYC/MAX heterodimer interacts with a plenty of other factors with diverse functions, like chromatin remodelers, demethylases, and other transcription factors (Hann, 2014). In principal, MYC can regulate genes transcribed by RNA polymerase (RNAP) I, II and III, as well as different RNA species including mRNA, long non-coding RNAs, tRNAs and microRNAs (Gomez-Roman, Grandori, Eisenman, & White, 2003; Grandori et al., 2005). Interestingly, genes transcribed by RNAP I and III are generally positively regulated by MYC occupancy (activation of transcription), whereas RNAP II transcribed target genes can either be positively or negatively be regulated by MYC (Sabo et al., 2014). However, it is still not completely clear how MYC functions in the cell and different models are existing. Although all active genes are bound by MYC, only a small subset responds to changes in MYC levels (Kress, Sabo, & Amati, 2015; Sabo et al., 2014; Walz et al., 2014; Yustein et al., 2010). This ‘specific-gene regulation model’ therefore suggests that MYC does not affect steady-state mRNA level of the downstream gene (Kress et al., 2015). Besides that, the ‘global gene activation model’ is based on the finding that MYC binds to all promoters of genes which are also bound by RNAP II (C. Y. Lin et al., 2012; Nie et al., 2012). This so-called ‘global amplifier’ model of MYC function suggests that MYC enhances the transcription rate of RNAP II, postulating this as the central oncogenic function of MYC. A third model is based on the fact that MYC’s affinity towards specific promoters differs although it is bound to virtually all open promoters (Baluapuri, Wolf, & Eilers, 2020). This ‘gene-specific affinity’ model differentiates between high and low affinity targets. At physiological levels of MYC, high-affinity promoters are already saturated, whereas oncogenic MYC levels are required for binding to low affinity promoters (Staller et al., 2001). This model further argues that factors interacting with the MYC/MAX heterodimer are relevant for the binding to low affinity targets at oncogenic MYC levels (Guo et al., 2014; Lorenzin et al., 2016).

1.3.2 Regulation of MYC

Given its universal role in cellular function and fate, proper levels of MYC are crucial for maintaining cellular homeostasis. Under physiological conditions, *MYC* expression is tightly controlled at every possible level of synthesis and degradation, like chromatin modification and remodeling, transcription, translation, as well as mRNA and protein degradation (Levens, 2013). It has been shown that even small differences in MYC protein levels can impact the proliferative behavior of normal cells (Shichiri, Hanson, & Sedivy, 1993), and multiple studies have shown that deregulated *MYC* expression is essential for both tumour initiation and progression in most types of cancers (Levens, 2013; Madden, de Araujo, Gerhardt, Fairlie, & Mason, 2021). In line with this, inhibiting *MYC* expression in already established tumours led to their regression, suggesting a general MYC-addiction of these cancer cells (Jain et al., 2002; Krenz et al., 2021; Weinstein, 2002). Elevated MYC levels were furthermore associated with genomic instability, accelerated cell cycle progression, angiogenesis and metastasis. In contrast, high MYC levels can also induce apoptosis, a fail-safe mechanism used by cells to avoid oncogenic transformation (Muthalagu et al., 2014). Generally, overexpression of the oncoprotein can be driven by different mechanisms at DNA, RNA and protein level. Genetic events leading to increased *MYC* gene expression include gene amplification and chromosomal translocations, especially occurring in Burkitt's lymphomas (Beroukhim et al., 2010; Dalla-Favera et al., 1982). However, high MYC levels in tumours mainly result from the loss or alteration of regulatory mechanisms concerning *MYC* mRNA and protein production.

1.3.2.1 Transcriptional regulation of MYC

Physiologically, *MYC* is an inducible gene, and its expression is regulated by specific growth signals in a cell-cycle-dependent manner. As 'immediate early gene', *MYC* is rapidly activated up to 40-fold within one to three hours upon stimulation (Kelly, Cochran, Stiles, & Leder, 1983). Principally, transcription of *MYC* can be initiated from four promoters (P0, P1, P2, P3) and the *MYC* mRNA contains three exons (**Figure 6**). Most of the transcripts derive from the weak P1 and the stronger P2 promoter, located in the 5' region of exon one (Levens, 2013). Several signaling pathways have been attributed a role in regulating *MYC* expression whose deregulation itself contributes to the development of certain tumours, e.g. Wnt/β-catenin, RAS/RAF/MAPK, JAK/STAT, TGFβ

and NFκB pathways (Dhanasekaran et al., 2022; Vervoorts, Luscher-Firzlaff, & Luscher, 2006). Furthermore, so-called super-enhancer (SE) sequences were detected in the surrounding of the *MYC* gene in various cancer cells, which further potentiate the transcription of the oncogene (Hnisz et al., 2013). In general, SEs are large clusters of transcriptional enhancers that are highly transcribed and bound by transcription factors, chromatin remodellers, and cofactors (Hnisz et al., 2013).

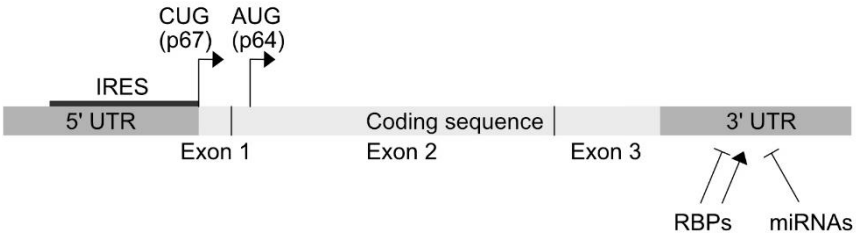

***Figure 6: Structure of the MYC mRNA**. The MYC mRNA contains three exons. A non-canonical CUG start codon is located in exon 1 and its use leads to synthesis of MYC p67. Translation usually initiates from the AUG start codon located in exon 2, leading to production of MYC p64. The MYC 5' UTR has a complex structure and an IRES element has been identified in this region (bold black line) which serves to maintain MYC synthesis under conditions when canonical, cap-dependent translation is inhibited. The 3' UTR is target of various RBPs and miRNAs, contributing to the regulation of MYC translation (Source: UCSC genome browser, (Kent et al., 2002)).*

1.3.2.2 Post-transcriptional regulation of MYC

In addition to transcriptional regulation, *MYC* expression is also controlled at the post-transcriptional and translational level. Post-transcriptional regulation of gene expression can occur at multiple levels including mRNA processing, modifications and export to the cytoplasm and numerous RNA-binding proteins (RBPs) and microRNAs (miRNAs) are involved in this process (Corbett, 2018). Once the mRNA has been successfully transported into the cytoplasm, and been translated, the MYC protein is also regulated in its function and stability by a series of post-translational modifications, such as phosphorylation, acetylation, glycosylation and ubiquitylation (Hann, 2006; Vervoorts et al., 2006). Under physiological conditions, MYC is highly unstable and subject to constant degradation by the ubiquitin/proteasome system (UPS) (Farrell & Sears, 2014). Various MYC-targeting ubiquitin ligases exist that mark MYC for proteasomal degradation, such as FBXW7 (Welcker et al., 2004; Yada et al., 2004). In CRC, mutations

are often present in the *FBXW7* gene, which ultimately leads to the stabilisation of MYC (Rajagopalan et al., 2004).

Besides that, *MYC* is also controlled at the translational level. The *MYC* mRNA contains long 5' and 3' UTRs which are targeted by various RBPs or miRNAs and thus regulate *MYC* expression under certain conditions (**Figure 6**) (Cannell et al., 2010; H. H. Kim et al., 2009; Lal et al., 2009; Mihailovich et al., 2015). For example, glutamine deprivation inhibits *MYC* translation via its 3' UTR in CRC cells, thereby coupling *MYC* translation to the cellular metabolic status (Dejure et al., 2017). Furthermore, an IRES element has been identified in the *MYC* 5' UTR, which plays an important role in *MYC* translation in cancer and will be described in more detail in the following sections (Nanbru et al., 1997; Paulin et al., 1996; Stoneley et al., 1998).

1.3.3 Alternative translation of MYC

As mentioned before, *MYC* is transcribed from four alternative promoters, with mRNA translation of P0, P1, and P2 transcripts being initiated from at least two different start codons (CUG and AUG) (Hann, King, Bentley, Anderson, & Eisenman, 1988). This results in two proteins of different lengths (MYC p67 and p64) which play distinct roles in the control of cell proliferation (Blackwood et al., 1994). As already mentioned in section 1.1.3, the translation of selected mRNAs under stress conditions or high levels of P-eIF2α can take place via an eIF2-independent mechanism (Koromilas, 2015). In this context, IRES-mediated translation plays a major role (Allam & Ali, 2010; Sonenberg & Hinnebusch, 2009; Subkhankulova, Mitchell, & Willis, 2001). In the *MYC* P0 and P2 mRNA, an IRES element has been detected which is located between nucleotides 811 and 1077 of the P0 transcript and mediates cap-independent translation of MYC p67 and p64 (Nanbru et al., 1997; Stoneley et al., 1998). In contrast to viral IRESs, cellular IRES elements cannot be classified according to their structure or sequence, as this differs greatly between mRNAs (Godet et al., 2019). The structure of the *MYC* 5' UTR or IRES was therefore modelled using an algorithm and two domains with secondary structure were identified (**Figure 7**) (Le Quesne et al., 2001). Domain 1 represents the larger and more complex structure, with two overlapping pseudo knots. Domain 2 was predicted to contain two helical segments separated by a large internal loop. It is assumed that domain 1 contains a ribosome landing patch from where the scanning process is initiated in a cap-independent manner.

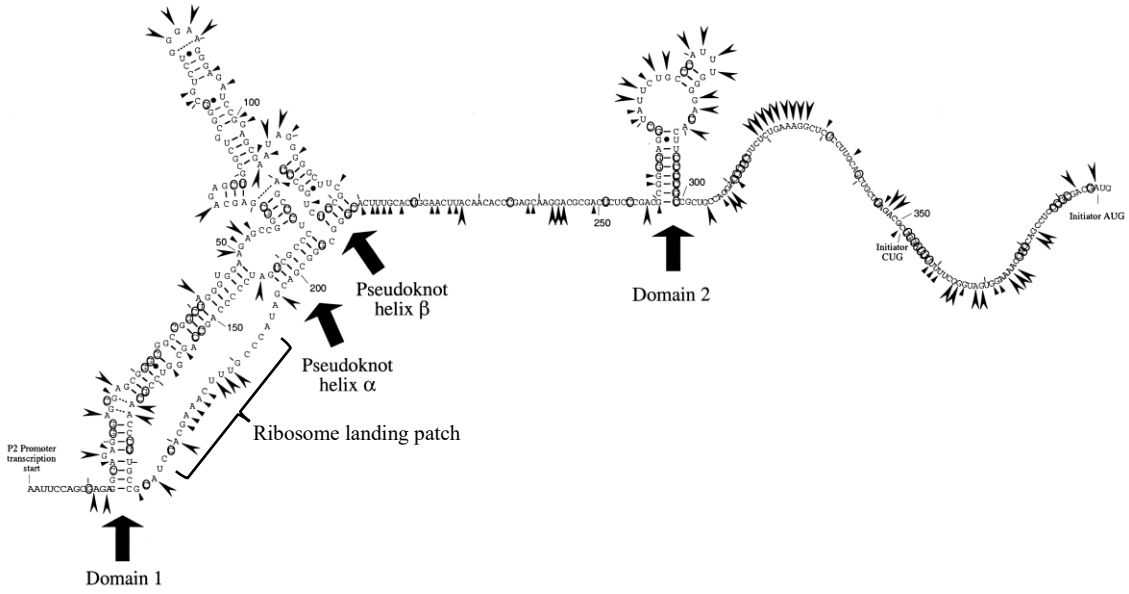

Figure 7: Secondary structure of the human MYC IRES*. Domain 1 is the larger and more complex and is predicted to contain two overlapping pseudoknots (helix α and helix β, respectively). Domain 2 contains only two helical segments, separated by a large internal loop. The ribosome is predicted to enter at some point between nucleotides 177 and 194 and then scans to the initiation codon, unwinding structural elements, including the double pseudoknot and domain 2. Adapted and modified from (Le Quesne, Stoneley, Fraser, & Willis, 2001) and reprinted with permission.*

The functions of the *MYC* IRES are diverse. First of all, it is active in almost all tissues during early embryonic development, whereby the activity is only tissue-specific as development progresses and is finally silenced in adult tissues (Creancier, Mercier, Prats, & Morello, 2001). Furthermore, the *MYC* IRES is thought to play a role during MYC-induced apoptosis (Stoneley et al., 2000). On the other hand it is also able to ensure translation of *MYC* and thus the survival of multiple myeloma (MM) cells through interaction with the Y-box binding protein 1 (YBX1) identified as ITAF (Bommert et al., 2013; Spriggs, Bushell, Mitchell, & Willis, 2005). In addition to its dependence on specific ITAFs, the *MYC* IRES has also been shown to interact with canonical translation initiation factors such as eIF4A, eIF4G as well as eIF3 (Spriggs et al., 2009). This suggests additional regulatory mechanisms that regulate the switch from canonical to IRES-mediated translation of *MYC*. Besides that, the modelability of IRES activity was demonstrated, whereby a C > T nucleotide transition within the structure significantly increased the internal initiation of *MYC* translation in MM (Chappell et al., 2000). In these tumours, the *MYC* IRES seems to play a particularly important role, but the transferability to other tumour systems has not yet been investigated much.

1.4 Post-transcriptional and translational regulation in colorectal cancer

In recent years, oncogenic cellular alterations have been linked to the translational machinery for many tumour entities (Chu et al., 2016; H. J. Kim, 2019; Truitt & Ruggero, 2016). In CRC, a generally increased rate of mRNA translation has been shown, so that intervention in protein synthesis represents a promising therapeutic approach in this type of cancer (Faller et al., 2015; S. Schmidt et al., 2019). As mentioned earlier, 95 % of all CRCs show mutations in the Wnt signalling pathway, with 80 % of these found in the *APC* gene (Fearon, 2011; Fearon & Vogelstein, 1990). The resulting activation of *MYC* leads to transcriptional activation of RNAP I - III and concomitant increased ribosome biogenesis and protein synthesis (Campbell & White, 2014; Gomez-Roman et al., 2003; Grandori et al., 2005; Oskarsson & Trumpp, 2005; van Riggelen, Yetil, & Felsher, 2010). In line with this, several components of the ribosome such as ribosomal proteins and RNAs were shown to be deregulated in CRC (S. Schmidt, Denk, & Wiegering, 2020). Besides that, many other genes are regulated by increased *MYC* expression, which, for example, regulate the activity of stress-associated eIF2α kinases and thereby the eIF2α/eIF2B complex (S. Schmidt et al., 2019). This mechanism is thought to be of great importance in regulating the stress response in CRC to ensure tumour cell survival. Another rate-limiting regulator of translation along the APC-MYC axis is eIF4E. Overexpression is associated with early adenoma stage and correlates with later stages and metastasis (Berkel, Turbat-Herrera, Shi, & de Benedetti, 2001; Gao et al., 2016; Xu et al., 2016). In addition to MYC, the RAS/RAF/MAPK and PI3K/AKT pathways, master regulators of protein synthesis, are also frequently deregulated in CRC (Fearon, 2011; Roux & Topisirovic, 2018). In this context, increased levels of phosphorylated mTOR (P-mTOR), phosphorylated S6K (P-S6K) as well as P-4EBP have been associated with metastasis and transition to invasive carcinoma (Y. Chen et al., 2017; Lu et al., 2015; Miao et al., 2017). In addition, loss of *APC* has also been directly linked to increased mTOR signalling (Fujishita, Aoki, Lane, Aoki, & Taketo, 2008). Furthermore, deregulation of translation elongation factors has been associated with enhanced translation rates in CRC (S. Schmidt et al., 2020). The examples above show that there is a connection between the genetic alterations during the adenoma-carcinoma sequence and the deregulation of the translational machinery.

In addition to translation and the factors involved, RBPs are generally considered to play a significant role in the post-transcriptional regulation of CRC (Garcia-Cardenas et al., 2019). In general, RBPs are involved in almost every aspect of RNA metabolism, such

as capping, splicing, polyadenylation, nucleoplasmic transport, stability, translation and degradation. Altered RBP expression or activity can therefore lead to impaired mRNA affinity or subcellular localisation and lead to an imbalance in cellular homeostasis (Iadevaia & Gerber, 2015). Just to mention few, aberrant or overexpression of *LIN28* and *Musashi* (MSI) were correlated with reduced patient survival and increased metastatic risk, respectively (Garcia-Cardenas et al., 2019). Furthermore, low expression and downregulation of *Quaking* (QKI) and *Tristetraprolin* (TTP) is associated with poorer prognosis and tumour aggressiveness, respectively. RBPs thus represent critical modulators in carcinogenesis and possible therapeutic intervention points.

1.5 Therapeutic approaches to target MYC (translation)

Given MYC's universal role in basically every cellular process and its involvement in tumourigenesis, the need for MYC inhibitors or strategies to target its oncogenic function is constantly increasing (Wolf & Eilers, 2020). There were several attempts to target MYC directly, specifically compounds that inhibit the ability of MYC to heterodimerize with MAX were tested (**Figure 8**). One of them is 10058-F4, which displaces MYC from chromatin and delays tumour growth and prolongs survival in a transgenic model of neuroblastoma (Zirath et al., 2013). Related to this, MAX stabilizers were developed that displace MYC from MYC/MAX heterodimers by stabilizing MAX homodimers and led to a delay of *MYC*-driven tumours *in vivo* (Jiang et al., 2009; Struntz et al., 2019). Furthermore, overexpression of a dominant-negative allele of *MYC* termed *Omomyc* led to tumour regression and prolonged survival in mouse models of different types of cancers (Annibali et al., 2014; Jung et al., 2017; Soucek, Nasi, & Evan, 2004; Soucek et al., 2008; Soucek et al., 2013). Therefore, another strategy is to deliver OmoMYC directly as a therapeutic peptide (Beaulieu et al., 2019). However, direct inhibition of MYC proteins is still challenging, thus, a lot of effort has been put into the identification of compounds that decrease *MYC* expression indirectly. Numerous strategies have been developed to inhibit *MYC* mRNA stability, *MYC* transcription, or *MYC* translation (**Figure 8**) (Wolf & Eilers, 2020).

MYC proteins are generally highly unstable and continuously turned over by the UPS and many individual MYC-associated ubiquitin ligases have been identified (Farrell & Sears, 2014). As antagonists of ubiquitin ligases, overexpression of deubiquitinating enzymes can lead to the stabilisation of MYC proteins. These include, among others,

USP7, USP22, USP28, USP36 and USP37 (Diefenbacher et al., 2015; Diefenbacher et al., 2014; Huber et al., 2016; Popov et al., 2007; Schülein-Völk et al., 2014; Welcker et al., 2004). Therefore, specific inhibition of individual deubiquitinating enzymes is a promising strategy to reduce cellular MYC levels (Turnbull et al., 2017).

Besides targeting MYC stability, inhibitors of *MYC* transcription have been studied extensively. One example is thieno-triazolo-1,4-diazepine JQ1, which was initially developed as an inhibitor of the bromodomain and extraterminal (BET) subfamily of human bromodomain proteins (Filippakopoulos et al., 2010). Although only low specificity for MYC, JQ1 exhibits antitumour activity by inhibiting MYC function. Multiple BET inhibitors are currently tested for their safety and potency as anticancer drugs (Stathis & Bertoni, 2018). In addition to BET inhibitors, inhibition of transcription-associated cyclin-dependent kinases (CDKs) has been tested as anticancer therapy due to their potential to reduce MYC expression (Chipumuro et al., 2014; Christensen et al., 2014; Kwiatkowski et al., 2014; Walsby, Lazenby, Pepper, & Burnett, 2011).

Another important field of research is the inhibition of cap- and IRES-dependent translation of *MYC*. In CRC, the mTOR pathway, which plays a crucial role in regulating cap-dependent translation, is a reasonable therapeutic target (Y.-J. Zhang et al., 2009). The widely used dual PI3K/mTOR inhibitor NVP-BEZ235 (hereafter referred to as BEZ235) reduced viability and delayed tumour growth of certain colon tumour models (Foley et al., 2017; Roper et al., 2011). However, BEZ235 failed to reduce MYC protein expression which could be counteracted by the natural compound silvestrol, an eIF4A helicase inhibitor that also led to reduced intestinal and lymphoid tumour growth (Bordeleau et al., 2008; Wiegering et al., 2015). Two other eIF4A inhibitors, elatol and FL3, successfully delayed tumour growth in different tumour models (W. L. Chen, Pan, Kinghorn, Swanson, & Burdette, 2016; Z. H. Chen et al., 2019; Peters et al., 2018; Thuaud et al., 2009; S. Wang, Darini, Desaubry, & Koromilas, 2016). Furthermore, IRES-mediated translation of *MYC* plays an essential role, especially in MM, and IRES inhibitors were tested in different studies. On the one hand, the cardiac glycosides (CGs) cymarin and somalin led to reduced *MYC* IRES activity in HEK293T cells (Didiot et al., 2013). Consequently, MYC protein expression and the viability of MYC-dependent ovarian cancer cell lines were significantly reduced. On the other hand, *MYC* IRES activity could be reduced by inhibiting the interaction with the ITAF hnRNP A1 (Holmes et al., 2016; Shi et al., 2022). In MM and glioblastoma (GB) cells, J007-IRES reduced

MYC protein expression and slowed proliferation. Therefore, targeting *MYC* translation represents a promising therapeutic approach in CRC treatment.

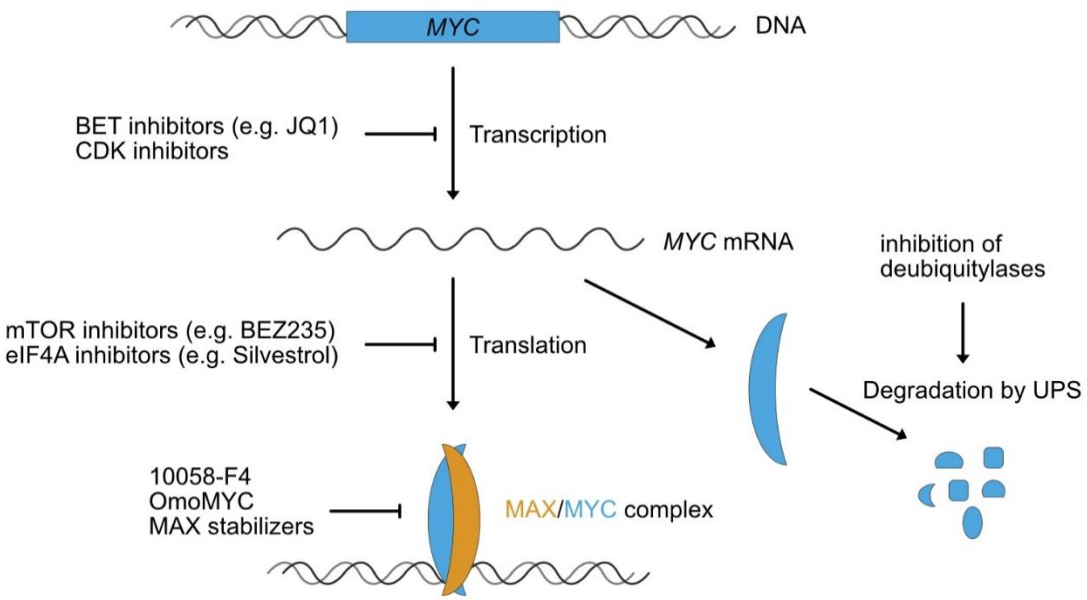

***Figure 8: Summary of strategies targeting MYC expression and function at multiple levels**. Shown are selected strategies to target MYC transcription, translation, its interaction with MAX and interference with the UPS to interfere with MYC stability. Adapted from (Wolf & Eilers, 2020).*

1.6 Aim of the thesis

CRC constitutes a very serious disease and the identification of new therapeutic targets is of great importance. In particular, targeting the deregulated expression of *MYC* in the course of the adenoma-carcinoma sequence is considered an important approach. In this work, on the one hand, we will investigate the role of the alternative, IRES-dependent translation of *MYC* in CRC and whether already published inhibitors of this structure could have a therapeutic benefit in CRC. Secondly, factors will be identified that contribute to the (alternative) translation of *MYC* in CRC and thus could open a new therapeutic window.

2 Materials

2.1 Cell lines & bacteria strains

2.1.1 Human cell lines

HEK293T	Human embryonic kidney cell line (ATCC)
DLD1	Colorectal adenocarcinoma cell line (ATCC)
LS174T	Colorectal adenocarcinoma cell line (ATCC)

2.1.2 Murine cell lines

MTO140	Tauriello *et al.* (Tauriello et al., 2018)

2.1.3 Competent bacteria

XL1 blue	*Escherichia coli*, genotype F-Φ80lacZΔM15 Δ lacZYA-argF) U169 recA1 endA1 hsdR17 (rK-, mK+) phoA supE44 λ-thi-1 gyrA96 relA1

2.2 Culture media & supplements

2.2.1 Cell culture media (cell lines)

All cell culture media and supplements were stored at 4 °C until use. Fetal bovine serum (FBS, Capricorn Scientific GmbH) was heat-inactivated at 56 °C for 30 min before application to culture media.

RPMI-1640, with L-Glutamine *10 % FBS, 1 % penicillin/ streptomycin (Sigma)*	Thermo Fisher Scientific
DMEM, high glucose, pyruvate *10 % FBS, 1 % penicillin/ streptomycin (Sigma)*	Capricorn Scientific GmbH

DMEM, high glucose, pyruvate — Capricorn Scientific GmbH
2 % FBS, 1 % penicillin/ streptomycin (Sigma)

OptiMEM reduced serum medium — Thermo Fisher Scientific

Freezing medium
70 % RPMI/DMEM (10 % FBS, 1 % penicillin/streptomycin), additional 20 % FBS, 10 % DMSO (Sigma)

2.2.2 Cell culture media (organoids)

Advanced DMEM F12 (ADF) 'base' — Thermo Fisher Scientific
1 % Glutamax, 1 % 1 M HEPES, 1 % pen/strep

ENR medium (working medium for murine organoids)
37 ml ADF 'base', 1 ml B27, 500 µl N2, 2.5 µl EGF (50 ng/ml), 1 ml Noggin condition medium, 5 ml RSPO condition medium; stored in fridge for > 2 weeks

Freezing medium
40 % ADF 'base' (1 % Glutamax, 1 % 1 M HEPES, 1 % pen/strep), 50 % FBS, 10 % DMSO (Sigma)

2.2.3 Supplements (general)

All supplements were obtained from Sigma, unless otherwise stated.

	Stock conc.	**Final conc.**
Polybrene (Hexadimethrine bromide)	4 mg/ml in H_2O (sterile filtered)	8 µg/ml
Cycloheximide	100 mg/ml in 100 % EtOH, freshly diluted before use	50 µg/ml
Doxycyclin	1 mg/ml in 100 % EtOH, stored at -20 °C	0.5 – 1 µg/ml
Puromycin (Invivogen)	10 mg/ml	2 - 4 µg/ml

2.2.4 Supplements (organoid culture)

HEPES 1M	Biochrom
Glutamax	ThermoFisherScientific
TrypLE Express Enzyme	ThermoFisherScientific

N2	Invitrogen
B27	Invitrogen
Recombinant murine EGF	Peprotech
R-spondin (RSPO)	self-made conditioned medium (L cells from Sansom lab (Beatson/Glasgow)
Noggin	self-made conditioned medium HEK293 cells from Stieneke lab, (Würzburg)
Nicotinamide	Sigma, 1 M in 1 x PBS
Chir99021	Sigma
Cultrex	RGF Basement Membrane Extract,Type 2, Select (Biotechne)
TrypLE Express Enzyme	Thermo Fisher Scientific

2.2.5 Cell transfection reagents

Lipofectamine® RNAiMAX Transfection Reagent	Thermo Fisher Scientific
Lipofectamine® 2000 Transfection Reagent	Thermo Fisher Scientific
Polyethyleneimine (PEI)	Sigma Aldrich

2.3 Bacteria culture media & supplements

2.3.1 Culture media

LB medium	10 % (w/v) bacto tryptone (Roth), 0.5 % (w/v) yeast extract (Roth), 1 % (w/v) NaCl (Roth)
LB agar	LB medium with 1.2 % (w/v) agar-agar (Roth); heated in a microwave, cooled down to 50 °C and addition of antibiotics, poured into 10 cm dishes

2.3.2 Antibiotics

Ampicillin and carbenicillin were obtained from Roth in form of powder, diluted to 100 mg/ml in H_2O and sterile filtered before use. Final concentration in media/LB plate was 100 µg/ml.

2.4 Chemicals, buffers & solutions

All buffers and solution were purchased from Sigma and Roth, unless otherwise indicated.

ROTIPHORESE®Gel 30	*ready-to-use*, acrylamide:bisacrylamide (37.5:1)
Ammonium persulfate (10 %)	5 g ammonium persulfate (APS) dissolved in 50 ml H_2O; stored at 4 °C
AnnexinV Binding Buffer	10 mM HEPES (pH 7.4), 140 mM NaCl, 2.5 mM $CaCl_2$
AnnexinV/Pacific blue	Life Sciences
Blotting Buffer (wet transfer) (5 X)	75 g Tris, 282.25 g Glycine; diluted in 5 L H_2O; diluted to 1 X with H_2O and 10 % methanol added before use
Bovine serum albumine (BSA)	diluted in RIPA buffer as Bradford standard; diluted in TBS-T (5 %) as blocking solution for PVDF membrane
Bradford Reagent	ROTI®Quant (Roth)
Chloroform	Applichem
Crystal Violet Solution	0.1 % (w/v) crystal violet in H_2O / 20% (v/v) EtOH
10 X Cut Smart Buffer	NEB

Deoxynucleotide triphosphate (dNTP) (100 nM stock)	50 µl each dNTP, mixed with 300 µl H_2O to final concentration of 10 mM; aliquoted and stored at -20 °C
DNAzol®	Invitrogen
DNA loading buffer (6 X)	NEB
ECL+ Western blot system	Amersham
EDTA (0.5 M)	93.05 g EDTA dissolved in 400 ml H_2O; while stirring, 9 – 10 g NaOH pellets were added; pH adjusted to 8.0 with 10 N NaOH and filled up to 1 L with H_2O
Ethidiumbromide solution (10 mg/ml)	1 g dissolved in 100 ml H_2O
Glutamax	Thermo Fisher Scientific
GlycoBlue™	Invitrogen
HEPES 1 M	Biochrom
Laemmli buffer (6 X) (Laemmli, 1970)	1.2 g SDS pellet, 6 mg bromphenol blue, 4.7 ml 100 % glycerol, 1.2 ml 0.5 M Tris (pH 6.8), 2.1 ml H_2O; heated up, then 0.93 g DTT dissolved; aliquoted and stored at -20 °C
5 X M-MLV reaction buffer	Promega (250mM Tris-HCl (pH 8.3 at 25°C), 375mM KCl, 15mM MgCl2, 50mM DTT)
Phosphate-buffered saline (PBS, 1 X)	137 mM NaCl, 2.7 mM KCl, 10.1 mM Na_2HPO_4, 1.76 mM KH_2PO_4; autoclaved after preparation
peqGOLD Trifast™	VWR

Phosphatase inhibitor	Phosphatase inhibitor cocktail 2 and 3 (Sigma); aliquoted and stored at -20 °C, used 1:100 each
Polyethylene glycol (PEG) 8000	Roth; 80 g PEG dissolved in 80 ml H_2O + 20 ml 10 X PBS + 14 g NaCl, pH adjusted to 7.0 – 7.2 and filled up to 200 ml with H_2O; sterile filtered (0.2 µm) solution was stored at 4 °C
Polyethyleneimine (PEI)	450 µl PEI (10 %), 150 µl HCl (2 N), 49.5 ml H_2O
Polysome profile lysis buffer	100mM KCl, 20mM Tris (pH 7.5), 5mM MgCl2, 1mM DTT, 0,5% NP40
PowerUp™ SYBR® Green Master Mix	Applied Biosystems
Propidiumiodide stock solution	Fluka, 1 mg/ml in 1 X PBS
Protease inhibitor	Protease inhibitor cocktail; aliquoted and stored at -20 °C, used 1:1000
Random hexanucleotide primers (RP)	Roche; 2 µg/ml stock
Ready Mix™ Taq PCR reaction mix	Sigma-Aldrich
RIPA lysis buffer	150 mM NaCl, 1 % NP-40, 0.1 % sodium deoxycholate, 0.1 % SDS, 50 mM Tris, pH 8.0; protease and phosphatase inhibitors added freshly before use
RNase A (10 mg/ml)	Roche; 100 mg RNase A, 27 µl sodium acetate (3 M, pH 5.2), 9 ml H_2O; aliquoted into 450 µl; boiled 30 min at 100 °C, 50 µl Tris-HCl (1 M, pH 7.4) added to each aliquot; stored at -20 °C

ROTI®Aqua-P/C/I	Phenol-Chloroform-Isoamylalcohol (25:24:1), saturated with 10 mM Tris, pH = 8.0, 1 mM EDTA; *ready-to-use*
SDS separating gel	for 2 (10 %) gels: 5.1 ml ROTIPHORESE®Gel 30, 3.75 ml Tris (1.5 M, pH 8.8), 6 ml H_2O, 150 µl 10 % SDS, 150 µl 10 % APS, 15 µl TEMED
SDS stacking gel	for 2 gels: 650 µl ROTIPHORESE®Gel 30, 1.2 ml Tris (0.5 M, pH 6.8), 3 ml H_2O, 50 µl 10 % SDS, 50 µl 10 % APS, 5 µl TEMED
SDS running buffer (10 X)	25 mM Tris Base, 250 mM Glycine, 0.1 % SDS
Sodium acetate (3 M)	123.04 g Na-Acetate (anhydrous) or 204.05 g Na-Acetate-3H_2O dissolved in 400 ml H_2O; pH adjusted to 5.2 with glacial acetic acid and filled up to 500 ml with H_2O
Sodium Dodecyl Sulfate (SDS, 10 %)	100 g SDS pellets dissolved in 800 ml H_2O, filled up to 1 L
TAE (50 X)	2 M Tris (pH 8), 5.7 % acetic acid, 50 mM EDTA
TBS (20 X)	500 mM Tris Base, 2.8 M NaCl, pH adjusted to 7.4 with concentrated HCl
TBS-T	1 X TBS, 0.2 % Tween-20
TE	10 mM Tris (pH = 7.4), 1 mM EDTA (pH = 8)
TEMED	99%, p.a.

Trans-Blot Blotting Buffer (semi-dry blotting)	BioRad
Trypsin-EDTA	0,25 % Trypsin, 5 mM EDTA, 22,3 mM Tris (pH 7,4), 125 mM NaCl

2.5 Standards, enzymes & kits

2.5.1 Ladders & loading dyes

DNA marker	Gene Ruler 1kb Plus DNA ladder	Invitrogen
Protein marker	PageRuler™ Prestained Protein Ladder	Fermentas
DNA Loading Dye	6 X Gel Loading Dye, purple	NEB

2.5.2 Enzymes

Calf-Intestinal alkaline phosphatase (CIP)	NEB
M-MLV Reverse transcriptase	Promega
Phusion Hot Start II High Fidelity DNA Polymerase	Thermo Scientific
RNase-free DNAse	Qiagen
PowerUp™ SYBR® Green Master Mix	Thermo Scientific
T4 DNA Ligase	NEB
T4 DNA Ligase	Thermo Scientific
RiboLock RNase Inhibitor	40 U/µl, Thermo Scientific
Q5® High-Fidelity DNA Polymerase	NEB

2.5.3 Restriction enzymes

BamHI	20,000 U/ml	NEB
BsmBI-v2	10,000 U/ml	NEB
EcoRI-HF	20,000 U/ml	NEB
PacI	10,000 U/ml	NEB
XhoI	20,000 U/ml	NEB

2.5.4 Kits

CellTiter-Glo® 2.0 Cell Viability Assay	Promega
Chemiluminescent Nucleic Acid Detection Module	Thermo Scientific
GeneJet Gel Extraction Kit	Thermo Scientific
MagSi-NGS^{PREP} Plus	magtivio
MEGAscript® Kit	Life Technologies
NEBNext Multiplex Oligos for Illumina (Dual Index Primer Set 1)	NEB
NEBNext Poly(A) mRNA Magnetic Isolation Module	NEB
NEBNext Ultra RNA Library Prep Kit for Illumina	NEB
Pierce™ Magnetic RNA-Protein Pull-Down Kit	Thermo Scientific
Pierce™ RNA 3' End Desthiobiotinylation Kit	Thermo Scientific
PureYield™ Plasmid Miniprep System	Promega
PureLink™ HiPure Plasmid Maxiprep Kit	Life Technologies
RNeasy® Mini Kit	Qiagen

2.5.5 Magnetic beads

MagSi-NGS^{PREP} Plus magnetic beads	magtivio

2.6 Plasmids & oligonucleotides

2.6.1 Plasmids

Empty vectors:

Name	**description**
pLT3-GEPIR	Tet-ON miR-E-based RNAi expression vector (Fellmann et al., 2013)
pGIPZΔEcoRI	miR-E-based RNAi expression vector with deletion of second EcoRI restriction site (openbiosystem)

Plasmids available in the department of Prof. M. Eilers:

Name	**description**
pInducer21 HA-MYC	expression vector with *MYC* coding sequence (CDS) and C-terminal HA-tag (Jaenicke et al., 2016)
pInducer21 HA-5'UTR-MYC	expression vector with 5'UTR, *MYC* CDS and C-terminal HA-tag (Dejure et al., 2017)
pInducer21 HA-MYC-3'UTR	expression vector with *MYC* CDS, 3'UTR and C-terminal HA-tag (Dejure et al., 2017)
pInducer21-5'UTR-MYC-HA-3'UTR	expression vector with 5'UTR, *MYC* CDS, 3'UTR and C-terminal HA-tag (Dejure et al., 2017)

pCW57.1-4EBP1_4xAla	expression vector with phospho-dead eIF4EBP1 mutant carrying four alanine substitutions (Thoreen et al., 2012)

Plasmids generated in this study:

pLT3-GEPIR-shEIF3D (mouse) #1 – 5	shRNA expression vector, tetracycline-inducible
pGIPZΔEco-shEIF3D (human) #1 - 5	shRNA expression vector, constitutive

Plasmids for lentivirus production:

psPax.2	2nd generation lentiviral packaging plasmid; Addgene (Naldini et al., 1996)
pMD2.G	VSV-G envelope expressing plasmid; Addgene (Naldini et al., 1996)

2.6.2 Oligonucleotides & primers

All oligos were obtained from Sigma, synthesised at 0.025 µM scale and purified by desalting (primers) or HPLC (sg/shRNAs). Oligos were diluted in H_2O to 100 µM stock solution and stored at -20 °C. Primer design was performed with the online-based tools offered by NCBI and Primer-X, according to standard requirements.

For: forward

Rev: reverse

2.6.2.1 Primers for PCR/cloning

#	name	Sequence 5' → 3'
1	SD_mirE_EcoRI_PCR_r	TTAGATGAATTCTAGCCCCTTGAAGTCCGAGGCAGTAGGCA
2	SD_mirE_XhoI_PCR_f	TACAATACTCGAGAAGGTATATTGCTGTTGACAGTGAGCG
3	SS_T3_MYC_IRES_for	AATTAACCCTCACTAAAGGGTAATTCCAGCGAGAGGCAGAGG
4	SS_MYC_IRES_CTG_rev1	TTTTCCACTACCCGAAAAAAATCCAGC

2.6.2.2 qRT-PCR primers

#	name	species	Sequence 5' → 3'
5	*B2M* for	human	GTGCTCGCGCTACTCTCTC
6	*B2M* rev	human	GTCAACTTCAATGTCGGAT
7	*MYC* for	human	CACCAGCAGCGACTCTGA
8	*MYC* rev	human	GATCCAGACTCTGACCTTTTGC
9	*EIF3D* for	human	CTGGAGGAGGGCAAATACCT
10	*EIF3D* rev	human	CTCGGTGGAAGGACAAACTC
11	*MYC-HA* for	human	AAGAGGACTTGTTGCGGAAA
12	*MYC-HA* rev	human	AGCGTAATCTGGAACATCGT
13	*Actin-beta* for	human	CCTCGCCTTTGCCGATCC
14	*Actin-beta* rev	human	GGATCTTCATGAGGTAGTCAGTC
15	*Luciferase* for	firefly	CCAGGGATTTCAGTCGATGT
16	*Luciferase* rev	firefly	AATCTCACGCAGGCAGTTCT

2.6.2.3 shRNA sequences

#	target gene	species	Sequence 5' → 3'
17	*EIF3D #1*	human	TGCTGTTGACAGTGAGCGATCGGAACATG TTGCAGTTCAATAGTGAAGCCACAGATGTA TTGAACTGCAACATGTTCCGACTGCCTACT GCCTCGGA
18	*EIF3D #2*	human	TGCTGTTGACAGTGAGCGCACCAAGATAA GAGGTACACAATAGTGAAGCCACAGATGT ATTGTGTACCTCTTATCTTGGTATGCCTACT GCCTCGGA
19	*EIF3D #3*	human	TGCTGTTGACAGTGAGCGCTGGGATCAGA AATCACAGAAATAGTGAAGCCACAGATGTA TTTCTGTGATTTCTGATCCCATTGCCTACTG CCTCGGA
20	*EIF3D #4*	human	TGCTGTTGACAGTGAGCGATCAGTTGATG AAGATGCGCTATAGTGAAGCCACAGATGTA TAGCGCATCTTCATCAACTGAGTGCCTAC TGCCTCGGA
21	*EIF3D #5*	human	TGCTGTTGACAGTGAGCGAGCCCTAGAAT ACTACGACAAATAGTGAAGCCACAGATGTA TTTGTCGTAGTATTCTAGGGCCTGCCTACT GCCTCGGA
22	*EIF3D #1*	mouse	TGCTGTTGACAGTGAGCGACAGGTTTTAG AAGATGGCGAATAGTGAAGCCACAGATGTA TTCGCCATCTTCTAAAACCTGCTGCCTACT GCCTCGGA
23	*EIF3D #2*	mouse	TGCTGTTGACAGTGAGCGAGAGGAACATG GTGCAGTTCAATAGTGAAGCCACAGATGTA TTGAACTGCACCATGTTCCTCCTGCCTACT GCCTCGGA

24	*EIF3D #3*	mouse	TGCTGTTGACAGTGAGCGCCCAGGACAAG AGGTACACAAATAGTGAAGCCACAGATGTA TTTGTGTACCTCTTGTCCTGGTTGCCTACT GCCTCGGA
25	*EIF3D #4*	mouse	TGCTGTTGACAGTGAGCGCCGCCACTGAA TTGAAGAACAATAGTGAAGCCACAGATGTA TTGTTCTTCAATTCAGTGGCGATGCCTACT GCCTCGGA
26	*EIF3D #5*	mouse	TGCTGTTGACAGTGAGCGATCAGCTGATG AAGATGCGCTATAGTGAAGCCACAGATGTA TAGCGCATCTTCATCAGCTGAGTGCCTACT GCCTCGGA
27	*Renilla Luciferase* #1	sea pansy	TGCTGTTGACAGTGAGCGTAGGAATTATAA TGCTTATCTATAGTGAAGCCACAGATGTATA GATAAGCATTATAATTCCTATGCCTACTGCC TCGGA
28	*Renilla Luciferase* #2	sea pansy	TGCTGTTGACAGTGAGCGCTTCGAAATGT CCGTTCGGTTATAGTGAAGCCACAGATGTA TAACCGAACGGACATTTCGAAGTGCCTACT GCCTCGGA
29	*Renilla Luciferase* #3	sea pansy	TGCTGTTGACAGTGAGCGTCACAGAATCG TCGTATGCAGATAGTGAAGCCACAGATGTA TCTGCATACGACGATTCTGTGATGCCTACT GCCTCGGA
30	*GFP* #1	Aequorea victoria	TGCTGTTGACAGTGAGCGCGGCATGGATG AACTATACAAATAGTGAAGCCACAGATGTAT TTGTATAGTTCATCCATGCCATGCCTACTGC CTCGGA
31	*GFP* #2	Aequorea victoria	TGCTGTTGACAGTGAGCGCTGGACACAAA TTGGAATACAATAGTGAAGCCACAGATGTA TTGTATTCCAATTTGTGTCCAATGCCTACT GCCTCGGA

2.6.2.4 siRNAs

siRNAs (all human) were purchased from Horizon Discovery and resuspended in 1 X siRNA resuspension buffer (Horizon) to a concentration of 20 µM.

siRNA	**catalogue #**
ON-TARGETplus Non-targeting Control Pool	D-001810-10-20
ON-TARGETplus MYC siRNA Smart Pool	L-003282-02-0005
ON-TARGETplus eIF3D siRNA Smart Pool	L-017556-00-0005
ON-TARGETplus eIF3B siRNA Smart Pool	L-019196-00-0005
ON-TARGETplus RPL23A siRNA Smart Pool	L-012863-00-0005
ON-TARGETplus RPS11 siRNA Smart Pool	L-013569-02-0005
ON-TARGETplus RPS15A siRNA Smart Pool	L-013542-01-0005
ON-TARGETplus RPS20 siRNA Smart Pool	L-011137-02-0005
ON-TARGETplus RPS19 siRNA Smart Pool	L-003771-00-0005
ON-TARGETplus ILF3 siRNA Smart Pool	L-012442-00-0005
ON-TARGETplus RPS17 siRNA Smart Pool	L-011152-01-0005
ON-TARGETplus RPL26 siRNA Smart Pool	L-011132-01-0005

2.7 Antibodies

2.7.1 Primary antibodies

WB: Western blotting, IP: immunoprecipitation, CLIP: cross-linking and immunoprecipitation, IHC: immune histochemistry

Target	company	catalogue #	used for (dilution)
β-Actin	Sigma Aldrich	A5441	WB (1:2000)
c-MYC (Y69)	Abcam	ab32072	WB (1:2000)
4EBP1	Cell Signaling	9644	WB (1:1000)
eIF3B	Santa Cruz	271539	WB (1:1000)
eIF3D	Abcam	ab264228	WB (1:1000), IP (20 µg)
eIF3D	Proteintech	10219-1-AP	IHC (1:100)
HA	Abcam	ab9110	WB (1:2000)
NF90 (ILF3)	Santa Cruz	377406	WB (1:1000)
p-S6 (Ser240/244)	Cell Signaling	2215	WB (1:1000)
Puromycin	Sigma Aldrich	MABE343	WB (1:1000)
RPL23A	Abcam	ab157110	WB (1:1000)
RPS11	Abcam	ab157101	WB (1:1000)
RPS15A	Abcam	ab241420	WB (1:1000)
RPS17	Santa Cruz	100835	WB (1:1000)
RPS19	Santa Cruz	100836	WB (1:1000)
RPS6	Cell Signaling	2217	WB (1:1000)
Vinculin	Sigma Aldrich	V9131	WB (1:2000)

2.7.2 Secondary antibodies

Target	supplier	order #	dilution (WB)
Anti-Rabbit IgG-HRP	GE Healthcare	1079-4347	1:10,000
Anti-Mouse IgG-HRP	GE Healthcare	1019-6124	1:10,000

2.8 Consumables

All consumables, including disposable plastic items (cell culture dishes, pipette tips, reaction tubes, syringes, cuvettes, filters etc.), were purchased from VWR, Sarstedt, NUNC, Eppendorf, INTEGRA Biosciences, and Greiner Bio-One.

2.9 Equipment

Chemiluminescent imaging	LAS-4000 mini (Fijifilm)
Cell culture incubator	BBD 6220 (Heraeus)
Cell counter	Neubauer cell counting chamber Invitrogen™ Countess™ 3 FL Cell counter (Fisher Scientific)
Centrifuges	Avanti J-26 XP (Beckman Coulter) Multifuge 1S-R (Thermo Fisher Scientific) Centrifuge 5430 (Eppendorf) Centrifuge 5424R (Eppendorf)
Deep-sequencer	NextSeq 2000 (Illumina)
Flow cytometer	BD FACS Canto™ II (BD Biosciences) BD FACS Aria III (BD Biosciences)
Heating block	Dry Bath System (Starlab)
Hybridisation Membrane	Hybond®-N+ hybridisation membrane (Cytiva)
Microscopes	Axiovert 40 CFL (Zeiss) Operetta High Content Imaging System (Perkin Elmer)
PCR thermal cycler	C1000 Toch™ Thermal cycler (BioRad)
Plate reader	Spark® multimode microplate reader (TECAN)
Photometer	NanoDrop 3000 (Thermo Scientific) Ultrospec™ 3100 pro (Amersham Biosciences)

Power supply	Power Pac (Bio-Rad)
PVDF Transfer membrane	Immobilon®-P (Millipore)
qRT-PCR machine	StepOnePlus Real-Time PCR System (Applied Biosystems)
Rotator	Rotator SB2 (Stuart)
Roll mixer	RM5 roll mixer (CAT)
SDS gel running chamber (WB)	Mini-PROTEAN Tetra Cell electrophoresis chambers (BioRad)
Sterile bench	HeraSafe (Heraeus)
Thermo shaker	Mixer HC (starlab)
Ultra sonifier	Digital Sonifier W-250 D (Branson)
UV transilluminator	Maxi UV fluorescent table (peqlab)
UV crosslinker	UVP crosslinker CL-1000 (analytic jena)
Vortex mixer	Vortex™ Genie 2 (Scientific Industries)
Western Blot transfer system	Trans-Blot® Turbo™ Transfer System (BioRad) PerfectBlue Tank Electro Blotter Web S (peqlab)
Whatman filter paper	Gel Blotting Paper (Schleicher and Schuell)

2.10 Software & online programs

Adobe Acrobat DC	Adobe Inc.
Affinity Designer	Serif
ApE plasmid editor	by M. Wayne Davis
BD FACSDiva software v6.1.2	BD Biosciences
Endnote™ 20.5	Clarivate

GraphPad Prism v9.4.1	Dotmatics
Image J	by Wayne Rasband
Integrated Genome Browser (IGV) 2.15.2	(Nicol, Helt, Blanchard, Raja, & Loraine, 2009)
Mac OS Ventura 13.1	Apple Inc.
Multi Gauge	Fujifilm Corporation
Microsoft Office	Microsoft Corporation (Word, PowerPoint, Excel)
Perkin Elmer Harmony Software	Perkin Elmer
SnapGene Viewer	Dotmatics
StepOne software v2.3	Applied Biosystem

3 Methods

3.1 Cell biology methods

3.1.1 Cell lines and standard cell culture

All cell lines were obtained from ATCC and cell culture consumables were purchased from (VWR International/NUNC, Sarstedt, Greiner). Cell lines DLD1, LS174T and SW480 were maintained in Roswell Park Memorial Institute (RPMI) 1640 Medium (Gibco), HCT116 and HEK293T in Dulbecco's modified Eagle Medium (DMEM, Capricorn Scientific GmbH). Media were supplemented with 10 % (v/v) fetal bovine serum (FBS) and 1 % penicillin/streptomycin (pen/strep) solution (Sigma), and cells cultivated at 37 °C, 85 % humidity, 21 % O2 and 5 % CO_2. Cell lines were passaged on a regular basis (twice a week). At a confluency of 60 – 80 % cells were washed with 1 X phosphate-buffered saline (PBS) and detaching from cell culture plates was achieved using trypsin-EDTA. To stop trypsinisation reaction, cells were resuspended in fresh medium and a fraction of the cell suspension was transferred to a new dish.

3.1.2 Cell number determination

Cells were trypsinised and resuspended in fresh medium as described in the previous section. 10 µl cell suspension was transferred onto a Neubauer cell counting chamber and counted manually at the microscope or transferred onto cell counting slides (Invitrogen) and counted automatically by the Countess™ 3 FL Cell counter (Fisher Scientific).

3.1.3 Cell freezing

For long term storage, cells were collected as described in 3.1.1 and cell suspension was centrifuged (1,000 rpm, 4 min). Subsequently, cell pellets were resuspended in fresh cell culture medium containing additional 20 % (v/v) FBS and 10 % (v/v) dimethyl sulfoxide (DMSO) to lower the freezing temperature. The cell suspension (4 – 5 x 10^6 cells/ml) was transferred into cryovials and stored in a freezing container at – 80 °C for at least 24 h. Afterwards, cells were moved to the liquid nitrogen tank.

3.1.4 Cell thawing

Upon removal from liquid nitrogen, cryovials were thawed at 37 °C and transferred into a 15 ml tube containing 1 X PBS. After centrifugation (1,000 rpm, 4 min) the supernatant was discarded, the cell pellet was resuspended in fresh cell culture medium and transferred into a new dish. The next day, medium was changed to remove residual DMSO.

3.1.5 Cell Harvest

Medium was discarded, cells were washed with 1 X PBS, scraped from the cell culture dish and transferred to a 1.5 ml reaction tube. After centrifugation (4,000 rpm, 4 min, 4 °C) supernatant was removed and cell pellets were flash-frozen in liquid nitrogen. Samples were stored at – 80 °C until further processing for protein or RNA isolation.

3.1.6 Cell transfection

3.1.6.1 Transfection using polyethyleneimine (PEI)

This method was used for production of lentiviral particles (see section 3.1.10). The day before transfection, HEK293T cells were seeded in 10 cm cell culture dishes at 80 – 90 % confluency and cultivated in antibiotics-free medium, supplemented with 2 % (v/v) FBS. Transfection reactions were prepared as follows:

Solution 1: plasmid DNA in 500 µl 1 x PBS

Solution 2: 30 µl PEI (double amount of plasmid DNA) in 500 µl 1 X PBS

Solution 1 and 2 were mixed, incubated at room temperature for 15 min and dropped carefully into the cell culture dish.

3.1.6.2 Transfection using lipofectamine RNAiMAX

For transient gene silencing, cells were transfected with small interfering (si) RNAs and the amount of each reagent refers to a 6 cm dish. In one reaction tube 500 µl OptiMEM were mixed with 5 µl siRNA (from a 20 µM stock) at a final concentration of 20 nM. In

another reaction tube, 10 µl RNAiMAX (Invitrogen) were mixed with 500 µl OptiMEM. After 5 min incubation, both reactions were mixed, incubated 10 min at room temperature and added dropwise to the cells.

3.1.7 Passaging of organoids

Organoids were passaged on a regular basis (1 – 2 x/week). Medium was removed from well, organoids were dissociated in 1 ml 1 X PBS (blue 1000 µl pipette tip with small 10µl pipette tip on top), transferred to a 15 ml tube and 5 ml 1 X PBS were added. Organoid solution was centrifuged at 300 x g for 4 min and RT, supernatant was sucked off and organoid pellet was resuspended 80 % cultrex / 20 % ADF 'base'. Organoid/cultrex solution was dropped into a pre-warmed 6-well plate and incubated for at least 10 min in the incubator, before 2 ml ENR medium were added to each well.

3.1.8 Freezing of organoids

To freeze organoids, cells from one well of a 6-well plate were dissociated by pipetting, transferred into a 15 ml tube and 5 ml 1 X PBS were added. Organoid solution was centrifuged for 4 min at 300 x g and supernatant was removed. Organoid pellet was resuspended in 500 µl organoid freezing medium, transferred into a cryo vial and slowly frozen in a freezing container for at least one day at -80 °C. For long term storage, cells were transferred into a liquid nitrogen tank.

3.1.9 Thawing organoids

Upon removal from liquid nitrogen, cryovials were thawed at 37 °C and transferred into a 15 ml tube containing 5 ml ADF 'base'. After centrifugation (300 x g, 4 min) the supernatant was discarded, the cell pellet was resuspended in 150 µl 80 % cultrex/20 % ADF 'base' and several drops were put into a pre-warmed 6-well plate. After a 10-min pre-incubation in the incubator, 2 ml ENR medium was added to the well. The next days, medium was changed again, and organoids were passaged as soon as they looked viable and happy.

3.1.10 Production of lentiviral particles

To ensure safety while working with virus particles, a lentiviral system of the 2nd generation was used ("Addgene: Lentiviral guide,"). A single packaging plasmid (psPAX2) encodes the Gag, Pol, Rev, and Tat genes. The transfer plasmid contains the viral long terminal repeats (LTRs) and psi packaging signal, as well as the gene or short hairpin (sh) RNA, which should be introduced into cells. The envelope protein Env is encoded on a third separate plasmid (pMD2.G). As described in section 3.1.6.1, 4 – 5 x 10^6 HEK293T cells were plated on a 10 cm dish and transfected with PEI using 10 µg transfer plasmid, 3 µg psPAX2 and 1.5 µg pMD2.G. Next day, medium containing transfection reagents was removed from HEK293T cells and 6 ml fresh standard culture medium was added. The two following days, virus-containing medium was collected, filtered through 0.45 µM filters (INTEGRA Biosciences) and directly used for infection of cells or stored at – 80 °C for later use.

3.1.11 Lentiviral infection of cells

Per 15 cm cell culture dish, 3 x 10^6 cells diluted in 7 ml medium were seeded and 3 ml virus-containing medium was added. In order to enhance infection efficiency, 8 µg/ml polybrene (Sigma) was added, which neutralizes the charge repulsion between virions and the cell surface. The next day, medium was refreshed. Two days after infection, infected cells were selected either by fluorescence-activated cell sorting (FACS) or by addition of the respective antibiotics which is determined by the resistance marker introduced by the transfer plasmid. After selection cells were seeded for further experiments.

3.1.12 Production of lentiviral particles for organoid culture

Lentivirus-containing medium from HEK293T cells for organoid infection was produced as described in chapter 3.1.10 with the following modifications. For each infection, one to three 15 cm dishes of HEK cells were transfected with the respective shRNA-carrying vector and the amounts of vector, psPAX2, pMD2.G and DMEM medium were adjusted accordingly. After collecting the virus-containing supernatant, the virus was concentrated using a polyethylene glycol (PEG) 8000 solution. For this purpose, the supernatant was

first centrifuged for 10 min at RT and 800 x g and then carefully transferred to a new 50 ml tube. One volume of PEG was added to three volumes of supernatant and mixed by shaking for 1 min before the mixture was incubated in the refrigerator for at least 4 - 6 h. This was followed by a 60 min centrifugation step at 1,600 x g and 4 °C. The supernatant was removed, and the pellet resuspended in 1/10 to 1/20 of the original volume in appropriate organoid medium (without FBS and pen/strep). The concentrated virus solution was stored at -80 °C until use.

3.1.13 Lentiviral infection of organoids

For lentiviral infection of organoids, three wells of a 6-well plate were collected and resuspended in 1 X PBS as described in 3.1.7, followed by centrifugation for 5 min at 500 x g. Supernatant was removed and pellet resuspended in 500 µl TrypLE Express Enzyme and incubated for 3 min at 37 °C. After incubation, 3.5 ml ADF ‘base’ medium were added, followed by centrifugation for 5 min and 500 x g and virus was thawed in parallel in a water bath at 37 °C. After centrifugation, supernatant was removed from cells, pellet was resuspended in 3 ml virus solution and transferred into one well of a 6-well plate. Nicotinamide (1:100), Y27 (1:100), Chir99021 (1:500) and Polybrene (1:500) were added to the well, plate was wrapped in parafilm and spin-infection was carried out in the centrifuge for 1 h at 600 x g and 32 °C. After centrifugation, the plate was incubated at 37 °C for 4 h. Subsequently, infected organoids were collected from the plate, transferred to a 15 ml tube and centrifuged for 5 min at 800 x g. The pellet was resuspended in 200 – 300 µl cultrex and seeded dropwise into a pre-warmed 6-well plate, followed by 10 min incubation at 37 °C. ENR medium was supplemented with nicotinamide (1:100), Y27 (1:100) and Chir99021 (1:500) and added to the infected organoids. The following days, medium was changed regularly (supplemented with nicotinamide, Y27 and Chir99021) and selection antibiotics was added. After one week, normal instead of supplemented ENR medium was used again.

3.1.14 CellTiter-Glo® 2.0 Cell Viability Assay

For cell viability assay, organoids were collected and dissociated by pipetting as described in 3.1.7. and centrifuged with 5 ml cold 1 X PBS for 4 min at 300 x g. For a 96-well plate (96-well Pheno Plate (transparent bottom, Perkin Elmer)), the organoid

pellet was resuspended in 50 µl cultrex/PBS mixture (1:1) per well and dropped into the wells. For each condition to be tested, four to five replicates were seeded. The plate was incubated at 37 °C for at least 30 min before 100 – 200 µl ADF 'base' medium were carefully added. Four additional wells only containing ADF 'base' medium served as background control. Respective treatments/medium change was performed the following days and CellTiter-Glo® (CTG) 2.0 Cell Viability Assay was performed five to seven days after seeding. To each well, 100 µl CTG 2.0 (equilibrated to room temperature) per 100 µl medium were added and incubated 10 min in the dark. Luminescence was measured at the Spark® multimode microplate reader (TECAN) and mean of background values was subtracted from each mean of sample values.

3.1.15 Fluorescence-activated Cell Sorting (FACS)

3.1.15.1 AnnexinV/PI FACS

During apoptosis, membrane-located phosphatidylserine (PS) translocates from the inner side of plasma membrane to the surface (Ravi Hingorani, 2011). Annexin V is a phospholipid-binding protein with high affinity for PS. When labelled with a fluorochrome, this enables detection of exposed PS using flow cytometry. Since PS translocation is an early apoptotic event, Annexin V is used in combination with the vital dye propidium iodide (PI) for identification of early and late apoptotic cells. PI is excluded from viable cells with intact membranes, whereas membranes of dead and damaged cells are permeable to PI. For Annexin V/PI analysis medium from cell culture dishes was collected in 15 ml tubes, cells were washed with 1 X PBS and trypsinised for 15 min. Detached cells were resuspended in previously collected medium and centrifuged for 5 min at 1,500 rpm and 4 °C. Supernatant was discarded, pellets resuspended in 1 ml ice-cold 1 X PBS and transferred to a 1.5 ml tube. Cells were centrifuged for 5 min at 2,500 rpm and 4 °C. Subsequently, pellets were resuspended in 100 µl 1 x Annexin V binding buffer including 2 µl Annexin V/Pacific Blue and incubated for 15 min at room temperature in the dark. Finally, 400 µl 1 x Annexin V binding buffer containing 5 µl PI (1 mg/ml stock) was added to the samples which were directly used for FACS measurement (488 nm, 586/42 nm bandpass filter) according to the instrument's manual.

3.1.15.2 PI Cell Cycle Analysis

PI intercalates into double-stranded DNA thereby providing information about DNA content of cells during cell cycle. Cells were prepared as described in chapter 3.1.15.1 until the first centrifugation step. Supernatant was discarded, cells washed with 10 ml ice-cold 1 X PBS and again centrifuged for 5 min at 1,500 rpm and 4 °C. Supernatant was removed and cells resuspended in 1 ml ice-cold 1 X PBS. Next, cells were fixed by adding suspension dropwise into 4 ml ice-cold 100 % (v/v) ethanol in a 15 ml polystyrol tube (Sarstedt) while vortexing and incubated over night at – 20 °C. Next day, samples were centrifuged for 10 min at 1,500 rpm and 4 °C, supernatant was discarded, and cells washed with 5 ml ice-cold 1 X PBS. Pellets were finally resuspended in 400 µl 38 mM sodium citrate, 15 µl PI (1 mg/ml stock) and 1 µl RNAse A (10 mg/ml stock). After 30 min incubation at 37 °C in the dark samples were used for FACS analysis.

3.1.16 Crystal-violet Staining and Quantification

In order to analyse proliferation of cells under certain conditions, cells were stained with a crystal violet solution. For this purpose, medium was removed from the cell culture dish, cells were washed with 1 X PBS and fixed with 70 % (v/v) ethanol for 10 min. After removal of ethanol cells were air-dried for 15 min. A 0.1 % (w/v) crystal violet solution in 20 % (v/v) ethanol was then added to the cell culture dishes and incubated for 30 min before cells were finally washed with H_2O and air-dried overnight. For quantification of staining intensity, cells were de-stained with 10 % (v/v) acetic acid solution and incubated for 15 min on an orbital shaker. 100 µl of this solution (in technical triplicates) were transferred to a 96-well plate and absorbance at 590 nm was measured with Spark® multimode microplate reader (TECAN).

3.2 Bacterial Methods

3.2.1 Transformation of Competent Cells

Transformation of bacteria was performed according to Hanahan (Green & Sambrook, 2018). For each reaction, 20 µl competent *E. coli* XL1blue were thawed on ice and 5 µl ligation mix or 0.1 µg pure plasmid were added to bacteria. After incubation on ice for

30 min, bacteria were heat-shocked at 42 °C for 2 min followed by incubation on ice for another 2 min. 750 µl pre-warmed LB medium without antibiotic were added to the cells and cell suspension was incubated in a thermoshaker for 30 min at 37 °C. After a 10 s centrifugation step at full speed, 750 µl of supernatant were removed and bacteria were resuspended in remaining medium. Cells were spread on LB/antibiotic plate and grown overnight at 37 °C.

3.2.2 Mini DNA Isolation

For Mini DNA preparation, colonies were picked with a pipette tip from LB/antibiotic plate (see chapter 3.2.1) and grown overnight at 30 or 37 °C in 5 ml ampicillin-containing (100 µg/ml) LB medium in round-bottom tubes (Sarstedt). Next day, Mini DNA isolation was performed using PureYield™ Plasmid Miniprep System (Promega) according to the manufacturer's instructions. Initially, 600 µl of bacterial culture were transferred to a 1.5 ml reaction tube and 100 µl Cell Lysis Buffer were added and mixed by inverting the tube 6 times. 350 µl of cold Neutralisation Solution were added to the mixture and mixed thoroughly by inverting the tube followed by a 3 min centrifugation step at maximum speed. Supernatant was transferred to a PureYield™ Minicolumn placed in a Collection Tube and again centrifuged at maximum speed for 15 s. Flowthrough was discarded and 200 µl Endotoxin Removal Wash solution was added to the minicolumn and again centrifuged for 15 s. Subsequently, 400 µl Column Wash Solution were added to the column and centrifuged for 30 s. The minicolumn was transferred to a clean 1.5 ml reaction tube and 30 µl ddH2O were added to the column matrix. DNA was eluted by a 15 s centrifugation step and stored at – 20 °C. Correct DNA sequence was confirmed by Sanger sequencing (LGC Genomics).

3.2.3 Maxi DNA Isolation

For DNA isolation from Maxi preparations, 4 ml of Mini culture (see 3.2.2) were expanded by addition of 200 ml LB medium + ampicillin (100 µg/ml) and grown overnight at 37 °C. Next day, DNA was isolated using the PureLink™ HiPure Plasmid Maxiprep Kit according to the manufacturer's instructions. In brief, bacterial suspension was pelleted by centrifugation (8,000 rpm for 25 min at 4 °C) and resuspended in 10 ml Resuspension Buffer. Subsequently, 10 ml Lysis Buffer were added, swirled gently incubated for 5 min

at room temperature. Then, 10 ml of Precipitation Buffer were added, swirled gently and the precipitate was pelleted by centrifugation (8,000 rpm for 25 min at 21 °C). For DNA binding, the column was prepared by addition of 30 ml Equilibration Buffer and the resulting supernatant after centrifugation was loaded onto the equilibrated column through a paper filter. After the solution drained by gravity flow, column was washed twice with 30 ml Wash Buffer and eluted in 15 ml Elution Buffer. Afterwards, 10.5 ml isopropanol were added to eluted DNA, incubated on ice for 20 min followed by 30 min centrifugation at 8,000 rpm. Supernatant was removed, pellet washed with 5 ml 70 % (v/v) ethanol and centrifuged for 25 min at 8,000 rpm. After removal of ethanol, pellet was air-dried at room temperature and resuspended in 200 – 1000 µl H2O (final DNA concentration 1 µg/µl) and stored at – 20 °C. Correct DNA sequence was confirmed by Sanger sequencing (LGC Genomics).

3.3 Molecular biological methods

3.3.1 DNA extraction

Genomic DNA from cell lysates was isolated using the DNAzol® reagent (Invitrogen) according to the manufacturer's instructions. In brief, pellets (1/5 of 10 cm cell culture dish) were lysed in 0.5 ml DNAzol® reagent by gently pipetting with a wide bore pipette tip. Subsequently, samples were centrifuged for 10 min at 10,000 x g and 4 °C. The resulting viscous supernatant was transferred into a fresh 1.5 ml tube to get rid of RNA. Then, 0.5 ml 100 % (v/v) ethanol was added, mixed by inversion and stored at room temperature for 1 – 3 min until a cloudy precipitate had formed. By spooling with a pipette tip, the DNA precipitate was transferred into a clean tube where it was washed twice with ethanol. Therefore, DNA was suspended in 1 ml 75 % (v/v) ethanol by inverting the tube 3 – 6 times and centrifuged for 1 min at 10,000 rcf and 4 °C. After second wash, ethanol was removed completely by pipetting and the DNA precipitate was transferred into a new tube with 40 µl of freshly prepared 8 mM NaOH + 0.9 µl 1 M HEPES. DNA was dissolved by pipetting.

3.3.2 Phenol-chloroform extraction of total RNA

RNA from whole cell lysates was extracted using TriFast reagent (VWR) according to the manufacturer's instructions. Briefly, cell pellets were resuspended in 0.5 – 1 ml TriFast reagent, incubated at room temperature for 5 min before 0.1 – 0.2 ml chloroform was added. Samples were mixed properly and centrifuged for 5 min at 14,000 x rpm and 4 °C to separate RNA-, DNA- and protein-containing phases. The upper RNA-containing phase was carefully transferred to a new 1.5 ml reaction tube containing 0.25 – 0.5 ml 100 % (v/v) isopropanol and 1 µl Glycoblue precipitation reagent (Invitrogen). Samples were incubated at – 20 °C for at least 1 h, before they were centrifuged for 5 min at 14,000 x rpm and 4 °C to pellet RNA. Supernatant was discarded and pellets were washed twice with 70 % (v/v) ethanol, air-dried and finally dissolved in 25 – 50 µl nuclease-free H_2O. Concentration of RNA was determined as described in 3.3.3.

3.3.3 Quantification of Nucleic Acids

Determination of nucleic acid's concentration was carried out spectrophotometrically using the NanoDrop 3000 (Thermo Scientific). Before measurement the photometer was calibrated with nuclease-free H_2O. Absorbance at $\lambda = 260$ nm was detected and the ratio to the absorption at $\lambda = 280$ nm was determined to verify purity of nucleic acid solution. Ratio for pure DNA should be around 1.8, for pure RNA around 2.0.

3.3.4 cDNA synthesis

Cellular expression of mRNA was assessed by quantitative real time PCR. For this purpose, single-stranded complementary DNA (cDNA) was generated from 0.2 – 0.5 µg of RNA (isolated as described in 3.3.2) using M-MLV Reverse Transcriptase (Promega). RNA was diluted in 10 µl nuclease-free H_2O and incubated for 2 min at 65 °C and 2 min at 4 °C. Subsequently, an equal volume of reaction mix (**Table 1**) was added to RNA and incubated for 10 min at 22 °C, 50 min at 37 °C and 15 min at 70 °C before samples were cooled down to 4 °C. Finally, cDNA was diluted with 130 µl H_2O and stored at – 20 °C.

Component	Volume [µl]	Final Conc.
5X M-MLV Reaction Buffer	4	1 X
Primer random p(dN)6 (2 µg/ml)	1	2 µg
10 mM dNTP mixture	0.5	250 µM
M-MLV reverse transcriptase (200 U/µl)	0.5	100 U
Ribolock RNase inhibitor (40 U/µl)	0.1	4 U
nuclease-free H_2O	3.9	
total	**10**	

***Table 1**: Components of a single reverse transcription reaction*

3.3.5 Quantitative real-time PCR (qRT-PCR)

To assess mRNA expression of genes of interest (GOI), total cellular RNA was initially transcribed *in vitro* as described in 3.3.4. qRT-PCR was performed using the PowerUp™ SYBR® Green Master Mix (Thermo Scientific) where a SYBR Green dye specifically binds double-stranded cDNA. This interaction provides a measurable fluorescent signal that reflects the amount of DNA produced during PCR via primers targeting the GOI. As an endogenous control, the housekeeping gene β-2-microglobulin (B2M) was used to correct sample preparation-related variations. qRT-PCR reactions were set up as indicated in **Table 2** and every sample was measured in technical triplicates. In parallel, a non-template control was tested for each primer pair used to ensure proper experimental handling and exclusion of DNA/RNA contamination of any reaction mixture component.

Component	Volume [µl]	Final Conc.
2 X Power SYBR® Green PCR Master Mix	5	1 X
Primer mix (forward + reverse) (10 µM)	1	1 µM
cDNA	4	
total	10	

***Table 2**: Components of single qRT-PCR reaction prepared in 96-well plates.*

The qRT-PCR was performed applying the following protocol (**Table 3**) on the Applied StepOne Real-Time PCR System.

Step	Temperature	Duration	
Initial Denaturation	98 °C	30 s	
Denaturation	98 °C	7 s	30 x
Annealing	60.5 °C	20 s	
Extension	72 °C	10 s	
Final Extension	72 °C	10 min	

***Table 3**: qRT-PCR thermal cycler program.*

To calculate the relative expression levels of a GOI, the comparative C_T method (Schmittgen & Livak, 2008) was applied using the StepOne Software. Here, the C_T (threshold cycle) value for every transcript in each sample represents the cycle number at which accumulation of a fluorescent signal crosses the internal set threshold. Data were normalised using the double delta C_T ($\Delta\Delta C_T$) method. First, C_T values of technical replicates of each sample were averaged and the ΔC_T between expression of the reference (B2M) and the GOI was determined. Second, the fold change of mRNA expression was calculated ($2^{-\Delta\Delta CT}$) and biological replicates were averaged to perform statistical analyses.

3.3.6 Agarose gel electrophoresis

To validate PCR-amplified DNA or restriction enzyme-based linearised plasmids, nucleic acid solutions in 6 X loading dye were loaded onto a pre-cast 1 – 2 % agarose gel containing 1 µg/ml ethidium bromide. Additionally, 1 kb DNA ladder was loaded to compare the size of DNA fragments. Nucleic acid separation was carried out at 140 V for one hour in an electrophoresis chamber containing 1 x TAE buffer. Finally, UV transillumination imaging was carried out at the Maxi UV fluorescent table (peqlab).

3.3.7 Gel purification of nucleic acid fragments

Purification of DNA fragments from agarose gels was performed using the GeneJET Gel Extraction Kit (Thermo Scientific). All steps were carried out according to the manufacturer's instructions for using centrifuge. In brief, a 1:1 volume of Binding Buffer

was added to gel slice and incubated at 55 °C until gel slice was dissolved. Solubilised gel solution was loaded onto purification column and centrifuged for 1 min at 12,000 x g. Immobilised nucleic acid in the column was washed by adding 700 µl Wash Buffer and centrifugation for 1 min. Empty GeneJET purification column was centrifuged for an additional 1 min to completely remove residual wash buffer and DNA was finally diluted in 20 – 50 µl H_2O.

3.3.8 Cloning shRNAs into pLT3/pGIPZ

To achieve stable expression of shRNAs in cells, shRNAs were cloned into pLT3-GEPIR or pGIPZΔEcoRI vector for inducible or constitutive expression, respectively. Initially, single stranded shRNA oligos were diluted to 60 ng/µl and amplified using primers #1 and #2 to add respective restriction sites for cloning into the vector. PCR reaction was set up based on the manufacturer's recommendations for Phusion Hot Start II High Fidelity DNA Polymerase Kit (Thermo Scientific) as listed in **Table 4**. For each shRNA, two reactions were prepared and pooled after PCR amplification.

Component	Volume [µl]	Final Conc.
Diluted oligo	1	60 ng
Phusion Hot Start II Polymerase (2 U/µl)	0.5	1 U
5 X Phusion HF Buffer	10	1 X
dNTP mix (10 mM)	1	200 µM each dNTP
Primer forward (10 µM)	2.5	500 nM
Primer reverse (10 µM)	2.5	500 nM
DMSO	2.5	5 % (v/v)
H_2O	30	
total	**50**	

***Table 4**: Preparation of PCR reaction mixture for amplification of shRNAs.*

Amplification was performed in a thermal cycler using the following parameters (**Table 5**):

Step	Temperature	Duration	
Initial Denaturation	98 °C	2 min	
Denaturation	98 °C	25 s	20 x
Annealing	62 °C	25 s	
Extension	72 °C	20 s	
Final Extension	72 °C	5 min	

***Table 5**: Thermal Cycler program for amplification of shRNAs.*

Subsequently, 5 µl of pooled PCR reaction were loaded onto a 3 % agarose gel as quality control of the PCR. The remaining 95 µl were purified using the GeneJET Gel Extraction Kit as described in section 3.3.7 using protocol for PCR product purification. Purified oligos were digested with respective restriction enzymes (EcoRI-HF and XhoI (NEB)) according to the manufacturer's recommendations, incubated in a thermal cycler at 37 °C for 30 min followed by another purification step. In parallel, 10 µg pLT3-GEPIR or pGIPZΔEcoRI, respectively, were digested by EcoRI-HF and XhoI (NEB) (37 °C for 45 min), loaded onto a 1 % agarose gel, cut out and purified. Digested vector (30 ng) and 7 µl oligo were ligated using T4 DNA ligase (NEB) according to the manufacturer's protocol and incubated at room temperature for 1 h. In the end, 2.5 µl ligation mix were added to 50 µl competent bacteria and proceeded as described in section 3.2.1.

3.3.9 *In vitro* RNA pulldown

To identify MYC 5' UTR-binding proteins, an in vitro RNA pulldown was performed, the individual steps of which are described in detail in the following sections and illustrated in **Figure 9**. Briefly, the sequence of the *MYC* 5' UTR was amplified from pInducer21-5'UTR-MYC-HA-3'UTR and a T3 promoter site was attached for efficient *in vitro* transcription. The transcribed RNA was biotinylated, purified and RNA-binding proteins were identified by streptavidin pulldown followed by LC/MS analysis.

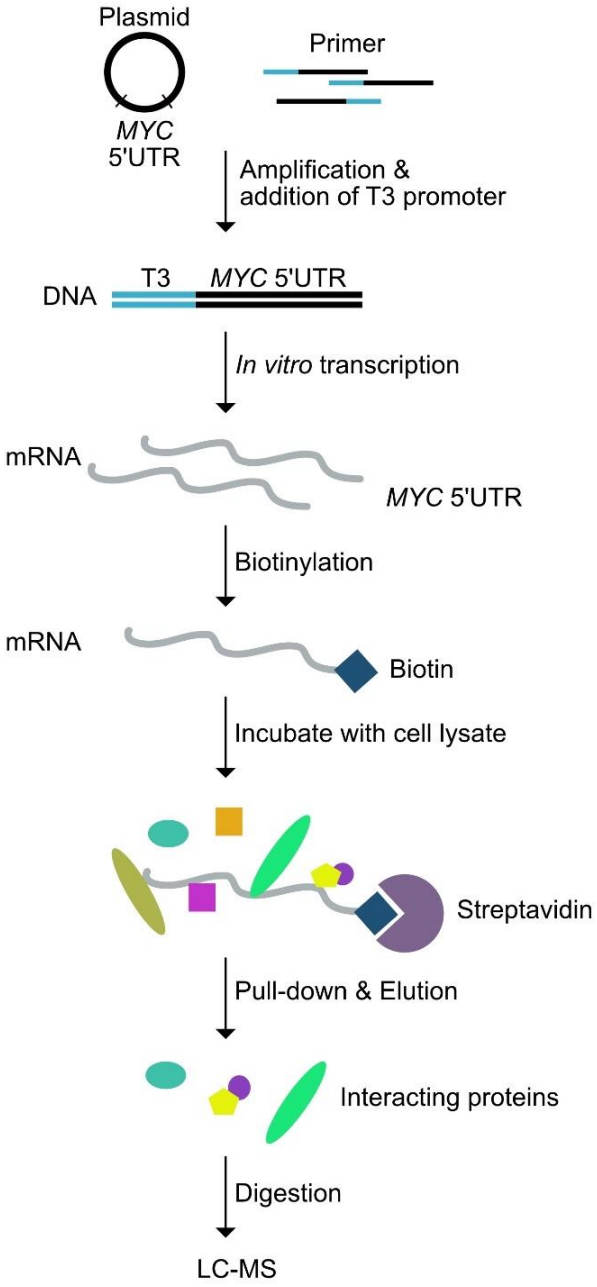

Figure 9: Schematic illustration of the in vitro RNA pulldown for identification of MYC 5' UTR-binding proteins*. Initially, sequence of the MYC 5'UTR was amplified and linked to T3 promoter for in vitro transcription. Transcribed RNA was biotinylated, incubated with DLD1 whole cell lysate and interacting proteins were pulled down using magnetic streptavidin beads and analysed by LC/MS.*

3.3.9.1 PCR amplification of MYC 5'UTR constructs

MYC 5' UTR constructs were amplified from plasmid DNA template (pInducer21-5'UTR-MYC-HA-3'UTR) and endowed with the RNA polymerase promoter site (T3 promoter) at the 5' end using oligos #3 and #4 to enable *in vitro* transcription. To ensure high fidelity and low error rate during amplification, Phusion Hot Start II DNA Polymerase (Thermo Scientific) was used. The PCR reaction setup is shown in **Table 6** and cycling conditions are listed in **Table 7**. Amplified DNA was stored at – 20 °C.

Component	Volume [µl]	Final Conc.
5 X Phusion HF Buffer	10	1 X
Template DNA	X	1 µg
Phusion Hot Start II Pol	0.2	0.02 U/µl
dNTP mix (10 mM)	0.4	200 µM each dNTP
Primer forward (10 µM)	2.5	500 nM
Primer reverse (10 µM)	2.5	500 nM
H_2O	X	
total	**50**	

***Table 6**: PCR reaction setup for amplification of MYC 5'UTR from pInducer21 HA-5'UTR-MYC.*

Step	Temperature	Duration	
Initial Denaturation	98 °C	30 s	
Denaturation	98 °C	7 s	30 x
Annealing	67.3 °C	20 s	
Extension	72 °C	10 s	
Final Extension	72 °C	10 min	

***Table 7**: Cycling instructions for amplification of MYC 5'UTR from pInducer21 HA-5'UTR-MYC-3'UTR.*

3.3.9.2 In vitro transcription

In vitro transcription of the *MYC* 5' UTR mRNA was performed using the MEGAscript T3 transcription kit (Thermo Scientific) according to the manufacturer's instructions. PCR-

amplified DNA fragment (see 3.3.9.1) was directly used as template and transcription reaction was assembled at room temperature as indicated in **Table 8**.

Component	Amount
ATP solution	2 µl
CTP solution	2 µl
GTP solution	2 µl
UTP solution	2 µl
10X Reaction Buffer	2 µl
PCR product template	200 ng
Enzyme Mix	2 µl
H_2O	X µl
total	**20 µl**

***Table 8**: Reaction setup for in vitro transcription of MYC 5' UTR PCR amplicon.*

Reaction mixtures were incubated overnight at 37 °C under constant agitation. Next day, 1 µl of TURBO DNase (2 U/µl) was added to the mixture and incubated for another 15 min at 37 °C to digest the DNA template. Subsequently, 115 µl nuclease-free H_2O and 15 µl Ammonium Acetate Stop Solution were added to the transcription reaction mixture and extracted with phenol/chloroform as described in section 3.3.2.

3.3.9.3 Biotinylation of RNA

In order to identify 5'UTR-binding factors, the *in vitro* transcribed RNA fragments were covalently coupled to biotin using Pierce RNA 3'-end Desthiobiotinylation Kit according to the manufacturer's recommendations. A poly(A)25 RNA was biotinylated and treated in parallel during the following pulldown procedure. In brief, RNA from the *in vitro* transcription reaction was purified via phenol/chloroform extraction to remove remaining nucleotides and enzyme prior to a biotinylation reaction. To remove secondary structures within the MYC 5'UTR constructs, *in vitro* transcribed RNA was heated in the presence of 25 % (v/v) DMSO for 5 min at 85 °C and immediately placed on ice. RNA ligation reaction was prepared as indicated in **Table 9** and incubated overnight at 16 °C. The

following day, 70 µl nuclease-free H_2O were added to the ligation reaction and biotinylated RNA was extracted as described in section 3.3.10.

Component	Volume [µl]	Final Conc.
Nuclease-free H_2O	3	
10X RNA Ligase Reaction Buffer	3	1 X
RNase Inhibitor	1	40 U
Non-labeled RNA Control/ Test RNA	5	50 pmol
Biotinylated Cytidine Bisphosphate	1	1 nmol
T4 RNA Ligase	2	40 U
PEG 30 %	15	15 % (v/v)
total	**30**	

***Table 9**: Reaction setup for biotinylating mRNA, adapted from Pierce RNA 3'-end Desthio-biotinylation Kit.*

3.3.10 Phenol-isoamyl alcohol extraction of biotinylated RNA

To extract RNA ligase from the biotinylation reaction, 100 µl chloroform:isoamylalcohol (24:1, v/v) were added to the reaction, vortexed and centrifuged for 3 min at 14,000 x g and 4 °C to allow phase separation. The top (aqueous) phase was carefully transferred to a fresh tube. Precipitation of RNA was achieved by addition of 10 µl of 5 M NaCl, 1 µl glycogen and 300 µl ice-cold 100 % (v/v) ethanol and an incubation step at – 20°C for at least 1 h. Afterwards, samples were centrifuged for 15 min at 14,000 x g at 4 °C. The supernatant was removed, pellets washed with 300 µl ice-cold 70 % (v/v) ethanol and air-dried. Finally, pellets were resuspended in 20 µl of nuclease-free H_2O.

3.3.11 Determining labelling efficiency by dot blotting

Detection of biotinylated RNA was performed using the Chemiluminescent Nucleic Acid Detection Module (Thermo Fisher Scientific) according to the manufacturer's instructions. In brief, dilution series of biotinylated control RNA (provided with the Pierce™ RNA 3' End Desthiobiotinylation Kit) and test RNA was prepared and spotted onto a positively charged hybridisation membrane (Cytiva) and allowed to absorb.

Subsequently, the membrane was UV-crosslinked for 15 min at 100 % intensity and immediately used for detection analysis. Crosslinked membrane was blocked in Blocking Buffer while shaking for 15 min at room temperature. Then, Stabilised Streptavidin-Horseradish Peroxidase Conjugate was added to fresh Blocking Buffer and the membrane was incubated for another 15 min with gentle shaking. The membrane was briefly rinsed with 1 X wash solution and washed 5 min each in 1 X wash solution. Then, the membrane was transferred to a new container and incubated for 5 min in Equilibration Buffer before Substrate Working Solution (6 mL Luminol/Enhancer Solution to 6mL Stable Peroxide Solution) was added and incubated for 5 min. Moist membrane was wrapped in plastic wrap and chemiluminescent detection was carried out at the LAS-4000 (Fujifilm).

3.3.12 Sample preparation for RNA pulldown-analysis

In order to identify proteins that bind to the different MYC 5'UTR constructs, respective RNAs were *in vitro* transcribed and biotinylated (see section 3.3.9.2 and 3.3.9.3) and protein lysates were prepared as described in section 3.5.1. To enable binding of RNA-interacting proteins to RNA the PierceTM Magnetic RNA-Protein Pull-Down Kit (Thermo Fisher Scientific) was used according to the manufacturer's protocol. In brief, 50 pmols of each biotinylated Test RNA and negative Control RNA provided with the kit were bound to 50 µl streptavidin beads, respectively, and incubated for 30 min at room temperature with constant agitation. Subsequently, Master Mix of RNA-Protein binding reaction (see **Table 10**) was added to RNA-bound beads and incubated 60 min at 4 °C with rotation. RNA-Protein complexes were washed, and RNA-binding proteins were eluted in 50 µl Elution Buffer, heated at 95 °C for 10 min and stored at – 20 °C until further analysis.

Reagent	Volume per 100 µl reaction
Nuclease-free H_2O	to 100 µl
10X Protein-RNA Binding Buffer	10 µl
Lysate (protein conc. > 2 mg/ml)	1 – 30 µl
50 % (v/v) glycerol	30 µl
total	**100 µl**

***Table 10**: RNA-protein binding reaction components, adapted from PierceTM Magnetic RNA-Protein Pull-Down Kit (Thermo Fisher Scientific) manual.*

3.3.13 siRNA screen and immunofluorescence staining of MYC

The siRNA-mediated knockdown screen was performed by Dr. Christina Schülein-Völk and Dr. Ursula Eilers, who are running the screening unit of the department of Prof. Martin Eilers. Main steps are described in the following section.

One day before transfection, stock plate for control and test siRNAs was prepared. Single siRNAs were diluted to 1 µM final concentration in 10 µl volume in a Sapphire 96-well microplate (Greiner). Next day, triplicates from each siRNA stock (2.5 µl each) were transferred to a 96-well Pheno Plate (transparent bottom, Perkin Elmer), 7.5 µl OptiMEM was added to each well and incubated for 5 min at room temperature. Then, 10 µl OptiMEM + RNAiMax (1:50 of final volume) were added to each well and incubated for 20 min at room temperature, before 5,000 cells in 80 µl medium (w/o antibiotics) were added to each well. Transfected cells were incubated at 37 °C and transfection medium was replaced by normal medium (10 % (v/v) FBS, 1 % (v/v) pen/strep) the following day. Three days after transfection, cells were fixed with 3.7 % (v/v) formaldehyde solution and permeabilised with 0.2 % Triton X-100 in PBS and incubation at room temperature for 10 min. Cells were washed with PBS and blocked with 3 % BSA in PBS for 30 min at room temperature, before MYC protein abundance was detected by immunofluorescence staining. Primary antibody (MYC Y-69, abcam) was diluted 1:1000 in 3 % BSA in PBS and cells were incubated overnight at 4 °C. Next day, cells were washed three times with PBS before secondary antibody (Alexa Fluor 488 goat anti-rabbit IgG, Invitrogen) was added at a 1:400 dilution. To be able to count cells and to distinguish between cytoplasm and nucleus cells were additionally stained by Hoechst-33342 (Sigma, 2.5 µg/ml in PBS) and incubated for 5 min at room temperature in the dark. Cells were washed twice with PBS and staining was visualised using the Operetta CLS High-Content Imaging System (Perkin Elmer) and analysis was performed with Perkin Elmer Harmony Software.

3.4 Biochemical Methods

3.4.1 Preparation of Whole Cell Lysates

Cells were washed with cold 1 X PBS, harvested by scraping and collected into a 1.5 ml reaction tube. Subsequently, cells were centrifuged at 4,000 rpm and 4 °C and cell pellet

was resuspended in RIPA Buffer (supplemented with protease and phosphatase inhibitors), using a 2:1 ratio (volume RIPA:pellet). Samples were incubated on ice for 30 min followed by a 10 min centrifugation step at 14,000 rpm and 4 °C. Cleared lysates were transferred to a new 1.5 ml tube and protein concentration was determined with the Bradford Assay (see section 3.4.2). Lysates were flash frozen in liquid nitrogen and stored at -80 °C or directly prepared for SDS-PAGE (see section 3.4.3).

3.4.2 Total Protein Quantification by Bradford Assay

Protein concentration in whole cell lysates was determined by using ROTI®Quant (Roth) Bradford reagent according to the manufacturer's manual. Briefly, ROTI®Quant was diluted 1:5 with H2O and 1 ml diluted reagent was transferred into cuvettes and mixed with 1 µl cell lysate. Absorbance at 595 nm was measured in a spectrophotometer relative to a blank control sample. Absolute protein concentration was determined according to a pre-calculated standard curve.

3.4.3 SDS-Polyacrylamid Gel Electrophoresis (PAGE)

For SDS-PAGE, 15 µg protein lysate were mixed with an appropriate amount of 3 X Laemmli buffer and boiled at 95 °C for 5 min. SDS-polyacrylamide gels were prepared in advance and assembled in Mini-PROTEAN Tetra Cell electrophoresis chambers (Biorad), filled with 1 X SDS Running Buffer. Samples were loaded onto the gel and electrophoresis was performed at 80 – 130 V to separate proteins according to their molecular weight. PageRuler Pre-Stained Protein Ladder (Fermentas) was used as reference.

3.4.4 Western Blot

After protein lysates were separated by SDS-PAGE, proteins were transferred onto a PVDF membrane (activated for 1 min in methanol and washed with H_2O). Transfer was performed by wet or semi-dry blotting. For wet blotting, the immunoblot sandwich was assembled in a cassette in transfer buffer as follows (starting from the negatively charged site of the immunoblot chamber): one sponge, two Whatman filter paper, gel, PVDF

membrane, two Whatman filter paper, sponge. The cassette was placed into the tankblotter (VWR) which was filled with 1 X Tank blot buffer. Transfer was carried out at 280 mA for 2.5 – 3 h at 4 °C. Alternatively, semi-dry transfer was performed with the Trans-Blot® Turbo™ System (Biorad) according to the supplier's protocol and the pre-installed blotting programs for 1.5 mm mini gels (2.5 A, 25 V, 10 min). Afterwards, membranes were blocked in 5 % (w/v) BSA in TBS-T for 1 h under constant shaking at room temperature and subsequently incubated with the primary antibody at 4 °C overnight. Next day, membranes were washed with TBS-T three times 10 min followed by incubation in an HRP-coupled secondary antibody dilution (1:10,000 in TBS-T) and another three times 10 min washing steps. Antibody binding was visualised using the Immobilon Western Chemiluminescence HRP Substrate (Millipore Corporation) and detected with the LAS-4000 imager (Fujifilm).

3.4.5 Polysome profiling

For each condition, DLD1 cells were seeded in triplicates on 15 cm dishes at 50 % confluency and transfected with non-targeting siRNA or siRNA against *eIF3D* the next day (see section 3.1.6.2). After 48 h siRNA exposure, cells were treated with 25 µg/ml cycloheximide (CHX) in their respective medium for 5 min. Then, cells were washed and detached with 10 ml ice cold PBS supplemented with 100 µg/ml CHX / 15 cm culture dish and collected at 1,000 rpm for 5 minutes at 4°C. Lysis was performed by adding 200 µl Polysome Profile lysis buffer, freshly supplemented with 100 µg/ml CHX, 40 U/ml Ribolock RNase inhibitor and protease/phosphatase inhibitors (1:1000) followed by a 10 min incubation on ice. Cell debris was pelleted at 10,000 rpm for 10 min and 20 µl cleared lysate were kept as input. Remaining sample (≈ 180 µl) was layered on a 5-45 % linear sucrose gradient (100mM KCl, 20mM Tris pH 7.5, 5 mM MgCl2) and subjected to ultracentrifugation for 2 h at 34,500 rpm in a SW60 swing-out rotor (Beckmann Coulter). Gradients were harvested with a Biocomb PGFip Piston Gradient Fractionator into 12 x 300 µl fractions. Loading samples on gradient, ultracentrifugation and fractionation were performed by Dr. Cornelius Schneider (Group of Prof. Utz Fischer, Biocenter, University of Würzburg).

3.4.6 Puromycin labelling assay

A non-radioactive method for quantification of global protein synthesis can be achieved by measuring Puromycin incorporation into nascent polypeptide chains (E. K. Schmidt, Clavarino, Ceppi, & Pierre, 2009). Puromycin resembles the 3' end of (aa)tRNA, where a modified adenosine base is covalently linked to a tyrosine amino acid but with a different bond between amino acid and ribose (Aviner, 2020). Puromycin can enter the A-site of the ribosome and its free amino group binds to the nascent polypeptide chain of the peptidyl-tRNA at the ribosomal P-site. However, the peptide bond between the two moieties of Puromycin cannot be cleaved by another incoming aa-tRNA, thereby preventing additional extension, and leading to premature termination of translation. For Puromycin labelling, cells were treated with Puromycin (1 µg/ml) for 10 min at 37 °C (incubator), washed three times with 1 X PBS and incubated another 50 min at 37 °C. Then, cells were harvested in 1ml 1 X PBS and centrifuged 4 min at 4,000 rpm and 4 °C. Cell pellets were directly lysed in 1 X Laemmli buffer (1:10 volume (pellet:buffer)) and boiled at 95 °C for 10 min. Samples were subjected to SDS-PAGE (see section 3.4.3) and puromycylated peptides were detected by immunoblotting (see section 3.4.4) by using a Puromycin-specific antibody.

3.5 Proteomics

LC-MS/MS analysis of RNA-binding proteins identified by RNA pulldown (see section 3.3.9) was performed in collaboration with the group of Prof. Andreas Schlosser (Rudolf-Virchow Center, Würzburg). Gel electrophoresis, in-gel digestion, NanoLC-MS/MS Analysis and MS data analysis were executed by Stephanie Lamer as described in the following sections.

3.5.1 Preparation of protein lysates

For RNA pulldown lysates, cells were harvested and lysed in nuclease-free, ice-cold IP lysis buffer (25 mM Tris-HCl pH 7.4, 150 mM NaCl, 1 mM EDTA, 1 % (v/v) NP-40, 5 % (v/v) glycerol) supplemented with protease and phosphatase inhibitor cocktails. After 10 min incubation at 4 °C under constant shaking, the sample was centrifuged at maximum speed at 4 °C. Supernatant was transferred into a new reaction tube and

protein concentration was determined as described in section 3.4.2. Lysates were used for protein-RNA binding reaction as described in section 3.3.12.

3.5.2 Gel electrophoresis

Protein precipitation was performed overnight at -20 °C with 4-fold volume of acetone. Pellets were washed three times with acetone at -20 °C. Precipitated proteins were dissolved in NuPAGE® LDS sample buffer (Life Technologies), reduced with 50 mM DTT at 70 °C for 10 min and alkylated with 120 mM iodoacetamide at room temperature for 20 min. Separation was performed on NuPAGE® Novex® 4-12 % Bis-Tris gels (Life Technologies) with MOPS buffer according to manufacturer's instructions. Gels were washed three times for 5 min with H_2O and stained for 60 min with Simply Blue™ Safe Stain (Life Technologies). After washing with H_2O for 1 h, each gel lane was cut into fifteen slices.

3.5.3 In-Gel Digestion

The excised gel bands were destained with 30 % (v/v) acetonitrile in 0.1 M NH_4HCO_3 (pH 8), shrunk with 100 % (v/v) acetonitrile, and dried in a vacuum concentrator (Concentrator 5301, Eppendorf, Germany). Digests were performed with 0.1 µg trypsin per gel band overnight at 37 °C in 0.1 M NH_4HCO_3 (pH 8). After removing the supernatant, peptides were extracted from the gel slices with 5 % (v/v) formic acid and extracted peptides were pooled with the supernatant.

3.5.4 NanoLC-MS/MS Analysis

NanoLC-MS/MS analyses were performed on an Orbitrap Fusion (Thermo Scientific) equipped with a PicoView Ion Source (New Objective) and coupled to an EASY-nLC 1000 (Thermo Scientific). Peptides were loaded on capillary columns (PicoFrit, 30 cm x 150 µm ID, New Objective) self-packed with ReproSil-Pur 120 C18-AQ, 1.9 µm (Dr. Maisch) and separated with a 30 min linear gradient from 3 % to 30 % (v/v) acetonitrile and 0.1 % (v/v) formic acid and a flow rate of 500 nl/min. Both MS and MS/MS scans were acquired in the Orbitrap analyzer with a resolution of 60,000 for MS scans and

7,500 for MS/MS scans. HCD fragmentation with 35 % normalised collision energy was applied. A Top Speed data-dependent MS/MS method with a fixed cycle time of 3 s was used. Dynamic exclusion was applied with a repeat count of one and an exclusion duration of 30 s; singly charged precursors were excluded from selection. Minimum signal threshold for precursor selection was set to 50,000. Predictive AGC was used with AGC a target value of 2e5 for MS scans and 5e4 for MS/MS scans. EASY-IC was used for internal calibration.

3.5.5 MS data analysis

Raw MS data files were analysed with MaxQuant version 1.6.2.2 (Cox & Mann, 2008). Database search was performed with Andromeda, which is integrated in the utilised version of MaxQuant. The search was performed against the UniProt Human Reference Proteome database (January 2020, UP000005640, 74788 entries). Additionally, a database containing common contaminants was used. The search was performed with tryptic cleavage specificity with three allowed miscleavages. Protein identification was under control of the false-discovery rate (FDR; <1 % FDR on protein and peptide spectrum match (PSM) level). In addition to MaxQuant default settings, the search was performed against following variable modifications: Protein N-terminal acetylation, Gln to pyro-Glu formation (N-term. Gln) and oxidation (Met). Carbamidomethyl (Cys) was set as fixed modification. Further data analysis was performed using R scripts developed in-house. LFQ intensities were used for protein quantitation (Cox et al., 2014). Proteins with less than two razor/unique peptides were removed. Missing LFQ intensities were imputed with values close to the baseline. Data imputation was performed with values from a standard normal distribution with a mean of the 5 % quantile of the combined log10-transformed LFQ intensities and a standard deviation of 0.1. For the identification of significantly enriched proteins, median log2 transformed protein ratios were calculated from the two replicate experiments and boxplot outliers were identified in intensity bins of at least 300 proteins. Log2 transformed protein ratios of sample versus control with values outside a 1.5x (significance 1) or 3x (significance 2) interquartile range (IQR), respectively, were considered as significantly enriched in the individual replicates.

3.6 Transcriptomics

3.6.1 RNA-sequencing (RNA-seq)

3.6.1.1 RNA isolation and library preparation

The experiment was performed in triplicates for each condition. RNA was extracted using the RNeasy® Mini Kit (Qiagen) according to the manufacturer's protocol. In brief, cells were harvested and lysed by directly adding 600 µl RLT buffer (including β-2-mercaptoethanol), homogenised and frozen at - 80 °C. RNA was isolated, including an on-column DNase digestion step and eluted in 40 µl RNase-free H2O. 2.5 µl were quality-checked on a Bioanalyzer and 1 µg RNA was used for library preparation. cDNA library was generated using the NEBNext Ultra RNA library prep kit for Illumina with MagSi-NGSPREP Plus magnetic beads (magtivio) and NEBNext Multiplex Oligos for Illumina (Dual Index Primer Set 1) according to the manufacturer´s instructions. H_2O was used as negative control to check the purity of the preparation. PCR amplification of cDNA was performed in 14 cycles and PCR products were purified using MagSi-NGSPREP Plus magnetic beads. The quality of the purified DNA was verified on the Bioanalyzer, and all samples were mixed at equimolar concentration of 50 nM before sequencing was performed on the NextSeq 2000 system (Illumina).

3.6.1.2 Sequencing data analysis

RNA-seq data analysis was performed by Dr. Carsten Ade (Group of Prof. Martin Eilers, Biocenter, University of Würzburg) and the main steps are described in the following.

Following sequencing on the NextSeq2000 system (Illumina), base calling was done with Illumina's FASTQ generation software (bcl2fastq v1.1.0) and only high-quality PF-reads were demultiplexed and allocated to sample-specific FASTQ files. The quality of these FASTQ files was analysed with the program FastQC (v0.11.8). The reads in the FASTQ files were aligned to the human reference genome hg19 using the splice-aware mapper HISAT2 (v2.1.0) in a paired-end alignment approach with parameters that only reported concordant alignments. To quantify the number of read-pairs that aligned to distinct genes, the software featureCounts (v1.6.4) was used. The count tables generated by featureCounts for all mapped samples were joined into a tabular count matrix and annotated using the bioconductor tool annotateMyIDs (v3.7.0) to assign gene IDs, gene

names and gene symbols to the quantified read-pairs. To analyse sample correlations, PCA plots (principal component analysis) using ggplot2 (v2.2.1) and hierarchical clustering plots using hierarchical clustering (v1.0.0) were generated in an R environment. The differential expression analysis between conditions was calculated with the bioconductor software edgeR (v3.24.1) using default settings and applying the TMM method to estimate scale factors for the normalisation of samples. The gene expression fold-changes between samples that were calculated by edgeR were used to generate pre-ranked lists as input files for a subsequent gene-set enrichment analysis. To this end, the GSEA tool from the Broad Institute (v4.1.0) was used with the MSigDB (molecular signature database) collection (v7.4) (Liberzon et al., 2015; Subramanian et al., 2005) for hallmark gene sets (h) and ontology gene sets (c5).

3.6.2 CLIP-sequencing (CLIP-seq)

CLIP-seq experiments were performed in collaboration with the group of Prof. Mathias Munschauer (Helmholtz Institute for RNA-based Infection Research, Würzburg). Immunoprecipitation and library preparation were performed by Sabina Ganskih. Sequencing was performed by Dr. Carsten Ade and sequencing results were analyzed by Yuanjie Wei and Dr. Dimitrios Papadopoulos.

3.6.2.1 Crosslinking of cells

Cells were seeded on two 15 cm dishes and grown until they reached 70 – 80 % confluency. Then, culture medium was removed, cells were rinsed with ice-cold 1 X PBS and UV-crosslinked in the UVP crosslinker CL-1000 (analytic jena) with 0.4 J/cm2 UV light. Crosslinked cells were scraped off the plate in 3 ml ice-cold PBS and collected by centrifugation at 400 x g for 5 min and 4 °C. Cell pellet was washed with 10 ml ice-cold PBS, centrifuged again at 400 x g for 5 min and 4 °C and frozen at -80 °C until further use.

3.6.2.2 eIF3D immunoprecipitation

CLIP protocol was adapted from (Van Nostrand et al., 2016), and modifications are briefly described as follows. Frozen cell pellets were lysed in 2 X CLIP lysis buffer (100 mM Tris-HCl pH 7.4, 300 mM NaCl, 2 mM EDTA, 2 % (v/v) NP40, 1 % (w/v) sodium deoxycholate, 0.5 mM DTT), incubated for 30 min at room temperature, centrifuged and stored at – 80 °C. To adjust lysis buffer to a 1 X concentration, an equal amount of nuclease-free H2O was added to frozen lysates. Immunoprecipitates were washed twice with 1 ml of 1 X CLIP lysis buffer, twice in immunoprecipitation wash buffer (50 mM Tris-HCl pH 7.4), 300 mM NaCl, 1 mM EDTA, 1 % (v/v) NP40, 0.5 % (w/v) sodium deoxycholate, 0.25 mM DTT), followed by two washing steps in 50 mM Tris-HCl pH 7.4), 1 mM EDTA and 0.5 % (v/v) NP40. All other steps were carried out as described in the eCLIP protocol (Van Nostrand et al., 2016). For one immunoprecipitation reaction, 5 µg EIF3D antibody (Abcam) and 50 µl beads per mg protein were used and RNA dephosphorylation was carried out using FastAP (Thermo Scientific). Samples were loaded onto E-Gel™ EX agarose gels (Invitrogen™) and gel extraction was performed with Zymoclean Gel DNA Recovery Kit (Zymo Research).

3.6.2.3 Library preparation and sequencing

RNA was purified and cDNA was synthesised as described in (Van Nostrand et al., 2016). Quality of cDNA library was checked on the Bioanalyzer and sequencing was performed on the NextSeq 2000 system (Illumina).

3.6.2.4 Sequencing data analysis

Data analysis from CLIP-seq was performed as described in (Gonzalez-Perez et al., 2021) or (N. Schmidt et al., 2021) and main steps are described in the following. Paired-end sequencing reads were trimmed using a custom Python script that simultaneously identified the unique molecular identifier (UMI) associated with each read. Trimmed reads were then aligned to the human genome (Hg38/Ensembl v100) using the Burrows-Wheeler Aligner (H. Li & Durbin, 2009) and PCR duplicates were removed using the UMI-aware deduplication functionality in Picard's MarkDuplicates. The generated .bam files were converted to .bw (bigwig format) using bamCoverage (Ramirez et al., 2016)

for visualisation. The enriched region of eIF3D binding sites was identified as peaks that were enriched against a size-matched input (SMI) control. MACS2 (version 2.2.7.1) callpeak (Y. Zhang et al., 2008) was used with the parameters -f BAM –keep-dup all –nomodel –extsize 50 –d-min 5 –scale-to small -B. Visualisation of binding regions was rendered from .bw files using the Integrative Genomics Viewer (IGV).

3.7 Statistics

Statistical analyses were performed using GraphPad Prism v9.4.1 (Dotmatics). All data are presented as mean ± standard deviation (SD) and sample sizes are indicated in figure legends. Significance between groups was tested by two-tailed Student's t-test and significance levels were set at *$0.01 < p < 0.05$, **$0.001 < p < 0.01$, *** $p \leq 0.001$.

4 Results

4.1 *MYC* expression is maintained under inhibition of cap-dependent translation

Preliminary work has shown that *MYC* is, among others, deregulated at the post-transcriptional level in CRC, and this is most likely via mRNA translation rather than MYC stability (Wiegering et al., 2015). However, it has been shown that inhibition of cap-dependent translation alone does not lead to the expected reduction in *MYC* expression. More specifically, the use of the dual PI3K/mTOR inhibitor BEZ235 consistently led to enhanced *MYC* expression at 500 nM in CaCo2, SW620, LS174T and HCT116 CRC cells. To test another CRC cell line carrying the most common mutations found in CRC (amongst others, *APC*, *KRAS*, *TP53*), DLD1 were treated with the PI3K/mTOR inhibitor. Again, MYC expression was increased at 50, 200, and 500 nM BEZ235 (**Figure 10 (A)**). The inhibition of the pathway was tested using the downstream target S6, whose phosphorylation by S6 kinase (S6K) is thought to initiate cap-dependent cellular translation but generally used as read-out for mTOR complex (mTORC) activity (Bohlen, Roiuk, & Teleman, 2021; Ruvinsky & Meyuhas, 2006). Already at a concentration of 50 nM BEZ235, no phosphorylation of S6 (P-S6) could be detected at the protein level (**Figure 10 (A)**). To test whether *MYC* is indeed translated independently of the eIF4F complex in CRC, an eIF4E-binding protein mutant (pCW57.1-4EBP1_4xAla; (Thoreen et al., 2012)), carrying alanine substitutions at four serine/threonine residues that are targets for mTORC1-dependent phosphorylation, was overexpressed in DLD1 cells (DLD1-4EBP1-4A). The mutation prevents phosphorylation of 4EBP1, which in the hypo-phosphorylated state binds increasingly to eIF4E and prevents recruitment of other components of the eIF4F complex, such as eEIF4A and G (Gingras, Gygi, et al., 1999). Induction of the mutant should therefore lead to a shut-down of cap- or eIF4F- dependent translation, respectively. Expression of exogenous 4EBP1-4A was induced by increasing concentrations of doxycycline (DOX), and protein levels exceeded those of endogenous 4EBP1 at concentrations as low as 0.01 ug/ml. Surprisingly, this had no effect on MYC expression compared to the DMSO-treated control (**Figure 10 (B)**).

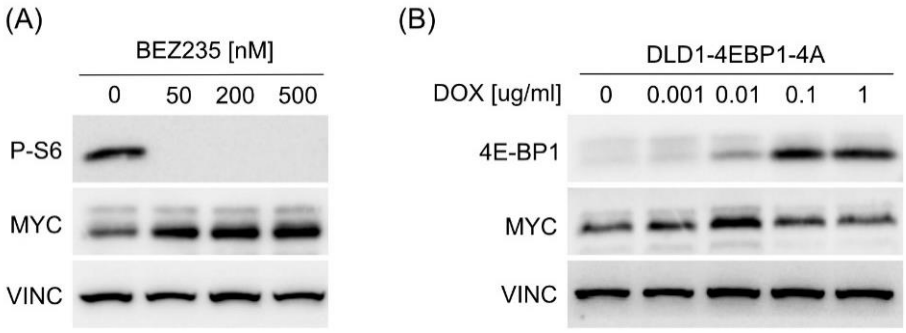

Figure 10: MYC levels are maintained upon inhibition of cap-dependent translation. *(A) DLD1 cells were treated with indicated concentration of BEZ235 for 24 h and representative immunoblot analyses are shown. n = 2. (B) A non-phosphorylatable form of 4EBP1 (4EBP1-4A) was inducibly overexpressed in DLD1 cells and immunoblot analyses were performed at indicated concentrations of doxycycline (DOX) after 24 h. n = 2. Vinculin (VINC) was used as loading control.*

To investigate the involvement of eIF4F in the translation of MYC more closely, individual components of the complex were depleted in the next step. DLD1 cells were treated for 48 h with siRNAs against *EIF4A*, *EIF4E* and *EIF4G* and MYC expression was analysed at the protein level. Interestingly, none of the knockdowns led to a reduction in MYC levels (**Figure 11**).

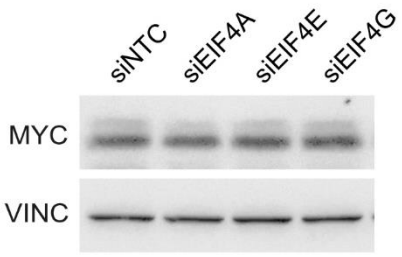

***Figure 11**: **MYC levels are maintained upon disruption of the eIF4F complex.** (A) DLD1 cells were treated with indicated siRNAs for 48 h and representative immunoblot analyses are shown. n = 2.*

The stable expression of MYC after inhibition of a pathway that contributes to canonical translation initiation and the independence of MYC expression on the eIF4F complex suggests an alternative mechanism of translation initiation for *MYC*, which will be explored in more detail in the following chapters.

4.2 Published *MYC* IRES inhibitors affect various cellular functions

The majority of cellular mRNAs possess numerous regulatory sequences in their 5' and 3' UTRs, which lead to an adaptation of the translation of the corresponding mRNA under different cellular conditions. *MYC* was shown to harbour an IRES in its 5’ UTR which under stress conditions or in certain types of cancer contributes to enhanced expression of this oncogene. To test the hypothesis that *MYC* is translated in a cap-independent way via its IRES, a CRISPR/Cas9-induced 250 bp deletion within the *MYC* 5' UTR was generated and evaluated in previous work. The deletion resulted in a substantial reduction in MYC protein levels, with no direct correlation to *MYC* mRNA expression (Sarah Denk, 2017). This led to the assumption that the *MYC* 5' UTR or a part of it plays an essential role in the translation of the transcription factor in CRC.

4.2.1 MYC IRES inhibitor J007 has no effect on *MYC* expression in CRC cells

As already mentioned in the introduction, (*MYC*) IRES-mediated translation relies on several ITAFs for optimal function. For example, in MM it was shown that *MYC* expression increases with progressive disease, and this is accompanied by increasing *hnRNP A1* expression (Shi et al., 2022). A1 belongs to the group of heterogeneous nuclear ribonucleoproteins which are associated with pre-mRNAs in the nucleus, thereby influencing processing and transport of the latter (Clarke, Thibault, Salapa, & Levin, 2021). Shi *et al.* demonstrated that hnRNP A1 acts as ITAF by binding to the *MYC* IRES, and *A1*-depleted MM cells showed decreased MYC expression and inhibition of growth (Shi et al., 2008; Shi et al., 2022). In order to chemically inhibit hnRNPA1-IRES interaction, the small molecule inhibitor J007-IRES was developed and utilised to block IRES-dependent translation of *MYC* in GB and MM cells (Holmes et al., 2016; Shi et al., 2022). To investigate a potential effect of J007-IRES in CRC, DLD1 cells were treated with the inhibitor at concentrations from 200 – 600 nM for 24 h. Even at the highest concentration, J007-IRES had only a negligible effect on MYC protein abundance (**Figure 12**). This led to the assumption that hnRNP A1 inhibition alone does not influence *MYC* translation in CRC.

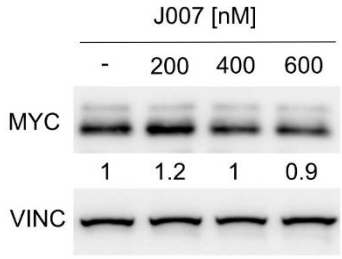

***Figure 12**: **MYC IRES inhibitor J007 has no effect on MYC expression in CRC cells.** DLD1 cells were treated with J007 at indicated concentrations for 24 h and representative immunoblot and quantification of two experiments is shown. Vinculin was used as loading control.*

4.2.2 Cymarin induces downregulation of MYC expression in CRC cells

To address the demand for inhibitors of IRES-mediated-/cap-independent translation initiation, Didiot *et al*. developed a click beetle, dual luciferase cell-based assay and identified a series of small molecules as inhibitors of IRES-directed translation (Didiot et al., 2013). In the screen, cymarin, a plant-based compound from the genus *Apocycnum*, was identified as one of the most promising compounds (Tilford, 1997). Cymarin has been used primarily in patients with congestive heart failure and cardiac arrhythmias and thus belongs to the group of CGs. In principle, its mode of action is to slow down the heart rate by inhibiting the cell membrane-localised sodium-potassium ATPase and thus increase the output force (Patel, 2016). However, a wide variety of biochemical effects have been attributed to CGs and thus have also been suggested to be used as anti-cancer drugs (Riganti et al., 2011). Indeed, treatment with cymarin resulted in decreased MYC protein expression and induction of apoptosis in ovarian cancer cell lines (Didiot et al., 2013). To evaluate a potentially equal effect of the CG in CRC cell lines, DLD1 and LS174T were treated with 10 – 100 nM cymarin, and MYC protein and mRNA expression were analysed after 8 h. In both cell lines, low concentrations of cymarin (10 and 30 nM) led to a slight upregulation of MYC protein expression. However, a significant dose-dependent reduction in MYC protein level could be observed at ≥ 50 nM cymarin (**Figure 13 (A)**). However, cymarin had no effect on *MYC* mRNA expression in DLD1 cells at neither concentration. In contrast, LS174T showed stronger downregulation of *MYC* RNA expression which correlated with reduced MYC protein expression (**Figure 13 (B)**).

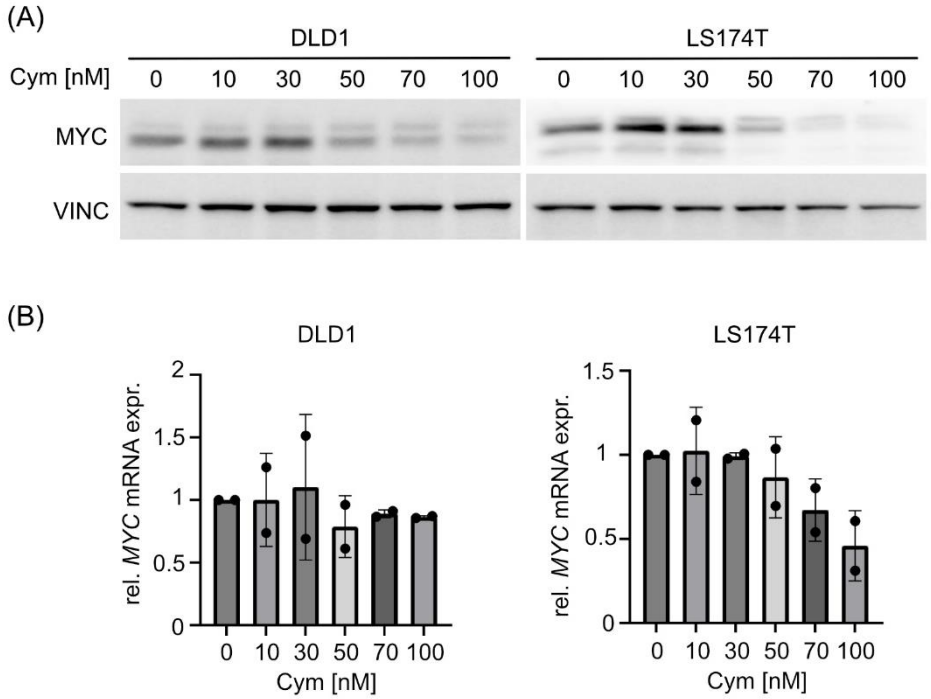

Figure 13: Cymarin induces downregulation of MYC expression. *(A) DLD1 and LS174T cells were treated with indicated concentrations of cymarin (Cym) for 8 h and representative immunoblot analyses are shown. Vinculin was used as loading control. (B) DLD1 and LS174T cells were treated with indicated concentrations of cymarin (Cym) for 8 h and subjected to qRT-PCR analysis. Shown is mean ± SD (n = 2, each measurement was performed in technical triplicates).*

4.2.3 Cymarin impacts proliferation by inducing cell cycle arrest in CRC cells

To further investigate the effect of cymarin on proliferation and viability, DLD1 cells were treated with 50, 70 and 100 nM cymarin over five days and cell number was determined every day. A strong proliferation arrest upon 50, 70 and 100 nM cymarin could be observed from day three on (**Figure 14 (A)**). However, there was no increase in apoptosis upon cymarin treatment for 72 h compared to control cells (10.7 % apoptotic cells) **(Figure 14 (B)**). Instead, a decrease to 6.4, 8.7, and 10.8 % at 50, 70 and 100 nM, respectively, could be observed being only significant at 50 nM cymarin. As induction of apoptosis could be excluded as cause of the lower cell numbers, a PI cell cycle analysis was performed to investigate potential effects leading to growth arrest. By combining data obtained from the growth curve (**Figure 14 (A)**) with PI cell cycle analysis, the length

of the different cell cycle phases was calculated. Indeed, cymarin treatment for 72 h led to a prolongation of all cell cycle phases (**Figure 14 (C)**). In detail, 50 nM cymarin led to 2-, 2.2- and 5.7-fold increased duration of G1, S and G2/M phase, respectively. The effect was even stronger at 70 nM cymarin where the different phases were found to be prolonged 12.2-, 10.8-, and 11.9-fold, respectively.

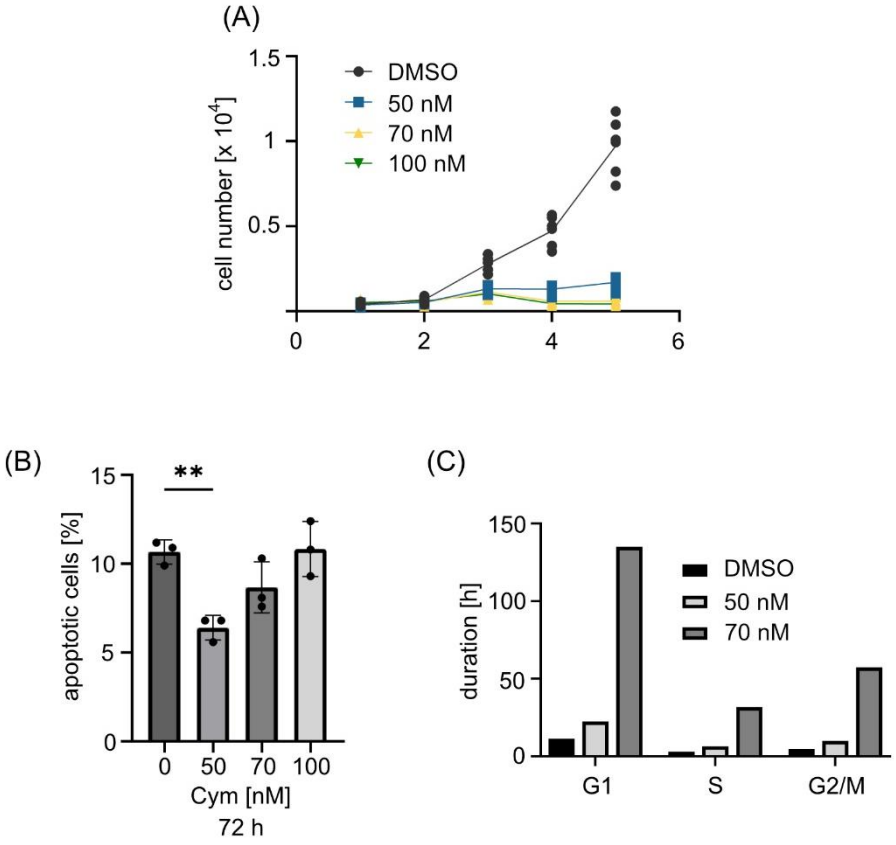

***Figure 14**: **Cymarin treatment impairs proliferation of CRC cells.** (A) DLD1 cells were treated with indicated concentrations of cymarin (Cym) for four days and cell number was normalised to day 1. Summary of two independent experiments is shown. (B) AnnexinV/PI FACS of cymarin-treated DLD1 cells was performed after 72 h. Results represent mean ± SD (n = 3). (C) cell cycle analysis was performed after 72 h and duration of each cell cycle phase was calculated by including data from growth curve.*

4.2.4 Cymarin impacts viability and MYC expression in PDOs

To test whether the cymarin-induced phenotype on MYC protein expression and proliferation is limited to 2-D cell culture or transferrable to 3-D organoid models, two human patient-derived colon cancer organoid lines (T4 and T5) with different mutation background were utilised. Panel-seq revealed T4 being mutated for *PIK3CA*, *APC* and

RB1 and T5 being mutated for *PIK3CA*, *APC*, *MET* and *TP53* (S. Schmidt et al., 2019). Treatment with cymarin at doses from 30 – 100 nM for 8 h strongly repressed MYC protein abundance in both lines, and the effect was more pronounced in T5 organoids **(Figure 15 (A)**).

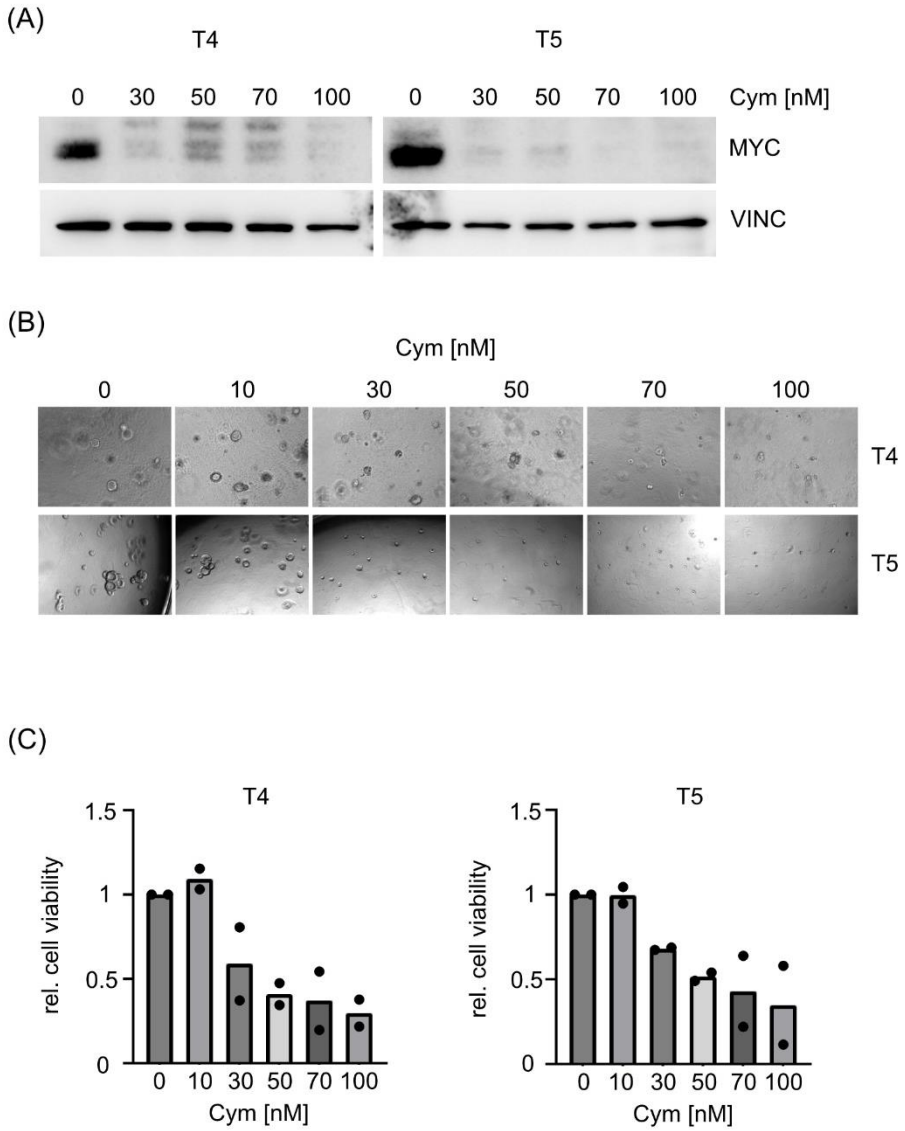

***Figure 15: Cymarin downregulates MYC expression and impairs viability of patient-derived CRC organoids (PDOs)**. (A) Immunoblot analyses of T4 and T5 PDOs treated with indicated concentrations of cymarin (Cym) for 8 h are shown. Vinculin was used as loading control. (B) T4 and T5 PDOs were treated with indicated concentration of cymarin for three days and representative pictures from two independent experiments are shown. (C) Cell Titer Glo Assay was performed after three days cymarin treatment in T4 and T5 PDOs and results represent mean ± SD (n = 2, measurements were performed in five technical replicates).*

Furthermore, a dose-dependent reduction in cell viability could be observed in both organoid lines (**Figure 15 (C)**). In T4 organoids, viability decreased significantly from a concentration of 30 nM, reaching only 59, 41, 37.1 and 29.8 % at 30, 50, 70 and 100 nM cymarin, respectively, compared to DMSO-treated control. T5 organoids reacted to cymarin in a similar way and showed 68, 51.6, 42.9, 34.8 % viable cells at 30, 50, 70 and 100 nM cymarin, respectively, compared to control-treated cells (**Figure 15 (C)**). The effect on viability was also reflected by reduced organoid formation (**Figure 15 (B) + (C)**). In summary, organoids showed a comparable downregulation of MYC protein abundance as it was observed in tested CRC cell lines. Additionally, viability was significantly impacted in organoids which could be due to an increase in apoptosis or slowed proliferation as observed in 2-D cell lines. However, this was not further analysed here.

4.2.5 Cymarin affects MYC expression independently of its UTRs

As Didiot *et al*. showed that cymarin regulates translation of a bicistronic reporter construct harbouring the *MYC* IRES sequence (Didiot et al., 2013) this raised the question whether cymarin could affect *MYC* expression similarly in CRC. In order to evaluate the regulatory mechanism, exogenous *MYC* constructs were used to test their regulation under cymarin treatment. They comprised either the *MYC* coding sequence (CDS) alone, starting from the canonical AUG site or the CDS with 5' UTR or 3' UTR (Dejure et al., 2017) **(Figure 16 (A)**). If cymarin controls *MYC* expression via the 5' UTR, it would be expected that the expression of this exogenous construct is reduced after cymarin treatment. In contrast, the other two constructs containing only the CDS or the CDS with 3' UTR should be able to rescue this effect. The transgenes were expressed in a DOX-inducible manner and C-terminally HA-tagged to discriminate between the endogenous and exogenous form of MYC. DLD1 cells expressing either of these constructs were generated, and protein and mRNA expression of exogenous *MYC* were analysed after 8 h DOX and cymarin treatment, respectively. Consistent with previous data, cymarin decreased endogenous total MYC protein at all concentrations applied (**Figure 16 (B)**). However, exogenous MYC-HA expression was reduced by cymarin as well, although to a lesser extent. In detail, 50 and 70 nM cymarin led to a 10 and 20 % reduction in MYC-HA protein expression of both 5’ and 3’ UTR constructs, whereas with the MYC-CDS construct exogenous MYC was reduced by 20 and 50 %, respectively.

Thus, it can be assumed that cymarin in this cell system does not regulate MYC expression via its 5' UTR (or IRES) but rather via post-translational mechanisms.

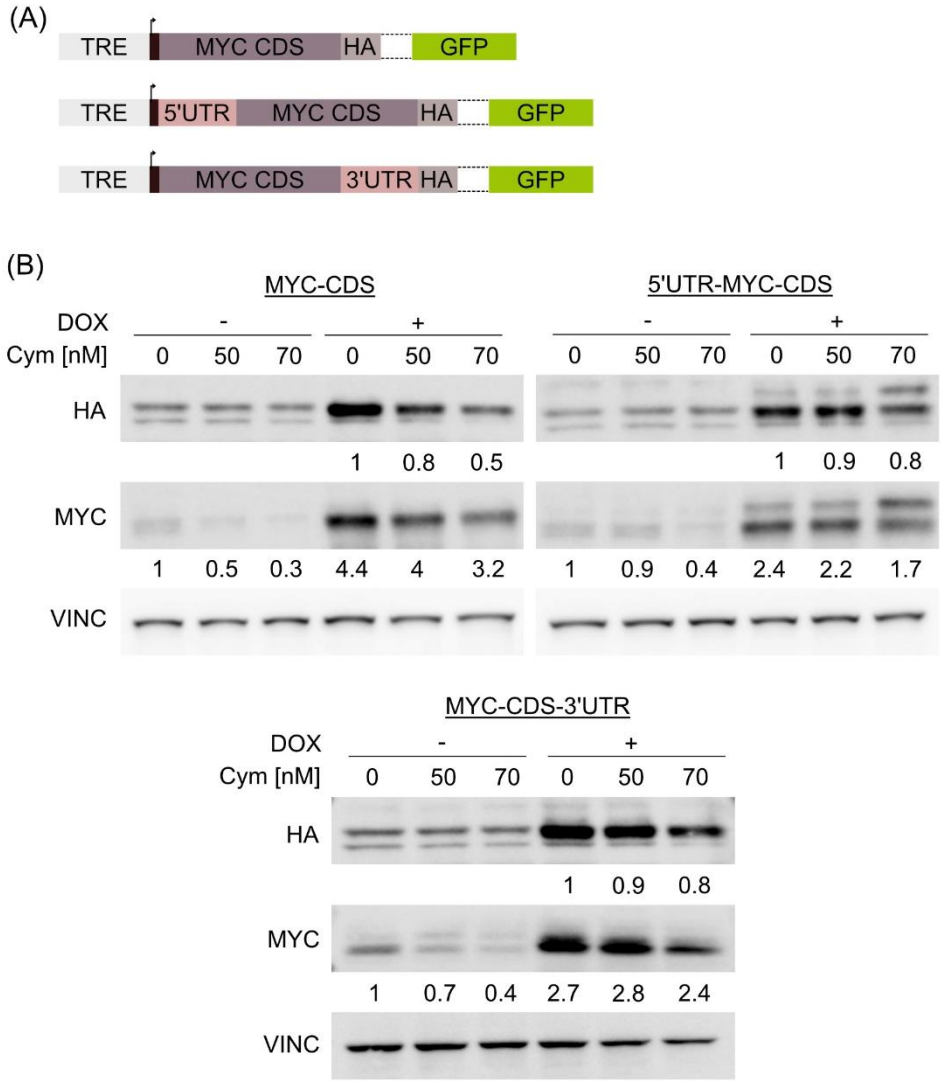

Figure 16: Cymarin affects MYC expression independently of its 5' and 3' UTR. *(A) Scheme of doxycycline (DOX)-inducible and HA-tagged MYC overexpression constructs which were stably integrated into DLD1 cells. (B) - (D) Representative immunoblots (n = 3) of DLD1 cells harbouring either of the constructs shown in (A). Exogenous MYC was induced by 0.5 µg/ml DOX for 8 h and at the same time cells were treated with cymarin (Cym) at indicated concentrations. Numbers represent relative MYC and MYC-HA levels, quantified from three independent experiments. Vinculin was used as loading control.*

4.2.6 Cymarin does not affect MYC stability

Since cymarin regulated MYC expression independently of its UTRs, the question arose whether cymarin is involved in MYC degradation in a proteasome-dependent manner. DLD1 cells were treated with 50, 70 or 100 nM cymarin and, in addition, the proteolytic function of the proteasome (Kisselev & Goldberg, 2001) was blocked by the inhibitor MG132 (20 µM, 3 h). MYC protein levels decreased at increasing concentrations of cymarin and could not be rescued by proteasomal inhibition (**Figure 17**). Thus, increased proteasomal degradation could be excluded as potential reason for reduced MYC protein expression.

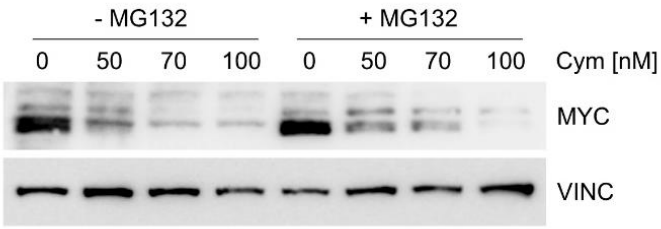

Figure 17: Cymarin does not affect MYC degradation. *DLD1 cells were treated with cymarin (Cym) at indicated concentrations for 8 h and in addition proteasomal degradation was blocked by 20 µM MG132 for 3 h. n = 1. Vinculin was used as loading control.*

4.2.7 Cymarin globally reduces *de novo* protein synthesis

As a transcription factor and oncogene *MYC* has multiple cellular functions, and deregulated expression can therefore lead to severe changes in cellular homeostasis. Independently of that, cymarin was primarily found to inhibit the activity of the cellular sodium-potassium ATPase which performs several functions in the cell like maintaining the resting potential, involvement in transport or acting as signal transducer/integrator to regulate, for example, the MAPK pathway or intracellular calcium signalling (Ozaki, Nagase, & Urakawa, 1984; Reddy, Kumavath, Barh, Azevedo, & Ghosh, 2020). Since the MAPK pathway is known to play a regulatory role in cap-dependent translation (Roux & Topisirovic, 2012), and MYC itself can do so as well (van Riggelen et al., 2010), it should be examined whether cymarin, in addition to MYC expression, influences global protein synthesis. To test this, a puromycin labelling assay was performed as described in section 3.4.6 to visualize total *de novo* protein synthesis. Puromycin incorporation into

growing polypeptide chains was analysed upon increasing concentrations of cymarin. At all concentrations applied, cymarin led to a significant decrease of puromycin incorporation with 40, 60, and 70 % reduced *de novo* protein synthesis at 50, 70, and 100 nM cymarin, respectively (**Figure 18**). From this result, it cannot be deduced whether this effect is due to the reduced MYC protein expression, but it suggests that cymarin causes a global change in protein synthesis.

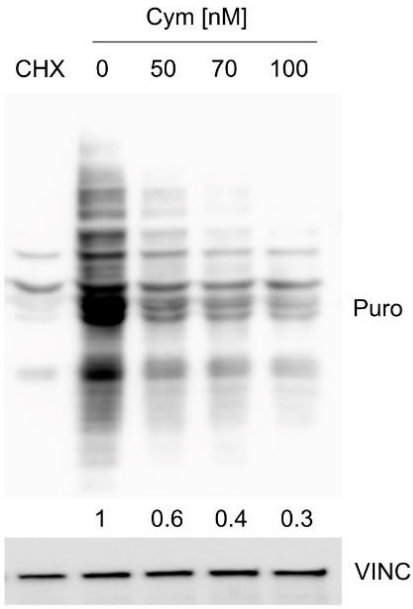

Figure 18: Cymarin impacts global de novo protein synthesis. *DLD1 cells were treated with cymarin at indicated concentrations for 8 h and puromycin incorporation was analysed by immunoblotting. 50 µg/ml cycloheximide (CHX) was used as positive control by inhibiting translation elongation. Numbers represent relative puromycin incorporation quantified from two independent experiments. Vinculin was used as loading control.*

4.2.8 Cymarin regulates immune signalling pathways

To further investigate the global effects of cymarin, an RNA-seq experiment in DLD1 cells treated with 100 nM cymarin for 72 h was performed as described in section 3.6.1. Sequencing data were subjected to Gene Set Enrichment Analysis (GSEA) and hallmark gene sets were examined. Surprisingly, no down-regulated gene sets were identified in neither condition compared to DMSO-treated control cells; instead, immune signalling-related gene sets in particular were affected and upregulated by cymarin (**Figure 19**). ‘TNFα signaling via NFκB’ was the most upregulated gene set, followed by ‘Inflammatory

response'. Furthermore, 'IL6-JAK-STAT3 signaling' and 'IL2-STAT5 signaling' were found among the strongest regulated hallmark gene sets at 100 nM cymarin. Additionally, 'Apoptosis' showed a relatively high normalised enrichment score (NES) and especially inhibitors (e.g. *JUN*, *BCL-2*, *BIRC3*, *MCL-1*) as well as activators of cell death (e.g. *BCL2L11*, *CASP2*, *PEA*-15, *DIABLO*) were upregulated. In addition, cell cycle regulators like *CDKN1B*, *CDKN1A*, or *WEE1* appeared in the list of upregulated genes. Surprisingly, hallmark gene sets MYC targets (v1 and v2) were not significantly changed compared to DMSO-treated cells (FDR > 0.6), although MYC protein level were consistently reduced in these conditions (**Figure 13 (A)**).

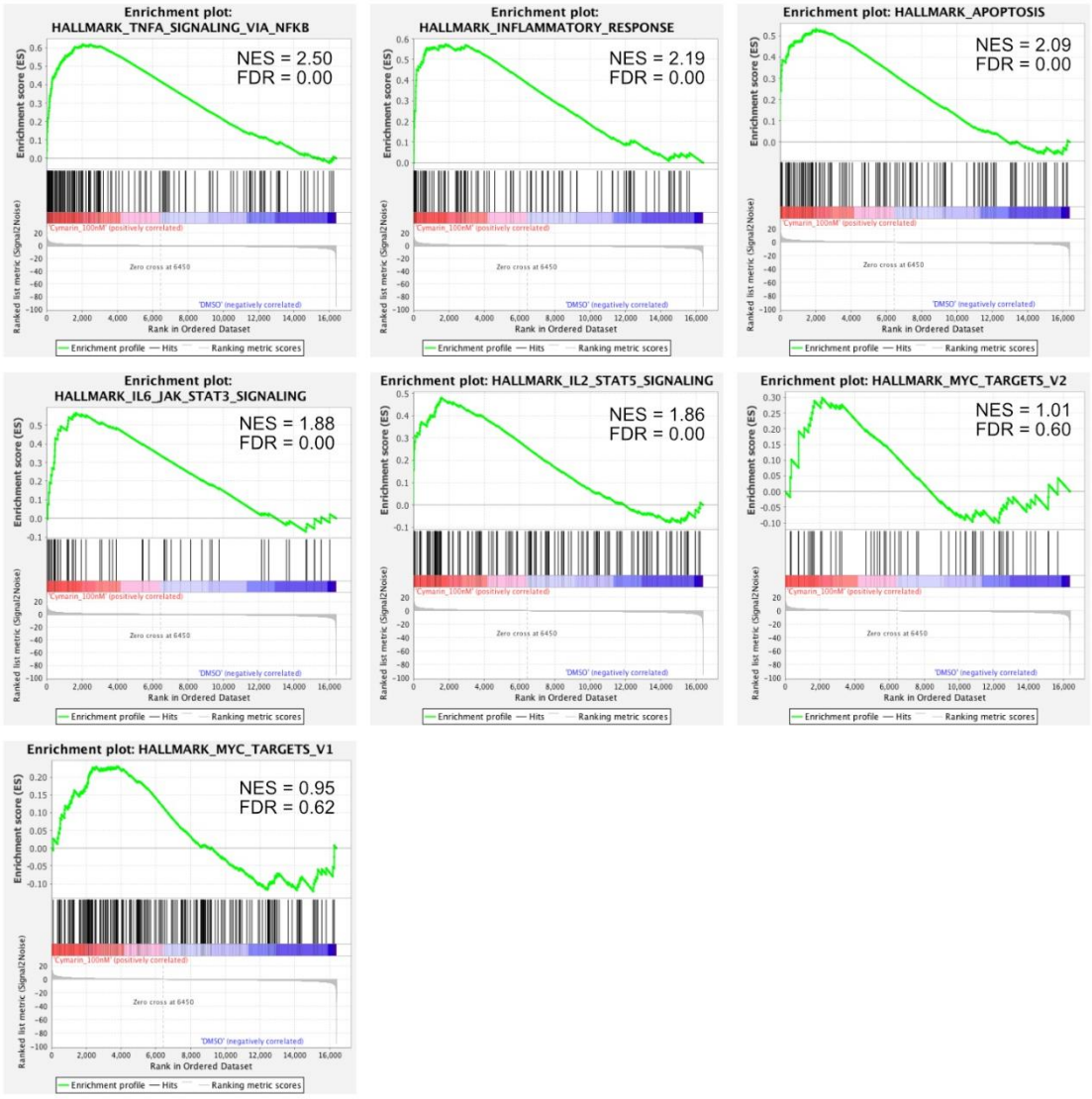

***Figure 19: Cymarin predominantly activates genes associated with immune signalling**. GSEA analysis from RNA-seq data obtained from DLD1 cells treated with 100 nM cymarin for 72 h. n = 3. NES = normalised enrichment score, FDR = False Discovery Rate.*

The RNA-seq experiment clearly showed that cymarin treatment causes much larger and more complex changes in CRC cells, which cannot be entirely attributed to altered translation of *MYC*. However, as this work aims to elucidate the mechanism and relevance of 5' UTR-mediated translation of *MYC*, the mechanism by which the cardiac glycoside exerts its cellular effects especially on immune signalling pathways was not further pursued here.

In summary, neither J007-IRES nor cymarin regulate translation of *MYC* in CRC. Nevertheless, the question remains how MYC expression can be maintained after global inhibition of eIF4F-dependent translation.

4.3 RNA pulldown reveals numerous *MYC* 5’ UTR-binding factors that have the potential to regulate *MYC* expression

4.3.1 *In vitro* RNA pulldown identifies already known and new *MYC* 5’ UTR binding proteins

As shown in the previous sections, cymarin and J007-IRES do not have an effect on *MYC* translation in CRC. Therefore, it is still largely unclear how the non-canonical translation of MYC in CRC is accomplished and which factors are involved in this pathway. It was previously shown that the oncoprotein CIP2A regulates the translation of *MYC* via its 5' UTR and knockdown of *CIP2A* leads to reduced MYC protein synthesis and decreased proliferation of CRC cells (S. Denk et al., 2021). Based on that, the question arose whether there could be additional factors responsible for alternative translation of *MYC* that contribute to its 5’ UTR-dependent and possibly eIF4F-independent translation. To address this, an *in vitro* RNA pulldown experiment with subsequent LC/MS proteome analysis was performed as illustrated in **Figure 9** and described in section 3.3.9. As template for the *in vitro* transcription reaction, 377 bp of the *MYC* 5’ UTR were amplified from pInducer21 HA-5’UTR-MYC-3’UTR using primers #1 and #2 and an unrelated poly(A)$_{25}$ RNA was treated in parallel during the procedure to exclude unspecific binders. In total, 370 *MYC* 5’ UTR-binding proteins were identified by LC/MS measurement from two independent replicates and from those, a total of 69 hits could be filtered out that were significantly enriched in two replicates (**Figure 20**). Interestingly, many factors emerged that have been previously identified as IRES-transacting factors and are thus thought to play a role in the regulation of 5' UTR-

mediated translation of various mRNAs. Just to mention few, NCL (*p53*, *VEGFD*) (Morfoisse et al., 2016; Takagi, Absalon, McLure, & Kastan, 2005), HNRNPM (*FGF1*) (Ainaoui et al., 2015), RPS19 (*BAG1*) (Horos et al., 2012), ILF3 (*p53*) (Halaby, Harris, Miskimins, Cleary, & Yang, 2015), RPL26 (*p53*) (Takagi et al., 2005), and HNRNPD (*NRF*) (Omnus et al., 2011; Reboll et al., 2007) have previously been attributed a role as ITAFs for different mRNA targets (*in brackets*) contributing to their translation under different cellular conditions or diseases. Interestingly, SFPQ, YBX1, GRSF1, NONO (Cobbold et al., 2008), HNRNPA1 (Jo et al., 2008) and PTBP1 (Cobbold et al., 2010) have previously been attributed a role as *MYC* 5' UTR regulators and their appearance in the screen speaks for the reliability of the result.

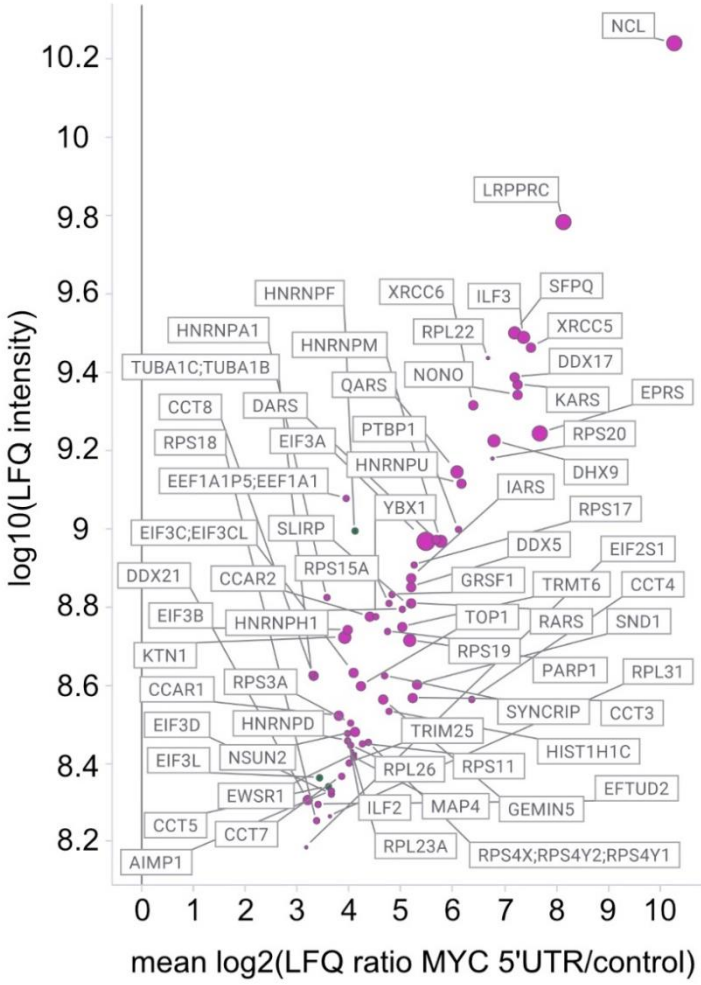

***Figure 20**: **In vitro RNA pulldown identifies MYC 5'UTR-binding proteins**. Scatter plot of 69 proteins specifically binding the MYC 5' UTR over the unrelated poly(A)25 control RNA. Mean of two biological replicates is shown, visualised with TIBCO Spotfire. The size of the circle is an indication of how many peptides have been identified for the respective protein.*

In addition, numerous translation (initiation) factors could be identified, in particular several subunits of the eIF3 complex (eIF3A, B, C, D, L) as well as various RPs of the small (RPS3A, 4X, 11, 15A, 17, 18, 19, 20) and large ribosomal (RPL22, 23A, 26, 31) subunit.

For more detailed functional analysis, the identified binding proteins were grouped according to their protein class by Gene Ontology (GO) analysis using PANTHER (pantherdb.org). Not surprisingly, most of the identified *MYC* 5 'UTR binding proteins were translation (initiation) factors (41.4 %), followed by RNA metabolising/processing proteins (25.7 %) and chaperones (7.1 %) (**Figure 21**). The remaining binding proteins were associated with DNA metabolism (5.7 %) and protein-modifying enzymes (2.9 %) as well as transport proteins, transcription regulators and cytoskeletal proteins, which each accounted for 1.4 %. The function of the proteins and the fact that many have been previously identified as ITAFs suggests that the pulldown worked technically well and can serve as a reliable basis for further validation experiments.

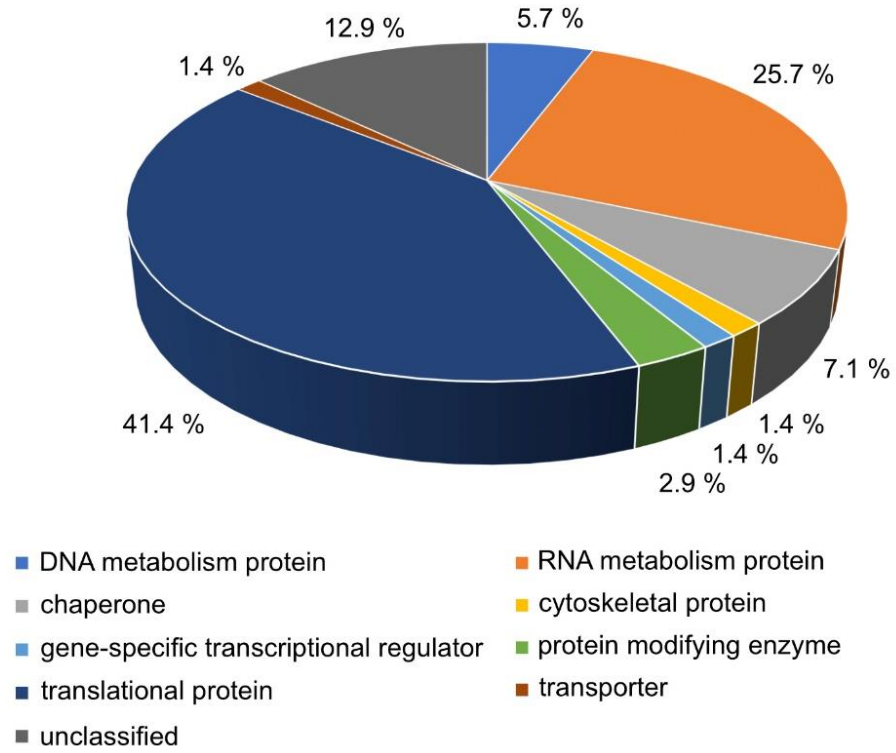

Figure 21: PANTHER classification of identified MYC 5'UTR-binding proteins reveals their cellular function.

4.3.2 siRNA screen identifies negative regulators of *MYC* expression

To further investigate the influence of the newly discovered *MYC* 5' UTR binding proteins on *MYC* translation, an siRNA screen was performed by Dr. Christina Schülein-Völk and Dr. Ursula Eilers as described in section 3.3.13 and MYC protein expression was analysed by IF staining at the Operetta screening microscope. An siRNA against *MYC* served as a positive control for the downregulation of MYC expression, and a non-targeting control siRNA (siCTR) was used as a negative control. MYC expression among all tested siRNAs was normalised to siCTR and the mean of three independent experiments was taken. The hits were sorted according to their efficiency to reduce MYC protein abundance and all those that resulted in > 50% reduction were considered highly interesting. Those were siRNAs against *RPL23A*, *EIF3D*, *RPS11*, *RPS15A* and *RPS20*, which downregulated MYC by a mean of 58.7, 55.8, 55, 53.1 and 52.3 %, respectively (**Figure 22).** In addition, *RPS17* and *RPS19* were considered interesting targets, as they were responsible for a reduction in MYC expression by 49.5 and 45.9 %, respectively. Besides that, eIF3B, another subunit of the eIF3 complex, reduced MYC expression by 46.1 %. In addition, the screen also identified factors whose knockdown led to an upregulation of MYC expression compared to siCTR (**Figure 22**). These included HNRNPA1, NONO, GRSF1, GEMIN5 and ILF3 which led to an increase by 2, 2.3, 4.4, 5.9 and 12.5 %, respectively.

The top MYC “down regulators” (meaning that they are actually promoting MYC expression when present) identified in the screen were subsequently subjected to further validation experiments.

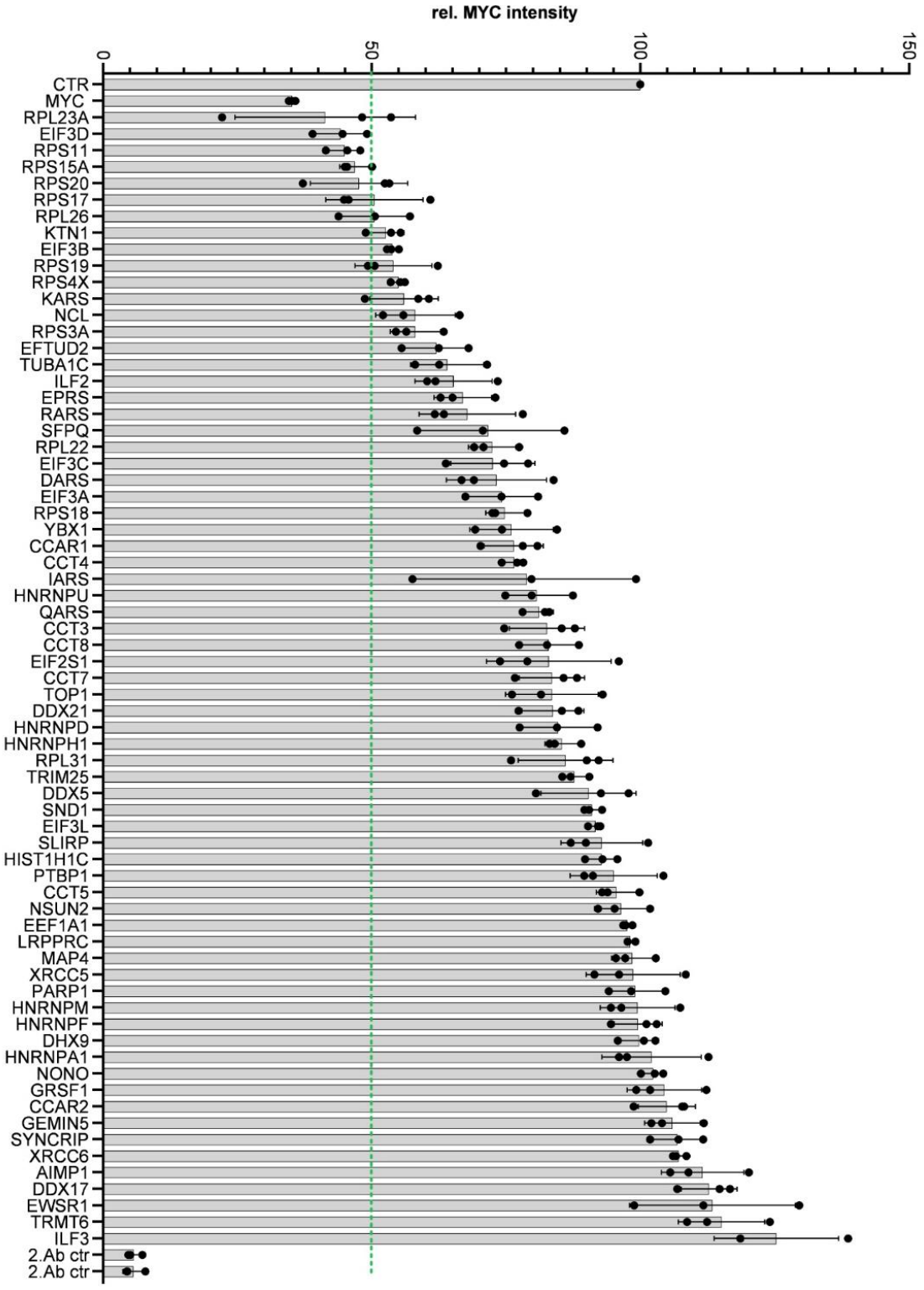

Figure 22: Hit validation of previously identified MYC 5' UTR-binding proteins and their effect on MYC protein expression. *DLD1 cells were transfected with siRNA pools against 69 hits from pulldown and MYC expression was analysed 72 h after transfection. MYC staining intensity was normalised to siCTR. Results represent mean ± SD of three independent experiments. Green dashed line illustrates a 50 % reduction in MYC expression compared to siCTR.*

4.4 Investigating the relevance of *MYC* 5' UTR-binding factors in CRC cells

4.4.1 siRNAs against top hits partially reduce MYC protein but not mRNA expression

As the proteins highlighted in section 4.3.2 play a role in a wide variety of cancers, the impact on CRC cells should be investigated further. For this purpose, siRNA pools each composed of four individual siRNAs targeting *EIF3B*, *EIF3D*, *RPL23A*, *RPS11*, *RPS15A*, *RPS17*, *RPS19*, *RPS20* and (as negative control) *ILF3* were used to transfect DLD1 cells. Additionally, siRNAs against *MYC* and a non-targeting control (NTC) siRNA pool were taken as controls, and 48 h after transfection, knockdown efficiency and MYC expression were examined. Efficient knockdown was achieved for *ILF3*, *EIF3D*, *RPS17* and *RPS11* with reduction in target gene expression of 76.3, 70.1, 55.2 and 47.2 %, respectively **Figure 23 (A) + (B)**). In contrast, lower knockdown efficiencies were recorded for *EIF3B*, *RPS15A*, *RPS19* and *RPS20*, which amounted to 33, 36.8, 29.5 and 26.3 %, respectively. No knockdown of the target gene could be achieved with the siRNA pool against *RPL23A*. However, the analysis of MYC expression showed that despite partially strong knockdown efficiency, only the knockdown of *EIF3D* led to a significant reduction of MYC protein levels by a mean of 48.7 % compared to siNTC (**Figure 24 (A) + (B)**).

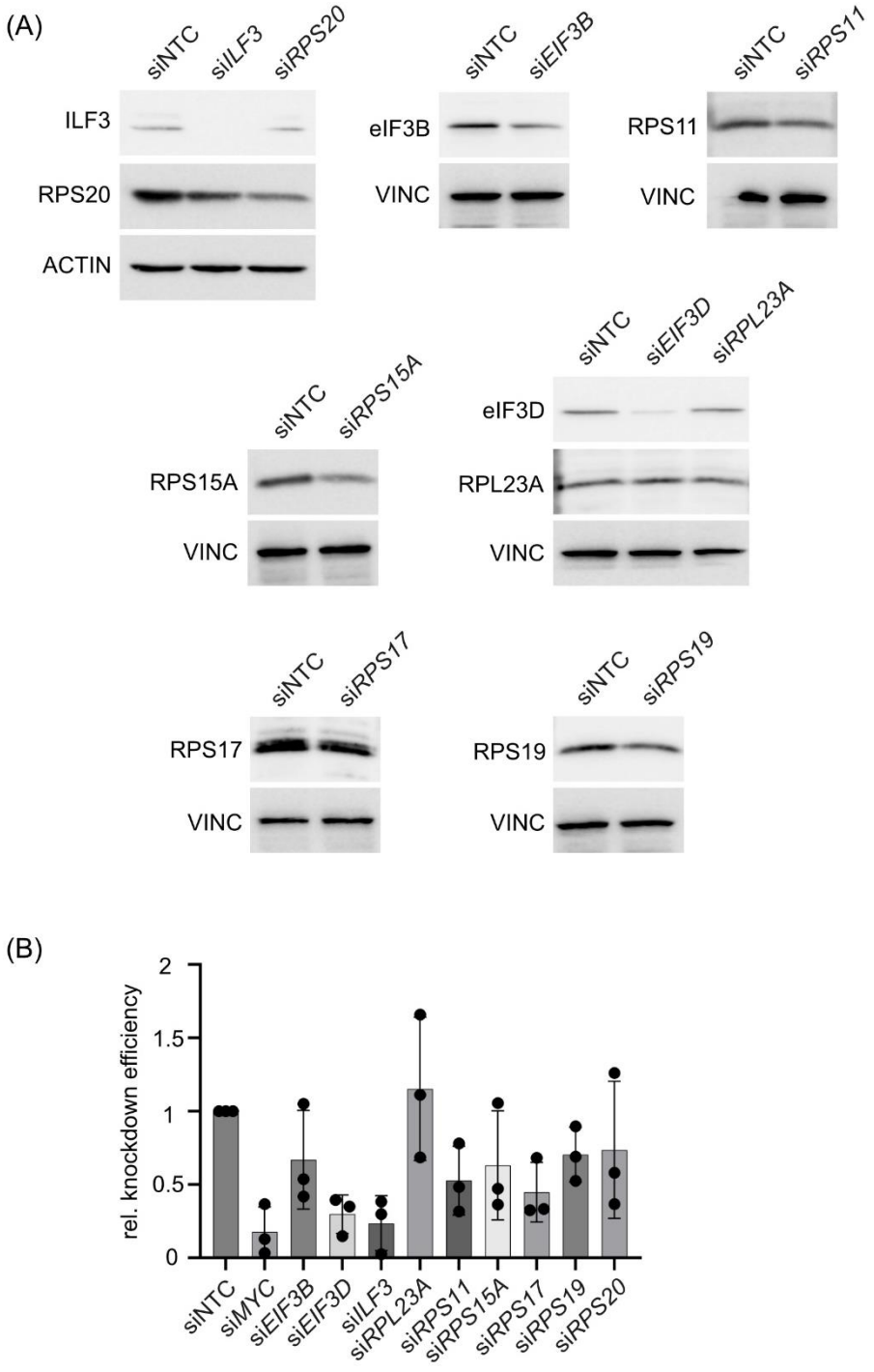

Figure 23: Testing potency of siRNA pools against previously identified MYC 5' UTR-binding proteins*. (A) DLD1 cells were transfected with siRNA pools against top hits from the siRNA screen and knockdowns were validated after 48 h by immunoblotting. (B) Knockdown efficiency was quantified and normalised to siNTC. Shown is mean ± SD of three independent experiments.*

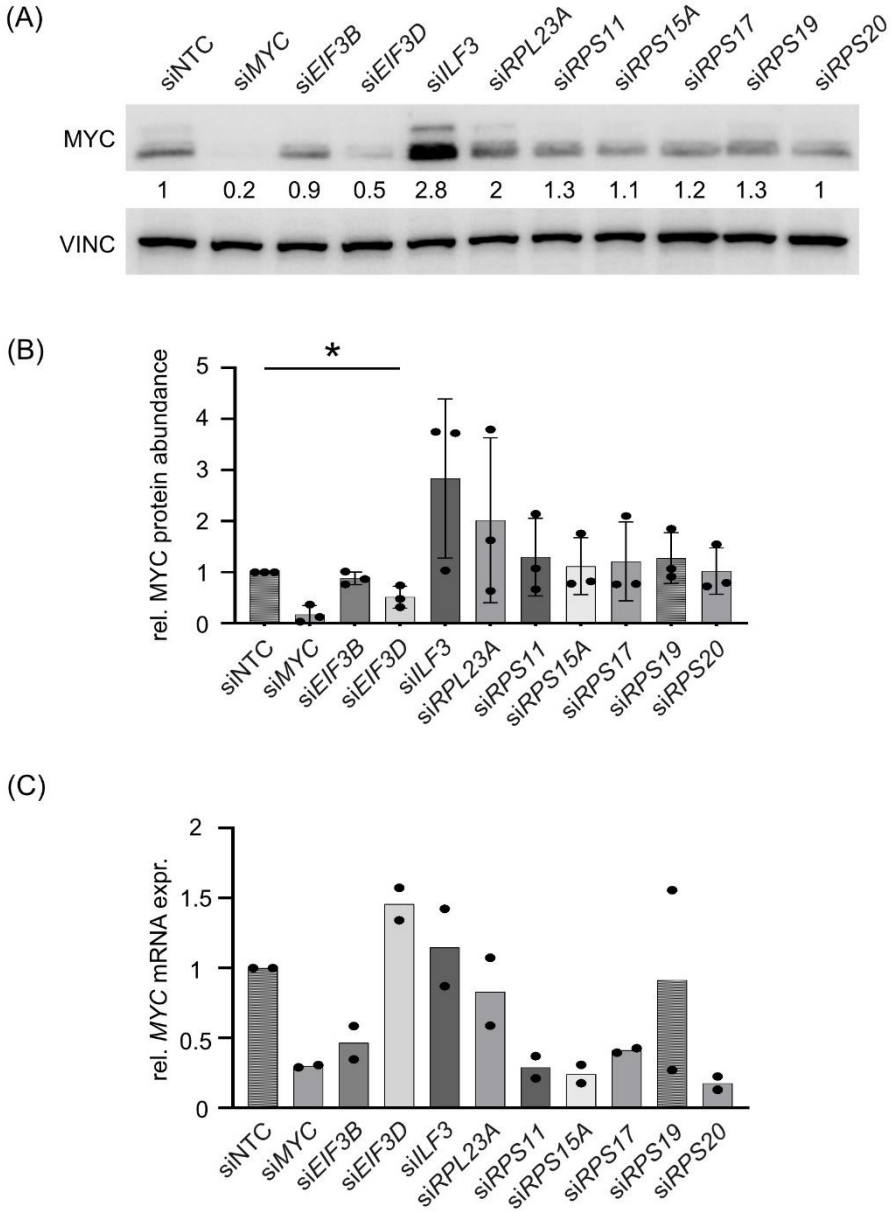

Figure 24: Hit validation of previously identified MYC 5' UTR-binding proteins and their effect on MYC expression. *(A) DLD1 cells were transfected with siRNA pools against top hits from the siRNA screen and MYC protein expression was investigated by immunoblotting 48 h after transfection. n = 3. (B) MYC expression was quantified and normalized to siNTC, shown is mean ± SD of three independent experiments. (C) DLD1 cells were transfected with siRNA pools against top hits from the siRNA screen and MYC mRNA expression was evaluated by qRT-PCR 48 h after transfection. Mean of two independent experiments is shown.*

The next step was to check whether the low MYC protein levels result from a decreased protein expression or whether there is already an altered *MYC* mRNA expression. For this purpose, qRT-PCR analysis was performed after siRNA knockdown of the targets

shown in **Figure 24 (A) + (B)**. It turned out that upon knockdown of *EIF3B* and *RPS17*, *MYC* mRNA expression is downregulated by 54.4 and 48.9 %, respectively. In contrast, siRNAs against *RPS11*, *RPS15A, and RPS20* reduced MYC mRNA levels by 70.9, 75.7, and 82.2 %, respectively, which is comparable to the 70.1 % decrease induced by si*MYC* **(Figure 24 (C))**. *ILF3* and *RPS19* knockdown had almost no effect on MYC mRNA level showing a 14.7 % increase and 8.9 % decrease in mRNA expression, respectively, compared to siNTC. Furthermore, si*RPL23A* induced a decrease by 16.9 %. Interestingly, knockdown of *EIF3D* which had the strongest effect on MYC protein expression (**Figure 24 (A)**) led to an upregulation of *MYC* mRNA expression by a mean of 45.8 % compared to siNTC.

In summary, in the validation experiments performed after the siRNA screen, only the knockdown of *EIF3D* led to a significant downregulation of MYC protein expression. In great contrast, *MYC* mRNA levels were not downregulated after si*EIF3D* compared to siNTC, suggesting a potential translational mechanism.

4.4.2 Knockdown of top hits from siRNA screen impairs proliferation of CRC cells

In parallel with analysis of the individual knockdowns and their effect on MYC levels, the effect on CRC cell proliferation was investigated to narrow down potential therapeutic targets. DLD1 cells were transfected with the corresponding siRNA pools and the proliferation behaviour was analysed after 72 h by crystal violet staining. In detail, si*RPS11*, si*RPS15A*, si*RPS17*, si*RPS20* and si*RPS19* reduced cell numbers by 64.4, 62.2, 62.2, 56.1 and 53.1 % (**Figure 25**). Comparable effects were achieved by knocking down eIF3B and eIF3D, which reduced growth by 51.6 and 56.1 %, respectively. si*MYC* caused a slowdown of proliferation (21.3 %), whereas si*RPL23A* and si*ILF3* showed no negative effect on growth compared to the control.

In summary, proliferation of DLD1 cells was strongly impaired after knockdown of the individual factors, except RPL23 and ILF3. However, it is still open whether this growth defect results from an increase in apoptosis or a slow down or arrest of cell cycle progression.

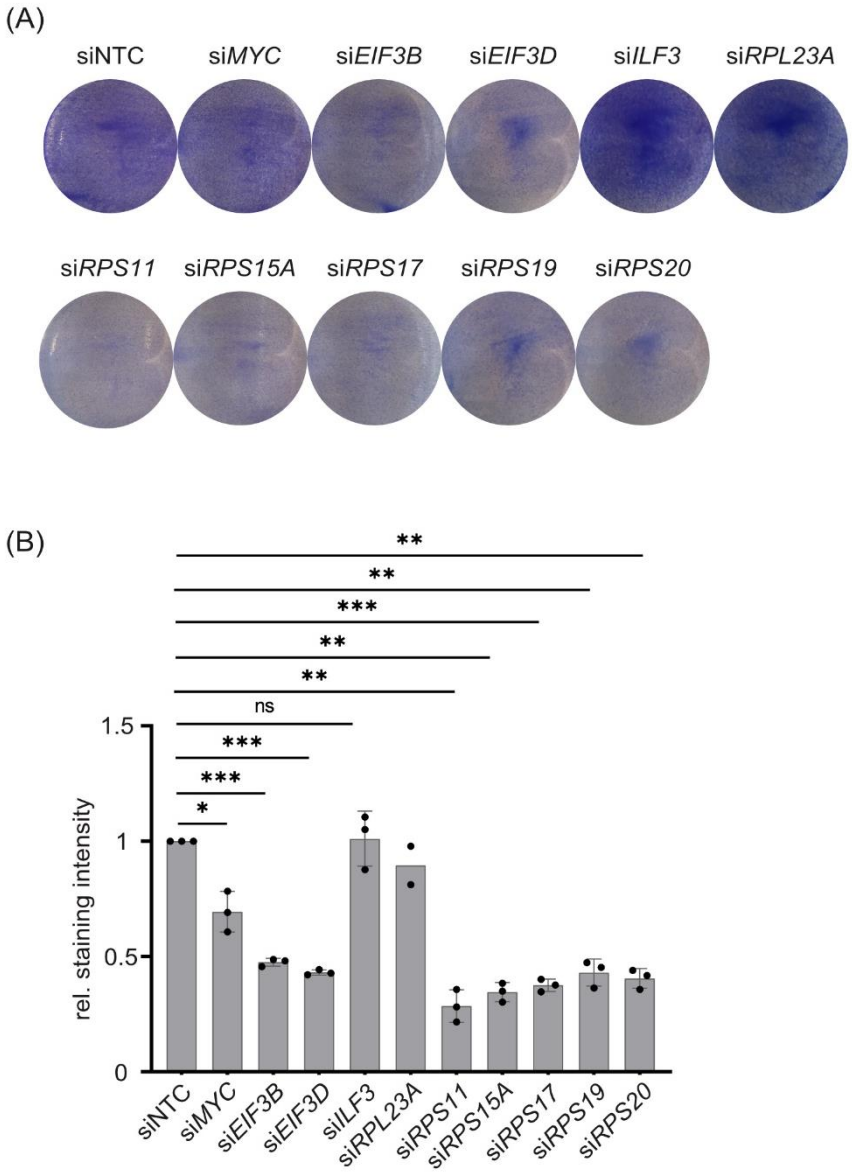

Figure 25: Knockdown of top hits from siRNA screen impairs proliferation of CRC cells. *(A) DLD1 cells were transfected with siRNA pools against hits from siRNA screen and proliferation behaviour was analysed by crystal violet staining. (B) Staining intensity was measured and shown is mean absorbance at 590 nm ± SD of three independent experiments (n = 2 for RPL23A), normalised to siNTC.*

4.4.3 Evaluating the impact of top hits from the siRNA screen on apoptosis and cell cycle distribution

To investigate whether the reduced cell numbers upon depletion of the top hits from the siRNA screen was due to an increase in apoptosis, an Annexin V/PI FACS was performed after knockdown of the corresponding targets as described in section 3.1.15.1. Surprisingly, compared to the control with 10.8 % apoptotic cells, none of the knockdowns led to an induction of apoptosis but showed very low numbers of apoptotic cells (**Figure 26**). Comparing the results of the crystal violet staining (**Figure 25**) with the FACS data of the respective knockdowns suggests that the reduced growth is not due to an increased apoptosis rate, but possibly mediated by a change in cell cycle distribution. To test the hypothesis, a PI cell cycle FACS was carried out in parallel, as described in section 3.1.15.2. Notably, siNTC, si*MYC*, si*RPL23A* and si*RPS17* displayed a proportion of cells in the subG1 phase. However, for most of the tested hits, there was a decrease in the amount of cells in subG1 phase compared to control cells, reflecting the result from the AnnexinV/PI FACS analysis (**Figure 26**) where no induction of apoptosis was observed. Besides that, most of the knockdowns led to an enrichment of cells in G1 phase compared to control with 51.4 %. In detail, si*EIF3B*, si*EIF3D*, si*RPS11*, si*RPS15A*, si*RPS19* and si*RPS20* showed 62.2, 67.2, 64.2, 61.8, 58.7 and 61.7 %, respectively, of cells in G1 phase. In contrast, si*MYC* and si*RPS17* increased the number of cells in G1 phase only to 56.4 and 52.6 %, respectively, whereas si*RPL23A* and si*ILF3* decreased the number to 47.9 and 41.5 %. Furthermore, there were less cells detectable in S phase upon knockdown of *MYC* (6.4 %), *EIF3D* (8.5 %), *RPL23A* (9.8 %) and *RPS17* (7.1 %), whereas knockdown of *EIF3B*, *ILF3*, *RPS11*, *RPS15A*, *RPS19* and *RPS20* did not lead to major changes compared to control knockdown (12.7 %). Additionally, only si*MYC*, si*RPL23A* and si*RPS17* reduced the number of cells in G2/M phase (14.5, 19.9 and 13.5 %, respectively) which at the same time were the siRNAs that resulted in an enrichment of cells in subG1 phase.

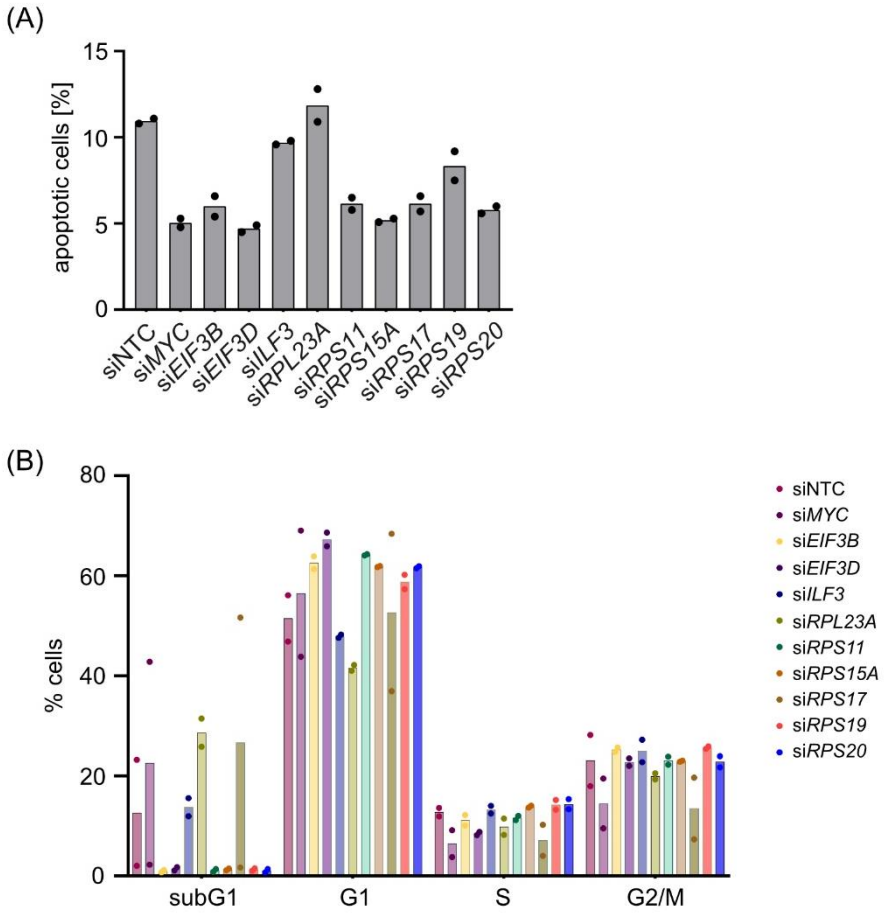

Figure 26: Identified MYC 5'UTR-binding proteins do not induce apoptosis but affect cell cycle distribution. *(A) DLD1 cells were transfected with respective siRNA pools and AnnexinV/PI FACS was performed. Rate of apoptosis was determined and shown is mean from two independent experiments. (B) siRNA-transfected DLD1 cells (48 h) were subjected to FACS-based cell cycle analysis. PI incorporation was measured and results represent mean of two experiments.*

In summary, considering the effects on MYC expression, proliferation behaviour as well as the distribution of cell cycle phases, eIF3D in particular stood out. A strong downregulation of MYC protein levels after siRNA-mediated knockdown of *EIF3D*, which is associated with slowed proliferation and increased proportion of cells in G1 phase, suggests an essential role of the translation initiation factor in CRC cells. For further investigations, the focus was therefore placed on eIF3D and its role in the translation of *MYC* in CRC.

4.5 shRNA-mediated knockdown of *EIF3D* affects *MYC* expression and proliferation of CRC cells

The results so far suggest that eIF3D may play a major role in the regulation of *MYC* expression and should therefore be investigated further. Since siRNA-mediated knockdown constitutes a transient depletion of the target gene, the next step was to investigate the cellular effect of a stable, shRNA-mediated knockdown of *EIF3D* in different cell lines. For this purpose, DLD1 and LS174T with a stably integrated shRNA against *EIF3D* were generated. The five best rated shRNAs against human *EIF3D* were selected from the list published by Fellmann et al. (Fellmann et al., 2013) and cloned into the expression vector pGIPZΔEcoRI (see section 3.3.8). All five shRNAs were tested in preliminary experiments in DLD1 (data not shown) and based on this, shRNAs #2 and #3 were selected for further experiments.

4.5.1 shRNA-mediated knockdown of *EIF3D* reduces *MYC* expression in DLD1 cells

Cell lines stably expressing a non-targeting control shRNA (shNTC) or the shRNAs against *EIF3D* were generated and knockdown efficiency and the effect on *MYC* expression were investigated after six days in selection medium. Using shRNAs, a similar knockdown efficiency on eIF3D protein level could be achieved (77.3 % with sh*EIF3D*#2 and 77 % with sh*EIF3D* #3) **(Figure 27 (A)**) compared to the previously used siRNA pool (**Figure 23 (B)**). The reduced eIF3D protein abundance was accompanied by 84.8 and 84.9 % decrease in *EIF3D* mRNA expression (**Figure 27 (C)**). However, the effect on MYC protein expression was significantly stronger than upon si*EIF3D* treatment, and shRNA-mediated knockdown of *EIF3D* resulted in 74.5 and 59.8 % decrease with shRNA #2 and #3, respectively. In parallel, the effect of *EIF3D* knockdown on *MYC* mRNA expression was investigated. It was found that the amount of mRNA also decreased significantly by 66.3 % for shRNA #2 and 46.8 % for shRNA #3 (**Figure 27 (B)**).

Taken together, stable and constitutive knockdown of *EIF3D* by shRNA showed similar knockdown efficiency as si*EIF3D*, however, the negative effect on MYC protein expression was significantly stronger. Although a reduction in *MYC* mRNA expression was observed at the same time, this was not as strong as the effect at the protein level.

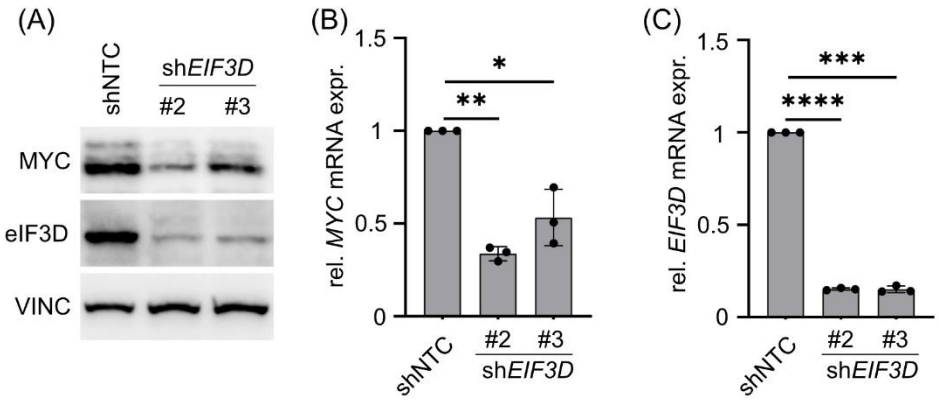

Figure 27: shRNA-mediated knockdown of EIF3D reduces MYC expression in DLD1 cells. *(A) DLD1 cells were stably infected with lentiviral plasmid pGIPZ carrying respective shRNAs against EIF3D. Representative immunoblots and qRT-PCR analyses ((B) + (C) showing mean ± SD of three independent experiments are shown. Vinculin was used as loading control.*

4.5.2 shRNA-mediated knockdown of *EIF3D* impairs proliferation and viability of DLD1 cells

The strong reduction in *MYC* expression observed in the previous section suggests that there is also a proliferation disadvantage in CRC cells after shRNA-induced knockdown of *EIF3D*. Proliferation behaviour of DLD1 cells was investigated by crystal violet staining and, similar to siRNA knockdown, growth of *EIF3D*-depleted DLD1 cells was significantly reduced. After six days, 85.3 % fewer cells were detected with sh*EIF3D*#2, with sh*EIF3D*#3 80.1 % less compared to shNTC (**Figure 28 (A) + (B)**). To find out whether the slowed growth was due to an increase in apoptosis rate, an AnnexinV/PI FACS was performed after sh*EIF3D* and five days of selection medium. Indeed, knockdown of *EIF3D* by both shRNAs led to an enrichment of dead cells to 35.5 and 39.6 %, respectively, compared to the control with 19.3 % (**Figure 28 (C)**).

In summary, shRNA-mediated knockdown of *EIF3D* led to a growth defect stronger than observed with siRNA-mediated knockdown. In contrast to siRNA-based experiments, sh*EIF3D* strongly induced apoptosis in DLD1 cells.

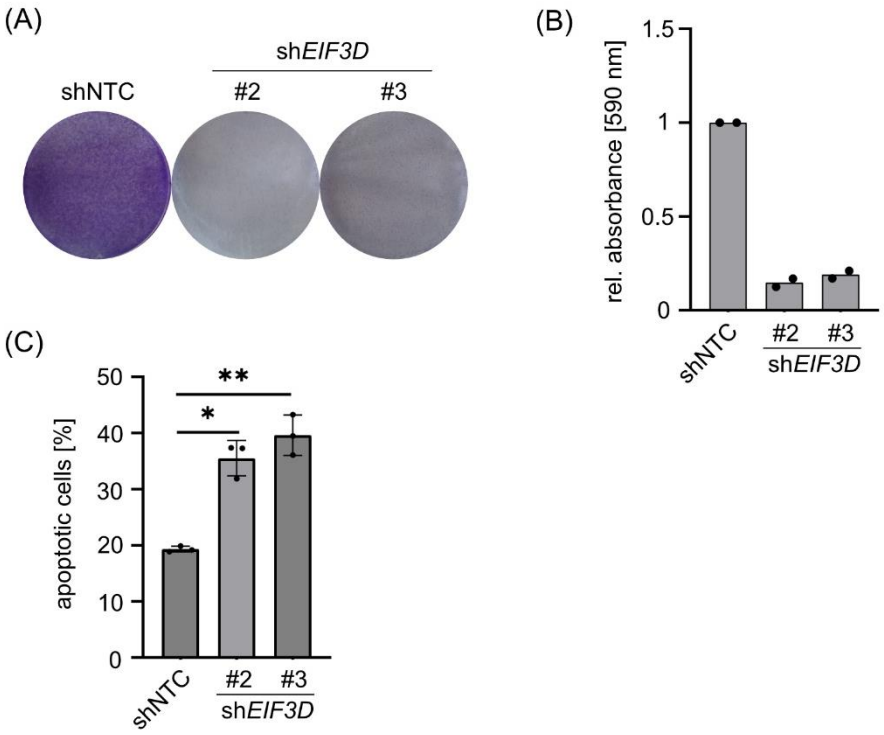

Figure 28: shRNA-mediated knockdown of EIF3D impairs proliferation and viability of DLD1 cells. *DLD1 cells were stably transfected with lentiviral plasmid pGIPZ carrying respective shRNAs against EIF3D. Cells were kept under selection for two days before they were seeded for experiments (in selection medium). (A) Crystal violet staining was performed six days after seeding, representative picture of two experiments is shown and quantified in (B). (B) Mean of absorbance at 590 nm from two independent experiments is shown. (C) AnnexinV/PI FACS was measured 72 h after seeding and mean ± SD of three independent experiments is shown.*

4.5.3 shRNA-mediated knockdown of *EIF3D* reduces *MYC* expression in LS174T cells

To test to what extent the mutation status of the cell line plays a role in the downregulation of *MYC* expression after *EIF3D* knockdown, LS174T cells with stably integrated sh*EIF3D* were generated in parallel. In contrast to DLD1, LS174T are not mutated in the *TP53* or *APC* locus but instead show a *CTNNB1* mutation, leading to dysregulated Wnt/β-catenin signalling (Berg et al., 2017). Compared to DLD1, a higher knockdown efficiency for *EIF3D* could be achieved with both shRNAs (82.9 and 88.2 % for #2 and #3, respectively) (**Figure 29 (A)**) and this was accompanied by 88.5 and 85 % decrease in *EIF3D* mRNA expression (**Figure 29 (C)**). Besides that, MYC protein expression was reduced by

85.5 % with shEIF3D#2 and 72.9 % with shEIF3D#3, along with a 76.4 and 66.8 % decrease in mRNA abundance (**Figure 29 (B)**).

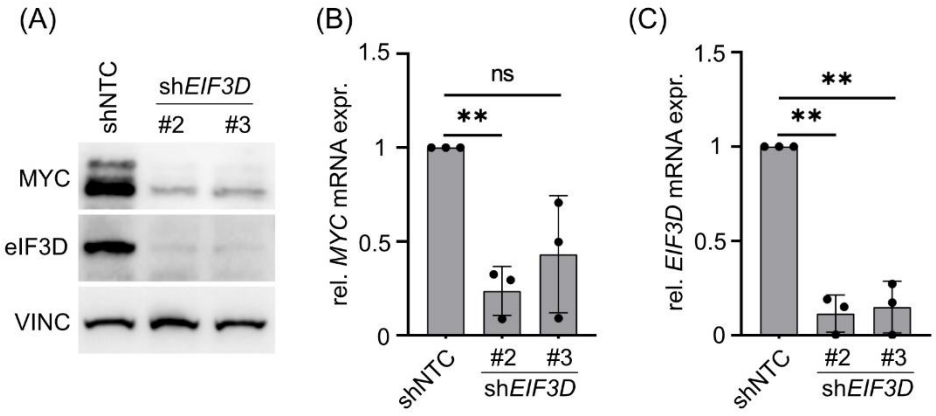

Figure 29: shRNA-mediated knockdown of EIF3D reduces MYC expression in LS174T cells. *(A) LS174T cells were stably infected with lentiviral plasmid pGIPZ carrying respective shRNAs against EIF3D. Representative immunoblots and qRT-PCR analyses ((B) + (C)) showing mean ± SD of three independent experiments are shown. Vinculin was used as loading control.*

To summarize, shRNA-induced knockdown of *EIF3D* in LS174T cells led to similar negative effects on MYC protein and mRNA expression as in DLD1 cells, although a stronger knockdown efficiency could be achieved with LS174T.

4.5.4 shRNA-mediated knockdown of *EIF3D* impairs proliferation and viability of LS174T cells

To further analyse proliferation behaviour of LS174T cells upon sh*EIF3D*, crystal violet staining was performed, and similar to DLD1 cells, growth was significantly reduced. After five days, 68.9 % fewer cells were detected with sh*EIF3D*#2 and 57.4 % less with sh*EIF3D*#3 compared to control (**Figure 30 (A) + (B)**). To check whether the slowed growth was due to an increase in apoptosis rate, an AnnexinV/PI FACS was performed after sh*EIF3D* and five days of selection medium. Indeed, knockdown of *EIF3D* by both shRNAs led to an enrichment of dead cells to 66.2 and 42 %, respectively, compared to shNTC with 31.8 % (**Figure 30 (C)**).

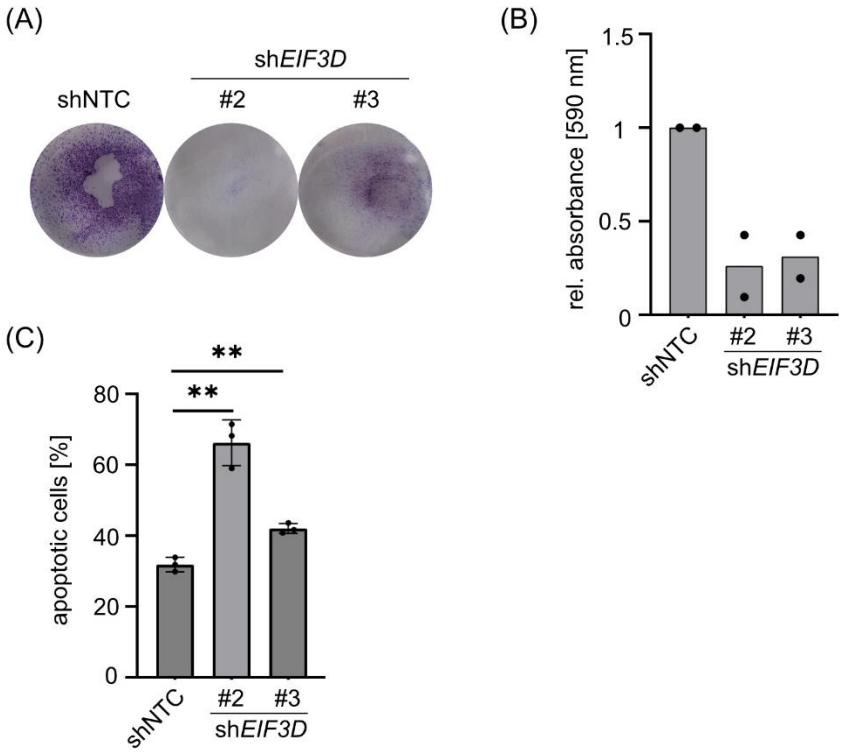

Figure 30: shRNA-mediated knockdown of EIF3D impairs proliferation and viability of LS174T cells. *LS174T cells were stably transfected with lentiviral plasmid pGIPZ carrying respective shRNAs against EIF3D. Cells were kept under selection for two days before they were seeded for experiments (in selection medium). (A) Crystal violet staining was performed six days after seeding, representative pictures of two experiments are shown and quantified in (B). (B) Mean of absorbance at 590 nm from two independent experiments is shown. (C) AnnexinV/PI FACS was measured 72 h after seeding and mean ± SD of three independent experiments is shown.*

In summary, although LS174T show a higher basal apoptosis rate compared to DLD1 cells, the number of dead cells after sh*EIF3D*#2 was similarly increased in both cell types. In contrast, after sh*EIF3D*#3, there was only a slightly increased apoptosis rate in LS174T.

4.6 *Eif3d* knockdown impairs viability of murine tumour organoids

After the knockdown of *EIF3D* in human CRC cell lines had been analysed extensively, the next step was to investigate whether the effects could be transferred to other models that are more physiological and genetically defined. For this purpose, mouse small

intestinal organoids were utilised and the following experiments with MTO140 cells and the LAKTP organoids were conducted by Dr. Stefanie Schmidt.

4.6.1 Testing shRNAs against *Eif3d* in an organoid-derived murine cell line

Before experiments with organoids were carried out, shRNAs against murine *Eif3d* were tested in a cell line derived from mouse tumour organoids (MTO). This was MTO140 established from the LAKTP (*Lgr5*$^{eGFP\text{-}creERT2}$*Apc*$^{-/-}$*Kras*$^{G12D/+}$*Tgfbr2*$^{-/-}$*Trp53*$^{-/-}$) quadruple mutant organoid line (Tauriello et al., 2018). The five best rated shRNAs against murine *Eif3d* were selected from the list published by Fellmann et al. (Fellmann et al., 2013) and cloned into the tetracycline-inducible expression vector pLT3-GEPIR (see section 3.3.8). All five shRNAs were tested in MTO140 and *Eif3d* knockdown efficiency and MYC protein expression were analysed upon 48 h shRNA induction. At protein level, eIF3D abundance was similarly decreased for all tested shRNAs (**Figure 31 (A)**). Besides that, analysis of *Eif3d* mRNA expression showed clear differences between the individual shRNAs, with a decrease by 81, 76.8, 64.3, 36 and 71.9 % induced by shRNA #1, #2, #3, #4 and #5, respectively, after induction by DOX (**Figure 31 (B)**). Notably, the control shRNA against Renilla luciferase (shLuc) used here also shows a downregulation of *Eif3d* mRNA expression by 26.7 % under DOX treatment. However, the effect on MYC protein expression in this assay was not clear but appeared to be upregulated with shRNA#1, downregulated with shRNA#3 and #4, and not regulated at all with shRNA #2 and #5 (**Figure 31 (A)**). As it has already been found to be difficult to perform MYC immunoblotting in organoid-derived cells, the shRNAs against *Eif3d* were selected for the further experiments according to their knockdown efficiency and not according to their effect on MYC protein levels. On the one hand, sh*Eif3d* #1 was selected for its strongest effect on *Eif3d* mRNA expression. On the other hand, sh*Eif3d* #3, which showed a moderate knockdown at the mRNA level, should also be tested further to be able to control *off-target* effects.

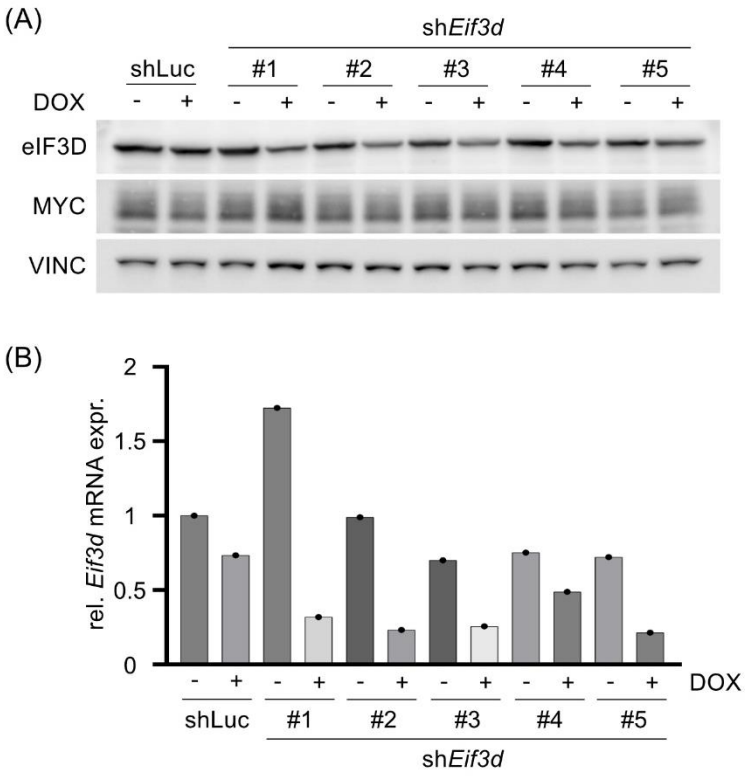

Figure 31: Validating shRNAs against Eif3d in MTO140. *Mouse tumour organoid-derived cel line MTO140 was stably infected with pLT3 vector carrying shRNAs against Luciferase (Luc) or Eif3d. shRNA expression was induced by 1µg/ml doxycycline (DOX) for 48 h and immunoblots (A) and qRT-PCR analyses (B) were performed. n = 1. Vinculin was used as loading control.*

4.6.2 *Eif3d* knockdown impairs viability of LAKTP organoids

In the next step, shRNAs #1 and #3 against *Eif3d* validated in the MTO140 cell line were used for stable infection of LAKTP organoids. As already mentioned, these are characterised by their mutation status ($Apc^{fl/fl}$, $Kras^{LSL\text{-}G12D}$, $Trp53^{fl/fl}$, $Tgfbr2^{fl/fl}$) and thus represent the status of advanced human colorectal adenocarcinoma. Lentiviral transduction was carried out as described in sections 3.1.12 and 3.1.13 and selection was carried out for five days, before they were seeded as single cells for viability assay. The day after, shRNAs were induced by DOX treatment for four days before CellTiter-Glo® 2.0 Cell Viability Assay (Promega) was performed as described in section 3.1.14. The induction of shRNAs against *Eif3d* led to a clear growth defect in the LAKTP organoids, which were significantly smaller after loss of *Eif3d* (**Figure 32 (A)**). This was accompanied by reduced viability, with sh*Eif3d* #1 reducing it by 40.4 % and sh*Eif3d* #3

by 54.8 % (**Figure 32 (B)**). At the protein level, sh*Eif3d* #1 led to reduced eIF3D expression by a mean of 41.3 %, whereas sh*Eif3D* #3 reduced it by 49.3 % upon induction by DOX (**Figure 32 (C) + (D)**). As in the previous experiment with the MTO140 cell line, no change in MYC protein levels could be detected in the immunoblot (**Figure 32 (C)**).

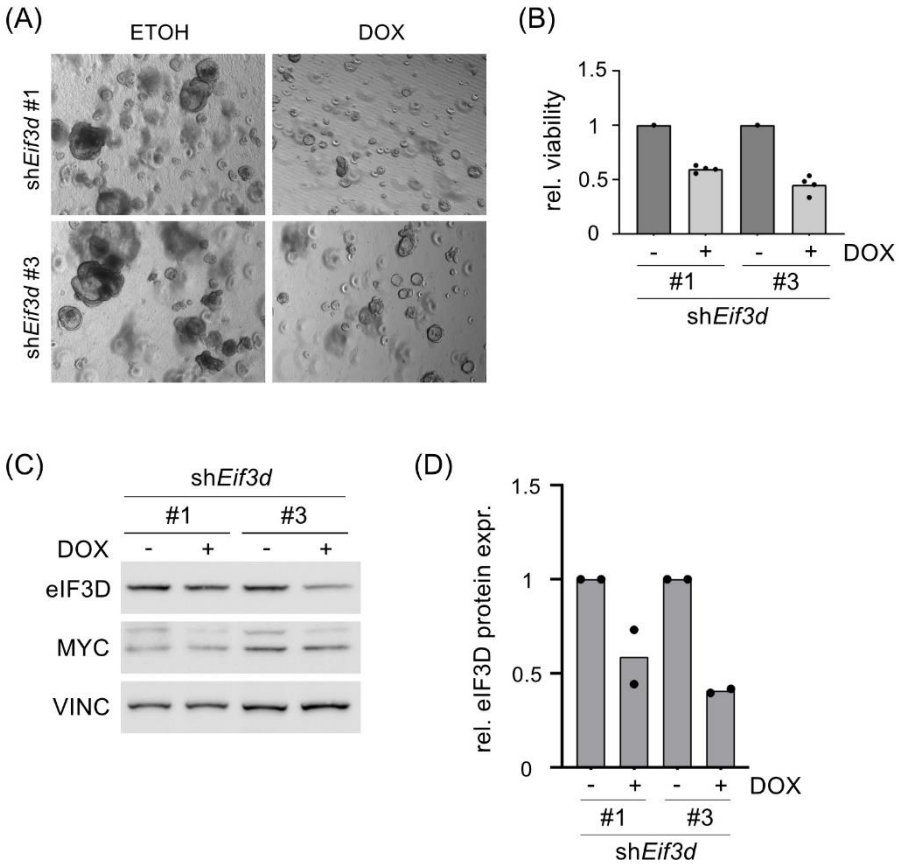

***Figure 32**: **Eif3d knockdown impairs viability of LAKTP murine tumour organoids.** LAKTP mouse tumour organoids were stably transfected with pLT3 vector carrying shRNAs against Eif3d. (A) Organoids were seeded as single cells and shRNA expression was induced by 1 µg/ml doxycycline (DOX) for four days. Representative pictures are shown. (B) CellTiter-Glo® 2.0 Cell Viability Assay was performed with organoids shown in (A) and analysis was conducted from four technical replicates. (C) Organoids were seeded, and shRNA expression was induced by 1 µg/ml DOX for 48 h. Representative immunoblots from two experiments are shown. Vinculin was used as loading control. (D) eIF3D knockdown efficiency was quantified and shown is mean of two experiments.*

Although no change in MYC protein expression was detected by immunoblot, a clear growth defect of LAKTP organoids was observed, leading to the assumption that eIF3D also plays an essential role in murine tumour cells.

4.7 Investigating global effects after *EIF3D* knockdown

Previous analyses after knockdown of *EIF3D* focused mainly on the translation of *MYC* and the general effect on the proliferation of CRC cells. However, the eIF3 complex is thought to play an essential role during eukaryotic translation initiation, so that the knockdown of eIF3D might also have global translational effects. Notably, loss of eIF3D generally does not impair integrity of the whole eIF3 complex which is the case for other eIF3 subunits (Herrmannova et al., 2020; Wagner, Herrmannova, Sikrova, & Valasek, 2016). Thus, it is of great interest which global effects knockdown of eIF3D might have.

4.7.1 Loss of eIF3D impairs *de novo* protein synthesis

In order to investigate potential effects on global mRNA translation, *de novo* protein synthesis was measured by quantification of puromycin incorporation into newly synthesised polypeptide chains.

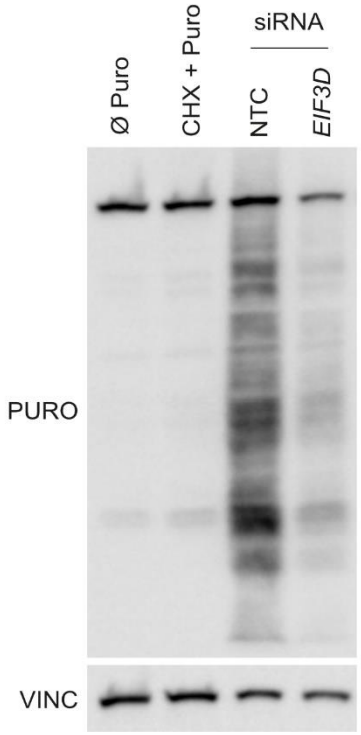

Figure 33: EIF3D knockdown globally reduces de novo protein synthesis. *DLD1 cells were transfected with siRNA for 48 h and puromycin incorporation was analysed by immunoblotting. 50 µg/ml Cycloheximide (CHX) was used as positive control by inhibiting translation elongation. n = 3. Vinculin was used as loading control.*

In detail, DLD1 cells were labelled with puromycin after treatment with siNTC or si*EIF3D* as described in section 3.4.6, and puromycin incorporation was analysed by immunoblotting. As controls, lysates from cells not treated with puromycin or cells treated with CHX to inhibit protein synthesis were also included. Compared to siNTC, si*EIF3D* strongly reduced puromycin incorporation, thereby reflecting reduced *de novo* protein synthesis **(Figure 33**).

4.7.2 Loss of eIF3D globally reduces polysomal mRNAs

Having already shown that global *de novo* protein synthesis is decreased by knockdown of *EIF3D*, the question arose as to the underlying mechanism. Thompson *et al.* recently demonstrated that global mRNA translation of HCMV-infected fibroblasts is dependent on eIF3D's cap-binding activity, and knockdown changed the global translation landscape which was accompanied by reduced polyribosome abundance (L. Thompson, Depledge, Burgess, & Mohr, 2022). To investigate whether there might be similar effects on polysome abundance in *EIF3D*-depleted CRC cells, polysome profile analysis was performed upon transient knockdown of *EIF3D,* together with Dr. Cornelius Schneider. This technique generally enables quantification of mRNA abundance in monosomal and polysomal fractions by sucrose density centrifugation thereby providing an assessment of global translational activity. DLD1 cells were transfected in triplicates with siRNA pools against *EIF3D* and NTC, respectively, and processed as described in section 3.4.5. Polysome profiles were measured after 48 h siRNA treatment. Compared to siNTC, knockdown of *EIF3D* clearly increased the abundance of mRNA in 80S ribosomal fractions and at the same time reduced the number of polyribosomal mRNAs (**Figure 34 (A)**). Knockdown of *EIF3D* was confirmed by immunoblotting and MYC protein levels were significantly decreased upon si*EIF3D* as observed before (**Figure 34 (B)**).

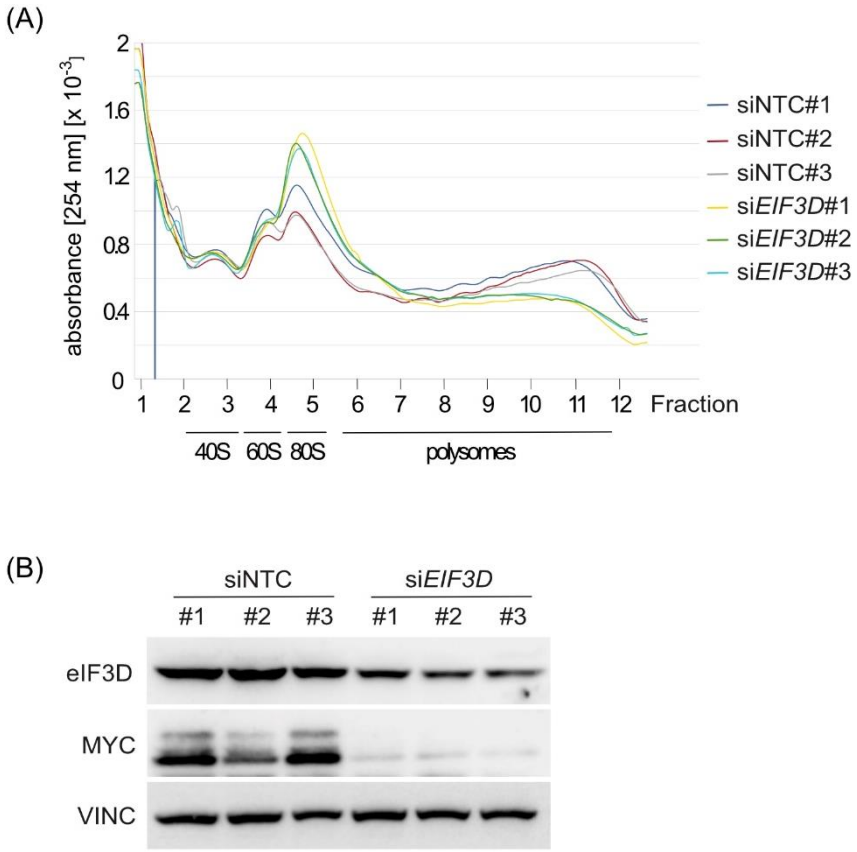

Figure 34: EIF3D knockdown globally reduces the amount of polysomal mRNAs. *(A) A254 nm absorbance profile of polysomes gradients from DLD1 cells transfected with siNTC or siEIF3D. Shown are three biological replicates #1 - #3. (B) Immunoblot analyses from samples used for gradient profiling. Vinculin was used as loading control.*

4.7.3 Loss of eIF3D affects similar gene sets as loss of MYC

In the previous sections, it was shown that the knockdown of *EIF3D* leads globally to a loss of polyribosomal mRNAs, which was associated with reduced *de novo* protein synthesis. However, since a 48-hour treatment with siRNA is required to achieve proper knockdown, it is possible that secondary effects also contribute to the observed phenotypes. Therefore, an RNA-seq experiment was performed to investigate to which extent cellular gene expression changes after loss of eIF3D. In addition, it should be compared whether the knockdown of *EIF3D* shows similar gene expression patterns as the knockdown of *MYC* in order to establish a potential connection. RNA-seq experiment was performed in DLD1 cells treated with siRNA for 48 h and described in 3.6.1.

Sequencing was followed by GSEA (Liberzon et al., 2015; Subramanian et al., 2005) and correlation of enrichment scores from hallmark gene sets between si*EIF3D* vs. siNTC and si*MYC* vs. siNTC was analysed. Interestingly, knockdown of *MYC* and *EIF3D* led to downregulation of many identical gene sets. The most strongly downregulated were 'MYC targets V1' and 'MYC targets V2', followed by 'Unfolded protein response', 'E2F targets' and 'mTORC1 signalling' (**Figure 35**). Besides that, immune signalling pathways were downregulated, such as 'TNF alpha signalling via NFκB' and 'Inflammatory response'. On the other side, gene sets upregulated in both *MYC* and *EIF3D* knockdown condition included 'Interferon gamma response' and 'Interferon alpha response'.

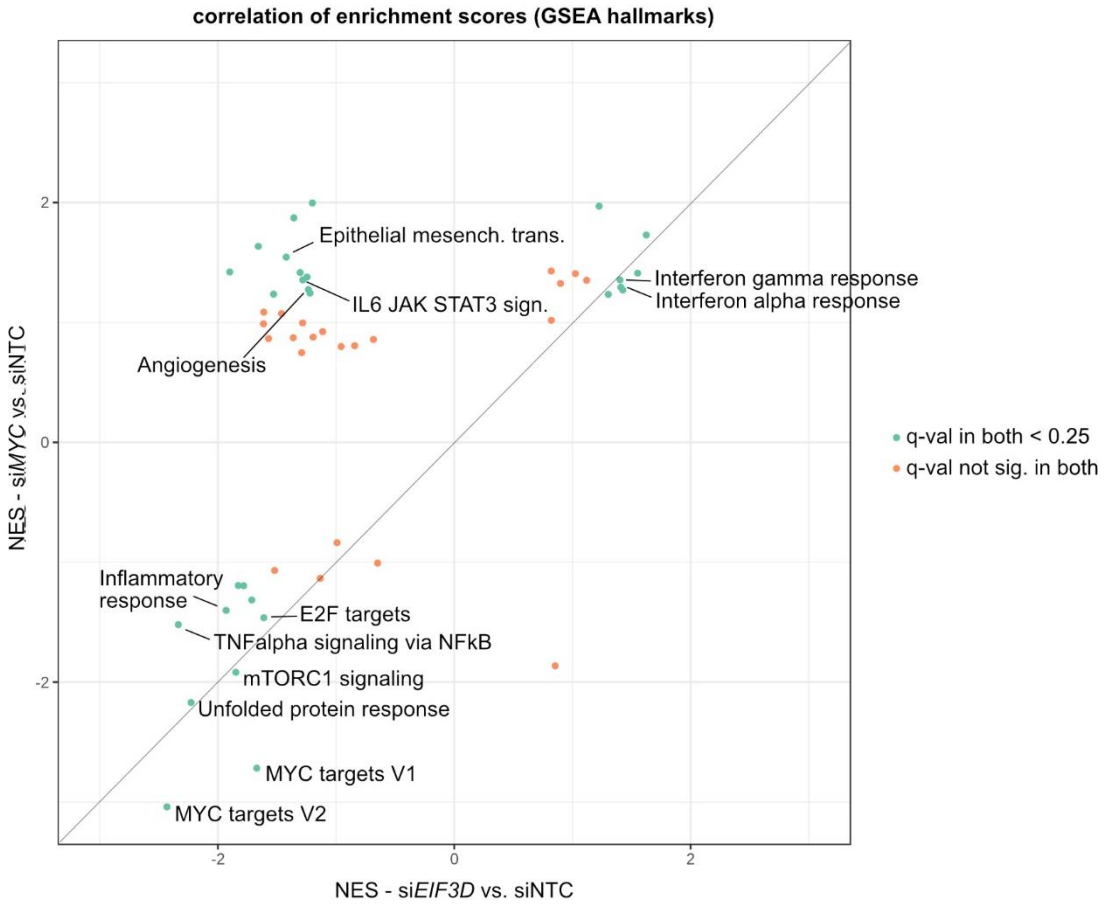

Figure 35: EIF3D knockdown influences similar gene sets as MYC knockdown. *DLD1 cells were transfected in triplicates with siRNA (NTC, MYC, EIF3D) and RNA-seq experiment was performed after 48 h. Shown is the correlation of enrichment scores from GSEA hallmarks, comparing siEIF3D and siMYC over siNTC, respectively. Green dots represent hallmarks that were significantly regulated in all replicates and both conditions. n = 3.*

Furthermore, gene sets were identified that are oppositely regulated in both knockdown conditions. Among others, 'Angiogenesis', 'IL6 JAK STAT3 signalling' and 'Epithelial mesenchymal transition' were upregulated under si*MYC* but downregulated after si*EIF3D*. Interestingly, no gene sets were identified that were upregulated upon *EIF3D* but at the same time downregulated upon *MYC* knockdown.

In summary, the analysis of RNA-seq clearly shows that *EIF3D* and *MYC* knockdown have similar effects on cellular gene expression.

4.7.4 eCLIP-seq identifies eIF3D binding sites in the *MYC* 5' UTR and exons 2 and 3

In order to validate eIF3D binding to the *MYC* mRNA under physiological conditions, an eCLIP-seq experiment was carried out in cooperation with the Munschauer group at the HIRI in Würzburg. In contrast to the *in vitro* pulldown, in which the binding of cellular proteins to a specific RNA was studied, the focus of an eCLIP experiment is on determining mRNA sequences bound by a specific protein. For the eCLIP procedure, DLD1 cells were UV-crosslinked to fix RNA-binding proteins on their potential target RNA and lysates were further processed as described in chapter 3.6.2.1. Subsequently, immunoprecipitation was performed with an eIF3D-targeting antibody, followed by cDNA library preparation from eIF3D-protected fragments and sequencing. Enriched sequences were aligned to human GRCh37/hg19 genome by Dr. Dimitrios Papadopoulos and significantly enriched binding sites of eIF3D were visualised using *IGV* software. Interestingly, eIF3D (orange) was found to be enriched at several positions on the *MYC* mRNA compared to SMI (blue) (**Figure 36**). On the one hand, binding was detected within the *MYC* 5' UTR, directly upstream of the alternative CTG start codon (MYC p67). On the other hand, eIF3D was found to bind in *MYC* exon 2, shortly after the ATG start codon (MYC p64). Additionally, eIF3D binding was detected in exon 3, downstream of an internal ATG start codon. In addition to *MYC*, the binding of eIF3D to already known binding sites was examined as a control. Several publications have shown that the eIF3 complex binds to highly structured UTRs of various mRNAs and can positively (e.g. *JUN*) or negatively (e.g. *BTG1*) regulate the translation of the corresponding genes via these (A. S. Lee et al., 2015). As expected, a significant

enrichment of eIF3D within the *JUN* 5' UTR could be detected (**Figure 37**). In contrast, the binding of eIF3D to the *BTG1* 5' UTR could not be detected (**Figure 38**).

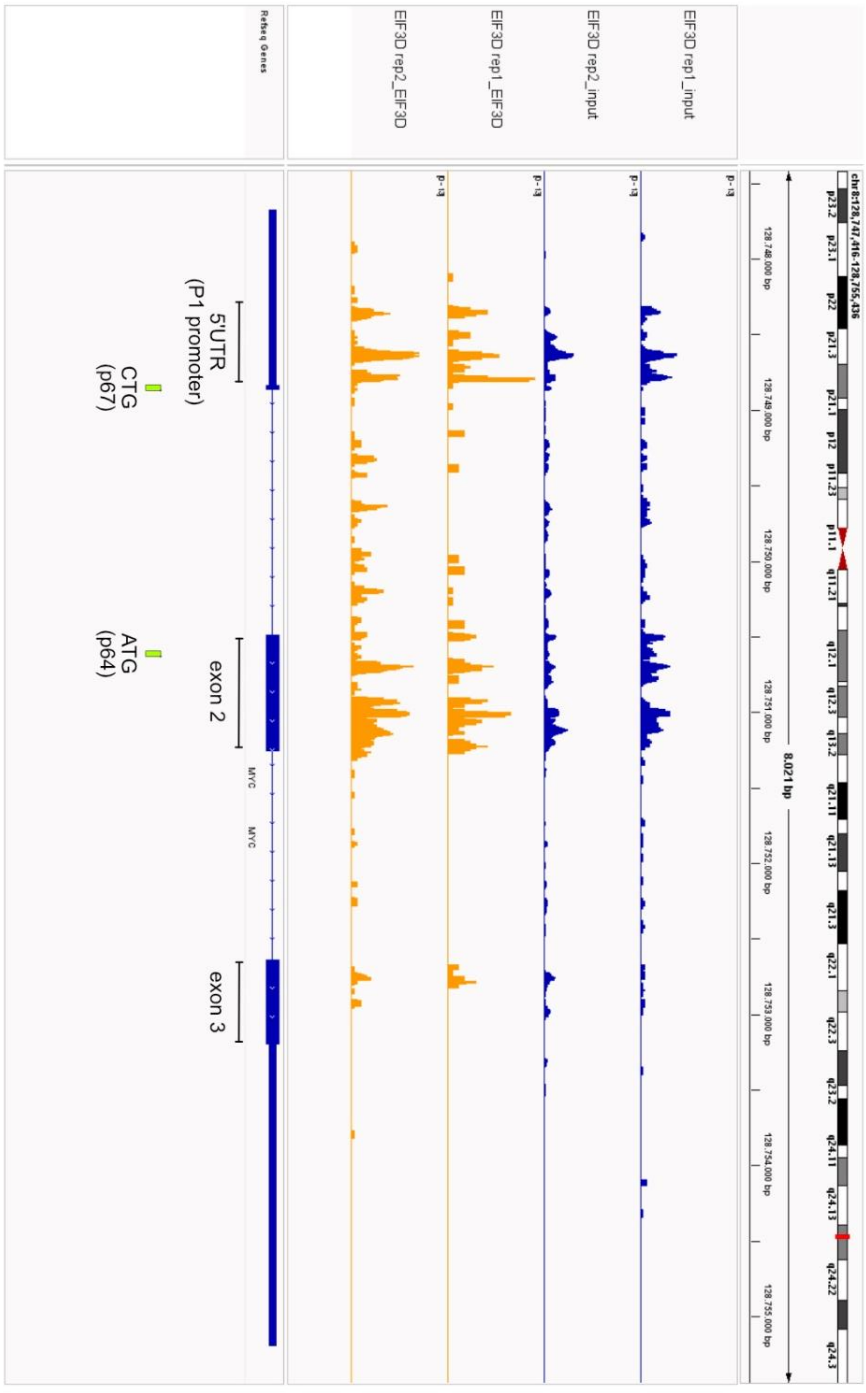

Figure 36: EIF3D binding is enriched on the MYC mRNA. *DLD1 cells were subjected to eCLIP-seq experiment and enrichment of eIF3D-bound RNA sequences over size-matched input (blue) was analysed. Shown are MYC tracks (orange) from two biological replicates, visualised by IGV software.*

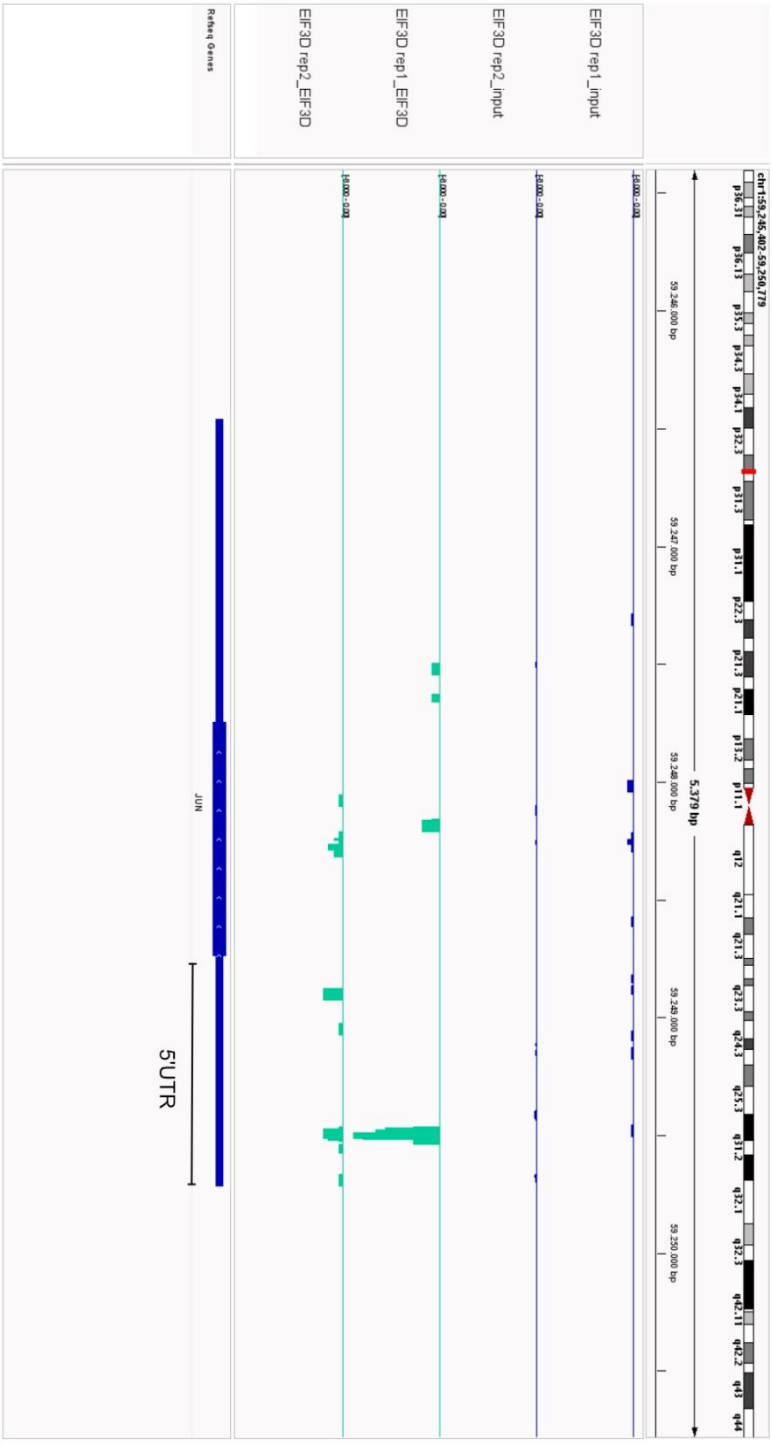

Figure 37: EIF3D binding is enriched on JUN mRNA. *DLD1 cells were subjected to eCLIP-seq experiment and enrichment of eIF3D-bound RNA sequences over SMI (blue) was analysed. Shown are tracks (turquoise) from two biological replicates, visualised by IGV software.*

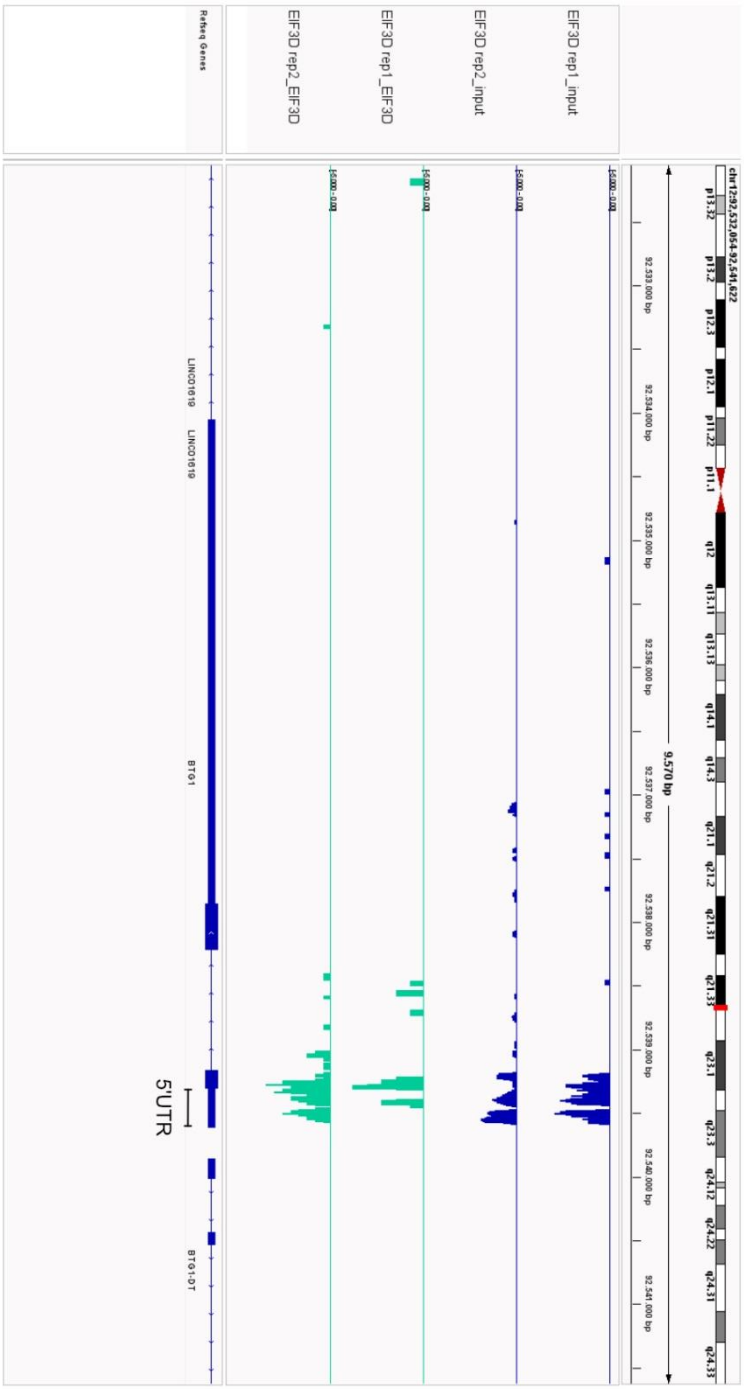

Figure 38: EIF3D binding is not enriched on BTG1 mRNA. *DLD1 cells were subjected to eCLIP-seq experiment and enrichment of eIF3D-bound RNA sequences over SMI (blue) was analysed. Shown are tracks (turquoise) from two biological replicates, visualised by IGV software.*

Even though no binding by eIF3D could be detected for *BTG1*, the enrichment in the *JUN* 5' UTR speaks for the reliability of the result and the *MYC* mRNA seems to be bound by eIF3D in its 5' UTR as well as in downstream sequences.

5 Discussion

5.1 MYC translation is eIF4F-independent in CRC cell lines

In the majority of tumours, activation of the *MYC* gene is found, which can be caused by genetic, epigenetic, transcriptional or post-transcriptional mechanisms (Dhanasekaran et al., 2022). Work from our own group has shown that, particularly in CRC, translation of *MYC* represents a therapeutic target (S. Denk et al., 2021; S. Schmidt et al., 2019; Wiegering et al., 2015). Inhibition of the PI3K-signaling pathway by the dual PI3K/mTOR inhibitor BEZ235 generally leads to the activation of 4EBP1 and to the sequestration of eIF4E. EIF4E is thus no longer available for the formation of the eIF4F complex, which means that translation can no longer be initiated via the canonical pathway (Gingras, Gygi, et al., 1999). Surprisingly, in the CRC cell lines tested, protein expression of MYC was not inhibited by BEZ235 despite inactivation of the PI3K/Akt/mTOR pathway, but instead was upregulated in a dose-dependent manner (**Figure 10 (A)**) (Wiegering et al., 2015). It was theorised that BEZ235-induced activation of 4EBP1 may be too low to affect translation of *MYC*. However, this was disproved by the overexpression of a 4EBP1 phospho-dead mutant. Although the expression of exogenous 4EBP1 by far exceeded that of cellular 4EBP1, no negative effect on MYC protein expression could be detected (**Figure 10 (B)**). Furthermore, knocking down components of the eIF4F complex did not lead to downregulation of MYC expression (**Figure 11**). The enhanced *MYC* expression under inhibition of a signalling pathway that regulates cap-dependent translation and the independence of MYC expression on the eIF4F complex supports the hypothesis that *MYC* might be translated via an alternative, eIF4F-independent mechanism in CRC. Many studies have shown that protein translation in tumours is characteristically altered depending on the type of tumour, resulting in tumour-specific therapeutic targets (S. Schmidt et al., 2020). In contrast to normal tissue, tumours exhibit an altered translation spectrum, which cannot be attributed exclusively to the altered transcription spectrum (Sendoel et al., 2017). In addition, an increased global translation rate has been demonstrated in lymphomas as well as solid tumours despite increased eIF2α phosphorylation, which generally would lead to the inhibition of cap-dependent translation (Faller et al., 2015; Lobo et al., 2000; Ruggero et al., 2004). The use of alternative translation initiation sites, e.g. alternative start codons or initiation via IRESs, is therefore becoming increasingly important in tumours (Cobbold et al., 2010; Sendoel et al., 2017). It is known that many regulatory elements are located in the *MYC* 5' UTR,

which influence the expression of the oncogene. The *MYC* IRES in particular has attracted great attention in the last two decades and has been attributed an essential role in the translation of *MYC* in MM (Chappell et al., 2000). Supportively, in GB, resistance to mTOR inhibitors has been associated with stimulation of IRES-induced translation, particularly of proteins that mediate resistance (Benavides-Serrato et al., 2023). It has been shown that especially the m^6A modification of IRES RNAs, such as *MYC* or *CCND1*, plays a major role in efficient translation and resistance to mTOR inhibition. The associated increased binding of the ITAF hnRNPA1 (discussed in more detail in the following section) has been linked to increased IRES activity. In this work, a possible m^6A modification of the *MYC* 5' UTR was not investigated, but intensive research was carried out to determine to what extent *MYC* translation is dependent on its 5' UTR and whether translation might be initiated via its IRES in CRC.

5.2 MYC IRES inhibitor J007-IRES does not affect MYC protein expression in CRC cells

Attention to IRES-mediated translation has been increasing strongly in recent years, especially as the regulatory mechanisms of viral IRES elements are progressively uncovered. Cellular IRES elements are now also thought to play an important role in the regulation of mRNA translation and IRES-like elements have been identified especially in genes that encode proteins essential for cellular processes and partly act as oncogenes (Godet et al., 2019). This additional regulatory mechanism opens new therapeutic windows, so that the demand and possibility for inhibitors is constantly increasing. Since the function of IRESs is dependent on the activity or presence of certain ITAFs, one approach to develop inhibitors is to prevent the interaction between IRESs and ITAFs. In MM, MYC expression increases as the disease progresses and this is accompanied by an increase in *HNRNP A1* expression (Shi et al., 2022). *A1*-depleted MM cells showed a severe growth defect and a marked decrease in *MYC* expression, most likely due to decreased *MYC* IRES activity as measured by dual luciferase assays. To chemically inhibit the interaction of hnRNP A1 with the *MYC* IRES, the small molecule inhibitor J007-IRES was developed, which led to a significant reduction in MYC expression in GB and MM cells (Holmes et al., 2016; Shi et al., 2022). In contrast, even high concentrations of J007-IRES had no effect on MYC protein expression in DLD1 CRC cells (**Figure 12**). hnRNP A1 plays multiple roles in the regulation of gene

expression and controls the processing of nascent mRNA transcripts. In this context, hnRNP A1 mainly modulates transcription, splicing, stability, nuclear export and translation of cellular and viral transcripts (Jean-Philippe, Paz, & Caputi, 2013), among others via IRESs. In general, *HNRNP A1* is considered an oncogene, is overexpressed in many cancers and is associated with poor prognosis in hepatocellular carcinoma (Z. J. Zhou et al., 2013) and breast cancer (Otsuka, Yamamoto, & Ochiya, 2018). In contrast, in CRC, high expression of the protein is associated with better survival (proteinatlas.org). Since treatment with J007-IRES in DLD1 cells had no effect on MYC protein expression, there are different hypotheses. On the one hand, it is possible that the applied dose of the inhibitor in CRC is not sufficient to prevent the MYC IRES-hnRNP A1 interaction, so that further tests would have to be carried out. Secondly, it is possible that hnRNP A1 does not play a major role in *MYC* IRES translation in CRC, as is the case in MM, because different types of tumours exhibit different needs for translation factors (S. Schmidt et al., 2020). Thus, hnRNP A1 probably does not serve as a therapeutic target in CRC. However, further analysis, such as luciferase assays with *MYC* 5' UTR constructs and *HNRNP A1* depletion, would be required to quantify *MYC* IRES activity and hnRNP A1's impact in CRC.

5.3 Cymarin impairs *MYC* expression, but not by regulating the *MYC* 5' UTR

A small-molecule screen conducted by Didiot *et al.* aimed to identify inhibitors of IRES-mediated translation, specifically of MYC (Didiot et al., 2013). Using a luciferase assay, in which IRES-mediated translation can be quantified independently of cap-dependent translation, the CGs cymarin and somalin were identified as top candidates for inhibiting *MYC* IRES translation under stress conditions in ovarian cancer cell lines. The authors hypothesised that inhibition of MYC protein synthesis is the critical mechanism that ultimately leads to reduced viability of cancer cells after treatment with CGs. In this work, it was shown that cymarin also leads to a significant reduction in MYC protein expression in CRC cell lines, which is accompanied by no (DLD1) or moderate (LS174T) reduction in mRNA expression (**Figure 13**). Even more pronounced effects on *MYC* expression were obtained when PDOs were treated with cymarin (**Figure 15**). The stronger effect of cymarin in PDOs can probably be attributed to the fact that organoids constitute a complex cell system, in which intercellular signalling plays a major role as they mimic

key functional, structural and biological complexity of an organ (Z. Zhao et al., 2022). It is therefore possible that the reduced *MYC* expression leads to more far-reaching changes in cell homeostasis than is the case in 2-D cell culture systems.

Regarding the mechanism underlying the reduction of MYC protein levels, the lack of correlation between mRNA and protein expression initially argues for post-transcriptional or translational regulation. However, an effect on MYC protein stability after cymarin treatment could be excluded in this work (**Figure 17**). As the *MYC* IRES was identified as a direct target of cymarin in the original screen conducted by Didiot *et al.*, *MYC* overexpression constructs were also used in this work to uncover the potential molecular mechanism. DLD1 cells were generated expressing the *MYC* CDS alone, the *MYC* CDS with 5' UTR, and the MYC CDS with 3' UTR. If cymarin mediates its effect via regulation of the IRES, reduced expression of the exogenous construct containing the 5' UTR would be expected. Overexpression of the *MYC* CDS, on the other hand, should rescue this effect. Surprisingly, both the 5' UTR and CDS constructs showed a decrease in exogenous MYC protein expression, suggesting a regulatory mechanism that is not specifically mediated via the 5' UTR or IRES of *MYC* (**Figure 16 (B)**).

In addition to the 5' UTR, elements in the 3' UTR also play a major role in MYC expression. Numerous miRNAs have been identified that regulate the oncogene's expression under certain cellular conditions by binding to the 3' UTR (Cannell et al., 2010; H. H. Kim et al., 2009; Lal et al., 2009; Mihailovich et al., 2015). The 3' UTR was previously shown to couple *MYC* translation to the cellular metabolic status, whereas the detailed mechanism remains to be determined (Dejure et al., 2017). As a third *MYC* construct, the CDS with 3' UTR was therefore tested as well and the expression of exogenous *MYC* after treatment with cymarin was quantified. Here, a decrease in exogenous *MYC* expression was also observed, comparable to the 5' UTR-CDS construct (**Figure 16 (B)**). However, further studies conducted in our group using *MYC* 3' UTR mutants suggested a 3' UTR-mediated regulation of *MYC* expression by cymarin (data not shown). The results support the assumption that cymarin induces a regulatory mechanism that is not specifically mediated via *MYC's* 5' UTR but generates more global changes in the cellular homeostasis.

5.4 Cymarin impairs proliferation and *de novo* protein synthesis in CRC cells

The primary target of CGs is the Na^+/K^+ ATPase (cell membrane-located sodium-potassium pump), which plays a decisive role in maintaining cellular homoeostasis. Cymarin suppresses the activity of the transporter, which reduces the intracellular concentration of K^+ ions and increases intracellular Na^+ and Ca^{2+} ions at the same time (Skubnik, Svobodova Pavlickova, Psotova, & Rimpelova, 2021). The Na^+/K^+ ATPase is therefore essential for maintaining the ion gradient across the cell membrane, to which the function of other transporters and the activity of several signalling pathways is coupled. Besides pumping, the Na^+/K^+ ATPase also plays an important role as a receptor, and protein tyrosine phosphorylation could be detected, although the ATPase itself does not possess a kinase domain. Instead, it was shown that the kinase activity is mediated by membrane-associated non-receptor tyrosine kinases from the Src family which are linked to several other partners like epidermal growth factor receptors (EGFR). The Na^+/K^+ ATPase therefore indirectly activates EGFR which, in turn, leads to activation of the RAS/RAF/MAPK signalling cascade, a pathway involved mainly in cell cycle progression and proliferation (Kometiani, Liu, & Askari, 2005; Liang, Cai, Tian, Qu, & Xie, 2006; Tian, Liu, Garlid, Shapiro, & Xie, 2003). In this work, DLD1 and LS174T cells showed a marked slowing of growth upon cymarin treatment at all concentrations applied, which was associated with a significant prolongation of cell cycle phases (**Figure 14**). However, the activity of cymarin's actual target, the Na^+/K^+ ATPase, was not verified in this study but its inhibition by cymarin could be an explanation for the observed phenotype. Furthermore, signalling pathways linked to the activity of the Na^+/K^+ ATPase could be investigated in more detail to elucidate cymarin's mode of action in CRC cells.

In the literature, CGs are also described as interactors of the regulatory network around mTOR, thereby influencing autophagy, cell growth, cell proliferation and cell death (Cerella, Gaigneaux, Dicato, & Diederich, 2015). Some CGs are considered inhibitors of PI3K/Akt/mTOR and negative regulators of global protein synthesis (Perne et al., 2009; D. M. Zhang et al., 2013). In line with this, reduced global protein synthesis after cymarin treatment was observed in this work, but the molecular mechanism was not investigated in more detail (**Figure 18**). Another CG, ouabain, was identified some time ago as a specific inhibitor of cap-dependent translation (Cao et al., 2014). Mechanistically, ouabain binds to eIF4E thereby preventing the association of eIF4E/eIF4G, but not of eIF4E to the mRNA. This results in a shift to cap-independent translation of certain

mRNAs and a change in the translation spectrum of the cell. It is possible that the reduced *de novo* protein synthesis after cymarin treatment is caused by a similar mechanism and might not only be caused by reduced MYC levels but rather by alteration of upstream signalling pathways.

5.5 Cymarin treatment affects immune signalling in CRC cells, rendering it a promising anti-cancer drug

The fact that cymarin induces global changes in gene expression of CRC cells was evident in the RNA-Seq experiment performed. Interestingly, cymarin treatment led to an upregulation of gene sets associated with immune-signalling pathways, especially of 'TNFα signalling via NFκB', 'inflammatory response', 'IL6-JAK-STAT3 signalling' and 'IL2-STAT5 signalling' pathways (**Figure 19**). On the one hand, this could be related to MYC's described role in the cellular immune response. For example, it has been shown that hyperactivation of *MYC* can lead to tumour-induced immunosuppression, mediated by programmed death ligand 1 (PD-L1) and CD47 (Casey et al., 2016; J. Li, Dong, Wu, Zhu, & Gu, 2023). PD-L1 mediates a so-called "don't find me" signal by blocking the engagement of T cells, whereas CD47 as a "don't eat me" signal blocks the activity of macrophages and T cells (Casey, Baylot, & Felsher, 2018). High MYC levels induce expression of both proteins, suppressing the immune response in numerous tumours and contributing to increased tumour growth of lymphomas, leukaemia, and liver cancer (Casey et al., 2016). The induction of immune signalling-related pathways after cymarin treatment may therefore be related to MYC's role in the cellular immune response and the mediators in this context would have to be identified in further studies. On the other hand, CGs themselves have also been attributed a role as regulators of immunogenic cell death (ICD) (Skubnik et al., 2021). ICD is the complete immunological response of an organism to infected or malignant cells, which are recognised initially by the presentation of antigens by T cells and finally eliminated (Galluzzi, Buque, Kepp, Zitvogel, & Kroemer, 2017). The most important molecules in mediating the ICD process are so-called damage-associated molecular patterns (DAMPs), which are released by cells under certain stress conditions. These include, above all, ER stress and the presence of reactive oxygen species (ROS). CGs also have the potential to induce ER stress or generate ROS via various signalling pathways (Xie & Cai, 2003) and thus trigger ICD (Menger et al., 2012). It is possible that the gene expression pattern of

immune signalling pathways observed in the RNA-seq experiment reflects this mechanism. However, further experiments would also have to be carried out here, for example to test the presentation of DAMPs characteristic of ICD such as ATP, calreticulin, type I interferon, annexin A1 or heat shock proteins 70 or 90.

As mentioned earlier, CGs were originally used as regulators of cardiovascular disorders. Later, epidemiological studies showed a positive correlation between the use of these compounds and the reduced incidence of some cancers (Haux, 1999). Numerous papers subsequently aimed to investigate this relationship and different mechanisms by which CGs induce apoptosis, cell cycle arrest or autophagy were identified (Reddy et al., 2020). One of the best studied CG is digitoxin, which has been linked to inhibition of global protein synthesis (Perne et al., 2009), antagonistic effects towards the estrogen receptor (J. Q. Chen et al., 2006), MAPK pathway-induced apoptosis (Kulikov, Eva, Kirch, Boldyrev, & Scheiner-Bobis, 2007), downregulation of the anti-apoptotic proteins Bcl-xL and Bcl-2 (Lopez-Lazaro, 2007), and production of ROS (Winnicka, Bielawski, & Bielawska, 2006). In contrast, the mode of action of cymarin in cancer cells has been rather poorly studied so far. It has been shown that cymarin suppresses the transcriptional activity of hypoxia-inducible factor 1 (HIF-1), which plays an important role in the adaptation of cancer cells to hypoxic conditions (H. Zhang et al., 2008). The effects observed in this work, such as reduction of *MYC* expression, slowing of proliferation, inhibition of global protein synthesis and induction of an immune response, suggest that cymarin could also gain importance as a potential anti-cancer drug. Regulation of the *MYC* IRES or 5' UTR could not be confirmed as the cause of the observed phenotype in the cell system used here and therefore the mechanisms were not further characterised in this work. Further studies should instead be conducted in a different context to investigate the molecular mechanism and specifically the influence in cancer cells to open a new therapeutic window in CRC.

5.6 Many of the identified *MYC* 5’ UTR binders are attributed a role in different types of cancers

In the experiments performed in this work, the *MYC* IRES inhibitors J007-IRES and cymarin did not show an exclusive effect on MYC mRNA translation. Assuming that these drugs do regulate IRES activity, it is possible that this structure does not play a decisive role in *MYC* translation in CRC. However, the *MYC* 5’ UTR is subject to various regulatory

mechanisms, so a different approach was subsequently pursued. In addition to eIF4E-dependent translation initiation, other possibilities exist to initiate protein synthesis in a cap-dependent manner, requiring an altered spectrum of translation initiation factors that interact with the 5' UTR. In addition, alternative translation initiation factors are sometimes used in tumours and there is an altered dependence on ribosomal proteins. Untransformed keratinocytes, for example, show a dependence on eIF2α, eIF2β and eIF5, whereas these are not essential in *SOX2*-transformed keratinocytes. Instead, these rely on the alternative initiation factor eIF2A (Sendoel et al., 2017). Tumours also exhibit an alternative dependence on ribosomal proteins. RPL24, for example, plays a central role in *MYC*-driven lymphomas and is haploinsufficient for tumour development, whereas deletion of one copy of the *RPL24* gene does not affect normal development in mice (Barna et al., 2008). Furthermore, eIF4A was identified as an essential factor in tumours to unwind mRNAs with complex structures in the 5' UTR (e.g. *MYC*) (Wiegering et al., 2015; Wolfe et al., 2014). The *in vitro* RNA pulldown performed here identified numerous proteins that specifically bind the *MYC* 5' UTR and thus have the potential to regulate it (**Figure 20**). In principle, the reliability of the pulldown result was confirmed by the presence of previously published binding proteins of the *MYC* 5' UTR, such as SFPQ, YBX1, GRSF1, NONO (Cobbold et al., 2008), hnRNPA1 (Jo et al., 2008), or PTBP1 (Cobbold et al., 2010) as well as binders of other 5' UTRs like NCL (Morfoisse et al., 2016; Takagi et al., 2005), hnRNPM (Ainaoui et al., 2015), RPS19 (Horos et al., 2012), ILF3 (Halaby et al., 2015), RPL26 (Takagi et al., 2005), and hnRNPD (Omnus et al., 2011; Reboll et al., 2007). Interestingly, several subunits of the eIF3 complex (eIF3A, B, C, D, L) were present in the pulldown as well as various ribosomal proteins of the small (RPS3A, 4X, 11, 15A, 17, 18, 19, 20) and large (RPL22, 23A, 26, 31) ribosomal subunit. Surprisingly, eIF2α (*EIF2S1*) also appeared in the list of MYC 5' UTR binding proteins. Many solid tumours as well as lymphomas exhibit increased translation rates despite elevated phosphorylation of eIF2α (Faller et al., 2015; Lobo et al., 2000; Ruggero et al., 2004; S. Schmidt et al., 2019). High levels of P-eIF2α prevent formation of the TC, leading to inhibition of canonical cap-dependent translation (Jennings et al., 2013). Therefore, a relevant amount of eIF2α-independent translation is thought to occur in tumours, e.g. by using alternative translation initiation factors and/or IRES structures in the corresponding mRNA (Koromilas, 2015). In principle, eIF2α is required for both cap-dependent and cap-independent translation, however, the activity of some IRESs is enhanced by phosphorylation of eIF2α (Fernandez et al., 2002). Interestingly, activity of the MYC IRES has been shown to be dependent on the availability of the TC in HeLa

cells (Spriggs et al., 2009). Since eIF2α has been identified as a binding protein *in vitro*, it can be assumed that 5' UTR-mediated translation of *MYC* is eIF2α-dependent in CRC cells.

Potential positive regulators of the *MYC* 5' UTR were identified in an siRNA knockdown screen following the pulldown (**Figure 22**). Of 69 screened hits, the top candidates identified were *RPL23A*, *EIF3D*, *RPS11*, *RPS15A*, *RPS20, RPS17*, *RPS19,* and *eIF3B*, whose knockdown led to a significant decrease in MYC protein expression. A closer look revealed that all identified MYC regulators play roles in different types of tumours. RPS15A has been attributed a role in lung, GB, gastric, liver and CRC and RPS20 has also been identified as a critical factor in the development of hereditary nonpolyposis colorectal cancer and gastric cancer (J. Kang et al., 2021). In CRC, RPS15A is thought to promote malignant transformation through misregulation of the p53 signalling pathway and high expression was associated with poor prognosis of CRC patients (J. Chen et al., 2016). In addition, it was shown for RPS20 that crosstalk with Guanine nucleotide binding protein like 1 (GNL1) is critical to promote cell proliferation in primary colon and gastric cancers (Krishnan, Boddapati, & Mahalingam, 2018) and mutated *RPS20* leads to a defect in pre-ribosomal RNA maturation and predisposition to microsatellite-stable (MSS) colon cancer (Nieminen et al., 2014). Besides that, high RPS11 expression in hepatocellular carcinoma was associated with poor survival of patients after curative resection (C. Zhou et al., 2020) and predicted poor survival of patients with primary glioblastoma (Yong et al., 2015). Amplification of *RPL23A* was more frequently found among highly aggressive endometrial tumours and increased expression was observed for prostate and liver cancer (El Khoury & Nasr, 2021; Fancello, Kampen, Hofman, Verbeeck, & De Keersmaecker, 2017). In addition, RPS17 was associated with microsatellite instability (MSI) in CRC (C. Yu et al., 2019) and RPS19 was shown to be increased in colon and prostate cancer (J. Kang et al., 2021). Furthermore, RPS19 is thought to be implicated in IRES-mediated translation of erythroblast proliferation and differentiation factors *BAG1* and *CSDE1* in Diamond-Blackfan anemia (Horos et al., 2012). Interestingly, two subunits of the eIF3 complex, eIF3B and D, were among the top MYC regulators. eIF3 constitutes the largest and most complex eIF, and is generally crucial for translation initiation, termination, ribosome recycling, and in the stimulation of stop codon read-through (Gomes-Duarte, Lacerda, Menezes, & Romao, 2018). Additionally, eIF3 is thought to act as translational activator or repressor by binding to structured sequences in 5’ UTRs of specific mRNAs (A. S. Lee et al., 2015; Thakor et al., 2017). Dysregulated eIF3D expression in particular was associated with advanced

tumour stage of gall bladder cancer (GBC) and metastasis (F. Zhang et al., 2017). Besides that, eIF3B (together with eIF3A) functions as a core component of the whole eIF3 complex around which all other subunits assemble in an ordered way (Gomes-Duarte et al., 2018). It is therefore not surprising that dysregulation of eIF3B leads to worse outcome in bladder cancer, esophagus squamous-cell carcinoma, prostate cancer and breast cancer. The literature clearly shows that all potential MYC regulators play a role in the development and maintenance of tumours and were worthy of closer examination in further validation experiments.

5.7 Knockdown experiments reveal eIF3D as the top candidate for regulating MYC protein expression

In the further course, individual siRNA pools against the corresponding genes identified in the pulldown and the siRNA screen were tested for their potential to regulate MYC expression at the protein and mRNA level as well as the proliferation behaviour of CRC cells. After analysing the knockdown efficiencies, it was found that despite a partially strong decrease in the expression of the respective protein, only the knockdown of eIF3D led to a significant reduction in MYC protein expression (**Figure 24 (A) + (B)**). This was associated with an increase in MYC mRNA expression (**Figure 24 (C)**), suggesting regulation at the translational level. Nevertheless, knockdown of almost all hits tested (except ILF3 and RPL23A) resulted in a proliferation defect which could not be attributed to an increased apoptosis rate but rather a shift in cell cycle phase distribution (**Figure 25** + **Figure 26**). This suggests that EIF3B, EIF3D, RPS11, RPS15A, RPS17, RPS19 and RPS20 are generally essential for CRC cell growth. However, except for EIF3D, this phenotype is not due to a regulation of *MYC* translation, but rather speaks for a general importance of these factors. Various studies have shown that eukaryotic ribosomes do not have a fixed stoichiometry of their core ribosomal proteins, but that this is adapted depending on the tissue type and the physiological conditions via the expression of the RPs (Gilbert, 2011; Xue & Barna, 2012). Mutations in core RPs specifically affect the translation of certain mRNAs, whereas others are not affected and thus an adaptation of the cellular translation spectrum can occur. In addition, it has been shown, especially in yeast models, that some RPs have extraribosomal functions and thus influence certain cellular functions (Warner & McIntosh, 2009). It is therefore possible that the RPs identified in the pulldown bind to the *MYC* 5' UTR, but knockdown of these factors results

in far more global effects. In the further course of the work, the focus was therefore on eIF3D as the most promising MYC regulator.

5.8 eIF3 holds a special role in cellular protein synthesis

As already mentioned, with its 800 kDa, eIF3 is the largest of all initiation factors, composed of the thirteen subunits A - M, and has the most diverse functions in almost every step of eukaryotic translation (Cate, 2017). Cryo-electron microscopy reconstruction of eIF3 revealed a five-lobe architecture with binding sites for the 40S ribosomal subunit as well as other initiation factors and mRNA structures (**Figure 39**) (Siridechadilok, Fraser, Hall, Doudna, & Nogales, 2005; Srivastava, Verschoor, & Frank, 1992).

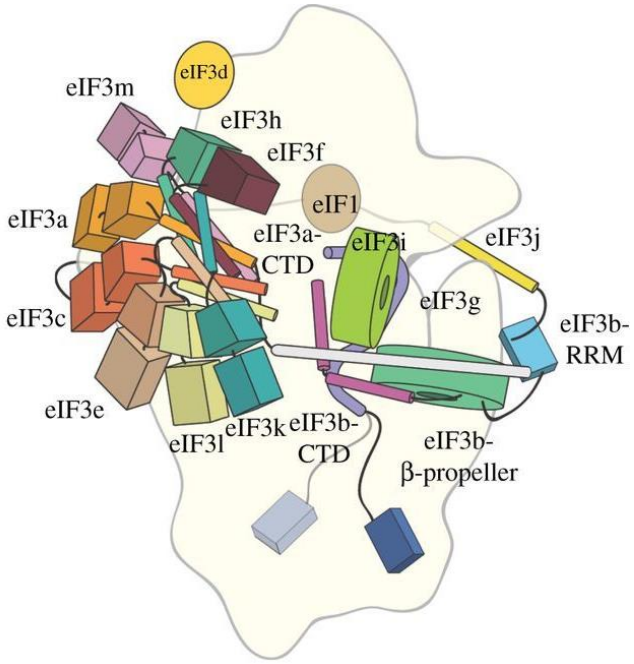

***Figure 39: Model of mammalian eIF3 bound to the 40S ribosomal subunit**. Reprinted from (Cate, 2017).*

Deletion analyses showed that the evolutionarily conserved subunits eIF3A, B and C and the non-conserved subunits E, F and H comprise the functional core and are essential for general translation initiation activity (Masutani, Sonenberg, Yokoyama, & Imataka, 2007). In contrast, subunits D, I, J, K, L, and M are thought to be dispensable for

translation initiation. Regarding its functions, eIF3 is essentially involved in the formation of the TC by enabling the binding of Met-tRNAi to the 40S ribosomal subunit even in the absence of an mRNA (Schreier & Staehelin, 1973). In addition, eIF3 controls the rate and processivity of the scanning process and is instrumental in start codon selection (Karaskova et al., 2012; Valasek, Nielsen, Zhang, Fekete, & Hinnebusch, 2004). eIF3 does not appear to be actively involved in the attachment of the 60S ribosomal subunit, but it remains bound to the 80S ribosome during the early elongation phase (Mohammad, Munzarova Pondelickova, Zeman, Gunisova, & Valasek, 2017). It is assumed that by remaining connected to the 80S complex, re-initiation at downstream start codons is facilitated (Szamecz et al., 2008). Furthermore, the eIF3 complex contributes to ribosome recycling and prevents premature assembly of the 40 and 60S subunit (Kaempfer & Kaufman, 1972; Kolupaeva, Unbehaun, Lomakin, Hellen, & Pestova, 2005). In addition to its role in canonical translation initiation, the eIF3 complex or certain of its subunits have independently been attributed specific functions in the translation of defined mRNAs (see section 1.1.3.4) and in the regulation of protein stability (S. Ma, Liu, & Zhang, 2023). However, in addition to its role in cellular translation, eIF3 has also been shown to be instrumental in the translation of encephalomyocarditis viral RNA as well as in hepatitis C virus (HCV) translation via an IRES (Strycharz, Ranki, & Dahl, 1974; Sun et al., 2013). Furthermore, eIF3 has been suggested to link translation initiation to nonsense-mediated mRNA decay activation, thereby leading to translation initiation repression (Isken et al., 2008). The multiple functions of eIF3 suggest that this factor plays a crucial role in cellular protein synthesis and may regulate it via both the canonical and non-canonical mechanisms of translation initiation. Overexpression of eIF3 is associated with various types of cancer, so that the underlying mechanism is of great importance for finding a therapeutic target (Hershey, 2010; L. Zhang, Pan, & Hershey, 2007). In one study, photoactivatable ribonucleoside-enhanced (PAR-) CLIP was used to identify genome-wide transcripts that interact with the eIF3 complex (A. S. Lee et al., 2015). These were a highly specific set of mRNAs involved in cell growth-related processes such as cell cycle, differentiation and apoptosis. In particular, eIF3 was shown to contribute to translational activation (shown for *JUN*) or repression (shown for *BTG1*) via binding and regulation of the 5' UTR. *JUN*, as a member of the immediate early response transcription factor AP1 and a positive mitotic regulator was shown to be translated independently of the eIF4F complex but instead relies on a 5’ cap-binding activity in eIF3D which is universally conserved in multicellular eukaryotes (Cate, 2017; A. S. Lee et al., 2016; Wisdom, Johnson, & Moore, 1999). However, MYC did not appear

in the list of eIF3-regulated mRNAs obtained from the PAR-CLIP experiment (A. S. Lee et al., 2015). Thus, it is of great interest whether there might be a similar, so far unknown mechanism for eIF3-dependent *MYC* translation.

5.9 eIF3D is linked to *MYC* expression and proliferation of CRC cells and MTOs

Therefore, DLD1 and LS174T cells were generated in which stable knockdown of *EIF3D* was achieved by constitutive expression of shRNAs. Again, MYC protein levels were significantly reduced after *EIF3D* knockdown (**Figure 27** + **Figure 29**). In contrast to the siRNA-induced knockdown of *EIF3D*, negative effects on *MYC* mRNA expression were now also observed. However, these were weaker than at the protein level, meaning that there may be a secondary effect due to the 6-day depletion of *EIF3D* and MYC's role as global regulator of gene expression. Besides the effects on *MYC* expression, a clear proliferation defect was also observed after shRNA-mediated knockdown, but in contrast to siRNA-mediated knockdown, this was accompanied by an increase in the apoptosis rate (**Figure 28** + **Figure 30**). DLD1 cells carry mutations in the *TP53*, *KRAS*, and *APC* genes, whereas LS174T are mutated for *β-catenin*, *KRAS* and *BRAF* (Berg et al., 2017). Since similar results were achieved in both tested cell lines, it can be assumed that the mutation status does not play a decisive role here. To further validate *EIF3D* depletion in a more complex cell system, LAKTP MTOs were utilised that carry mutations in *APC*, *KRAS*, *TP53*, *TGFBR2* genes, representing the status of advanced human colorectal adenocarcinoma (Tauriello et al., 2018). These were genetically modified to express inducible shRNAs against *Eif3d*. Similar to the cell lines tested, a clear reduction in cell viability could be observed which was accompanied by a growth defect represented by markedly smaller organoids upon *Eif3d* depletion (**Figure 32 (A) + (B)**). However, *Eif3d* knockdown efficiency was not as strong as in the 2-D cell system, most likely because a different lentiviral vector was used here (pInducer instead of pLT3) and the induction of the shRNA was less efficient than constitutive expression. Furthermore, no difference in Myc protein expression upon *Eif3d* depletion was detected, which is probably caused by a technical issue and needs to be further addressed (**Figure 32 (C)**). Additionally, a non-targeting control should be included in the experiments to confirm an *Eif3d*-knockdown-induced phenotype. Also, the comparison to non-transformed wild-type organoids would be of great interest, as the hypothesis is that eIF3D is essential for tumour but not for

healthy tissue. In addition, other organoids with different mutation backgrounds (e.g. *APC*, *APC/TP53*, *APC/KRAS*, *APC/KRAS/TP53*) should be tested for effects after *Eif3d* depletion. Analysis of *Myc* expression, morphology, cell viability and expression of differentiation, proliferation or stem cell markers will provide information on whether all oncogenic mutant organoids are equally sensitive to *Eif3d* depletion. Following MTO-based experiments, the results should be validated on a series of human PDOs in order to obtain an indication of the therapeutic window.

5.10 Depletion of *EIF3D* is associated with reduced *de novo* protein synthesis and global loss of polyribosomal mRNAs

As already mentioned, eIF3D is not a core component and its loss should not impair the integrity of the whole eIF3 complex. Therefore, it is of great interest which global effects knockdown of *EIF3D* might have. As shown above, siRNA-mediated knockdown of *EIF3D* induced a marked decrease in global *de novo* protein synthesis, reflected by decreased puromycin incorporation (**Figure 33**). However, from this result it is not possible to determine whether the effect on global protein synthesis is directly mediated by the loss of eIF3D or whether secondary effects, e.g. due to low MYC levels, contribute to this effect. MYC is also involved in the control of translation by regulating the expression of rRNAs and tRNAs, which could be a possible explanation for the decreased translation rate (van Riggelen et al., 2010). In this context, polysome profiling analysis was performed to examine the distribution of all cellular mRNAs among monosomal and polysomal fractions, respectively, to obtain information about the global translation status. After knockdown of *EIF3D*, an accumulation of mRNAs in the monosomal 80S fraction was observed, whereas significantly fewer polysomal mRNAs were present compared to the control (**Figure 34**). It was previously shown that *EIF3D* depletion in Normal Human Dermal Fibroblasts (NHDFs) results in reduced initiation of translation, being evidenced by modestly increased 80S and 40S/60S ribosomal subunits and slightly decreased polyribosome abundance (L. Thompson et al., 2022). These modest effects were attributed to the fact that the majority of mRNAs are translated in an eIF3D-independent manner depending on eIF4E-driven ribosome loading and cap recognition (de la Parra et al., 2018; A. S. Lee et al., 2015; A. S. Lee et al., 2016). In this work, the effects were more pronounced after knockdown of *EIF3D*. It is therefore possible that there is a greater dependence of mRNA translation on eIF3D

in CRC, which should be investigated by further analyses. Furthermore, it seems like the loss of *EIF3D* does not affect the general assembly of the ribosome to mRNAs, which is one of the functions attributed to eIF3. However, the attachment of further ribosomes seems to be impaired. Another function of the eIF3 complex is to support dissociation of the 80S ribosome into 40S and 60S subunits after translation of an mRNA has completed (Kolupaeva et al., 2005). Possibly, this function is suppressed by the loss of eIF3D, leaving the ribosomes attached to the mRNA bound and no pool of free 40S and 60S subunits in the cell to initiate further translation events. However, the polysome profile shown here represents only the average of all cellular mRNAs and does not indicate whether a particular subset of mRNAs is specifically regulated. It would therefore be of great interest to perform RNA-seq from the different ribosomal fractions to identify those mRNAs that are differentially regulated and whether they are involved in specific cellular processes. In order to examine this in a more clinical context, polysome profiles from wild-type organoids and differently mutated tumour organoids (e.g. *APC, APC/TP53, APC/KRAS, APC/KRAS/TP53*) could also be created with and without knockdown of *Eif3d*. By performing RNA-seq from individual ribosomal fractions, it could be determined whether the dependence on eIF3D is related to increasing mutation load and which mRNAs are particularly influenced. If there is a different regulation of mRNA translation after eIF3D knockdown in tumour and wild-type organoids, this would strengthen the hypothesis that eIF3D plays a special role in CRC.

5.11 Depletion of *EIF3D* and *MYC* similarly change gene expression in CRC cells suggesting a link between eIF3D and MYC expression

The results so far indicate that the loss of eIF3D has a global effect, such as reduced *de novo* protein synthesis or loss of polyribosomal mRNAs. To investigate this phenotype in more detail, the cellular gene expression pattern after siRNA-induced *EIF3D* knockdown was examined using RNA-seq. In parallel, the extent to which this overlapped with the knockdown of *MYC* was examined to find a possible correlation. Interestingly, many gene sets were identified that were regulated in the same way after knockdown of *MYC* and *eIF3D,* respectively (**Figure 35**). Surprisingly, the most down-regulated gene sets in both conditions were 'MYC targets V1' and 'MYC targets V2'. In conjunction with the previously observed reduction in MYC protein levels, this may suggest a dependence of *MYC* expression on eIF3D. However, it is not possible to conclude from this experiment

whether the regulation takes place at the transcriptional or translational level, as both could lead to the same result. Furthermore, decreased expression was found in genes involved in the 'Unfolded Protein Response' (UPR). The ER provides a complex network of chaperones, foldases, cofactors and quality control mechanisms for the secretory pathway, and perturbations in this system lead to the accumulation of unfolded or misfolded proteins in the ER lumen (Schwarz & Blower, 2016; M. Wang & Kaufman, 2014). This stress activates the UPR, which leads to increased expression of chaperones and inhibition of translation or initiation of the apoptotic pathway, depending on the severity of the stress (Hetz, Chevet, & Oakes, 2015; I. Kim, Xu, & Reed, 2008; Ruggiano, Foresti, & Carvalho, 2014; Walter & Ron, 2011). Many tumours take advantage of the UPR to cope with increased protein synthesis or to adapt to the tumour microenvironment, which is often characterised by hypoxia or nutrient deprivation (T. Zhang, Li, Sun, Jin, & Sheng, 2020). Notably, the ER-stress-activated UPR is an adaptive response and encompasses the activation of the ISR by phosphorylation of eIF2α (Pakos-Zebrucka et al., 2016). Interestingly, Mukhopadhyay *et al*. recently showed that the persistent ISR is driven by eIF3D, acting as a regulator of core stress response orchestrators (Mukhopadhyay, Amodeo, & Lee, 2023). In detail, during chronic stress, eIF3D translationally activates GCN2, one of the stress-related kinases that phosphorylates eIF2α, thus inhibiting general protein synthesis. At the same time, eIF3D induces the expression of the m^6A demethylase ALKBH5 to drive 5' UTR-specific demethylation of stress response genes, e.g. *ATF4*, thereby inducing their translation. Thus, the switch to eIF3D-specialised translation represents an essential regulatory mechanism by which cellular survival is ensured. Inhibition of *EIF3D* expression might therefore lead to dysfunctional stress signalling and induction of cell death, rendering it a promising target in tumour cells. Besides that, activation of *MYC* also represents an intrinsic stress by increasing the protein synthetic capacity of the cell, thereby enhancing cell survival, proliferation and genome instability in tumours (Dai & Lu, 2008; Ruggero, 2009; van Riggelen et al., 2010). Subsequently, increased protein synthesis can lead to induction of the UPR (Nguyen et al., 2018; Tameire, Verginadis, & Koumenis, 2015). A direct link between MYC and the UPR has also been proposed, e.g. through direct regulation of components of the PERK pathway (another stress-related eIF2α kinase) such as binding and activation of the *ATF4* promoter. It is therefore not surprising that after knockdown of *MYC*, the 'Unfolded protein response' was downregulated and this, together with eIF3D's important function, could open a therapeutic window in which

components of the UPR signalling pathway may be targeted in *MYC*-hyperactivated colorectal tumours.

Another master regulator of protein synthesis is mTOR kinase, whose activity is often deregulated in tumours (X. Wang & Proud, 2006; Zoncu, Efeyan, & Sabatini, 2011). As part of mTORC1, mTOR controls protein synthesis, at least in part, by direct phosphorylation of 4EBPs and S6K (Brown et al., 1995; Gingras, Kennedy, O'Leary, Sonenberg, & Hay, 1998). In B-lymphocytes of a *Eμ-Myc* transgenic mouse model, *Myc* overexpression was shown to result in hyperphosphorylation of 4EBP1 (Pourdehnad et al., 2013). In the hyperphosphorylated state, 4EBPs are unable to bind eIF4E, which is thus available for the formation of the eIF4F complex to initiate protein synthesis (Somers et al., 2013). Therefore, regulation of the activity of the tumour suppressor 4EBP1 is thought to be part of the *Myc* oncogenic programme at the earliest stage of tumour development. The downregulation of mTORC1 signalling observed in RNA-seq after *MYC* and *EIF3D* knockdown may be explained by this mechanism.

Surprisingly, depletion of *MYC* and *EIF3D* led to a decrease in expression of gene sets that have previously been identified as targets for repression by MYC (Krenz et al., 2021). Specifically, ‘TNF alpha signalling via NFκB’ and ‘Inflammatory response’ were significantly downregulated in both conditions, arguing for an alternative regulatory mechanism than in pancreatic ductal adenocarcinoma. Another gene set downregulated by *MYC* and *EIF3D* knockdown, respectively, were ‘E2F targets‘. Here, ‘E2F’ is the collective term used for at least seven different transcription factors (E2F1–E2F7), which are of high importance in both cell cycle progression and cancer (Muller & Helin, 2000; J. R. Nevins, 2001). Previous studies have shown that MYC induces transcription of E2F1, E2F2 and E2F3 and that *Myc*-induced S phase and apoptosis requires distinct E2F activities in mouse embryo fibroblasts (Leone et al., 2001). *MYC* in turn, as well as various other transcription factors (e.g. *JUN*) and cell cycle regulators (e.g. *CCND1, CCND3*) have been identified as E2F targets (Bracken, Ciro, Cocito, & Helin, 2004). This suggests a regulatory loop in which the coupling of MYC and E2F activity is used to control cell proliferation and cell fate decisions. On the other hand, it is not yet clear whether there is also a link between eIF3D and *E2F* expression. Interestingly, knockdown of another eIF3 subunit, eIF3B, led to a marked decrease in *E2F1* expression and was associated with slowed proliferation and migration of gastric cancer cells (F. Ma et al., 2019). It is therefore possible that in CRC, eIF3D regulates a similar mechanism.

In addition to all the downregulated gene sets, 'interferon gamma response' and 'interferon alpha response' were identified as equally upregulated gene sets after *MYC* and *EIF3D* depletion. Supporting this, a previous study showed that MYC overexpression in triple negative breast cancer (TNBC) leads to a strong downregulation of interferon signalling pathways and thus mediates immune evasion in these tumours (Zimmerli et al., 2022). The increased expression of interferon signalling pathways after *MYC* knockdown leads to the assumption that a similar mechanism exists in CRC.

For all the regulated gene sets described above, there are already published correlations with *MYC* expression, which speaks for a high reliability of the RNA-seq result. The fact that all these gene sets are also influenced by knockdown of eIF3D suggests a direct link between *EIF3D* and *MYC* expression. Interestingly, in addition to the equally regulated gene sets, some were also identified that are induced after *MYC* knockdown but are repressed by the knockdown of *EIF3D*. These included 'Epithelial mesenchymal transition' (EMT), 'Angiogenesis', and 'IL6 JAK STAT3 signalling'. EMT describes a mechanism where cells undergo a developmental switch from a polarised epithelial phenotype to a highly motile mesenchymal phenotype which is associated with invasion and motility of cancer cells (Cho, Cho, Lee, & Kang, 2010). In contrast to the observed upregulation upon *MYC* knockdown in the RNA-seq experiment, overexpression of *MYC* was shown to induce EMT in mammary epithelial cells. Thus, in CRC, MYC seems to be involved in EMT in a different way. However, eIF3D in conjunction with DAP5 is thought to play a role in the selective translation of certain mRNAs (Alard et al., 2023). Cap-dependent, DAP5/eIF3D-mediated translation is thought to contribute primarily to the expression of EMT-associated transcription factors and regulators, cell survival and angiogenesis factors. Loss of eIF3D could therefore disrupt this regulatory mechanism and lead to the observed downregulation of the EMT gene set. Similarly, this could also explain the repression of the angiogenesis gene set, a process by which tumours secure their supply of oxygen and nutrients by forming new blood vessels (Lugano, Ramachandran, & Dimberg, 2020). Although MYC was previously shown to be essential for vasculogenesis and angiogenesis during development and tumour progression (Baudino et al., 2002), the RNA-seq experiment clearly showed an upregulation of the associated gene set upon *MYC* depletion. Thus, like EMT, it seems like this pathway is also differentially regulated in CRC. Furthermore, *MYC* depletion here also led to an upregulation of ‘IL6 JAK STAT3 signalling’, whereas this pathway was downregulated upon *EIF3D* depletion. JAK/STAT signalling is one of the main pathways critical for cell growth, proliferation and migration and it was previously found that this signalling

cascade is especially upregulated under mTOR inhibition (Hua, Kong, Yin, Zhang, & Jiang, 2020; Shin et al., 2023). In this context, it was also shown that the inhibition of mTOR signalling leads to the selective translation of eIF3D-dependent mRNAs and that the interaction of eIF3D with other RNA-binding proteins plays a crucial role. The results of the RNA-seq carried out here support this hypothesis, so that the next step is to define those mRNAs that are specifically regulated by eIF3D in CRC. For this purpose, a gene expression analysis from the monosomal and polysomal fractions of the previously performed polysome profiling after *EIF3D* knockdown using RNA-seq is planned as described in section 5.10. In parallel, a proteome analysis upon si*EIF3D* will be carried out to investigate global effects on protein abundance. The comparison of the RNA-seq data with the proteome data will provide information on whether specifically translation of certain mRNAs is dependent on eIF3D.

5.12 eIF3D has multiple binding sites in the *MYC* mRNA

As mentioned previously, binding of eIF3 to a secondary structure in the *JUN* mRNA induces its eIF4F-independent translation but is instead dependent on a cap-binding activity in eIF3D (Cate, 2017). Cap-binding by eIF3D requires prior allosteric activation of the cap binding pocket, to which access usually is blocked by eIF3D's 'RNA gate'. Binding of the eIF3 complex to secondary structures in the 5' UTR is thought to induce this conformational change, thereby promoting translation of eIF4F-independent mRNAs. As the *in vitro* transcribed *MYC* mRNA from the pulldown did not include a cap structure, it is possible that eIF3D was either pulled down as indirect *MYC* 5' UTR binding protein, embedded in the eIF3 complex or that it has additional binding sites in the *MYC* mRNA. The first hypothesis is supported by the presence of other eIF3 subunits like eIF3A, B, C, and L in the pulldown (**Figure 20**). However, Lee *et al*. demonstrated that the majority of eIF3-bound mRNAs contain single eIF3-binding sites and that these interact with distinct combinations of eIF3A, B, D and G subunits (A. S. Lee et al., 2015). To identify the eIF3D binding sites in the *MYC* mRNA in more detail, an eCLIP-seq experiment was conducted in this work. EIF3D binding sites were detected within the *MYC* 5' UTR directly upstream of the alternative CTG start codon (MYC p67) and in MYC exon 2, shortly after the ATG start codon (MYC p64) (**Figure 36**). Additionally, a short region in exon 3 was bound by eIF3D, downstream of an internal ATG codon. She et al. recently linked eIF3D to start codon selectivity (She, Luo, & Weissman, 2023). In detail,

it was shown that knockdown of *EIF3D* leads to a significantly more frequent use of alternative CUG start codons and that the N-terminal tail of eIF3D plays a crucial role in the selection of AUG start codons. Considering this, it is not surprising that eIF3D is mainly found in the vicinity of start codons in the eCLIP-seq experiment. However, it is still unclear whether this mechanism is related to eIF3D's cap-binding activity. *MYC* 5' UTR luciferase constructs should therefore be utilised to further understand eIF3D's role in translation of *MYC*. After depletion of *EIF3D*, a reduced luminescence signal of a MYC 5' UTR^{wt} reporter would be expected in the case of dependence. In parallel, *MYC* 5' UTR reporters containing mutations of different lengths in the 5' UTR (MYC-5' UTR^{del}), targeting the identified binding sites from the eCLIP-seq, should be tested to validate the binding of eIF3D to a specific region in the *MYC* 5' UTR. If the expression of the deleted constructs is altered after depletion of eIF3D, the corresponding regions will be further investigated. In this context, an *in vitro* pulldown of biotinylated MYC-5'UTR^{wt} or MYC-5'UTR^{del} RNA with subsequent immunoblot could provide information on whether eIF3D or other subunits of the complex are bound and whether this binding is altered by deletion of certain regions in the 5' UTR.

As a control for the validity of the eCLIP-seq experiment, binding of eIF3D was detected in the *JUN* 5' UTR (**Figure 37**). As mentioned above, eIF3 binds to a secondary structure in the *JUN* 5' UTR, thereby mediating its eIF4F-independent translation. To investigate whether a similar mechanism exists for *MYC*, the secondary structure of the *MYC* 5' UTR should be reconstructed by means of selective 2'-hydroxyl acylation analysed by primer extension (SHAPE) to 1) check by mutation analyses whether this is essential for binding by eIF3D and 2) to investigate whether there is similarity to the already published structure in the *JUN* mRNA. In contrast to *JUN*, no significant enrichment of eIF3D was detected in the *BTG1* mRNA, which may be due to technical issues (**Figure 38**). Overall, the CLIP-seq experiment showed a clear variance between both replicates on the one hand and a rather weak enrichment of reads in the eIF3D IP compared to the control on the other hand. Since these two criteria are crucial for the quality of the eCLIP-seq experiment, it will be repeated with the help of technical improvements and an adaptation of the CLIP protocol. For further validation regarding binding to the MYC mRNA, a "manual" CLIP experiment could be carried out. For this, instead of sequencing, the eIF3D IP is followed by a manual check of the eIF3D binding sites using qRT-PCR with specific primers. The exact binding site of eIF3D in the *MYC* mRNA could be determined in this way and provide further information about the mechanism. Furthermore, global analyses of all identified eIF3D-bound mRNAs could provide information about whether

they share common cellular functions, are involved in particular cellular processes and maybe also harbour secondary structures in their 5’ UTR. If so, this would suggest a general, eIF3D-specialised translation landscape in CRC.

5.13 Is translation of MYC in CRC eIF4F-independent but cap-dependent?

At the beginning of this work, it was hypothesised on the basis of previous data that translation of *MYC* in CRC occurs via an eIF4F-independent, alternative pathway. However, the data shown here suggest that this is not mediated by the published IRES structure in the *MYC* mRNA, as initially assumed, but rather the entire *MYC* 5' UTR and regulatory mechanisms linked to it seem to play a crucial role. EIF3D has been identified as one of the binding proteins that have the potential to positively affect MYC protein expression, although the exact molecular mechanism could not be evaluated in this work. Although MYC levels were not influenced by knocking down components of the eIF4F complex, this does not provide direct information on whether the components bind to the *MYC* mRNA or whether an active translational complex is formed. For this purpose, an *in vitro* translation assay could be performed in which a cytosolic cell lysate is enriched with additional molecules essential for translation (hereafter called ‘translation extract’) and incubated with an *in vitro* transcribed *MYC* or control mRNA. This enables the formation of 48S translation initiation complexes, which can subsequently be separated on a sucrose gradient. The detection of eIF3D or the eIF4F subunits is then carried out by immunoblot. If the hypothesis that *MYC* is translated eIF4F-independently is correct, a lower or absent accumulation of the eIF4F components would be expected. In addition to the involvement of the eIF4F complex, the dependence of *MYC* translation on the m7G cap should also be tested. For this purpose, as described above, *in vitro* transcribed *MYC* 5' UTR luciferase constructs could be used. These are incubated with translation extracts from CRC cells, which may or may not contain an m7G cap analogue as a competitor. If *MYC* translation is cap-dependent, reduced luciferase expression in the presence of the cap competitor would be expected. Altogether, this would suggest a new regulatory mechanism where a switch from eIF4F- to eIF3D-and cap-dependent translation is exploited to ensure differential gene expression under certain circumstances.

5.14 Is *EIF3D* expression dependent on tumour localisation or cell type?

Expression data from The Cancer Genome Atlas (TCGA) show that *EIF3D* is expressed approximately 1.5-fold higher in colorectal adenocarcinomas compared to normal tissue (https://oncodb.org/cgi-bin/ genomic_normal_ expression_search.cgi). Tumours are generally composed of a heterogeneous cell population and so far, it is unclear whether the expression of *EIF3D* is dependent on the cell compartment or whether individual cell populations are particularly sensitive to a depletion of *EIF3D*. To address these issues, histological sections of human CRCs should first be stained for eIF3D by IHC and compared with healthy small and large intestinal mucosa. In parallel, the expression of specific markers for the individual compartments should be determined. This will show whether the expression of eIF3D is ubiquitous or restricted to individual compartments and whether there are general differences in the distribution of eIF3D between tumour centre or peripheral areas. Furthermore, it should be investigated whether certain cell populations are particularly sensitive to *EIF3D* depletion. For this purpose, total RNA from MTOs carrying an shRNA against *Eif3d* could be isolated and targeted organoid sequencing (TORNADO-seq) could be used to identify gene signatures for specific cell populations and to analyse a shift in the profile (e.g. towards differentiation) (Norkin, Ordonez-Moran, & Huelsken, 2021). It would also be interesting here to see whether there are overlaps with MYC-dependent cell compartments to further validate the link between eIF3D and MYC in CRC.

5.15 Outlook

In this work, it was shown that MYC translation in CRC is most likely initiated via an eIF4F-independent mechanism and that eIF3D is a *MYC* 5’ UTR binding protein that has the potential to regulate *MYC* expression. However, further mechanistic studies are needed to investigate whether eIF3 has a specific function in *MYC* translation. Since in the initial *EIF3D* knockdown experiments it was suspected that the long-term loss of eIF3D leads to increased secondary effects in the cell, an acute depletion of *EIF3D* would be particularly desirable for the elucidation of eIF3D’s mode of action. For this purpose, the auxin-inducible degron (AID) system could be used which is based on widely used PROTAC approaches. The plant-based E3 ligase *TIR1* is exogenously expressed in cells and at the same time a so-called AID-tag is cloned to the endogenous protein of interest (Békés, Langley, & Crews, 2022; Shetty, Reim, & Winston, 2019). The plant hormone

auxin specifically links the AID-tagged protein to TIR1, thereby inducing its ubiquitin-mediated degradation. With this approach, time-course experiments could be performed to separate the effects on MYC protein expression from global effects resulting from this. Another important point to check is whether eIF3D has a special function in translation specifically in tumour cells. In yeast, eIF3D has been defined as non-essential and transferring it to human cells could render it a potential therapeutic target structure (S. Ma et al., 2023). Therefore, in addition to the validation in MTOs or human PDOs, it should be investigated how the depletion of *EIF3D* affects the whole organism and in particular whether it is an essential protein in adult healthy tissue.

With the help of the aforementioned follow-up experiments, the mechanism of eIF3D-mediated translation of *MYC*, as well as other global effects, should be investigated in more detail. The further goal should be to validate eIF3D as a potential target in CRC in order to obtain a therapeutic benefit from it. To date, no eIF3D-specific inhibitor exists, so further research would also be needed in this regard. It is possible that the expression of eIF3D is regulated by specific factors that control it depending on cellular conditions. As an example, eIF3D was found to be activated in response to metabolic stress and activation required reduced CK2-mediated phosphorylation close to eIF3D's cap-binding pocket (Lamper, Fleming, Ladd, & Lee, 2020). The identification of other eIF3D-regulating factors and the potential targetability would be a first approach to open a new therapeutic window. However, intensive further investigations are needed to uncover the still incomplete puzzle of eIF3D-specialised translation in tumours and pathways that might be influenced by it.

6 Literature

Addgene: Lentiviral guide. Retrieved from https://www.addgene.org/guides/lentivirus/#second-generation

Adhikary, S., & Eilers, M. (2005). Transcriptional regulation and transformation by Myc proteins. *Nat Rev Mol Cell Biol, 6*(8), 635-645. doi:10.1038/nrm1703

Ainaoui, N., Hantelys, F., Renaud-Gabardos, E., Bunel, M., Lopez, F., Pujol, F., . . . Prats, A. C. (2015). Promoter-Dependent Translation Controlled by p54nrb and hnRNPM during Myoblast Differentiation. *PLoS One, 10*(9), e0136466. doi:10.1371/journal.pone.0136466

Aitken, C. E., & Lorsch, J. R. (2012). A mechanistic overview of translation initiation in eukaryotes. *Nat Struct Mol Biol, 19*(6), 568-576. doi:10.1038/nsmb.2303

Alard, A., Katsara, O., Rios-Fuller, T., Parra, C., Ozerdem, U., Ernlund, A., & Schneider, R. J. (2023). Breast cancer cell mesenchymal transition and metastasis directed by DAP5/eIF3d-mediated selective mRNA translation. *Cell Rep, 42*(6), 112646. doi:10.1016/j.celrep.2023.112646

Allam, H., & Ali, N. (2010). Initiation factor eIF2-independent mode of c-Src mRNA translation occurs via an internal ribosome entry site. *J Biol Chem, 285*(8), 5713-5725. doi:10.1074/jbc.M109.029462

Annibali, D., Whitfield, J. R., Favuzzi, E., Jauset, T., Serrano, E., Cuartas, I., . . . Soucek, L. (2014). Myc inhibition is effective against glioma and reveals a role for Myc in proficient mitosis. *Nat Commun, 5*, 4632. doi:10.1038/ncomms5632

Arnaud, E., Touriol, C., Boutonnet, C., Gensac, M. C., Vagner, S., Prats, H., & Prats, A. C. (1999). A new 34-kilodalton isoform of human fibroblast growth factor 2 is cap dependently synthesized by using a non-AUG start codon and behaves as a survival factor. *Mol Cell Biol, 19*(1), 505-514. doi:10.1128/MCB.19.1.505

Aviner, R. (2020). The science of puromycin: From studies of ribosome function to applications in biotechnology. *Comput Struct Biotechnol J, 18*, 1074-1083. doi:10.1016/j.csbj.2020.04.014

Baluapuri, A., Wolf, E., & Eilers, M. (2020). Target gene-independent functions of MYC oncoproteins. *Nat Rev Mol Cell Biol, 21*(5), 255-267. doi:10.1038/s41580-020-0215-2

Barna, M., Pusic, A., Zollo, O., Costa, M., Kondrashov, N., Rego, E., . . . Ruggero, D. (2008). Suppression of Myc oncogenic activity by ribosomal protein haploinsufficiency. *Nature, 456*(7224), 971-975. doi:10.1038/nature07449

Baudino, T. A., McKay, C., Pendeville-Samain, H., Nilsson, J. A., Maclean, K. H., White, E. L., . . . Cleveland, J. L. (2002). c-Myc is essential for vasculogenesis and angiogenesis during development and tumor progression. *Genes Dev, 16*(19), 2530-2543. doi:10.1101/gad.1024602

Beaulieu, M. E., Jauset, T., Masso-Valles, D., Martinez-Martin, S., Rahl, P., Maltais, L., . . . Soucek, L. (2019). Intrinsic cell-penetrating activity propels Omomyc from proof of concept to viable anti-MYC therapy. *Sci Transl Med, 11*(484). doi:10.1126/scitranslmed.aar5012

Békés, M., Langley, D. R., & Crews, C. M. (2022). PROTAC targeted protein degraders: the past is prologue. *Nature Reviews Drug Discovery, 21*(3), 181-200. doi:10.1038/s41573-021-00371-6

Benavides-Serrato, A., Saunders, J. T., Kumar, S., Holmes, B., Benavides, K. E., Bashir, M. T., . . . Gera, J. (2023). m(6)A-modification of cyclin D1 and c-myc IRESs in glioblastoma controls ITAF activity and resistance to mTOR inhibition. *Cancer Lett, 562*, 216178. doi:10.1016/j.canlet.2023.216178

Berg, K. C. G., Eide, P. W., Eilertsen, I. A., Johannessen, B., Bruun, J., Danielsen, S. A., . . . Lothe, R. A. (2017). Multi-omics of 34 colorectal cancer cell lines - a resource for biomedical studies. *Mol Cancer, 16*(1), 116. doi:10.1186/s12943-017-0691-y

Berkel, H. J., Turbat-Herrera, E. A., Shi, R., & de Benedetti, A. (2001). Expression of the translation initiation factor eIF4E in the polyp-cancer sequence in the colon. *Cancer Epidemiol Biomarkers Prev, 10*(6), 663-666. Retrieved from https://www.ncbi.nlm.nih.gov/pubmed/11401917

Beroukhim, R., Mermel, C. H., Porter, D., Wei, G., Raychaudhuri, S., Donovan, J., . . . Meyerson, M. (2010). The landscape of somatic copy-number alteration across human cancers. *Nature, 463*(7283), 899-905. doi:10.1038/nature08822

Blackwood, E. M., Lugo, T. G., Kretzner, L., King, M. W., Street, A. J., Witte, O. N., & Eisenman, R. N. (1994). Functional analysis of the AUG- and CUG-initiated forms of the c-Myc protein. *Mol Biol Cell, 5*(5), 597-609. doi:10.1091/mbc.5.5.597

Bohlen, J., Roiuk, M., & Teleman, A. A. (2021). Phosphorylation of ribosomal protein S6 differentially affects mRNA translation based on ORF length. *Nucleic Acids Res, 49*(22), 13062-13074. doi:10.1093/nar/gkab1157

Bommert, K. S., Effenberger, M., Leich, E., Kuspert, M., Murphy, D., Langer, C., . . . Bommert, K. (2013). The feed-forward loop between YB-1 and MYC is essential for multiple myeloma cell survival. *Leukemia, 27*(2), 441-450. doi:10.1038/leu.2012.185

Bordeleau, M. E., Robert, F., Gerard, B., Lindqvist, L., Chen, S. M., Wendel, H. G., . . . Pelletier, J. (2008). Therapeutic suppression of translation initiation modulates chemosensitivity in a mouse lymphoma model. *J Clin Invest, 118*(7), 2651-2660. doi:10.1172/JCI34753

Bracken, A. P., Ciro, M., Cocito, A., & Helin, K. (2004). E2F target genes: unraveling the biology. *Trends Biochem Sci, 29*(8), 409-417. doi:10.1016/j.tibs.2004.06.006

Braunstein, S., Karpisheva, K., Pola, C., Goldberg, J., Hochman, T., Yee, H., . . . Schneider, R. J. (2007). A hypoxia-controlled cap-dependent to cap-independent translation switch in breast cancer. *Mol Cell, 28*(3), 501-512. doi:10.1016/j.molcel.2007.10.019

Brown, E. J., Beal, P. A., Keith, C. T., Chen, J., Shin, T. B., & Schreiber, S. L. (1995). Control of p70 s6 kinase by kinase activity of FRAP in vivo. *Nature, 377*(6548), 441-446. doi:10.1038/377441a0

Buttgereit, F., & Brand, M. D. (1995). A hierarchy of ATP-consuming processes in mammalian cells. *Biochem J, 312 (Pt 1)*(Pt 1), 163-167. doi:10.1042/bj3120163

Campbell, K. J., & White, R. J. (2014). MYC regulation of cell growth through control of transcription by RNA polymerases I and III. *Cold Spring Harb Perspect Med, 4*(5). doi:10.1101/cshperspect.a018408

Camps, J., Nguyen, Q. T., Padilla-Nash, H. M., Knutsen, T., McNeil, N. E., Wangsa, D., . . . Difilippantonio, M. J. (2009). Integrative genomics reveals mechanisms of copy number alterations responsible for transcriptional deregulation in colorectal cancer. *Genes Chromosomes Cancer, 48*(11), 1002-1017. doi:10.1002/gcc.20699

Cancer Genome Atlas, N. (2012). Comprehensive molecular characterization of human colon and rectal cancer. *Nature, 487*(7407), 330-337. doi:10.1038/nature11252

Cannell, I. G., Kong, Y. W., Johnston, S. J., Chen, M. L., Collins, H. M., Dobbyn, H. C., . . . Bushell, M. (2010). p38 MAPK/MK2-mediated induction of miR-34c following DNA damage prevents Myc-dependent DNA replication. *Proc Natl Acad Sci U S A, 107*(12), 5375-5380. doi:10.1073/pnas.0910015107

Cao, J., He, L., Lin, G., Hu, C., Dong, R., Zhang, J., . . . Yang, B. (2014). Cap-dependent translation initiation factor, eIF4E, is the target for Ouabain-mediated inhibition of HIF-1alpha. *Biochem Pharmacol, 89*(1), 20-30. doi:10.1016/j.bcp.2013.12.002

Casey, S. C., Baylot, V., & Felsher, D. W. (2018). The MYC oncogene is a global regulator of the immune response. *Blood, 131*(18), 2007-2015. doi:10.1182/blood-2017-11-742577

Casey, S. C., Tong, L., Li, Y., Do, R., Walz, S., Fitzgerald, K. N., . . . Felsher, D. W. (2016). MYC regulates the antitumor immune response through CD47 and PD-L1. *Science, 352*(6282), 227-231. doi:10.1126/science.aac9935

Cate, J. H. (2017). Human eIF3: from 'blobology' to biological insight. *Philos Trans R Soc Lond B Biol Sci, 372*(1716). doi:10.1098/rstb.2016.0176

Cerella, C., Gaigneaux, A., Dicato, M., & Diederich, M. (2015). Antagonistic role of natural compounds in mTOR-mediated metabolic reprogramming. *Cancer Lett, 356*(2 Pt A), 251-262. doi:10.1016/j.canlet.2014.02.008

Chappell, S. A., LeQuesne, J. P., Paulin, F. E., deSchoolmeester, M. L., Stoneley, M., Soutar, R. L., . . . Willis, A. E. (2000). A mutation in the c-myc-IRES leads to enhanced internal ribosome entry in multiple myeloma: a novel mechanism of oncogene de-regulation. *Oncogene, 19*(38), 4437-4440. doi:10.1038/sj.onc.1203791

Chen, H., Liu, H., & Qing, G. (2018). Targeting oncogenic Myc as a strategy for cancer treatment. *Signal Transduct Target Ther, 3*, 5. doi:10.1038/s41392-018-0008-7

Chen, J., Wei, Y., Feng, Q., Ren, L., He, G., Chang, W., . . . Qin, X. (2016). Ribosomal protein S15A promotes malignant transformation and predicts poor outcome in colorectal cancer through misregulation of p53 signaling pathway. *Int J Oncol, 48*(4), 1628-1638. doi:10.3892/ijo.2016.3366

Chen, J. Q., Contreras, R. G., Wang, R., Fernandez, S. V., Shoshani, L., Russo, I. H., . . . Russo, J. (2006). Sodium/potassium ATPase (Na+, K+-ATPase) and ouabain/related cardiac glycosides: A new paradigm for development of anti- breast cancer drugs? *Breast Cancer Res Treat, 96*(1), 1-15. doi:10.1007/s10549-005-9053-3

Chen, W. L., Pan, L., Kinghorn, A. D., Swanson, S. M., & Burdette, J. E. (2016). Silvestrol induces early autophagy and apoptosis in human melanoma cells. *BMC Cancer, 16*, 17. doi:10.1186/s12885-015-1988-0

Chen, Y., Wang, J., Fan, H., Xie, J., Xu, L., & Zhou, B. (2017). Phosphorylated 4E-BP1 is associated with tumor progression and adverse prognosis in colorectal cancer. *Neoplasma, 64*(5), 787-794. doi:10.4149/neo_2017_518

Chen, Z. H., Qi, J. J., Wu, Q. N., Lu, J. H., Liu, Z. X., Wang, Y., . . . Wang, F. (2019). Eukaryotic initiation factor 4A2 promotes experimental metastasis and oxaliplatin resistance in colorectal cancer. *J Exp Clin Cancer Res, 38*(1), 196. doi:10.1186/s13046-019-1178-z

Chipumuro, E., Marco, E., Christensen, C. L., Kwiatkowski, N., Zhang, T., Hatheway, C. M., . . . George, R. E. (2014). CDK7 inhibition suppresses super-enhancer-linked oncogenic transcription in MYCN-driven cancer. *Cell, 159*(5), 1126-1139. doi:10.1016/j.cell.2014.10.024

Cho, K. B., Cho, M. K., Lee, W. Y., & Kang, K. W. (2010). Overexpression of c-myc induces epithelial mesenchymal transition in mammary epithelial cells. *Cancer Lett, 293*(2), 230-239. doi:10.1016/j.canlet.2010.01.013

Christensen, C. L., Kwiatkowski, N., Abraham, B. J., Carretero, J., Al-Shahrour, F., Zhang, T., . . . Wong, K. K. (2014). Targeting transcriptional addictions in small cell lung cancer with a covalent CDK7 inhibitor. *Cancer Cell, 26*(6), 909-922. doi:10.1016/j.ccell.2014.10.019

Chu, J., Cargnello, M., Topisirovic, I., & Pelletier, J. (2016). Translation Initiation Factors: Reprogramming Protein Synthesis in Cancer. *Trends Cell Biol, 26*(12), 918-933. doi:10.1016/j.tcb.2016.06.005

Clarke, J. P., Thibault, P. A., Salapa, H. E., & Levin, M. C. (2021). A Comprehensive Analysis of the Role of hnRNP A1 Function and Dysfunction in the Pathogenesis of Neurodegenerative Disease. *Front Mol Biosci, 8*, 659610. doi:10.3389/fmolb.2021.659610

Cobbold, L. C., Spriggs, K. A., Haines, S. J., Dobbyn, H. C., Hayes, C., de Moor, C. H., . . . Willis, A. E. (2008). Identification of internal ribosome entry segment (IRES)-trans-acting factors for the Myc family of IRESs. *Mol Cell Biol, 28*(1), 40-49. doi:10.1128/MCB.01298-07

Cobbold, L. C., Wilson, L. A., Sawicka, K., King, H. A., Kondrashov, A. V., Spriggs, K. A., . . . Willis, A. E. (2010). Upregulated c-myc expression in multiple myeloma by internal ribosome entry results from increased interactions with and expression of PTB-1 and YB-1. *Oncogene, 29*(19), 2884-2891. doi:10.1038/onc.2010.31

Colon-Ramos, D. A., Shenvi, C. L., Weitzel, D. H., Gan, E. C., Matts, R., Cate, J., & Kornbluth, S. (2006). Direct ribosomal binding by a cellular inhibitor of translation. *Nat Struct Mol Biol, 13*(2), 103-111. doi:10.1038/nsmb1052

Conte, C., Ainaoui, N., Delluc-Clavieres, A., Khoury, M. P., Azar, R., Pujol, F., . . . Prats, A. C. (2009). Fibroblast growth factor 1 induced during myogenesis by a transcription-translation coupling mechanism. *Nucleic Acids Res, 37*(16), 5267-5278. doi:10.1093/nar/gkp550

Corbett, A. H. (2018). Post-transcriptional regulation of gene expression and human disease. *Curr Opin Cell Biol, 52*, 96-104. doi:10.1016/j.ceb.2018.02.011

Cox, J., Hein, M. Y., Luber, C. A., Paron, I., Nagaraj, N., & Mann, M. (2014). Accurate proteome-wide label-free quantification by delayed normalization and maximal peptide ratio extraction, termed MaxLFQ. *Mol Cell Proteomics, 13*(9), 2513-2526. doi:10.1074/mcp.M113.031591

Cox, J., & Mann, M. (2008). MaxQuant enables high peptide identification rates, individualized p.p.b.-range mass accuracies and proteome-wide protein quantification. *Nat Biotechnol, 26*(12), 1367-1372. doi:10.1038/nbt.1511

Creancier, L., Mercier, P., Prats, A. C., & Morello, D. (2001). c-myc Internal ribosome entry site activity is developmentally controlled and subjected to a strong translational repression in adult transgenic mice. *Mol Cell Biol, 21*(5), 1833-1840. doi:10.1128/MCB.21.5.1833-1840.2001

Dai, M. S., & Lu, H. (2008). Crosstalk between c-Myc and ribosome in ribosomal biogenesis and cancer. *J Cell Biochem, 105*(3), 670-677. doi:10.1002/jcb.21895

Dalla-Favera, R., Bregni, M., Erikson, J., Patterson, D., Gallo, R. C., & Croce, C. M. (1982). Human c-myc onc gene is located on the region of chromosome 8 that is translocated in Burkitt lymphoma cells. *Proc Natl Acad Sci U S A, 79*(24), 7824-7827. doi:10.1073/pnas.79.24.7824

de la Parra, C., Ernlund, A., Alard, A., Ruggles, K., Ueberheide, B., & Schneider, R. J. (2018). A widespread alternate form of cap-dependent mRNA translation initiation. *Nat Commun, 9*(1), 3068. doi:10.1038/s41467-018-05539-0

Dejure, F. R., Royla, N., Herold, S., Kalb, J., Walz, S., Ade, C. P., . . . Eilers, M. (2017). The MYC mRNA 3'-UTR couples RNA polymerase II function to glutamine and ribonucleotide levels. *EMBO J, 36*(13), 1854-1868. doi:10.15252/embj.201796662

Denk, S. (2017). *IRES-vermittelte translationelle Regulation von MYC durch eIF2B5 im kolorektalen Karzinom.* (Masterthesis). Julius-Maximilians-Universität Würzburg, Würzburg.

Denk, S., Schmidt, S., Schurr, Y., Schwarz, G., Schote, F., Diefenbacher, M., . . . Wiegering, A. (2021). CIP2A regulates MYC translation (via its 5'UTR) in colorectal cancer. *Int J Colorectal Dis, 36*(5), 911-918. doi:10.1007/s00384-020-03772-y

Dever, T. E. (2002). Gene-specific regulation by general translation factors. *Cell, 108*(4), 545-556. doi:10.1016/s0092-8674(02)00642-6

Dever, T. E., & Green, R. (2012). The elongation, termination, and recycling phases of translation in eukaryotes. *Cold Spring Harb Perspect Biol, 4*(7), a013706. doi:10.1101/cshperspect.a013706

Dhanasekaran, R., Deutzmann, A., Mahauad-Fernandez, W. D., Hansen, A. S., Gouw, A. M., & Felsher, D. W. (2022). The MYC oncogene - the grand orchestrator of cancer growth and immune evasion. *Nat Rev Clin Oncol, 19*(1), 23-36. doi:10.1038/s41571-021-00549-2

Didiot, M. C., Hewett, J., Varin, T., Freuler, F., Selinger, D., Nick, H., . . . Parker, C. N. (2013). Identification of cardiac glycoside molecules as inhibitors of c-Myc IRES-mediated translation. *J Biomol Screen, 18*(4), 407-419. doi:10.1177/1087057112466698

Diefenbacher, M. E., Chakraborty, A., Blake, S. M., Mitter, R., Popov, N., Eilers, M., & Behrens, A. (2015). Usp28 counteracts Fbw7 in intestinal homeostasis and cancer. *Cancer Res, 75*(7), 1181-1186. doi:10.1158/0008-5472.CAN-14-1726

Diefenbacher, M. E., Popov, N., Blake, S. M., Schulein-Volk, C., Nye, E., Spencer-Dene, B., . . . Behrens, A. (2014). The deubiquitinase USP28 controls intestinal homeostasis and promotes colorectal cancer. *J Clin Invest, 124*(8), 3407-3418. doi:10.1172/JCI73733

El Khoury, W., & Nasr, Z. (2021). Deregulation of ribosomal proteins in human cancers. *Biosci Rep, 41*(12). doi:10.1042/BSR20211577

Faller, W. J., Jackson, T. J., Knight, J. R., Ridgway, R. A., Jamieson, T., Karim, S. A., . . . Sansom, O. J. (2015). mTORC1-mediated translational elongation limits intestinal tumour initiation and growth. *Nature, 517*(7535), 497-500. doi:10.1038/nature13896

Fancello, L., Kampen, K. R., Hofman, I. J., Verbeeck, J., & De Keersmaecker, K. (2017). The ribosomal protein gene RPL5 is a haploinsufficient tumor suppressor in multiple cancer types. *Oncotarget, 8*(9), 14462-14478. doi:10.18632/oncotarget.14895

Farrell, A. S., & Sears, R. C. (2014). MYC degradation. *Cold Spring Harb Perspect Med, 4*(3). doi:10.1101/cshperspect.a014365

Fearon, E. R. (2011). Molecular genetics of colorectal cancer. *Annu Rev Pathol, 6*, 479-507. doi:10.1146/annurev-pathol-011110-130235

Fearon, E. R., & Vogelstein, B. (1990). A genetic model for colorectal tumorigenesis. *Cell, 61*(5), 759-767. doi:10.1016/0092-8674(90)90186-i

Fellmann, C., Hoffmann, T., Sridhar, V., Hopfgartner, B., Muhar, M., Roth, M., . . . Zuber, J. (2013). An optimized microRNA backbone for effective single-copy RNAi. *Cell Rep, 5*(6), 1704-1713. doi:10.1016/j.celrep.2013.11.020

Fernandez, J., Yaman, I., Merrick, W. C., Koromilas, A., Wek, R. C., Sood, R., . . . Hatzoglou, M. (2002). Regulation of internal ribosome entry site-mediated translation by eukaryotic initiation factor-2alpha phosphorylation and translation of a small upstream open reading frame. *J Biol Chem, 277*(3), 2050-2058. doi:10.1074/jbc.M109199200

Filippakopoulos, P., Qi, J., Picaud, S., Shen, Y., Smith, W. B., Fedorov, O., . . . Bradner, J. E. (2010). Selective inhibition of BET bromodomains. *Nature, 468*(7327), 1067-1073. doi:10.1038/nature09504

Foley, T. M., Payne, S. N., Pasch, C. A., Yueh, A. E., Van De Hey, D. R., Korkos, D. P., . . . Deming, D. A. (2017). Dual PI3K/mTOR Inhibition in Colorectal Cancers with APC and PIK3CA Mutations. *Mol Cancer Res, 15*(3), 317-327. doi:10.1158/1541-7786.MCR-16-0256

Fujishita, T., Aoki, K., Lane, H. A., Aoki, M., & Taketo, M. M. (2008). Inhibition of the mTORC1 pathway suppresses intestinal polyp formation and reduces mortality in ApcDelta716 mice. *Proc Natl Acad Sci U S A, 105*(36), 13544-13549. doi:10.1073/pnas.0800041105

Galluzzi, L., Buque, A., Kepp, O., Zitvogel, L., & Kroemer, G. (2017). Immunogenic cell death in cancer and infectious disease. *Nat Rev Immunol, 17*(2), 97-111. doi:10.1038/nri.2016.107

Gao, M., Zhang, X., Li, D., He, P., Tian, W., & Zeng, B. (2016). Expression analysis and clinical significance of eIF4E, VEGF-C, E-cadherin and MMP-2 in colorectal adenocarcinoma. *Oncotarget, 7*(51), 85502-85514. doi:10.18632/oncotarget.13453

Garcia-Cardenas, J. M., Guerrero, S., Lopez-Cortes, A., Armendariz-Castillo, I., Guevara-Ramirez, P., Perez-Villa, A., . . . Paz, Y. M. C. (2019). Post-transcriptional Regulation of Colorectal Cancer: A Focus on RNA-Binding Proteins. *Front Mol Biosci, 6*, 65. doi:10.3389/fmolb.2019.00065

Gilbert, W. V. (2011). Functional specialization of ribosomes? *Trends Biochem Sci, 36*(3), 127-132. doi:10.1016/j.tibs.2010.12.002

Gingras, A. C., Gygi, S. P., Raught, B., Polakiewicz, R. D., Abraham, R. T., Hoekstra, M. F., . . . Sonenberg, N. (1999). Regulation of 4E-BP1 phosphorylation: a novel two-step mechanism. *Genes Dev, 13*(11), 1422-1437. doi:10.1101/gad.13.11.1422

Gingras, A. C., Kennedy, S. G., O'Leary, M. A., Sonenberg, N., & Hay, N. (1998). 4E-BP1, a repressor of mRNA translation, is phosphorylated and inactivated by the Akt(PKB) signaling pathway. *Genes Dev, 12*(4), 502-513. doi:10.1101/gad.12.4.502

Gingras, A. C., Raught, B., & Sonenberg, N. (1999). eIF4 initiation factors: effectors of mRNA recruitment to ribosomes and regulators of translation. *Annu Rev Biochem, 68*, 913-963. doi:10.1146/annurev.biochem.68.1.913

Godet, A. C., David, F., Hantelys, F., Tatin, F., Lacazette, E., Garmy-Susini, B., & Prats, A. C. (2019). IRES Trans-Acting Factors, Key Actors of the Stress Response. *Int J Mol Sci, 20*(4). doi:10.3390/ijms20040924

Gomes-Duarte, A., Lacerda, R., Menezes, J., & Romao, L. (2018). eIF3: a factor for human health and disease. *RNA Biol, 15*(1), 26-34. doi:10.1080/15476286.2017.1391437

Gomez-Roman, N., Grandori, C., Eisenman, R. N., & White, R. J. (2003). Direct activation of RNA polymerase III transcription by c-Myc. *Nature, 421*(6920), 290-294. doi:10.1038/nature01327

Gonzalez-Perez, A. C., Stempel, M., Wyler, E., Urban, C., Piras, A., Hennig, T., . . . Brinkmann, M. M. (2021). The Zinc Finger Antiviral Protein ZAP Restricts Human Cytomegalovirus and Selectively Binds and Destabilizes Viral UL4/UL5 Transcripts. *mBio, 12*(3). doi:10.1128/mBio.02683-20

Grandori, C., Gomez-Roman, N., Felton-Edkins, Z. A., Ngouenet, C., Galloway, D. A., Eisenman, R. N., & White, R. J. (2005). c-Myc binds to human ribosomal DNA and stimulates transcription of rRNA genes by RNA polymerase I. *Nat Cell Biol, 7*(3), 311-318. doi:10.1038/ncb1224

Green, M. R., & Sambrook, J. (2018). The Hanahan Method for Preparation and Transformation of Competent Escherichia coli: High-Efficiency Transformation. *Cold Spring Harb Protoc, 2018*(3). doi:10.1101/pdb.prot101188

Guo, J., Li, T., Schipper, J., Nilson, K. A., Fordjour, F. K., Cooper, J. J., . . . Price, D. H. (2014). Sequence specificity incompletely defines the genome-wide occupancy of Myc. *Genome Biol, 15*(10), 482. doi:10.1186/s13059-014-0482-3

Halaby, M. J., Harris, B. R., Miskimins, W. K., Cleary, M. P., & Yang, D. Q. (2015). Deregulation of Internal Ribosome Entry Site-Mediated p53 Translation in Cancer Cells with Defective p53 Response to DNA Damage. *Mol Cell Biol, 35*(23), 4006-4017. doi:10.1128/MCB.00365-15

Hann, S. R. (2006). Role of post-translational modifications in regulating c-Myc proteolysis, transcriptional activity and biological function. *Semin Cancer Biol, 16*(4), 288-302. doi:10.1016/j.semcancer.2006.08.004

Hann, S. R. (2014). MYC cofactors: molecular switches controlling diverse biological outcomes. *Cold Spring Harb Perspect Med, 4*(9), a014399. doi:10.1101/cshperspect.a014399

Hann, S. R., King, M. W., Bentley, D. L., Anderson, C. W., & Eisenman, R. N. (1988). A non-AUG translational initiation in c-myc exon 1 generates an N-terminally distinct protein whose synthesis is disrupted in Burkitt's lymphomas. *Cell, 52*(2), 185-195. doi:10.1016/0092-8674(88)90507-7

Harvey, R. F., & Willis, A. E. (2018). Post-transcriptional control of stress responses in cancer. *Curr Opin Genet Dev, 48*, 30-35. doi:10.1016/j.gde.2017.10.006

Hashem, Y., & Frank, J. (2018). The Jigsaw Puzzle of mRNA Translation Initiation in Eukaryotes: A Decade of Structures Unraveling the Mechanics of the Process. *Annu Rev Biophys, 47*, 125-151. doi:10.1146/annurev-biophys-070816-034034

Haux, J. (1999). Digitoxin is a potential anticancer agent for several types of cancer. *Med Hypotheses, 53*(6), 543-548. doi:10.1054/mehy.1999.0985

He, T. C., Sparks, A. B., Rago, C., Hermeking, H., Zawel, L., da Costa, L. T., . . . Kinzler, K. W. (1998). Identification of c-MYC as a target of the APC pathway. *Science, 281*(5382), 1509-1512. doi:10.1126/science.281.5382.1509

Herrmannova, A., Prilepskaja, T., Wagner, S., Sikrova, D., Zeman, J., Poncova, K., & Valasek, L. S. (2020). Adapted formaldehyde gradient cross-linking protocol implicates human eIF3d and eIF3c, k and l subunits in the 43S and 48S pre-initiation complex assembly, respectively. *Nucleic Acids Res, 48*(4), 1969-1984. doi:10.1093/nar/gkz1185

Hershey, J. W. (2010). Regulation of protein synthesis and the role of eIF3 in cancer. *Braz J Med Biol Res, 43*(10), 920-930. doi:10.1590/s0100-879x2010007500098

Hetz, C., Chevet, E., & Oakes, S. A. (2015). Erratum: Proteostasis control by the unfolded protein response. *Nat Cell Biol, 17*(8), 1088. doi:10.1038/ncb3221

Hinnebusch, A. G. (2014). The scanning mechanism of eukaryotic translation initiation. *Annu Rev Biochem, 83*, 779-812. doi:10.1146/annurev-biochem-060713-035802

Hnisz, D., Abraham, B. J., Lee, T. I., Lau, A., Saint-Andre, V., Sigova, A. A., . . . Young, R. A. (2013). Super-enhancers in the control of cell identity and disease. *Cell, 155*(4), 934-947. doi:10.1016/j.cell.2013.09.053

Holcik, M. (2015). Could the eIF2alpha-Independent Translation Be the Achilles Heel of Cancer? *Front Oncol, 5*, 264. doi:10.3389/fonc.2015.00264

Holmes, B., Lee, J., Landon, K. A., Benavides-Serrato, A., Bashir, T., Jung, M. E., . . . Gera, J. (2016). Mechanistic Target of Rapamycin (mTOR) Inhibition Synergizes with Reduced Internal Ribosome Entry Site (IRES)-mediated Translation of Cyclin D1 and c-MYC mRNAs to Treat Glioblastoma. *J Biol Chem, 291*(27), 14146-14159. doi:10.1074/jbc.M116.726927

Horos, R., Ijspeert, H., Pospisilova, D., Sendtner, R., Andrieu-Soler, C., Taskesen, E., . . . von Lindern, M. (2012). Ribosomal deficiencies in Diamond-Blackfan anemia impair translation of transcripts essential for differentiation of murine and human erythroblasts. *Blood, 119*(1), 262-272. doi:10.1182/blood-2011-06-358200

Hovanes, K., Li, T. W., Munguia, J. E., Truong, T., Milovanovic, T., Lawrence Marsh, J., . . . Waterman, M. L. (2001). Beta-catenin-sensitive isoforms of lymphoid enhancer factor-1 are selectively expressed in colon cancer. *Nat Genet, 28*(1), 53-57. doi:10.1038/ng0501-53

Hua, H., Kong, Q., Yin, J., Zhang, J., & Jiang, Y. (2020). Insulin-like growth factor receptor signaling in tumorigenesis and drug resistance: a challenge for cancer therapy. *J Hematol Oncol, 13*(1), 64. doi:10.1186/s13045-020-00904-3

Huber, A. L., Papp, S. J., Chan, A. B., Henriksson, E., Jordan, S. D., Kriebs, A., . . . Lamia, K. A. (2016). CRY2 and FBXL3 Cooperatively Degrade c-MYC. *Mol Cell, 64*(4), 774-789. doi:10.1016/j.molcel.2016.10.012

Huez, I., Creancier, L., Audigier, S., Gensac, M. C., Prats, A. C., & Prats, H. (1998). Two independent internal ribosome entry sites are involved in translation initiation of vascular endothelial growth factor mRNA. *Mol Cell Biol, 18*(11), 6178-6190. doi:10.1128/MCB.18.11.6178

Iadevaia, V., & Gerber, A. P. (2015). Combinatorial Control of mRNA Fates by RNA-Binding Proteins and Non-Coding RNAs. *Biomolecules, 5*(4), 2207-2222. doi:10.3390/biom5042207

Ingolia, N. T., Ghaemmaghami, S., Newman, J. R., & Weissman, J. S. (2009). Genome-wide analysis in vivo of translation with nucleotide resolution using ribosome profiling. *Science, 324*(5924), 218-223. doi:10.1126/science.1168978

Ingolia, N. T., Lareau, L. F., & Weissman, J. S. (2011). Ribosome profiling of mouse embryonic stem cells reveals the complexity and dynamics of mammalian proteomes. *Cell, 147*(4), 789-802. doi:10.1016/j.cell.2011.10.002

Isken, O., Kim, Y. K., Hosoda, N., Mayeur, G. L., Hershey, J. W., & Maquat, L. E. (2008). Upf1 phosphorylation triggers translational repression during nonsense-mediated mRNA decay. *Cell, 133*(2), 314-327. doi:10.1016/j.cell.2008.02.030

Jackson, R. J., Hellen, C. U., & Pestova, T. V. (2010). The mechanism of eukaryotic translation initiation and principles of its regulation. *Nat Rev Mol Cell Biol, 11*(2), 113-127. doi:10.1038/nrm2838

Jaenicke, L. A., von Eyss, B., Carstensen, A., Wolf, E., Xu, W., Greifenberg, A. K., . . . Popov, N. (2016). Ubiquitin-Dependent Turnover of MYC Antagonizes MYC/PAF1C Complex Accumulation to Drive Transcriptional Elongation. *Mol Cell, 61*(1), 54-67. doi:10.1016/j.molcel.2015.11.007

Jain, M., Arvanitis, C., Chu, K., Dewey, W., Leonhardt, E., Trinh, M., . . . Felsher, D. W. (2002). Sustained loss of a neoplastic phenotype by brief inactivation of MYC. *Science, 297*(5578), 102-104. doi:10.1126/science.1071489

Jean-Philippe, J., Paz, S., & Caputi, M. (2013). hnRNP A1: the Swiss army knife of gene expression. *Int J Mol Sci, 14*(9), 18999-19024. doi:10.3390/ijms140918999

Jennings, M. D., Zhou, Y., Mohammad-Qureshi, S. S., Bennett, D., & Pavitt, G. D. (2013). eIF2B promotes eIF5 dissociation from eIF2*GDP to facilitate guanine nucleotide exchange for translation initiation. *Genes Dev, 27*(24), 2696-2707. doi:10.1101/gad.231514.113

Jho, E. H., Zhang, T., Domon, C., Joo, C. K., Freund, J. N., & Costantini, F. (2002). Wnt/beta-catenin/Tcf signaling induces the transcription of Axin2, a negative regulator of the signaling pathway. *Mol Cell Biol, 22*(4), 1172-1183. doi:10.1128/MCB.22.4.1172-1183.2002

Ji, B., Harris, B. R., Liu, Y., Deng, Y., Gradilone, S. A., Cleary, M. P., . . . Yang, D. Q. (2017). Targeting IRES-Mediated p53 Synthesis for Cancer Diagnosis and Therapeutics. *Int J Mol Sci, 18*(1). doi:10.3390/ijms18010093

Jiang, H., Bower, K. E., Beuscher, A. E. t., Zhou, B., Bobkov, A. A., Olson, A. J., & Vogt, P. K. (2009). Stabilizers of the Max homodimer identified in virtual ligand screening inhibit Myc function. *Mol Pharmacol, 76*(3), 491-502. doi:10.1124/mol.109.054858

Jo, O. D., Martin, J., Bernath, A., Masri, J., Lichtenstein, A., & Gera, J. (2008). Heterogeneous nuclear ribonucleoprotein A1 regulates cyclin D1 and c-myc internal ribosome entry site function through Akt signaling. *J Biol Chem, 283*(34), 23274-23287. doi:10.1074/jbc.M801185200

Jung, L. A., Gebhardt, A., Koelmel, W., Ade, C. P., Walz, S., Kuper, J., . . . Eilers, M. (2017). OmoMYC blunts promoter invasion by oncogenic MYC to inhibit gene expression characteristic of MYC-dependent tumors. *Oncogene, 36*(14), 1911-1924. doi:10.1038/onc.2016.354

Kaempfer, R., & Kaufman, J. (1972). Translational control of hemoglobin synthesis by an initiation factor required for recycling of ribosomes and for their binding to messenger RNA. *Proc Natl Acad Sci U S A, 69*(11), 3317-3321. doi:10.1073/pnas.69.11.3317

Kang, J., Brajanovski, N., Chan, K. T., Xuan, J., Pearson, R. B., & Sanij, E. (2021). Ribosomal proteins and human diseases: molecular mechanisms and targeted therapy. *Signal Transduct Target Ther, 6*(1), 323. doi:10.1038/s41392-021-00728-8

Kang, M. J., Vasudevan, D., Kang, K., Kim, K., Park, J. E., Zhang, N., . . . Ryoo, H. D. (2017). 4E-BP is a target of the GCN2-ATF4 pathway during Drosophila development and aging. *J Cell Biol, 216*(1), 115-129. doi:10.1083/jcb.201511073

Karaskova, M., Gunisova, S., Herrmannova, A., Wagner, S., Munzarova, V., & Valasek, L. (2012). Functional characterization of the role of the N-terminal domain of the c/Nip1 subunit

of eukaryotic initiation factor 3 (eIF3) in AUG recognition. *J Biol Chem, 287*(34), 28420-28434. doi:10.1074/jbc.M112.386656

Karginov, T. A., Pastor, D. P. H., Semler, B. L., & Gomez, C. M. (2017). Mammalian Polycistronic mRNAs and Disease. *Trends Genet, 33*(2), 129-142. doi:10.1016/j.tig.2016.11.007

Kearse, M. G., & Wilusz, J. E. (2017). Non-AUG translation: a new start for protein synthesis in eukaryotes. *Genes Dev, 31*(17), 1717-1731. doi:10.1101/gad.305250.117

Kelly, K., Cochran, B. H., Stiles, C. D., & Leder, P. (1983). Cell-specific regulation of the c-myc gene by lymphocyte mitogens and platelet-derived growth factor. *Cell, 35*(3 Pt 2), 603-610. doi:10.1016/0092-8674(83)90092-2

Kent, W. J., Sugnet, C. W., Furey, T. S., Roskin, K. M., Pringle, T. H., Zahler, A. M., & Haussler, D. (2002). The human genome browser at UCSC. *Genome Res, 12*(6), 996-1006. doi:10.1101/gr.229102

Kim, H. H., Kuwano, Y., Srikantan, S., Lee, E. K., Martindale, J. L., & Gorospe, M. (2009). HuR recruits let-7/RISC to repress c-Myc expression. *Genes Dev, 23*(15), 1743-1748. doi:10.1101/gad.1812509

Kim, H. J. (2019). Cell Fate Control by Translation: mRNA Translation Initiation as a Therapeutic Target for Cancer Development and Stem Cell Fate Control. *Biomolecules, 9*(11). doi:10.3390/biom9110665

Kim, I., Xu, W., & Reed, J. C. (2008). Cell death and endoplasmic reticulum stress: disease relevance and therapeutic opportunities. *Nat Rev Drug Discov, 7*(12), 1013-1030. doi:10.1038/nrd2755

Kisselev, A. F., & Goldberg, A. L. (2001). Proteasome inhibitors: from research tools to drug candidates. *Chem Biol, 8*(8), 739-758. doi:10.1016/s1074-5521(01)00056-4

Kolupaeva, V. G., Unbehaun, A., Lomakin, I. B., Hellen, C. U., & Pestova, T. V. (2005). Binding of eukaryotic initiation factor 3 to ribosomal 40S subunits and its role in ribosomal dissociation and anti-association. *RNA, 11*(4), 470-486. doi:10.1261/rna.7215305

Kometiani, P., Liu, L., & Askari, A. (2005). Digitalis-induced signaling by Na+/K+-ATPase in human breast cancer cells. *Mol Pharmacol, 67*(3), 929-936. doi:10.1124/mol.104.007302

Koromilas, A. E. (2015). Roles of the translation initiation factor eIF2alpha serine 51 phosphorylation in cancer formation and treatment. *Biochim Biophys Acta, 1849*(7), 871-880. doi:10.1016/j.bbagrm.2014.12.007

Kozak, M. (1986). Point mutations define a sequence flanking the AUG initiator codon that modulates translation by eukaryotic ribosomes. *Cell, 44*(2), 283-292. doi:10.1016/0092-8674(86)90762-2

Kozak, M. (2002). Pushing the limits of the scanning mechanism for initiation of translation. *Gene, 299*(1-2), 1-34. doi:10.1016/s0378-1119(02)01056-9

Krenz, B., Gebhardt-Wolf, A., Ade, C. P., Gaballa, A., Roehrig, F., Vendelova, E., . . . Eilers, M. (2021). MYC- and MIZ1-Dependent Vesicular Transport of Double-Strand RNA Controls Immune Evasion in Pancreatic Ductal Adenocarcinoma. *Cancer Res, 81*(16), 4242-4256. doi:10.1158/0008-5472.CAN-21-1677

Kress, T. R., Sabo, A., & Amati, B. (2015). MYC: connecting selective transcriptional control to global RNA production. *Nat Rev Cancer, 15*(10), 593-607. doi:10.1038/nrc3984

Krishnan, R., Boddapati, N., & Mahalingam, S. (2018). Interplay between human nucleolar GNL1 and RPS20 is critical to modulate cell proliferation. *Sci Rep, 8*(1), 11421. doi:10.1038/s41598-018-29802-y

Kulikov, A., Eva, A., Kirch, U., Boldyrev, A., & Scheiner-Bobis, G. (2007). Ouabain activates signaling pathways associated with cell death in human neuroblastoma. *Biochim Biophys Acta, 1768*(7), 1691-1702. doi:10.1016/j.bbamem.2007.04.012

Kwiatkowski, N., Zhang, T., Rahl, P. B., Abraham, B. J., Reddy, J., Ficarro, S. B., . . . Gray, N. S. (2014). Targeting transcription regulation in cancer with a covalent CDK7 inhibitor. *Nature, 511*(7511), 616-620. doi:10.1038/nature13393

Laemmli, U. K. (1970). Cleavage of structural proteins during the assembly of the head of bacteriophage T4. *Nature, 227*(5259), 680-685. doi:10.1038/227680a0

Lal, A., Navarro, F., Maher, C. A., Maliszewski, L. E., Yan, N., O'Day, E., . . . Lieberman, J. (2009). miR-24 Inhibits cell proliferation by targeting E2F2, MYC, and other cell-cycle genes via binding to "seedless" 3'UTR microRNA recognition elements. *Mol Cell, 35*(5), 610-625. doi:10.1016/j.molcel.2009.08.020

Lamper, A. M., Fleming, R. H., Ladd, K. M., & Lee, A. S. Y. (2020). A phosphorylation-regulated eIF3d translation switch mediates cellular adaptation to metabolic stress. *Science, 370*(6518), 853-856. doi:10.1126/science.abb0993

Landry, D. M., Hertz, M. I., & Thompson, S. R. (2009). RPS25 is essential for translation initiation by the Dicistroviridae and hepatitis C viral IRESs. *Genes Dev, 23*(23), 2753-2764. doi:10.1101/gad.1832209

Le Quesne, J. P., Stoneley, M., Fraser, G. A., & Willis, A. E. (2001). Derivation of a structural model for the c-myc IRES. *J Mol Biol, 310*(1), 111-126. doi:10.1006/jmbi.2001.4745

Leary, R. J., Lin, J. C., Cummins, J., Boca, S., Wood, L. D., Parsons, D. W., . . . Velculescu, V. E. (2008). Integrated analysis of homozygous deletions, focal amplifications, and sequence alterations in breast and colorectal cancers. *Proc Natl Acad Sci U S A, 105*(42), 16224-16229. doi:10.1073/pnas.0808041105

Lee, A. S., Kranzusch, P. J., & Cate, J. H. (2015). eIF3 targets cell-proliferation messenger RNAs for translational activation or repression. *Nature, 522*(7554), 111-114. doi:10.1038/nature14267

Lee, A. S., Kranzusch, P. J., Doudna, J. A., & Cate, J. H. (2016). eIF3d is an mRNA cap-binding protein that is required for specialized translation initiation. *Nature, 536*(7614), 96-99. doi:10.1038/nature18954

Lee, K. M., Chen, C. J., & Shih, S. R. (2017). Regulation Mechanisms of Viral IRES-Driven Translation. *Trends Microbiol, 25*(7), 546-561. doi:10.1016/j.tim.2017.01.010

LeFebvre, A. K., Korneeva, N. L., Trutschl, M., Cvek, U., Duzan, R. D., Bradley, C. A., . . . Rhoads, R. E. (2006). Translation initiation factor eIF4G-1 binds to eIF3 through the eIF3e subunit. *J Biol Chem, 281*(32), 22917-22932. doi:10.1074/jbc.M605418200

Leone, G., Sears, R., Huang, E., Rempel, R., Nuckolls, F., Park, C. H., . . . Nevins, J. R. (2001). Myc requires distinct E2F activities to induce S phase and apoptosis. *Mol Cell, 8*(1), 105-113. doi:10.1016/s1097-2765(01)00275-1

Levens, D. (2013). Cellular MYCro economics: Balancing MYC function with MYC expression. *Cold Spring Harb Perspect Med, 3*(11). doi:10.1101/cshperspect.a014233

Li, H., & Durbin, R. (2009). Fast and accurate short read alignment with Burrows-Wheeler transform. *Bioinformatics, 25*(14), 1754-1760. doi:10.1093/bioinformatics/btp324

Li, J., Dong, T., Wu, Z., Zhu, D., & Gu, H. (2023). The effects of MYC on tumor immunity and immunotherapy. *Cell Death Discov, 9*(1), 103. doi:10.1038/s41420-023-01403-3

Liang, M., Cai, T., Tian, J., Qu, W., & Xie, Z. J. (2006). Functional characterization of Src-interacting Na/K-ATPase using RNA interference assay. *J Biol Chem, 281*(28), 19709-19719. doi:10.1074/jbc.M512240200

Liberman, N., Marash, L., & Kimchi, A. (2009). The translation initiation factor DAP5 is a regulator of cell survival during mitosis. *Cell Cycle, 8*(2), 204-209. doi:10.4161/cc.8.2.7384

Liberzon, A., Birger, C., Thorvaldsdottir, H., Ghandi, M., Mesirov, J. P., & Tamayo, P. (2015). The Molecular Signatures Database (MSigDB) hallmark gene set collection. *Cell Syst, 1*(6), 417-425. doi:10.1016/j.cels.2015.12.004

Lin, C. Y., Loven, J., Rahl, P. B., Paranal, R. M., Burge, C. B., Bradner, J. E., . . . Young, R. A. (2012). Transcriptional amplification in tumor cells with elevated c-Myc. *Cell, 151*(1), 56-67. doi:10.1016/j.cell.2012.08.026

Lin, J. C., Hsu, M., & Tarn, W. Y. (2007). Cell stress modulates the function of splicing regulatory protein RBM4 in translation control. *Proc Natl Acad Sci U S A, 104*(7), 2235-2240. doi:10.1073/pnas.0611015104

Lin, W., Wadlington, N. L., Chen, L., Zhuang, X., Brorson, J. R., & Kang, U. J. (2014). Loss of PINK1 attenuates HIF-1alpha induction by preventing 4E-BP1-dependent switch in protein translation under hypoxia. *J Neurosci, 34*(8), 3079-3089. doi:10.1523/JNEUROSCI.2286-13.2014

Lobo, M. V., Martin, M. E., Perez, M. I., Alonso, F. J., Redondo, C., Alvarez, M. I., & Salinas, M. (2000). Levels, phosphorylation status and cellular localization of translational factor eIF2 in gastrointestinal carcinomas. *Histochem J, 32*(3), 139-150. doi:10.1023/a:1004091122351

Lopez-Lazaro, M. (2007). Digitoxin as an anticancer agent with selectivity for cancer cells: possible mechanisms involved. *Expert Opin Ther Targets, 11*(8), 1043-1053. doi:10.1517/14728222.11.8.1043

Lorenzin, F., Benary, U., Baluapuri, A., Walz, S., Jung, L. A., von Eyss, B., . . . Wolf, E. (2016). Different promoter affinities account for specificity in MYC-dependent gene regulation. *Elife, 5*. doi:10.7554/eLife.15161

Lu, Q., Wang, J., Yu, G., Guo, T., Hu, C., & Ren, P. (2015). Expression and clinical significance of mammalian target of rapamycin/P70 ribosomal protein S6 kinase signaling pathway in human colorectal carcinoma tissue. *Oncol Lett, 10*(1), 277-282. doi:10.3892/ol.2015.3228

Lugano, R., Ramachandran, M., & Dimberg, A. (2020). Tumor angiogenesis: causes, consequences, challenges and opportunities. *Cell Mol Life Sci, 77*(9), 1745-1770. doi:10.1007/s00018-019-03351-7

Ma, F., Li, X., Ren, J., Guo, R., Li, Y., Liu, J., . . . Li, W. (2019). Downregulation of eukaryotic translation initiation factor 3b inhibited proliferation and metastasis of gastric cancer. *Cell Death Dis, 10*(9), 623. doi:10.1038/s41419-019-1846-0

Ma, S., Liu, J. Y., & Zhang, J. T. (2023). eIF3d: A driver of noncanonical cap-dependent translation of specific mRNAs and a trigger of biological/pathological processes. *J Biol Chem, 299*(5), 104658. doi:10.1016/j.jbc.2023.104658

Macejak, D. G., & Sarnow, P. (1991). Internal initiation of translation mediated by the 5' leader of a cellular mRNA. *Nature, 353*(6339), 90-94. doi:10.1038/353090a0

Madden, S. K., de Araujo, A. D., Gerhardt, M., Fairlie, D. P., & Mason, J. M. (2021). Taking the Myc out of cancer: toward therapeutic strategies to directly inhibit c-Myc. *Mol Cancer, 20*(1), 3. doi:10.1186/s12943-020-01291-6

Majzoub, K., Hafirassou, M. L., Meignin, C., Goto, A., Marzi, S., Fedorova, A., . . . Imler, J. L. (2014). RACK1 controls IRES-mediated translation of viruses. *Cell, 159*(5), 1086-1095. doi:10.1016/j.cell.2014.10.041

Mann, B., Gelos, M., Siedow, A., Hanski, M. L., Gratchev, A., Ilyas, M., . . . Hanski, C. (1999). Target genes of beta-catenin-T cell-factor/lymphoid-enhancer-factor signaling in human colorectal carcinomas. *Proc Natl Acad Sci U S A, 96*(4), 1603-1608. doi:10.1073/pnas.96.4.1603

Martinez-Salas, E., Pineiro, D., & Fernandez, N. (2012). Alternative Mechanisms to Initiate Translation in Eukaryotic mRNAs. *Comp Funct Genomics, 2012*, 391546. doi:10.1155/2012/391546

Masutani, M., Sonenberg, N., Yokoyama, S., & Imataka, H. (2007). Reconstitution reveals the functional core of mammalian eIF3. *EMBO J, 26*(14), 3373-3383. doi:10.1038/sj.emboj.7601765

Menger, L., Vacchelli, E., Adjemian, S., Martins, I., Ma, Y., Shen, S., . . . Kroemer, G. (2012). Cardiac glycosides exert anticancer effects by inducing immunogenic cell death. *Sci Transl Med, 4*(143), 143ra199. doi:10.1126/scitranslmed.3003807

Meyer, K. D., Patil, D. P., Zhou, J., Zinoviev, A., Skabkin, M. A., Elemento, O., . . . Jaffrey, S. R. (2015). 5' UTR m(6)A Promotes Cap-Independent Translation. *Cell, 163*(4), 999-1010. doi:10.1016/j.cell.2015.10.012

Meyer, K. D., Saletore, Y., Zumbo, P., Elemento, O., Mason, C. E., & Jaffrey, S. R. (2012). Comprehensive analysis of mRNA methylation reveals enrichment in 3' UTRs and near stop codons. *Cell, 149*(7), 1635-1646. doi:10.1016/j.cell.2012.05.003

Miao, Y., Chen, L., Shi, C., Fan, R., Chen, P., Liu, H., . . . Qian, H. (2017). Increased phosphorylation of 4E-binding protein 1 predicts poor prognosis for patients with colorectal cancer. *Mol Med Rep, 15*(5), 3099-3104. doi:10.3892/mmr.2017.6352

Mihailovich, M., Bremang, M., Spadotto, V., Musiani, D., Vitale, E., Varano, G., . . . Bonaldi, T. (2015). miR-17-92 fine-tunes MYC expression and function to ensure optimal B cell lymphoma growth. *Nat Commun, 6*, 8725. doi:10.1038/ncomms9725

Mitchell, S. A., Spriggs, K. A., Coldwell, M. J., Jackson, R. J., & Willis, A. E. (2003). The Apaf-1 internal ribosome entry segment attains the correct structural conformation for function via interactions with PTB and unr. *Mol Cell, 11*(3), 757-771. doi:10.1016/s1097-2765(03)00093-5

Mitchell, S. F., & Parker, R. (2015). Modifications on Translation Initiation. *Cell, 163*(4), 796-798. doi:10.1016/j.cell.2015.10.056

Miura, P., Coriati, A., Belanger, G., De Repentigny, Y., Lee, J., Kothary, R., . . . Jasmin, B. J. (2010). The utrophin A 5'-UTR drives cap-independent translation exclusively in skeletal muscles of transgenic mice and interacts with eEF1A2. *Hum Mol Genet, 19*(7), 1211-1220. doi:10.1093/hmg/ddp591

Mohammad, M. P., Munzarova Pondelickova, V., Zeman, J., Gunisova, S., & Valasek, L. S. (2017). In vivo evidence that eIF3 stays bound to ribosomes elongating and terminating on short upstream ORFs to promote reinitiation. *Nucleic Acids Res, 45*(5), 2658-2674. doi:10.1093/nar/gkx049

Morfoisse, F., Tatin, F., Hantelys, F., Adoue, A., Helfer, A. C., Cassant-Sourdy, S., . . . Garmy-Susini, B. H. (2016). Nucleolin Promotes Heat Shock-Associated Translation of VEGF-D to Promote Tumor Lymphangiogenesis. *Cancer Res, 76*(15), 4394-4405. doi:10.1158/0008-5472.CAN-15-3140

Mukhopadhyay, S., Amodeo, M. E., & Lee, A. S. Y. (2023). eIF3d controls the persistent integrated stress response. *Mol Cell*. doi:10.1016/j.molcel.2023.08.008

Muller, H., & Helin, K. (2000). The E2F transcription factors: key regulators of cell proliferation. *Biochim Biophys Acta, 1470*(1), M1-12. doi:10.1016/s0304-419x(99)00030-x

Muthalagu, N., Junttila, M. R., Wiese, K. E., Wolf, E., Morton, J., Bauer, B., . . . Murphy, D. J. (2014). BIM is the primary mediator of MYC-induced apoptosis in multiple solid tissues. *Cell Rep, 8*(5), 1347-1353. doi:10.1016/j.celrep.2014.07.057

Naldini, L., Blomer, U., Gallay, P., Ory, D., Mulligan, R., Gage, F. H., . . . Trono, D. (1996). In vivo gene delivery and stable transduction of nondividing cells by a lentiviral vector. *Science, 272*(5259), 263-267. doi:10.1126/science.272.5259.263

Nanbru, C., Lafon, I., Audigier, S., Gensac, M. C., Vagner, S., Huez, G., & Prats, A. C. (1997). Alternative translation of the proto-oncogene c-myc by an internal ribosome entry site. *J Biol Chem, 272*(51), 32061-32066. doi:10.1074/jbc.272.51.32061

Nevins, J. R. (2001). The Rb/E2F pathway and cancer. *Hum Mol Genet, 10*(7), 699-703. doi:10.1093/hmg/10.7.699

Nevins, T. A., Harder, Z. M., Korneluk, R. G., & Holcik, M. (2003). Distinct regulation of internal ribosome entry site-mediated translation following cellular stress is mediated by apoptotic fragments of eIF4G translation initiation factor family members eIF4GI and p97/DAP5/NAT1. *J Biol Chem, 278*(6), 3572-3579. doi:10.1074/jbc.M206781200

Nguyen, H. G., Conn, C. S., Kye, Y., Xue, L., Forester, C. M., Cowan, J. E., . . . Ruggero, D. (2018). Development of a stress response therapy targeting aggressive prostate cancer. *Sci Transl Med, 10*(439). doi:10.1126/scitranslmed.aar2036

Nicol, J. W., Helt, G. A., Blanchard, S. G., Jr., Raja, A., & Loraine, A. E. (2009). The Integrated Genome Browser: free software for distribution and exploration of genome-scale datasets. *Bioinformatics, 25*(20), 2730-2731. doi:10.1093/bioinformatics/btp472

Nie, Z., Hu, G., Wei, G., Cui, K., Yamane, A., Resch, W., . . . Levens, D. (2012). c-Myc is a universal amplifier of expressed genes in lymphocytes and embryonic stem cells. *Cell, 151*(1), 68-79. doi:10.1016/j.cell.2012.08.033

Nieminen, T. T., O'Donohue, M. F., Wu, Y., Lohi, H., Scherer, S. W., Paterson, A. D., . . . Peltomaki, P. (2014). Germline mutation of RPS20, encoding a ribosomal protein, causes predisposition to hereditary nonpolyposis colorectal carcinoma without DNA mismatch repair deficiency. *Gastroenterology, 147*(3), 595-598 e595. doi:10.1053/j.gastro.2014.06.009

Niu, Y., Zhao, X., Wu, Y. S., Li, M. M., Wang, X. J., & Yang, Y. G. (2013). N6-methyl-adenosine (m6A) in RNA: an old modification with a novel epigenetic function. *Genomics Proteomics Bioinformatics, 11*(1), 8-17. doi:10.1016/j.gpb.2012.12.002

Norkin, M., Ordonez-Moran, P., & Huelsken, J. (2021). High-content, targeted RNA-seq screening in organoids for drug discovery in colorectal cancer. *Cell Rep, 35*(3), 109026. doi:10.1016/j.celrep.2021.109026

Omnus, D. J., Mehrtens, S., Ritter, B., Resch, K., Yamada, M., Frank, R., . . . Reboll, M. R. (2011). JKTBP1 is involved in stabilization and IRES-dependent translation of NRF mRNAs by binding to 5' and 3' untranslated regions. *J Mol Biol, 407*(4), 492-504. doi:10.1016/j.jmb.2011.01.050

Oskarsson, T., & Trumpp, A. (2005). The Myc trilogy: lord of RNA polymerases. *Nat Cell Biol, 7*(3), 215-217. doi:10.1038/ncb0305-215

Otsuka, K., Yamamoto, Y., & Ochiya, T. (2018). Regulatory role of resveratrol, a microRNA-controlling compound, in HNRNPA1 expression, which is associated with poor prognosis in breast cancer. *Oncotarget, 9*(37), 24718-24730. doi:10.18632/oncotarget.25339

Ozaki, H., Nagase, H., & Urakawa, N. (1984). Sugar moiety of cardiac glycosides is essential for the inhibitory action on the palytoxin-induced K+ release from red blood cells. *FEBS Lett, 173*(1), 196-198. doi:10.1016/0014-5793(84)81045-5

Pakos-Zebrucka, K., Koryga, I., Mnich, K., Ljujic, M., Samali, A., & Gorman, A. M. (2016). The integrated stress response. *EMBO Rep, 17*(10), 1374-1395. doi:10.15252/embr.201642195

Patel, S. (2016). Plant-derived cardiac glycosides: Role in heart ailments and cancer management. *Biomed Pharmacother, 84*, 1036-1041. doi:10.1016/j.biopha.2016.10.030

Paulin, F. E., West, M. J., Sullivan, N. F., Whitney, R. L., Lyne, L., & Willis, A. E. (1996). Aberrant translational control of the c-myc gene in multiple myeloma. *Oncogene, 13*(3), 505-513. Retrieved from https://www.ncbi.nlm.nih.gov/pubmed/8760292

Peabody, D. S. (1989). Translation initiation at non-AUG triplets in mammalian cells. *J Biol Chem, 264*(9), 5031-5035. Retrieved from https://www.ncbi.nlm.nih.gov/pubmed/2538469

Perne, A., Muellner, M. K., Steinrueck, M., Craig-Mueller, N., Mayerhofer, J., Schwarzinger, I., . . . Mayerhofer, M. (2009). Cardiac glycosides induce cell death in human cells by inhibiting general protein synthesis. *PLoS One, 4*(12), e8292. doi:10.1371/journal.pone.0008292

Peters, T. L., Tillotson, J., Yeomans, A. M., Wilmore, S., Lemm, E., Jimenez-Romero, C., . . . Schatz, J. H. (2018). Target-Based Screening against eIF4A1 Reveals the Marine Natural Product Elatol as a Novel Inhibitor of Translation Initiation with In Vivo Antitumor Activity. *Clin Cancer Res, 24*(17), 4256-4270. doi:10.1158/1078-0432.CCR-17-3645

Popov, N., Wanzel, M., Madiredjo, M., Zhang, D., Beijersbergen, R., Bernards, R., . . . Eilers, M. (2007). The ubiquitin-specific protease USP28 is required for MYC stability. *Nat Cell Biol, 9*(7), 765-774. doi:10.1038/ncb1601

Pourdehnad, M., Truitt, M. L., Siddiqi, I. N., Ducker, G. S., Shokat, K. M., & Ruggero, D. (2013). Myc and mTOR converge on a common node in protein synthesis control that confers synthetic lethality in Myc-driven cancers. *Proc Natl Acad Sci U S A, 110*(29), 11988-11993. doi:10.1073/pnas.1310230110

Prats, A. C., & Prats, H. (2002). Translational control of gene expression: role of IRESs and consequences for cell transformation and angiogenesis. *Prog Nucleic Acid Res Mol Biol, 72*, 367-413. doi:10.1016/s0079-6603(02)72075-8

Prats, H., Kaghad, M., Prats, A. C., Klagsbrun, M., Lelias, J. M., Liauzun, P., . . . et al. (1989). High molecular mass forms of basic fibroblast growth factor are initiated by alternative CUG codons. *Proc Natl Acad Sci U S A, 86*(6), 1836-1840. doi:10.1073/pnas.86.6.1836

Preston, A. M., & Hendershot, L. M. (2013). Examination of a second node of translational control in the unfolded protein response. *J Cell Sci, 126*(Pt 18), 4253-4261. doi:10.1242/jcs.130336

Rajagopalan, H., Jallepalli, P. V., Rago, C., Velculescu, V. E., Kinzler, K. W., Vogelstein, B., & Lengauer, C. (2004). Inactivation of hCDC4 can cause chromosomal instability. *Nature, 428*(6978), 77-81. doi:10.1038/nature02313

Ramirez, F., Ryan, D. P., Gruning, B., Bhardwaj, V., Kilpert, F., Richter, A. S., . . . Manke, T. (2016). deepTools2: a next generation web server for deep-sequencing data analysis. *Nucleic Acids Res, 44*(W1), W160-165. doi:10.1093/nar/gkw257

Ravi Hingorani, J. D., Jeanne Elia, Catherine McIntyre, Dev Mittar. (2011). *Detection of Apoptosis Using the BD Annexin V FITC Assayon the BD FACSVerse™ System*.

Reboll, M. R., Oumard, A., Gazdag, A. C., Renger, I., Ritter, B., Schwarzer, M., . . . Nourbakhsh, M. (2007). NRF IRES activity is mediated by RNA binding protein JKTBP1 and a 14-nt RNA element. *RNA, 13*(8), 1328-1340. doi:10.1261/rna.545407

Reddy, D., Kumavath, R., Barh, D., Azevedo, V., & Ghosh, P. (2020). Anticancer and Antiviral Properties of Cardiac Glycosides: A Review to Explore the Mechanism of Actions. *Molecules, 25*(16). doi:10.3390/molecules25163596

Riganti, C., Campia, I., Kopecka, J., Gazzano, E., Doublier, S., Aldieri, E., . . . Ghigo, D. (2011). Pleiotropic effects of cardioactive glycosides. *Curr Med Chem, 18*(6), 872-885. doi:10.2174/092986711794927685

Roose, J., Huls, G., van Beest, M., Moerer, P., van der Horn, K., Goldschmeding, R., . . . Clevers, H. (1999). Synergy between tumor suppressor APC and the beta-catenin-Tcf4 target Tcf1. *Science, 285*(5435), 1923-1926. doi:10.1126/science.285.5435.1923

Roper, J., Richardson, M. P., Wang, W. V., Richard, L. G., Chen, W., Coffee, E. M., . . . Hung, K. E. (2011). The dual PI3K/mTOR inhibitor NVP-BEZ235 induces tumor regression in a genetically engineered mouse model of PIK3CA wild-type colorectal cancer. *PLoS One, 6*(9), e25132. doi:10.1371/journal.pone.0025132

Roux, P. P., & Topisirovic, I. (2012). Regulation of mRNA translation by signaling pathways. *Cold Spring Harb Perspect Biol, 4*(11). doi:10.1101/cshperspect.a012252

Roux, P. P., & Topisirovic, I. (2018). Signaling Pathways Involved in the Regulation of mRNA Translation. *Mol Cell Biol, 38*(12). doi:10.1128/MCB.00070-18

Ruggero, D. (2009). The role of Myc-induced protein synthesis in cancer. *Cancer Res, 69*(23), 8839-8843. doi:10.1158/0008-5472.CAN-09-1970

Ruggero, D., Montanaro, L., Ma, L., Xu, W., Londei, P., Cordon-Cardo, C., & Pandolfi, P. P. (2004). The translation factor eIF-4E promotes tumor formation and cooperates with c-Myc in lymphomagenesis. *Nat Med, 10*(5), 484-486. doi:10.1038/nm1042

Ruggiano, A., Foresti, O., & Carvalho, P. (2014). Quality control: ER-associated degradation: protein quality control and beyond. *J Cell Biol, 204*(6), 869-879. doi:10.1083/jcb.201312042

Ruvinsky, I., & Meyuhas, O. (2006). Ribosomal protein S6 phosphorylation: from protein synthesis to cell size. *Trends Biochem Sci, 31*(6), 342-348. doi:10.1016/j.tibs.2006.04.003

Ryoo, H. D., & Vasudevan, D. (2017). Two distinct nodes of translational inhibition in the Integrated Stress Response. *BMB Rep, 50*(11), 539-545. doi:10.5483/bmbrep.2017.50.11.157

Sabo, A., Kress, T. R., Pelizzola, M., de Pretis, S., Gorski, M. M., Tesi, A., . . . Amati, B. (2014). Selective transcriptional regulation by Myc in cellular growth control and lymphomagenesis. *Nature, 511*(7510), 488-492. doi:10.1038/nature13537

Safaee, N., Kozlov, G., Noronha, A. M., Xie, J., Wilds, C. J., & Gehring, K. (2012). Interdomain allostery promotes assembly of the poly(A) mRNA complex with PABP and eIF4G. *Mol Cell, 48*(3), 375-386. doi:10.1016/j.molcel.2012.09.001

Sansom, O. J., Meniel, V. S., Muncan, V., Phesse, T. J., Wilkins, J. A., Reed, K. R., . . . Clarke, A. R. (2007). Myc deletion rescues Apc deficiency in the small intestine. *Nature, 446*(7136), 676-679. doi:10.1038/nature05674

Schmidt, E. K., Clavarino, G., Ceppi, M., & Pierre, P. (2009). SUnSET, a nonradioactive method to monitor protein synthesis. *Nat Methods, 6*(4), 275-277. doi:10.1038/nmeth.1314

Schmidt, N., Lareau, C. A., Keshishian, H., Ganskih, S., Schneider, C., Hennig, T., . . . Munschauer, M. (2021). The SARS-CoV-2 RNA-protein interactome in infected human cells. *Nat Microbiol, 6*(3), 339-353. doi:10.1038/s41564-020-00846-z

Schmidt, S., Denk, S., & Wiegering, A. (2020). Targeting Protein Synthesis in Colorectal Cancer. *Cancers (Basel), 12*(5). doi:10.3390/cancers12051298

Schmidt, S., Gay, D., Uthe, F. W., Denk, S., Paauwe, M., Matthes, N., . . . Wiegering, A. (2019). A MYC-GCN2-eIF2alpha negative feedback loop limits protein synthesis to prevent MYC-dependent apoptosis in colorectal cancer. *Nat Cell Biol, 21*(11), 1413-1424. doi:10.1038/s41556-019-0408-0

Schmittgen, T. D., & Livak, K. J. (2008). Analyzing real-time PCR data by the comparative C(T) method. *Nat Protoc, 3*(6), 1101-1108. doi:10.1038/nprot.2008.73

Schreier, M. H., & Staehelin, T. (1973). Initiation of eukaryotic protein synthesis: (Met-tRNA f - 40S ribosome) initiation complex catalysed by purified initiation factors in the absence of mRNA. *Nat New Biol, 242*(115), 35-38. doi:10.1038/newbio242035a0

Schülein-Völk, C., Wolf, E., Zhu, J., Xu, W., Taranets, L., Hellmann, A., . . . Popov, N. (2014). Dual Regulation of Fbw7 Function and Oncogenic Transformation by Usp28. *Cell Reports, 9*(3), 1099-1109. doi:https://doi.org/10.1016/j.celrep.2014.09.057

Schwarz, D. S., & Blower, M. D. (2016). The endoplasmic reticulum: structure, function and response to cellular signaling. *Cell Mol Life Sci, 73*(1), 79-94. doi:10.1007/s00018-015-2052-6

Sendoel, A., Dunn, J. G., Rodriguez, E. H., Naik, S., Gomez, N. C., Hurwitz, B., . . . Fuchs, E. (2017). Translation from unconventional 5' start sites drives tumour initiation. *Nature, 541*(7638), 494-499. doi:10.1038/nature21036

She, R., Luo, J., & Weissman, J. S. (2023). Translational fidelity screens in mammalian cells reveal eIF3 and eIF4G2 as regulators of start codon selectivity. *Nucleic Acids Res, 51*(12), 6355-6369. doi:10.1093/nar/gkad329

Shetty, A., Reim, N. I., & Winston, F. (2019). Auxin-Inducible Degron System for Depletion of Proteins in Saccharomyces cerevisiae. *Curr Protoc Mol Biol, 128*(1), e104. doi:10.1002/cpmb.104

Shi, Y., Frost, P. J., Hoang, B. Q., Benavides, A., Sharma, S., Gera, J. F., & Lichtenstein, A. K. (2008). IL-6-induced stimulation of c-myc translation in multiple myeloma cells is mediated by myc internal ribosome entry site function and the RNA-binding protein, hnRNP A1. *Cancer Res, 68*(24), 10215-10222. doi:10.1158/0008-5472.CAN-08-1066

Shi, Y., Sun, F., Cheng, Y., Holmes, B., Dhakal, B., Gera, J. F., . . . Lichtenstein, A. (2022). Critical Role for Cap-Independent c-MYC Translation in Progression of Multiple Myeloma. *Mol Cancer Ther, 21*(4), 502-510. doi:10.1158/1535-7163.MCT-21-0016

Shichiri, M., Hanson, K. D., & Sedivy, J. M. (1993). Effects of c-myc expression on proliferation, quiescence, and the G0 to G1 transition in nontransformed cells. *Cell Growth Differ, 4*(2), 93-104. Retrieved from https://www.ncbi.nlm.nih.gov/pubmed/8494788

Shin, S., Han, M. J., Jedrychowski, M. P., Zhang, Z., Shokat, K. M., Plas, D. R., . . . Yoon, S. O. (2023). mTOR inhibition reprograms cellular proteostasis by regulating eIF3D-mediated selective mRNA translation and promotes cell phenotype switching. *Cell Rep, 42*(8), 112868. doi:10.1016/j.celrep.2023.112868

Shtutman, M., Zhurinsky, J., Simcha, I., Albanese, C., D'Amico, M., Pestell, R., & Ben-Ze'ev, A. (1999). The cyclin D1 gene is a target of the beta-catenin/LEF-1 pathway. *Proc Natl Acad Sci U S A, 96*(10), 5522-5527. doi:10.1073/pnas.96.10.5522

Siegel, R., Desantis, C., & Jemal, A. (2014). Colorectal cancer statistics, 2014. *CA Cancer J Clin, 64*(2), 104-117. doi:10.3322/caac.21220

Siridechadilok, B., Fraser, C. S., Hall, R. J., Doudna, J. A., & Nogales, E. (2005). Structural roles for human translation factor eIF3 in initiation of protein synthesis. *Science, 310*(5753), 1513-1515. doi:10.1126/science.1118977

Skubnik, J., Svobodova Pavlickova, V., Psotova, J., & Rimpelova, S. (2021). Cardiac Glycosides as Autophagy Modulators. *Cells, 10*(12). doi:10.3390/cells10123341

Somers, J., Poyry, T., & Willis, A. E. (2013). A perspective on mammalian upstream open reading frame function. *Int J Biochem Cell Biol, 45*(8), 1690-1700. doi:10.1016/j.biocel.2013.04.020

Sonenberg, N., & Hinnebusch, A. G. (2009). Regulation of translation initiation in eukaryotes: mechanisms and biological targets. *Cell, 136*(4), 731-745. doi:10.1016/j.cell.2009.01.042

Soucek, L., Nasi, S., & Evan, G. I. (2004). Omomyc expression in skin prevents Myc-induced papillomatosis. *Cell Death Differ, 11*(9), 1038-1045. doi:10.1038/sj.cdd.4401443

Soucek, L., Whitfield, J., Martins, C. P., Finch, A. J., Murphy, D. J., Sodir, N. M., . . . Evan, G. I. (2008). Modelling Myc inhibition as a cancer therapy. *Nature, 455*(7213), 679-683. doi:10.1038/nature07260

Soucek, L., Whitfield, J. R., Sodir, N. M., Masso-Valles, D., Serrano, E., Karnezis, A. N., . . . Evan, G. I. (2013). Inhibition of Myc family proteins eradicates KRas-driven lung cancer in mice. *Genes Dev, 27*(5), 504-513. doi:10.1101/gad.205542.112

Spriggs, K. A., Bushell, M., Mitchell, S. A., & Willis, A. E. (2005). Internal ribosome entry segment-mediated translation during apoptosis: the role of IRES-trans-acting factors. *Cell Death Differ, 12*(6), 585-591. doi:10.1038/sj.cdd.4401642

Spriggs, K. A., Cobbold, L. C., Jopling, C. L., Cooper, R. E., Wilson, L. A., Stoneley, M., . . . Willis, A. E. (2009). Canonical initiation factor requirements of the Myc family of internal ribosome entry segments. *Mol Cell Biol, 29*(6), 1565-1574. doi:10.1128/MCB.01283-08

Sriram, A., Bohlen, J., & Teleman, A. A. (2018). Translation acrobatics: how cancer cells exploit alternate modes of translational initiation. *EMBO Rep, 19*(10). doi:10.15252/embr.201845947

Srivastava, S., Verschoor, A., & Frank, J. (1992). Eukaryotic initiation factor 3 does not prevent association through physical blockage of the ribosomal subunit-subunit interface. *J Mol Biol, 226*(2), 301-304. doi:10.1016/0022-2836(92)90946-h

Staller, P., Peukert, K., Kiermaier, A., Seoane, J., Lukas, J., Karsunky, H., . . . Eilers, M. (2001). Repression of p15INK4b expression by Myc through association with Miz-1. *Nat Cell Biol, 3*(4), 392-399. doi:10.1038/35070076

Stathis, A., & Bertoni, F. (2018). BET Proteins as Targets for Anticancer Treatment. *Cancer Discov, 8*(1), 24-36. doi:10.1158/2159-8290.CD-17-0605

Stoneley, M., Chappell, S. A., Jopling, C. L., Dickens, M., MacFarlane, M., & Willis, A. E. (2000). c-Myc protein synthesis is initiated from the internal ribosome entry segment during apoptosis. *Mol Cell Biol, 20*(4), 1162-1169. doi:10.1128/MCB.20.4.1162-1169.2000

Stoneley, M., Paulin, F. E., Le Quesne, J. P., Chappell, S. A., & Willis, A. E. (1998). C-Myc 5' untranslated region contains an internal ribosome entry segment. *Oncogene, 16*(3), 423-428. doi:10.1038/sj.onc.1201763

Struntz, N. B., Chen, A., Deutzmann, A., Wilson, R. M., Stefan, E., Evans, H. L., . . . Koehler, A. N. (2019). Stabilization of the Max Homodimer with a Small Molecule Attenuates Myc-Driven Transcription. *Cell Chem Biol, 26*(5), 711-723 e714. doi:10.1016/j.chembiol.2019.02.009

Strycharz, W. A., Ranki, M., & Dahl, H. H. (1974). A high-molecular-weight protein component required for natural messenger translation in ascites tumor cells. *Eur J Biochem, 48*(1), 303-310. doi:10.1111/j.1432-1033.1974.tb03769.x

Subkhankulova, T., Mitchell, S. A., & Willis, A. E. (2001). Internal ribosome entry segment-mediated initiation of c-Myc protein synthesis following genotoxic stress. *Biochem J, 359*(Pt 1), 183-192. doi:10.1042/0264-6021:3590183

Subramanian, A., Tamayo, P., Mootha, V. K., Mukherjee, S., Ebert, B. L., Gillette, M. A., . . . Mesirov, J. P. (2005). Gene set enrichment analysis: a knowledge-based approach for interpreting genome-wide expression profiles. *Proc Natl Acad Sci U S A, 102*(43), 15545-15550. doi:10.1073/pnas.0506580102

Sun, C., Querol-Audi, J., Mortimer, S. A., Arias-Palomo, E., Doudna, J. A., Nogales, E., & Cate, J. H. (2013). Two RNA-binding motifs in eIF3 direct HCV IRES-dependent translation. *Nucleic Acids Res, 41*(15), 7512-7521. doi:10.1093/nar/gkt510

Szamecz, B., Rutkai, E., Cuchalova, L., Munzarova, V., Herrmannova, A., Nielsen, K. H., . . . Valasek, L. (2008). eIF3a cooperates with sequences 5' of uORF1 to promote resumption of scanning by post-termination ribosomes for reinitiation on GCN4 mRNA. *Genes Dev, 22*(17), 2414-2425. doi:10.1101/gad.480508

Tai, D., Wells, K., Arcaroli, J., Vanderbilt, C., Aisner, D. L., Messersmith, W. A., & Lieu, C. H. (2015). Targeting the WNT Signaling Pathway in Cancer Therapeutics. *Oncologist, 20*(10), 1189-1198. doi:10.1634/theoncologist.2015-0057

Takagi, M., Absalon, M. J., McLure, K. G., & Kastan, M. B. (2005). Regulation of p53 translation and induction after DNA damage by ribosomal protein L26 and nucleolin. *Cell, 123*(1), 49-63. doi:10.1016/j.cell.2005.07.034

Takahashi, K., Maruyama, M., Tokuzawa, Y., Murakami, M., Oda, Y., Yoshikane, N., . . . Yamanaka, S. (2005). Evolutionarily conserved non-AUG translation initiation in NAT1/p97/DAP5 (EIF4G2). *Genomics, 85*(3), 360-371. doi:10.1016/j.ygeno.2004.11.012

Tameire, F., Verginadis, II, & Koumenis, C. (2015). Cell intrinsic and extrinsic activators of the unfolded protein response in cancer: Mechanisms and targets for therapy. *Semin Cancer Biol, 33*, 3-15. doi:10.1016/j.semcancer.2015.04.002

Tauriello, D. V. F., Palomo-Ponce, S., Stork, D., Berenguer-Llergo, A., Badia-Ramentol, J., Iglesias, M., . . . Batlle, E. (2018). TGFbeta drives immune evasion in genetically reconstituted colon cancer metastasis. *Nature, 554*(7693), 538-543. doi:10.1038/nature25492

Thakor, N., & Holcik, M. (2012). IRES-mediated translation of cellular messenger RNA operates in eIF2alpha- independent manner during stress. *Nucleic Acids Res, 40*(2), 541-552. doi:10.1093/nar/gkr701

Thakor, N., Smith, M. D., Roberts, L., Faye, M. D., Patel, H., Wieden, H. J., . . . Holcik, M. (2017). Cellular mRNA recruits the ribosome via eIF3-PABP bridge to initiate internal translation. *RNA Biol, 14*(5), 553-567. doi:10.1080/15476286.2015.1137419

Thompson, L., Depledge, D. P., Burgess, H. M., & Mohr, I. (2022). An eIF3d-dependent switch regulates HCMV replication by remodeling the infected cell translation landscape to mimic chronic ER stress. *Cell Rep, 39*(5), 110767. doi:10.1016/j.celrep.2022.110767

Thompson, S. R. (2012). So you want to know if your message has an IRES? *Wiley Interdiscip Rev RNA, 3*(5), 697-705. doi:10.1002/wrna.1129

Thoreen, C. C., Chantranupong, L., Keys, H. R., Wang, T., Gray, N. S., & Sabatini, D. M. (2012). A unifying model for mTORC1-mediated regulation of mRNA translation. *Nature, 485*(7396), 109-113. doi:10.1038/nature11083

Thuaud, F., Bernard, Y., Turkeri, G., Dirr, R., Aubert, G., Cresteil, T., . . . Desaubry, L. (2009). Synthetic analogue of rocaglaol displays a potent and selective cytotoxicity in cancer cells: involvement of apoptosis inducing factor and caspase-12. *J Med Chem, 52*(16), 5176-5187. doi:10.1021/jm900365v

Tian, J., Liu, J., Garlid, K. D., Shapiro, J. I., & Xie, Z. (2003). Involvement of mitogen-activated protein kinases and reactive oxygen species in the inotropic action of ouabain on cardiac myocytes. A potential role for mitochondrial K(ATP) channels. *Mol Cell Biochem, 242*(1-2), 181-187. Retrieved from https://www.ncbi.nlm.nih.gov/pubmed/12619881

Tilford, G. (1997). *Edible & Medicinal Plants of West*.

Truitt, M. L., & Ruggero, D. (2016). New frontiers in translational control of the cancer genome. *Nat Rev Cancer, 16*(5), 288-304. doi:10.1038/nrc.2016.27

Tsukiyama-Kohara, K., Iizuka, N., Kohara, M., & Nomoto, A. (1992). Internal ribosome entry site within hepatitis C virus RNA. *J Virol, 66*(3), 1476-1483. doi:10.1128/JVI.66.3.1476-1483.1992

Turnbull, A. P., Ioannidis, S., Krajewski, W. W., Pinto-Fernandez, A., Heride, C., Martin, A. C. L., . . . Komander, D. (2017). Molecular basis of USP7 inhibition by selective small-molecule inhibitors. *Nature, 550*(7677), 481-486. doi:10.1038/nature24451

Valasek, L., Nielsen, K. H., Zhang, F., Fekete, C. A., & Hinnebusch, A. G. (2004). Interactions of eukaryotic translation initiation factor 3 (eIF3) subunit NIP1/c with eIF1 and eIF5 promote preinitiation complex assembly and regulate start codon selection. *Mol Cell Biol, 24*(21), 9437-9455. doi:10.1128/MCB.24.21.9437-9455.2004

Van Nostrand, E. L., Pratt, G. A., Shishkin, A. A., Gelboin-Burkhart, C., Fang, M. Y., Sundararaman, B., . . . Yeo, G. W. (2016). Robust transcriptome-wide discovery of RNA-binding protein binding sites with enhanced CLIP (eCLIP). *Nat Methods, 13*(6), 508-514. doi:10.1038/nmeth.3810

van Riggelen, J., Yetil, A., & Felsher, D. W. (2010). MYC as a regulator of ribosome biogenesis and protein synthesis. *Nat Rev Cancer, 10*(4), 301-309. doi:10.1038/nrc2819

Vervoorts, J., Luscher-Firzlaff, J., & Luscher, B. (2006). The ins and outs of MYC regulation by posttranslational mechanisms. *J Biol Chem, 281*(46), 34725-34729. doi:10.1074/jbc.R600017200

Vogelstein, B., Fearon, E. R., Hamilton, S. R., Kern, S. E., Preisinger, A. C., Leppert, M., . . . Bos, J. L. (1988). Genetic alterations during colorectal-tumor development. *N Engl J Med, 319*(9), 525-532. doi:10.1056/NEJM198809013190901

Wagner, S., Herrmannova, A., Sikrova, D., & Valasek, L. S. (2016). Human eIF3b and eIF3a serve as the nucleation core for the assembly of eIF3 into two interconnected modules: the yeast-like core and the octamer. *Nucleic Acids Res, 44*(22), 10772-10788. doi:10.1093/nar/gkw972

Walsby, E., Lazenby, M., Pepper, C., & Burnett, A. K. (2011). The cyclin-dependent kinase inhibitor SNS-032 has single agent activity in AML cells and is highly synergistic with cytarabine. *Leukemia, 25*(3), 411-419. doi:10.1038/leu.2010.290

Walter, P., & Ron, D. (2011). The unfolded protein response: from stress pathway to homeostatic regulation. *Science, 334*(6059), 1081-1086. doi:10.1126/science.1209038

Walther, A., Johnstone, E., Swanton, C., Midgley, R., Tomlinson, I., & Kerr, D. (2009). Genetic prognostic and predictive markers in colorectal cancer. *Nat Rev Cancer, 9*(7), 489-499. doi:10.1038/nrc2645

Walz, S., Lorenzin, F., Morton, J., Wiese, K. E., von Eyss, B., Herold, S., . . . Eilers, M. (2014). Activation and repression by oncogenic MYC shape tumour-specific gene expression profiles. *Nature, 511*(7510), 483-487. doi:10.1038/nature13473

Wang, C., Sarnow, P., & Siddiqui, A. (1994). A conserved helical element is essential for internal initiation of translation of hepatitis C virus RNA. *J Virol, 68*(11), 7301-7307. doi:10.1128/JVI.68.11.7301-7307.1994

Wang, M., & Kaufman, R. J. (2014). The impact of the endoplasmic reticulum protein-folding environment on cancer development. *Nat Rev Cancer, 14*(9), 581-597. doi:10.1038/nrc3800

Wang, S., Darini, C., Desaubry, L., & Koromilas, A. E. (2016). STAT1 Promotes KRAS Colon Tumor Growth and Susceptibility to Pharmacological Inhibition of Translation Initiation Factor eIF4A. *Mol Cancer Ther, 15*(12), 3055-3063. doi:10.1158/1535-7163.MCT-16-0416

Wang, X., & Proud, C. G. (2006). The mTOR pathway in the control of protein synthesis. *Physiology (Bethesda), 21*, 362-369. doi:10.1152/physiol.00024.2006

Wang, X. Q., & Rothnagel, J. A. (2004). 5'-untranslated regions with multiple upstream AUG codons can support low-level translation via leaky scanning and reinitiation. *Nucleic Acids Res, 32*(4), 1382-1391. doi:10.1093/nar/gkh305

Warner, J. R., & McIntosh, K. B. (2009). How common are extraribosomal functions of ribosomal proteins? *Mol Cell, 34*(1), 3-11. doi:10.1016/j.molcel.2009.03.006

Weinstein, I. B. (2002). Cancer. Addiction to oncogenes--the Achilles heal of cancer. *Science, 297*(5578), 63-64. doi:10.1126/science.1073096

Welcker, M., Orian, A., Jin, J., Grim, J. E., Harper, J. W., Eisenman, R. N., & Clurman, B. E. (2004). The Fbw7 tumor suppressor regulates glycogen synthase kinase 3 phosphorylation-dependent c-Myc protein degradation. *Proc Natl Acad Sci U S A, 101*(24), 9085-9090. doi:10.1073/pnas.0402770101

Wiegering, A., Uthe, F. W., Jamieson, T., Ruoss, Y., Huttenrauch, M., Kuspert, M., . . . Eilers, M. (2015). Targeting Translation Initiation Bypasses Signaling Crosstalk Mechanisms That Maintain High MYC Levels in Colorectal Cancer. *Cancer Discov, 5*(7), 768-781. doi:10.1158/2159-8290.CD-14-1040

Wilson, J. E., Pestova, T. V., Hellen, C. U., & Sarnow, P. (2000). Initiation of protein synthesis from the A site of the ribosome. *Cell, 102*(4), 511-520. doi:10.1016/s0092-8674(00)00055-6

Winnicka, K., Bielawski, K., & Bielawska, A. (2006). Cardiac glycosides in cancer research and cancer therapy. *Acta Pol Pharm, 63*(2), 109-115. Retrieved from https://www.ncbi.nlm.nih.gov/pubmed/17514873

Wisdom, R., Johnson, R. S., & Moore, C. (1999). c-Jun regulates cell cycle progression and apoptosis by distinct mechanisms. *EMBO J, 18*(1), 188-197. doi:10.1093/emboj/18.1.188

Wolf, E., & Eilers, M. (2020). Targeting MYC Proteins for Tumor Therapy. *Annual Review of Cancer Biology, 4*(1), 61-75. doi:10.1146/annurev-cancerbio-030518-055826

Wolfe, A. L., Singh, K., Zhong, Y., Drewe, P., Rajasekhar, V. K., Sanghvi, V. R., . . . Wendel, H. G. (2014). RNA G-quadruplexes cause eIF4A-dependent oncogene translation in cancer. *Nature, 513*(7516), 65-70. doi:10.1038/nature13485

Xie, Z., & Cai, T. (2003). Na+-K+--ATPase-mediated signal transduction: from protein interaction to cellular function. *Mol Interv, 3*(3), 157-168. doi:10.1124/mi.3.3.157

Xu, T., Zong, Y., Peng, L., Kong, S., Zhou, M., Zou, J., . . . Li, L. (2016). Overexpression of eIF4E in colorectal cancer patients is associated with liver metastasis. *Onco Targets Ther, 9*, 815-822. doi:10.2147/OTT.S98330

Xue, S., & Barna, M. (2012). Specialized ribosomes: a new frontier in gene regulation and organismal biology. *Nat Rev Mol Cell Biol, 13*(6), 355-369. doi:10.1038/nrm3359

Yada, M., Hatakeyama, S., Kamura, T., Nishiyama, M., Tsunematsu, R., Imaki, H., . . . Nakayama, K. I. (2004). Phosphorylation-dependent degradation of c-Myc is mediated by the F-box protein Fbw7. *EMBO J, 23*(10), 2116-2125. doi:10.1038/sj.emboj.7600217

Yamaguchi, S., Ishihara, H., Yamada, T., Tamura, A., Usui, M., Tominaga, R., . . . Oka, Y. (2008). ATF4-mediated induction of 4E-BP1 contributes to pancreatic beta cell survival under endoplasmic reticulum stress. *Cell Metab, 7*(3), 269-276. doi:10.1016/j.cmet.2008.01.008

Yong, W. H., Shabihkhani, M., Telesca, D., Yang, S., Tso, J. L., Menjivar, J. C., . . . Tso, C. L. (2015). Ribosomal Proteins RPS11 and RPS20, Two Stress-Response Markers of Glioblastoma Stem Cells, Are Novel Predictors of Poor Prognosis in Glioblastoma Patients. *PLoS One, 10*(10), e0141334. doi:10.1371/journal.pone.0141334

Yu, C., Hong, H., Zhang, S., Zong, Y., Ma, J., Lu, A., . . . Zheng, M. (2019). Identification of key genes and pathways involved in microsatellite instability in colorectal cancer. *Mol Med Rep, 19*(3), 2065-2076. doi:10.3892/mmr.2019.9849

Yu, Y., Ji, H., Doudna, J. A., & Leary, J. A. (2005). Mass spectrometric analysis of the human 40S ribosomal subunit: native and HCV IRES-bound complexes. *Protein Sci, 14*(6), 1438-1446. doi:10.1110/ps.041293005

Yustein, J. T., Liu, Y. C., Gao, P., Jie, C., Le, A., Vuica-Ross, M., . . . Dang, C. V. (2010). Induction of ectopic Myc target gene JAG2 augments hypoxic growth and tumorigenesis in a human B-cell model. *Proc Natl Acad Sci U S A, 107*(8), 3534-3539. doi:10.1073/pnas.0901230107

Zhang, D. M., Liu, J. S., Deng, L. J., Chen, M. F., Yiu, A., Cao, H. H., . . . Ye, W. C. (2013). Arenobufagin, a natural bufadienolide from toad venom, induces apoptosis and autophagy in human hepatocellular carcinoma cells through inhibition of PI3K/Akt/mTOR pathway. *Carcinogenesis, 34*(6), 1331-1342. doi:10.1093/carcin/bgt060

Zhang, F., Xiang, S., Cao, Y., Li, M., Ma, Q., Liang, H., . . . Liu, Y. (2017). EIF3D promotes gallbladder cancer development by stabilizing GRK2 kinase and activating PI3K-AKT signaling pathway. *Cell Death Dis, 8*(6), e2868. doi:10.1038/cddis.2017.263

Zhang, H., Qian, D. Z., Tan, Y. S., Lee, K., Gao, P., Ren, Y. R., . . . Semenza, G. L. (2008). Digoxin and other cardiac glycosides inhibit HIF-1alpha synthesis and block tumor growth. *Proc Natl Acad Sci U S A, 105*(50), 19579-19586. doi:10.1073/pnas.0809763105

Zhang, L., Pan, X., & Hershey, J. W. (2007). Individual overexpression of five subunits of human translation initiation factor eIF3 promotes malignant transformation of immortal fibroblast cells. *J Biol Chem, 282*(8), 5790-5800. doi:10.1074/jbc.M606284200

Zhang, T., Li, N., Sun, C., Jin, Y., & Sheng, X. (2020). MYC and the unfolded protein response in cancer: synthetic lethal partners in crime? *EMBO Mol Med, 12*(5), e11845. doi:10.15252/emmm.201911845

Zhang, X., Gaspard, J. P., & Chung, D. C. (2001). Regulation of vascular endothelial growth factor by the Wnt and K-ras pathways in colonic neoplasia. *Cancer Res, 61*(16), 6050-6054. Retrieved from https://www.ncbi.nlm.nih.gov/pubmed/11507052

Zhang, Y.-J., Dai, Q., Sun, D.-F., Xiong, H., Tian, X.-Q., Gao, F.-H., . . . Fang, J.-Y. (2009). mTOR Signaling Pathway Is a Target for the Treatment of Colorectal Cancer. *Annals of Surgical Oncology, 16*(9), 2617-2628. doi:10.1245/s10434-009-0555-9

Zhang, Y., Liu, T., Meyer, C. A., Eeckhoute, J., Johnson, D. S., Bernstein, B. E., . . . Liu, X. S. (2008). Model-based analysis of ChIP-Seq (MACS). *Genome Biol, 9*(9), R137. doi:10.1186/gb-2008-9-9-r137

Zhao, H., Ming, T., Tang, S., Ren, S., Yang, H., Liu, M., . . . Xu, H. (2022). Wnt signaling in colorectal cancer: pathogenic role and therapeutic target. *Mol Cancer, 21*(1), 144. doi:10.1186/s12943-022-01616-7

Zhao, Z., Chen, X., Dowbaj, A. M., Sljukic, A., Bratlie, K., Lin, L., . . . Yu, H. (2022). Organoids. *Nature Reviews Methods Primers, 2*(1), 94. doi:10.1038/s43586-022-00174-y

Zhou, C., Sun, J., Zheng, Z., Weng, J., Atyah, M., Zhou, Q., . . . Ren, N. (2020). High RPS11 level in hepatocellular carcinoma associates with poor prognosis after curative resection. *Ann Transl Med, 8*(7), 466. doi:10.21037/atm.2020.03.92

Zhou, Z. J., Dai, Z., Zhou, S. L., Fu, X. T., Zhao, Y. M., Shi, Y. H., . . . Fan, J. (2013). Overexpression of HnRNP A1 promotes tumor invasion through regulating CD44v6 and indicates poor prognosis for hepatocellular carcinoma. *Int J Cancer, 132*(5), 1080-1089. doi:10.1002/ijc.27742

Zimmerli, D., Brambillasca, C. S., Talens, F., Bhin, J., Linstra, R., Romanens, L., . . . Jonkers, J. (2022). MYC promotes immune-suppression in triple-negative breast cancer via inhibition of interferon signaling. *Nature Communications, 13*(1), 6579. doi:10.1038/s41467-022-34000-6

Zirath, H., Frenzel, A., Oliynyk, G., Segerstrom, L., Westermark, U. K., Larsson, K., . . . Henriksson, M. A. (2013). MYC inhibition induces metabolic changes leading to accumulation of lipid droplets in tumor cells. *Proc Natl Acad Sci U S A, 110*(25), 10258-10263. doi:10.1073/pnas.1222404110

Zitomer, R. S., Walthall, D. A., Rymond, B. C., & Hollenberg, C. P. (1984). Saccharomyces cerevisiae ribosomes recognize non-AUG initiation codons. *Mol Cell Biol, 4*(7), 1191-1197. doi:10.1128/mcb.4.7.1191-1197.1984

Zoncu, R., Efeyan, A., & Sabatini, D. M. (2011). mTOR: from growth signal integration to cancer, diabetes and ageing. *Nat Rev Mol Cell Biol, 12*(1), 21-35. doi:10.1038/nrm3025

7 Appendix

7.1 Abbreviations

7.1.1 Prefixes

p	pico
n	nano
µ	micro
c	centi
m	milli
k	kilo

7.1.2 Units

A	Ampere
°C	degree Celcius
Da	Dalton
g	gram
h	hour
l	liter
m	meter
min	minute
M	mol/l
s	second
U	units
V	Volt

w/v	weight per volume
v/v	volume per volume

7.1.3 Other abbreviations

aa	aminoacylated
ADF	Advanced DMEM F12
APS	ammoniumpersulfate
ATCC	American type culture collection
ATP	adenosin-5’-triphosphate
bp	base pair
cDNA	complementary DNA
CDS	coding sequence
CIP	calf-intestinal alkaline phosphatase
CLIP	crosslinking and immunoprecipitation
CHX	cycloheximide
CT	threshold cycle
DMEM	Dulbecco’s Modified Eagle Medium
DMSO	dimethylsulfoxide
DNA	desoxyribonucleic acid
DNase	nuclease
dNTPs	deoxynucleotide triphosphate
DOX	doxycycline
DTT	dithiothreitol
ECL	enhanced chemiluminescence
E. coli	*Escherichia coli*

EDTA	ethylendiamintetraacetate
e.g.	*exempla gratia*, for example
etc	et cetera
FACS	fluorescence-activated cell sorting
FBS	fetal bovine serum
FC	fold change
FDR	false discovery rate
Fig.	figure
for	forward
GFP	green fluorescent protein
GOI	gene of interest
HA	hemagglutinin
HEPES	2-[4-(2-hydroxyethyl)piperazin-1-yl]ethanesulfonic acid
HRP	horseradish peroxidase
IF	immunofluorescence
IgG	immunoglobulin
IHC	immunohistochemistry
IP	immunoprecipitation
IRES	internal ribosome entry site
LB	Luria-Bertani
LTR	long terminal repeat
M-MLV	Moloney-Murine Leukemia Virus
mRNA	messenger RNA
NES	negative enrichment score
p	phospho

PAGE	polyacrylamide gel electrophoresis
PBS	phosphate-buffered saline
PCR	polymerase chain reaction
PEG	polyehtylenglycol
PEI	polyethylenimine
pen/strep	penicillin/streptomycin
PI	propidium iodide
PS	phosphatidylserine
qRT-PCR	quantitative real-time PCR
RBP	RNA-binding protein
rev	reverse
RIPA	radioimmunoprecipitation assay buffer
RNA	ribonucleic acid
RNase	ribonuclease
RP	random hexanucleotide primers
rpm	revolutions per minute
RPMI	Roswell Park Memorial Institute
SD	standard deviation
SDS	sodium dodecyl sulfate
Seq	sequencing
shRNA	small hairpin RNA
siRNA	small interfering RNA
TAE	Tris-acetate-EDTA buffer
TBS	Tris-buffered saline
TBS-T	Tris-buffered saline with Tween-20

TE	Tris-EDTA buffer
TEMED	N, N, N’, N’-tetramethylehtylendiamine
tRNA	transfer RNA
UTR	untranslated region
UV	ultraviolet
WB	Western blotting
w/o	without

7.2 Publications

“A MYC-GCN2-eIF2α negative feedback loop limits protein synthesis to prevent MYC-dependent apoptosis in colorectal cancer.”

Schmidt S, Gay D, Uthe FW, **Denk S**, Paauwe M, Matthes N, Diefenbacher ME, Bryson S, Warrander FC, Erhard F, Ade CP, Baluapuri A, Walz S, Jackstadt R, Ford C, Vlachogiannis G, Valeri N, Otto C, Schülein-Völk C, Maurus K, Schmitz W, Knight JRP, Wolf E, Strathdee D, Schulze A, Germer CT, Rosenwald A, Sansom OJ, Eilers M, Wiegering A. Nat Cell Biol. 2019 Nov;21(11):1413-1424. doi: 10.1038/s41556-019-0408-0. Epub 2019 Nov 4.

“CIP2A regulates MYC translation (via its 5'UTR) in colorectal cancer.”

Denk S, Schmidt S, Schurr Y, Schwarz G, Schote F, Diefenbacher M, Armendariz C, Dejure F, Eilers M, Wiegering A. Int J Colorectal Dis. 2021 May;36(5):911-918. doi: 10.1007/s00384-020-03772-y. Epub 2020 Oct 19

“Targeting Protein Synthesis in Colorectal Cancer.”

Schmidt S, **Denk S**, Wiegering A. Cancers (Basel). 2020 May 21;12(5):1298. doi: 10.3390/cancers12051298.

7.3 Affidavit / Eidesstattliche Erklärung

I hereby confirm that my thesis entitled “Investigating non-canonical, 5’ UTR-dependent translation of MYC and its impact on colorectal cancer development” is the result of my own work. I did not receive any help or support from commercial consultants. All sources and / or materials applied are listed and specified in the thesis.

Furthermore, I confirm that this thesis has not yet been submitted as part of another examination process neither in identical nor in similar form.

Würzburg, _____ _____

Hiermit erkläre ich an Eides statt, die Dissertation „Untersuchung der nicht-kanonischen, 5‘ UTR-abhängigen Translation von MYC und ihres Einflusses auf die Entwicklung von Darmkrebs“ eigenständig, d.h. insbesondere selbständig und ohne Hilfe eines kommerziellen Promotionsberaters, angefertigt zu haben und keine anderen als die von mir angegebenen Quellen und Hilfsmittel verwendet zu haben.

Ich erkläre außerdem, dass die Dissertation weder in gleicher noch in ähnlicher Form bereits in einem anderen Prüfungsverfahren vorgelegen hat.

Würzburg, _____ _____